UNIVERSITY OF KWAZULU-NATAL

**MITIGATION TECHNIQUES THROUGH SPATIAL DIVERSITY
COMBINING AND RELAY-ASSISTED TECHNOLOGY IN A
TURBULENCE IMPAIRED AND MISALIGNED FREE SPACE
OPTICAL CHANNEL**

Kehinde Oluwasesan ODEYEMI

March, 2018

MITIGATION TECHNIQUES THROUGH SPATIAL DIVERSITY COMBINING AND RELAY-ASSISTED TECHNOLOGY IN A TURBULENCE IMPAIRED AND MISALIGNED FREE SPACE OPTICAL CHANNEL

by

Kehinde Oluwasesan ODEYEMI

IN FULFILLMENT OF THE DEGREE OF

Doctor of Philosophy in Electronic Engineering.

College of Agriculture, Engineering and Science,

University of KwaZulu-Natal, Durban

Supervised by:

Prof. Viranjay M. Srivastava

and

Prof. Pius A. Owolawi

March, 2018

As the candidate's Supervisors, we agree/do not agree to the submission of this thesis

Signed ………………………………… Date …………………………………….

Name: Prof. Viranjay M. Srivastava

Signed ………………………………….. Date ……………………………………

Name: Prof. Pius A. Owolawi

Declaration 1 - Plagiarism

I, **Kehinde Oluwasesan ODEYEMI**, with Student Number **216075046** and the thesis entitled "Mitigation Techniques through Spatial Diversity Combining and Relay-Assisted Technology in a Turbulence Impaired and Misaligned Free Space Optical Channel" hereby declare that:

1. The research reported in this thesis, except where otherwise indicated, is my original research.

2. This thesis has not been submitted for any degree or examination at any other university.

3. This thesis does not contain other persons' data, pictures, graphs or other information, unless specifically acknowledged as being sourced from other persons.

4. This thesis does not contain other persons' writing, unless specifically acknowledged as being sourced from other researchers. Where other written sources have been quoted, then:

   (a) Their words have been re-written but the general information attributed to them has been referenced;

   (b) Where their exact words have been used, then their writing has been placed inside quotation marks, and referenced.

5. This thesis does not contain text, graphics or tables copied and pasted from the Internet, unless specifically acknowledged, and the source being detailed in the thesis and in the References section.

Signed…………………………………. Date………………………………

    Kehinde Oluwasesan ODEYEMI

Declaration 2 - Publications

Details of contribution to publications that form part of the research presented in this thesis include publications in preparation, already submitted, in press and published. They give details of the contributions of each author to the experimental work, simulation and writing of each publication.

JOURNAL PUBLICATIONS

1. **Kehinde O. Odeyemi,** Pius A. Owolawi, and Viranjay M. Srivastava, "Performance analysis of decode-and-forward dual-hop optical spatial modulation with diversity combiner over atmospheric turbulence," *Optics Communication [Elsevier]*, vol. 402, pp. 242-251, November, 2017 (***Published***)

2. **Kehinde O. Odeyemi,** Pius A. Owolawi, and Viranjay M. Srivastava, "Block error rate performance of subcarrier intensity modulation FSO link with spatial diversity over Gamma-Gamma atmospheric channel," *International Journal of Microwave and Optical Technology (IJMOT),* vol. 12, pp. 123-133, March, 2017 (***Published***)

3. **Kehinde O. Odeyemi,** Pius A. Owolawi, and Viranjay M. Srivastava, "Optical spatial modulation with diversity combiner in dual-hops amplify-and-forward relay systems over atmospheric impairments," *Wireless Personal Communication [Springer],* vol. 96, pp. 1-24, June, 2017 (***Published***)

4. **Kehinde O. Odeyemi,** Pius A. Owolawi, and Viranjay M. Srivastava, "Performance analysis of free space optical system with spatial modulation and diversity combiners over the Gamma-Gamma atmospheric turbulence," *Optics Communication [Elsevier],* vol. 382, pp. 205-211, January, 2017 (***Published***)

5. **Kehinde O. Odeyemi,** Pius A. Owolawi, and Viranjay M. Srivastava, "Optical spatial modulation over Gamma-Gamma turbulence and pointing error induced fading channels," *Optik – International Journal for Light and Electron Optics [Elsevier]*, vol. 147, pp. 214-223, October, 2017 ***(Published)***

6. **Kehinde O. Odeyemi,** Pius A. Owolawi, and Viranjay M. Srivastava, "Free space optical system with spatial modulation and diversity combiners over atmospheric turbulent channel," *Journal of Communications* (***Accepted***)

CONFERENCE PROCEEDINGS

1. **Kehinde O. Odeyemi,** Pius A. Owolawi, and Viranjay M. Srivastava, "Performance analysis of a dual-hop spatial modulation relaying system with spatial diversity over asymmetric RF/FSO channels," *In proceedings of South African Telecommunication and Network Application Conference (SATNAC)*, Spain, September, 2017, pp. 62-67 (***Published***)

2. **Kehinde O. Odeyemi,** Pius A. Owolawi, and Viranjay M. Srivastava, **"**Performance Analysis of Block Error Rate for SIM-FSO System with Spatial Diversity over Gamma-Gamma fading and pointing error channel," *In proceedings of IEEE AFRICON Conference*, Cape town, South Africa, September, 2017, pp. 115-120 *(**Published**)*

3. **Kehinde O. Odeyemi,** Pius A. Owolawi, and Viranjay M. Srivastava, "A comparison between mathematical tools for analyzing FSO systems over Gamma-Gamma atmospheric channel," *In proceedings of IEEE AFRICON Conference*, Cape town, South Africa, September, 2017, pp. 549-554 *(**Published**)*

Signed…………………………………. Date …………………………………

Kehinde Oluwasesan ODEYEMI

Acknowledgements

Dedication

This thesis is dedicated to my beloved wife, Odeyemi Olajumoke and my son, Oluwasemire.

To God be the Glory.

Abstract

In recent times, spectrum resource scarcity in Radio Frequency (RF) systems is one of the biggest and prime issues in the area of wireless communications. Owing to the cost of spectrum, increase in the bandwidth allocation as alternative solution, employed in the recent past, does no longer offer an effective means to fulfilling high demand in higher data rates. Consequently, Free Space Optical (FSO) communication systems has received considerable attention in the research community as an attractive means among other popular solutions to offering high bandwidth and high capacity compared to conventional RF systems. In addition, FSO systems have positive features which include license-free operation, cheap and ease of deployment, immunity to interference, high security, etc. Thus, FSO systems have been favoured in many areas especially, as a viable solution for the last-mile connectivity problem and a potential candidate for heterogeneous wireless backhaul network. With these attractive features, however, FSO systems are weather-dependent wireless channels. Therefore, it is usually susceptible to atmospheric induced turbulence, pointing error and attenuation under adverse weather conditions which impose severe challenges on the system performance and transmission reliability. Thus, before widespread deployment of the system will be possible, promising mitigation techniques need to be found to address these problems.

In this thesis, the performance of spatial diversity combining and relay-assisted techniques with Spatial Modulation (SM) as viable mitigating tools to overcome the problem of atmospheric channel impairments along the FSO communication system link is studied. Firstly, the performance analysis of a heterodyne FSO-SM system with different diversity combiners such as Maximum Ratio Combining (MRC), Equal Gain Combining (EGC) and Selection Combining (SC) under the influence of lognormal and Gamma-Gamma atmospheric-induced turbulence fading is presented. A theoretical framework for the system error is provided by deriving the Average Pairwise Error Probability (APEP) expression for each diversity scheme under study and union bounding technique is applied to obtain their Average Bit Error Rate (ABER). Under the influence of Gamma-Gamma turbulence, an APEP expression is obtained through a generalized infinite power series expansion approach and the system performance is further enhanced by convolutional coding technique. Furthermore, the performance of proposed system under the combined effect of misalignment and Gamma-Gamma turbulence fading is also studied using the same mathematical approach.

Moreover, the performance analysis of relay-assisted dual-hop heterodyne FSO-SM system with diversity combiners over a Gamma-Gamma atmospheric turbulence channel using Decode-and-Forward (DF) relay and Amplify-and-Forward (AF) relay protocols also is presented. Under DF dual-hop FSO system, power series expansion of the modified Bessel function is used to derive the closed-form expression for the end-to-end APEP expressions for each of the combiners under study over Gamma-Gamma channel, and a tight upper bound on the ABER per hop is given. Thus, the overall end-to-end ABER for the dual-hop FSO system is then evaluated. Under AF dual-hop FSO system, the statistical characteristics of AF relay in terms of Moment Generating Function (MGF), Probability Density Function (PDF) and Cumulative Distribution Function (CDF) are derived for the combined Gamma-Gamma turbulence and/or pointing error distributions channel in terms of Meijer-G function. Based on these expressions, the APEP for each of the under studied combiners is determined and the ABER for the system is given by using union bounding technique. By utilizing the derived ABER expressions, the effective capacity for the considered system is then obtained.

Furthermore, the performance of a dual-hop heterodyne FSO-SM asymmetric RF/FSO relaying system with MRC as mitigation tools at the destination is evaluated. The RF link experiences Nakagami-m distribution and FSO link is subjected to Gamma-Gamma distribution with and/or without pointing error. The MGF of the system equivalent SNR is derived using the CDF of the system equivalent SNR. Utilizing the MGF, the APEP for the system is then obtained and the ABER for the system is determined.

Finally, owing to the slow nature of the FSO channel, the Block Error Rate (BLER) performance of FSO Subcarrier Intensity Modulation (SIM) system with spatial diversity combiners employing Binary Phase Shift Keying (BPSK) modulation over Gamma-Gamma atmospheric turbulence with and without pointing error is studied. The channel PDF for MRC and EGC by using power series expansion of the modified Bessel function is derived. Through this, the BLER closed-form expressions for the combiners under study are obtained.

Table of Contents

CHAPTER FOUR

List of Tables

List of Abbreviations

AC	Alternating Current
AF	Amplify-and-Forward
APD	Avalanche Photo-Diode
ABER	Average Bit Error Rate
APEP	Average Pairwise Error Probability
AWGN	Additive White Gaussian Noise
BPSK	Binary Phase Shift Keying
BLER	Block Error Rate
CBFSK	Coherent Binary Frequency Shift Keying
CBPSK	Coherent Binary Phase Shift Keying
CSI	Channel State Information
CDF	Cumulative Distribution Function
CRC	Cyclic Redundancy Check
DBPSK	Differential Binary Phase Shift Keying
DF	Decode-and-Forward
DC	Direct Current
EGC	Equal Gain Combining
FOV	Field of View
FSO	Free Space Optical
HD	High Definition
IID	Independent and Identical Distribution
IM/DD	Intensity Modulation with Direct Detection

LOS	Line of Sight
LO	Local Oscillator
MZM	March-Zehnder Modulator
MLSD	Maximum Likehood Sequence Detection
ML	Maximum Likelihood
MRC	Maximum Ratio Combining
MMSE	Minimum Mean Square Error
MGF	Moment Generating Function
MIMO	Multiple Input Multiple Output
OOK	On/Off Keying
OFDM	Orthogonal Frequency Division Multiplexing
PD	Photo-Detector
PIN	Positive-Intrinsic Negative
PDF	Probability Density Function
PPAM	Pulse Position Amplitude Modulation
PPM	Pulse Position Modulation
RF	Radio Frequency
SI	Scintillation Index
SC	Selection Combining
SNR	Signal-to-Noise Ratio
SD	Spatial Diversity
SIM	Subcarrier Intensity Modulation

CHAPTER ONE

Introduction

1.1 Background Information and Motivation

The transmission of information using optical carrier is an old-age technology which roots can be traced back to antiquity. In ancient time, around 800BC and 150BC, smoke and fire beacons signals were used for signaling purpose in military operations [1, 2]. In 1821, a solar telegraphy called *heliography* was invented by Carl Friedrich Gauss for geodetic survey where a pair of mirror was used to reflect a controlled beam of sunlight over a great distant [3]. Also, French sea Navigators during 1790-1794 used *Semaphore* as means of optical signaling to convey information over long distances [3]. In December 14, 1880, the first known optical wireless communication system called *photophone* was invented and patented by *Alexandra Graham Bell* as illustrated in Figure 1.1. In his experiment, voice signal was used to modulate intensity of sunlight and transmitted over a distance of 200 m to a parabolic mirror receiver having selenium crystal at the focal point to convert optical energy to electrical current [4-6]. The simple experiment set-up suffered a lot of challenges due to the intermittent nature of the sunlight and the crudity of the devices employed. Optical communication system was quantum leap in 1960s through the advent of new optical sources such Laser invented by *Theodore Maiman* [7]. It was during this time the earliest full duplex laser link was demonstrated by Nippon Electric Company (NEC) in Japan for commercial use [8]. Thus, from this time, optical communication has found usefulness in military operations and deep space applications.

The successful records of optical communication in military applications and the new development in optical techniques rejuvenated and fueled the research interest in the optical broadband access technology for civil applications [9]. Nowadays, with the number of users growing exponentially, the demand for high data rate transmission for present and emerging applications such as file transfer or video and audio streaming, VoIP, video conferencing, high-definition TV, is higher than ever and hence demanding more transmission bandwidth. Nevertheless, as the optical fiber infrastructure known as network backbone is capable of subsisting the current demands of bandwidth in global communication network, the issues of '*last mile*' problem is still the major bottleneck experienced by the end users which limit the

availability of data rate or download rate [10, 11]. This is mostly as a result of bandwidth limitations of copper-based connections and Radio Frequency (RF) wireless services employed by the end users to access the backbone. In this case, it was revealed that the RF band of electromagnetic spectrum is highly limited in capacity as the number of users increases and its allocation is progressively more expensive.

Recently, free space optical communication systems have received considerable attention as a viable alternative technology to its RF communication systems counterpart. It offers comparable huge bandwidth in the order of Terabyte similar to optical fiber link at a low cost without trenches digging. Free Space Optical (FSO) communication systems have seamless feature of wireless systems which make it easy to be integrated with the existing access networks [12, 13]. Moreover, when comparing FSO with RF technology, the formal requires less power, unlicensed spectrum, high security and ease of design and implementation for various applications [6, 14]. Practically, FSO was found useful in facilitating high definition (HD) video transmission during 2010 FAFA world cup events between temporary studios in Cape Town, South Africa due to its high speed capability. Furthermore, because FSO is very easy to deploy, it was then employed during September 11, 2001 terrorist attack on world trade center in New York, USA as a temporary communication means for post disaster recovery [11].
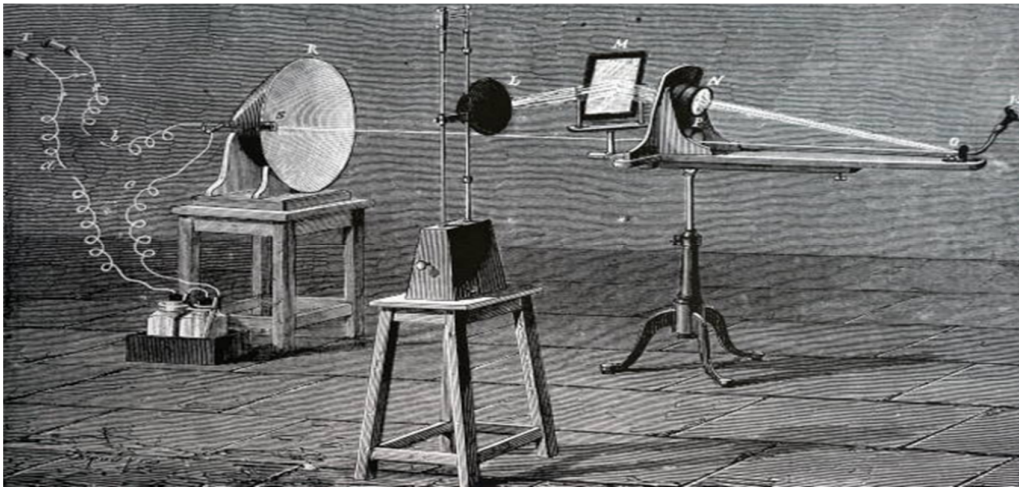
Figure 1.1: Photophone invented by *Alexandra Graham Bell* [15]

Despite these great attributes aforementioned, FSO systems are still facing a lot of challenges which degrade its performance. This is because, the transmission of information in FSO systems is via unguided media such as free space and it requires Line of Sight (LOS) between

2

the transmitter and the receiver. As a result, the system is highly vulnerable to adverse weather conditions resulting in absorption, scattering and atmospheric turbulence. These challenges hamper the transmission data rate, link range, availability and maximum performance of the system [14]. Absorption and scattering phenomenon depend on the laser wavelength and the types of particle present in atmosphere. The particles that cause absorption and scattering of light beam along FSO link could be fog, rain, snow, dust, aerosols, smoke and others. These particles attenuate the optical power by absorbing some degree of transmitted laser light energy. They also scatter laser light by deflecting it from its direction leading to spatial, angular and temporal spread. In this respect, scattering coefficient may be very high in some cases when the particles diameter is on the order of light wavelength [3, 16-18]. For instance, attenuation caused by fog and haze as a result of comparable diameter with the laser wavelength is far higher than that of the rain and snow. It is reported in [19, 20] that attenuation due to dense fog is about *350 dB/km* compared to *> 45 dB/km* loss caused by snow and *20-30 dB/km* loss at the rate of *150 mm/h* caused by rain. These attenuation losses can hamper the availability of the system and limit its range to short distance especially under a very dense fog. In this regard, additional optical power would be needed to mitigate this effect, such as the use of RF technology as back-up in order to achieve *99.99%* carrier-grade link availability for the FSO systems [21-23]. Therefore, the effects of absorption and scattering on FSO systems are deterministic and these can be predicted by using different software such as LOWTRAN, FASCODE, MODTRAN, HITRAN, and LNPCWIN as a function of wavelength [17, 24, 25].

Under clear weather conditions, however, FSO links may still be susceptible to the effect due to atmospheric turbulence which simple means fluctuation in the refractive index as a result of variation in temperature and pressure of the atmospheric medium. This impairment becomes more pronounced especially over a distance of *1 km* or more and can degrade the performance and availability of an FSO link [26, 27]. In addition to atmospheric turbulence, when the receiver employs no tracking mechanism, pointing error is another impairment that can deteriorate the FSO systems performance. This occurs as a result of a misalignment between the transmitter and the receiver due to the narrowness of the beam divergence angle and small receiver Field of View (FOV). Thus, building sway in respect to thermal expansion, dynamic wind loads, and weak earthquakes can effectively interrupt the systems link [28, 29]. Hence, atmospheric turbulence and pointing error are the serious impairments that can significantly degrade the performance of FSO link.

1.2 Literature Review on FSO Systems

Over the past decade, the need for higher data rate, higher spectral efficiency and quality of service in the wireless communication systems are growing exponentially due to the increase in number of users. As result of this, next-generation wireless communication systems are expected to offer various broadband wireless services such as the high-definition television, computer network applications (up to 100 Mbps), mobile videophones, video conferencing, high-speed Internet access, and so on. However, the disruptive nature of wireless communication channels due to multipath signal propagation and induced-fading effect has posed intriguing challenges from achieving these highly demanding goals. Therefore, in order to overcome these limitations that is particular with wireless systems; different technologies have been proposed which include the copper and coaxial cables, wireless Internet access, broadband RF (millimeter and microwave radio) and fiber optics [19]. These technologies, especially the RF based, has limitations such as congested spectrum, an expensive licensing, security issues and a high cost of installation which prevent in meeting all the aforementioned communication requirements for today services. Consequently, FSO technology is considered as one of the most promising alternative technology which can bring superior quality, wideband services to users' premises. Recently, FSO communication has drawn attention in research community due to its various characteristics including high capacity and free large bandwidth with security, compared to its RF communication counterpart [14]. Moreover, it is very easy and cheap to deploy without digging of trenches. Hence, it is found useful in several applications where high data rate is required. With all these virtues, the FSO systems suffer from atmospheric induced turbulence and pointing errors which significantly limit its operations to a short transmission distance and also degrade its performance. As a consequence, powerful mitigation techniques need to be employed for the FSO systems to surmount over the stated challenges and this is the focus of this thesis.

As mention earlier, FSO systems are prone to atmospheric turbulence. As a result, different statistical distributions have been proposed to evaluate the effect of turbulence conditions on its performance. Unfortunately, a general model that is valid for all types of turbulence conditions has not been established in the literature due to mathematical complexity in modeling the atmospheric turbulence. Notwithstanding, previous researches have shown that lognormal turbulence model is found suitable for the case of a weak turbulence condition especially over a distance less than 1 km in range [27, 30-34]. In the work presented in [35-38], it was confirmed that the K-distribution tends to be appropriate for the case of strong

atmospheric turbulence condition. Under saturation regime, irradiance fluctuations can be modelled accurately by negative exponential distribution [32, 39, 40]. Moreover, Gamma-Gamma distribution proposed by *Andrew et al* has received considerable attention as it is found used in various FSO research works [41]. This is as a result of its excellent fitness with experimental measured data for a wide turbulence regime and it has also made it useful to model weak to strong turbulence conditions [41, 42]. In addition to these models, other distributions proposed in the literature include the I-K distribution [43, 44], exponentiated Weibull [45] and log-normal Rice model (Beckmann) [44, 46, 47].

In addition to atmospheric turbulence effect, pointing error due to misalignment between the transmitter and receiver can also degrade the performance of FSO systems. In this case, various studies have been carried out on the combined effect of pointing errors with atmospheric turbulence under different weather conditions. The combined effect of these impairments was first analyzed by *Arnon* for On/Off Keying (OOK)-based FSO systems, but the effect of detector size was assumed to be negligible [48, 49]. Later, *Farid and Hranilovic* presented a composite model for FSO system over the lognormal and Gamma-Gamma turbulence conditions [50]. The authors specifically considered the effect of beam waist, jitter variance and detector size in obtaining the PDF for the composite channels, and the model with Gamma-Gamma turbulence was obtained in terms of integral. However, the pursuit of a closed-form expression for the composite channel model under Gamma-Gamma turbulence has led to further studies on pointing errors. In [51, 52], *Sandalidis et al* provided the PDF for the combined effect of strong turbulence with pointing errors to study the performance of the FSO system and the composite channel was obtained in terms of the Meijer-G function. Based on this, most works have employed this model to evaluate the performance of FSO system under the combined effects of the two impairments as it is found used in [53-58]. In spite of this, *Song et al* applied series expansion approach to study the combined effect of pointing errors over Gamma-Gamma turbulence for subcarrier binary phase shift keying modulated FSO system [59] and the analysis provides more insight for the system. In all the aforementioned works, the pointing error was modeled by Rayleigh distribution with the assumption that the jitter variance in the horizontal and vertical direction is the same. However, in [60], *Gappmair et al* employed Hoyt distribution to model the radial displacement at the receiver by assuming different jitters in orthogonal direction and this led to a finite series expression for the BER performance of the FSO system. In considering the boresight, Yang et al, developed a non-zero boresight pointing error for OOK-based FSO

system [61].The authors obtained a closed-form PDF for the composite lognormal and finite series approximation PDF for the composite Gamma-Gamma turbulence channels.

Basically, there are two types of detection for FSO systems and these include Intensity Modulation with Direct Detection (IM/DD) and coherent detection (that is, heterodyne and homodyne). In IM/DD, the photo-detector directly detects the change of light intensity emitted from the laser. In coherent detection, the optical field is mixed with the locally generated optical field before photo-detection [62]. It was reported that coherent detection offers better background noise rejection and increases the receiver sensitivity compared to IM/DD [63-65]. Also, power and bandwidth efficiency are the two most critical factors that need to be considered in selecting a modulation scheme for any FSO applications. Power efficiency of a modulation implies the maximum achievable data rate at a BER target while the bandwidth efficiency refers to the information transmission rate for a given bandwidth without considering the required transmit power [19, 66]. The most widely used signal format for FSO-based systems is well known to be On/Off Keying (OOK) modulation due to its simplicity and low cost. However, this modulation scheme requires adaptive detection threshold in order to achieve its optimum performance owing to its high sensitivity to channel turbulence [67]. This can be costly to implement at the expense of channel estimation errors. Thus, a predetermined fixed detection threshold is employed for practical implementation of OOK IM/DD systems for FSO applications but this suboptimal technique usually leads to undesirable irreducible error floors especially under strong turbulence conditions [68]. In addition to the need of adaptive detection threshold, OOK has a relatively poor energy and spectral efficiency [3, 69, 70]. Alternatively, Pulse Position Modulation (PPM) has been proposed for FSO systems to overcome the deficiency in OOK modulation scheme. It has superior energy efficiency and requires no adaptive detection threshold for optimal detection. However, PPM suffers from poor bandwidth efficiency due to short duration pulses and requires tight synchronization resulting in complex transceiver design [66]. To overcome the limitations of the conventional modulations (OOK and PPM), Subcarrier Intensity Modulation (SIM) technology was proposed by *Huang et al* in [69] for FSO applications. The idea of SIM is drawn from the well-known Orthogonal Frequency Division Multiplexing (OFDM) system where several data streams are modulated onto different RF subcarrier frequencies and the composite RF is used to modulate the laser irradiance [71]. The performance of SIM modulation in FSO systems has been studied in various works under atmospheric conditions [68-75]. However, this modulation yields a significantly higher

transceiver complexity as the number of subcarrier increases and also causes poor optical average power efficiency due to an increase in the number of required DC biases [19, 75].

Recently, optical spatial modulation (SM) emerged as a powerful transmission technique for FSO communication systems. It has been known to be an efficient low complex Multiple Input Multiple Output (MIMO) technique compared with other conventional MIMO schemes such as spatial multiplexing (Vertical Bell Labs Layered Space-Time Architecture) and repetitive coding [76]. SM makes use of the index of an activated Laser to convey information data at an instant while other Lasers remain idle [77]. As a result of this, it has advantages of avoiding inter-channel interference, eliminating the needs of inter-antenna synchronization, and provides a robust system against channel estimation errors [78, 79]. The concept was studied for indoor FSO in [80-83] and later applied for outdoor FSO systems. In [82, 84], it was reported that SM can increase the data rate of FSO systems when compared with OOK and PPM by a factor of 2 and 4 respectively with significant reduction in receiver complexity and system design. In [85], SM was proposed for FSO communication systems where SIM was combined with SM to enhance the FSO system performance. The results from this work showed that SM offered better performance compared to SIM. *Popoola et al* employed channel gain measurement to study the combined effect of SM with PPM for FSO system [86]. Later, in [87] the behaviour of optical spatial modulation system was experimentally carried out and measurement of symbol error rate at different distance was obtained. Likewise *Pham et al* evaluate the effect of combining SM with PPM for FSO system over weak turbulence channel. The results showed that the system benefit from the simplicity of the SM and the energy efficiency of the PPM [88]**.** In [89], SM was integrated with Pulse Position and Amplitude Modulation (PPAM) under the lognormal and Gamma-Gamma atmospheric turbulence. *Peppas et al* proposed SM for a coherent detection FSO system under H-K atmospheric turbulent channel in [90].

Based on the fact that FSO systems are susceptible to atmospheric turbulence, several counter-fading techniques have been proposed to mitigate the effect of turbulence induced fading along the system link. Thus, Maximum Likelihood Sequence Detection (MLSD) was also proposed by [91] as a means of combating fading over FSO links. This technique however, suffers from excessive computational complexity since its analysis requires complicated multidimensional integration. Moreover, aperture averaging is another mitigation technique which has been widely used in practical FSO applications and studied in literatures as a simple solution to reduce fading effect [92-98]. The drawback of this

technique is that, the system receiver needs a relatively large lens for the scheme to be efficient that is, aperture lens must be larger than the fading correlation length. Therefore, the increase in aperture size in aperture averaging amount to increase in background noise collected at the receiver [95]. A significant fading reduction can also be achieved when using adaptive optics. This is mostly employed in optical astronomy and deep space optical communication to deliver undistorted beam [2, 99]. The technique involves the use of wave-front sensor and deformable mirrors to reduce the distortion induced in the wave-front resulting from atmospheric turbulence[2]. However, while the technique is feasible, it is highly costly and complex to implement. In [100], error control coding in-conjunction with interleaving was used as mitigation tools for FSO systems. However, this is impracticable because its effectiveness requires large interleave as a result of slow/quasi-static fading nature of the FSO channels; thus it is more useful under weak turbulence conditions [96, 101]. Under moderate to strong conditions, error control coding is also significantly efficient, provided that it is combined with other mitigation techniques [96].

Spatial Diversity (SD) technique is a suitable alternative mitigation tool compared to the aforementioned mitigation techniques. It has an advantage of improving the error performance and reliability of the link by using multiple lasers at the transmitter and /or multiple photo-detectors at the receiver. It also prevents laser misalignment and temporary blockage of beam by obstructions [102]. This method of combating fading effect was first proposed in FSO system by *Ibrahim et al* [103]. In [31], the performance of different spatial diversity combining was investigated under clear weather, and MRC outperformed EGC. *Zhu et al* used maximum likelihood detector with spatial diversity to study the symbol-by-symbol performance of MIMO FSO system over independent and correlated lognormal channel [33]. Under a K-distribution channel, *Tsiftsis et al* studied the performance of OOK IM/DD FSO system using various spatial diversity combiners [26]. *Wilson et al* evaluated the performance of PPM and *Q-ary* PPM of MIMO FSO system under Rayleigh and lognormal fading channel [32]. *Popoola et al* investigated the performance of SIM FSO system using MRC, EGC and SC under lognormal turbulence conditions [104]. MIMO IM/DD FSO link error performance over a Gamma-Gamma channel was evaluated by *Bayaki et al* using MRC and EGC as mitigation tools [105]. *Song et al* studied the error rate performance of MIMO SIM-FSO system with repetition coding under Gamma-Gamma turbulence condition [106]. Also, *Niu et al*, considered the three diversity combining techniques to study the performance of coherent SIM FSO system [37]. In [107], the spatial modulation was used in-conjunction with

diversity combiners to improve the performance of SIM-FSO system over the lognormal fading channel but the analysis has no traceable closed-form expression for the system error rate.

Owing to the distance-dependent nature of atmospheric fading, relay-assisted transmission technique has been considered as a promising solution to improve the coverage area and reliability of FSO links. The scheme involves the use of relay devices to convey information between the source and destination nodes. Generally, relay can be categorized into two protocols comprising Amplify–and-Forward (AF) and Decode-and-Forward (DF) relays. The former amplifies any incoming signal from the source and retransmits it to the destination while the latter decodes any received signal from the source re-encodes and then re-transmits the decoded information to the destination [108, 109]. A relay-assisted technique was first proposed in FSO systems by Acampora and Krishnamurthy [110] and results from the study showed that the technique can increase the link range of FSO system. Few years later, error performance due to visibility conditions was first developed by *Akella et al* for a single hop relay FSO system [111]. Later, *Tsiftsis et al* studied the outage performance of multi-hops FSO system with AF and DF relays over strong Gamma-Gamma turbulence channels [112]. The Bit Error Rate (BER) performance of a DF based relay-assisted FSO system over the Gamma-Gamma turbulence with pointing error was studied by *Fu et al* [113]. The end-to-end performance of multi-hop FSO system with AF relays over Gamma-Gamma fading channel was extensively studied by *Datsikas et al* and subcarrier phase shift keying and differential phase shift keying (DPSK) were considered as modulation schemes [114]. *Aggarwal et al* investigated the performance of SIM-based DF relayed FSO system under the combined influence of turbulence and pointing error impairment [115]. These authors also evaluated the capacity performance of dual-hop CSI relay SIM based FSO system under the same channel conditions [71]. *Tang et al* studied the error probability and outage probability of a multi-hops FSO link employing CSI-assisted and fixed gain relays over Gamma-Gamma and pointing error channels using heterodyne detection [116]. *Zedini et al* studied the end-to-end performance of multi-hops FSO system with AF-CSI relaying using IM/DD technique over Gamma-Gamma fading with pointing error impairment [117]. *Castillo-Vazquez et al* studied the outage performance of DF-relay-assisted FSO system under the combined effects of Gamma-Gamma distribution and pointing error using time diversity [118]. In this work however, the time diversity introduced several delays in the system due to slow nature of the atmospheric turbulence channel. *Dang et al* combined techniques of *M*-ary PPM, spatial

diversity and multi-hops transmission for DF relay FSO system to overcome the impairments caused by strong atmospheric turbulence and pointing error [119].

Recently, asymmetric RF/FSO relaying technique emerged as the means of facilitating radio over free space optical communication. In some cases where optical fibers are not enough, this scheme offers advantage of multiplexing large number of RF users/devices into the backbone network. Due to high capacity of FSO systems compared to RF links, the scheme increases the end-to-end system throughput. Asymmetric RF/FSO technique was first employed in FSO systems by *Lee et al* where the authors studied the outage performance of AF dual-hop SIM based FSO system and RF and FSO links were assumed respectively to be Rayleigh and Gamma-Gamma fading [120]. Performance analysis of asymmetric RF/FSO dual-hop AF relay SIM based FSO system for Unmanned Aerial Vehicle (UAV) applications was studied by *Park et al* with RF link undergone Rayleigh fading and FSO link experienced Gamma-Gamma distribution [121]. *Ansari et al* investigated the impact of pointing error on the performance on the Gamma-Gamma turbulence FSO link of mixed RF/FSO AF dual-hop system over the RF Rayleigh fading channel [122]. *Zhang et al* proposed a mixed RF/FSO AF dual-hop system with RF undergone generalized $\kappa - \mu$ or $\eta - \mu$ distributions while FSO experiences Gamma-Gamma distribution [123]. In [124, 125], the performance of AF dual-hop relay system over the asymmetric link, with RF link undergone Nakagami-*m* and FSO link experienced the combined effect of Gamma-Gamma distribution and pointing error was investigated. *Anees et al* later evaluate the capacity of a DF based dual-hop asymmetric RF/FSO system where RF link was assumed to be Nakagami-*m* and FSO link was characterized by path loss, Gamma-Gamma and pointing error impairments [126].

In a communication system which transmits data in block of N bits, the probability $P\,(M, N)$ of more than M bits error in a block can be estimated by average Block Error Rate (BLER). Typically, the influence of atmospheric turbulence on the FSO links has been described as a slow varying channel with its coefficient resulting in the corruption of block of data bits [127]. Previous works have shown the needs to evaluate the block data transmission performance under the slow varying fading condition so as to establish good data transmission. RF research works, specifically in [127-129], have considered the systems BLER performance over a very slow fading Rayleigh channel. From our findings, works on BLER performance in FSO systems are still at infancy stage. Recently, *Zhang et al* [130] presented the BLER performance of SIM-FSO system for both coherent and non-coherent binary modulations over different atmospheric channels. However, the study did not consider

diversity combiners at the receiver end. Also, *Cheng et al* [131] studied the BLER of FSO link with pointing error over non-Kolmogorov turbulence channel, but the work did not consider combiners and SIM-BPSK binary modulation.

1.3   Aim and Objectives of the Research

This thesis aim at investigating the performance of spatial diversity combining and relay-assisted technique as mitigation tools against the effects of atmospheric turbulence and pointing error induced-fading on FSO systems. The objectives of this thesis are:

1. To investigate the performance of heterodyne optical spatial modulation based FSO system with diversity combining over lognormal and Gamma-Gamma atmospheric turbulence channels and to study the impact of combined effect of pointing error with Gamma-Gamma turbulence conditions on the proposed system.

2. To investigate the performance of relay-assisted dual-hop DF and AF optical spatial modulation with diversity combining as alternative mitigation technique over Gamma-Gamma turbulence channel.

3. To evaluate the performance of dual-hop AF Asymmetric RF/FSO optical spatial modulation with diversity combining and the influence of pointing error on the system performance.

4. To investigate the BLER performance of FSO-SIM system with diversity combining over Gamma-Gamma turbulence channel and the effect of pointing error on the system performance.

1.4 Thesis Organization

The total number of chapters arranged in this thesis is seven. Chapter 1 provides some background information about the evolution and development of the FSO communication systems. A comprehensive literature review on the FSO is presented in this chapter.

Technical background details needed for the whole thesis is presented in chapter 2. An overview of FSO system configuration with detection schemes is reported. Different statistical models for atmospheric turbulence induced fading and pointing errors are discussed. In addition, we describe different diversity combining techniques for fading mitigation as well as relay technology. A comparison between the mathematical tools in analyzing FSO system over Gamma-Gamma channel using SIM-FSO system as case study is illustrated in order to complete the chapter.

In chapter 3, the error performance of optical spatial modulation based FSO system with different diversity combiner over atmospheric turbulence conditions is analyzed. The closed-form expressions for the error performance of each under studied combiner is obtained using Gauss-Laguerre quadrature and power series expansion respectively over lognormal and Gamma-Gamma atmospheric induced fading channels. The impact of pointing error on the system performance under the Gamma-Gamma turbulence condition by using power series expansion approach is examined in the chapter.

The error performance of the optical spatial modulation with diversity combiner in dual-hop AF and DF relaying systems over Gamma-Gamma turbulence channel is presented in chapter 4. For dual-hop DF relaying system, a derived closed-form expression for the end-to-end APEP expression for each of the combiners under study and a tight upper bound on the ABER per hop is given. Thus, the overall end-to-end ABER for the dual-hops system is then evaluated. For the AF relaying system, the statistical characteristics of CSI-assisted AF relay in terms of MGF, PDF and CDF are derived for combined effect of Gamma-Gamma turbulence with and/or without pointing error. Based on these expressions, the APEP for each of the combiner is determined and the ABER for the system is also given by using union bounding technique. By utilizing the derived ABER expressions, the effective capacity for the considered system is then obtained. These are the core interest of chapter 4.

In chapter 5, the performance of a dual-hop spatial modulation asymmetric RF/FSO relaying system with heterodyne detection and MRC as mitigation tools at the destination is evaluated. Nakagami-m distribution is adopted to represent the RF channel distribution while the FSO links is subjected to Gamma-Gamma distribution with and/or without pointing error. The MGF of the system equivalent SNR is derived using the CDF of the system equivalent SNR. Utilizing the MGF, the APEP for the system is then obtained. Through this, the ABER for the system is determined using the union bounding technique.

In chapter 6, the BLER performance of SIM-based FSO system with spatial diversity combiners employing BPSK modulation over Gamma-Gamma atmospheric turbulence was discussed. The channel Probability Density Function (PDF) for MRC and EGC by using power series expansion of the modified Bessel function was derived and used to provide selection for the evaluation. Through this solution, the BLER closed-form expressions for the combiners are obtained. Also within this chapter, the influence of pointing error on the BLER performance on the system was illustrated over the Gamma-Gamma turbulence channel.

Research summary and future work are detailed in chapter 7.

1.5 Original Contributions

The contributions of this thesis to the existing body of knowledge are listed below:

- Optical spatial modulation has been well studied in many FSO communication researches as it is reported in the literature review section. However, a general received diversity technique which involves multiple receive photo-detectors is being considered at the systems receiving end. By our findings, the consideration of spatial diversity combining in-conjunction with the optical SM as a mitigation tool has not been employed for FSO systems. Thus, the combination of optical SM with diversity combining for fading mitigation over atmospheric turbulence using heterodyne detection at the receiver is established in this thesis. The error performances of the proposed systems for various types of combiner over lognormal and Gamma-Gamma atmospheric turbulence channels are detailed in chapter 3. The impacts of pointing error with zero boresight for the spatial modulation based FSO system are reported and the closed-form expression for the error performance is obtained through infinite power series approach.

- By our knowledge, it shows that spatial modulation has been extensively investigated with relay technology mostly in RF wireless systems [77, 132-136] but this modulation scheme has not been found employed in the FSO relay-assisted systems. Thus, the performance of optical spatial modulation based FSO system with spatial diversity combiner at the destination and/or relay in a dual-hop AF and DF relaying system is presented in chapter 4. The results confirm that relay schemes improve the system performance than the direct transmission. It is also discovered that the used of optical spatial modulation has not been found useful for asymmetric RF/FSO relaying scenario. Therefore, the performance of asymmetric RF/FSO relaying system with MRC combiner is presented in chapter 5. The result shows that the proposed system offers better performance than the existing system under the same turbulence conditions.

- Due to the slow nature of atmospheric turbulence channel of FSO channel, BLER can also be used to study the performance of the system. To the best of our knowledge, the improvement on BLER through the use of diversity combiner was only employed in RF conventional systems [127-129] but has not yet been

considered for FSO system. Thus, the BLER performance of SIM-FSO system with diversity combiner is presented in chapter 6. The results indicate that diversity combining technique significantly improves the system BLER performance.

1.6 Publication in Journals and Conference Proceedings

1. **Kehinde O. Odeyemi,** Pius A. Owolawi, and Viranjay M. Srivastava, "Performance analysis of decode-and- forward dual-hop optical spatial modulation with diversity combiner over atmospheric turbulence," *Optics Communication [Elsevier]*, vol. 402, pp. 242-251, November, 2017 (***Published***)

2. **Kehinde O. Odeyemi,** Pius A. Owolawi, and Viranjay M. Srivastava, "Block error rate performance of subcarrier intensity modulation FSO link with spatial diversity over Gamma-Gamma atmospheric channel," *International Journal of Microwave and Optical Technology (IJMOT)*, vol. 12, pp. 123-133, March, 2017(***Published***)

3. **Kehinde O. Odeyemi,** Pius A. Owolawi, and Viranjay M. Srivastava, "Performance analysis of free space optical system with spatial modulation and diversity combiners over the Gamma-Gamma atmospheric turbulence," *Optics Communication [Elsevier],* vol. 382, pg. 205-211, January, 2017 (***Published***)

4. **Kehinde O. Odeyemi,** Pius A. Owolawi, and Viranjay M. Srivastava, "Optical spatial modulation with diversity combiner in dual-hops amplify-and-forward relay systems over atmospheric impairments," *Wireless Personal Communication [Springer],* vol. 96, pp. 1-24, June, 2017 (***Published***)

5. **Kehinde O. Odeyemi,** Pius A. Owolawi, and Viranjay M. Srivastava, "Optical spatial modulation over Gamma-Gamma turbulence and pointing error induced fading channels," *Optik – International Journal for Light and Electron Optics [Elsevier]*, vol. 147, pp. 214-223, October, 2017 *(**Published**)*

6. **Kehinde O. Odeyemi,** Pius A. Owolawi, and Viranjay M. Srivastava, "Free space optical system with spatial modulation and diversity combiners over atmospheric turbulent channel," *Journal of Communications* (***Accepted***)

7. **Kehinde O. Odeyemi,** Pius A. Owolawi, and Viranjay M. Srivastava, "Performance analysis of a dual-hop spatial modulation relaying system with spatial diversity over asymmetric RF/FSO channels", *In proceedings of South*

African Telecommunication and Network Application Conference (SATNAC) Spain, September, 2017, pp. 62-67 (***Published***)

8. **Kehinde O. Odeyemi,** Pius A. Owolawi, and Viranjay M. Srivastava, **"**Performance analysis of block error rate for SIM-FSO system with spatial diversity over Gamma-Gamma fading and pointing error channel," *In proceedings of IEEE AFRICON Conference*, Cape town, South Africa, September, 2017, pp. 115-120 *(**Published**)*

9. **Kehinde O. Odeyemi,** Pius A. Owolawi, and Viranjay M. Srivastava, "A comparison between mathematical tools for analyzing FSO systems over Gamma-Gamma atmospheric channel," *In proceedings of IEEE AFRICON Conference*, Cape town, South Africa, September, 2017, pp. 549-554 *(**Published**)*

CHAPTER TWO

General Overview of Free Space Optical Systems

2.1 FSO Communication Systems Configuration

The block diagram of a FSO system configuration is illustrated in Figure 2.1. Similar to other types of communication systems, a FSO system comprises of three basic units which include the transmitter, transmission channel, and the receiver. Each of these units is detailed in the sections of this chapter.
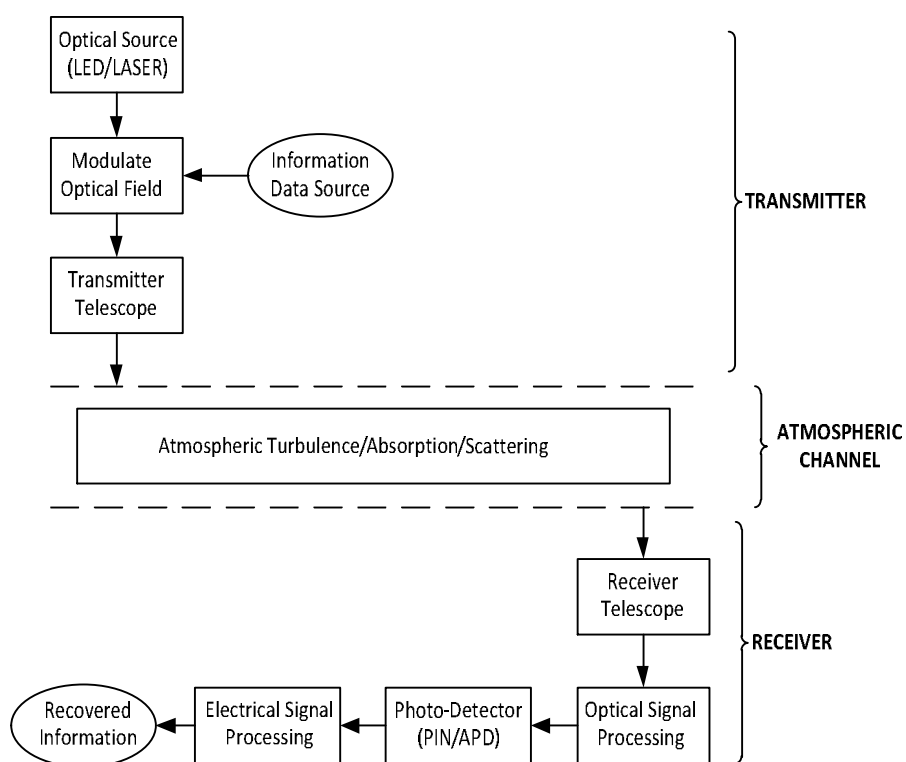
Figure 2.1: Illustration of a FSO communication system

2.1.1 FSO Transmitter System

In an FSO transmitter system, information data to be transmitted from the transmitter are modulated onto the optical field carrier produced by light source(s). Optionally, the modulated beam may be allowed to pass through the optical amplifier to boost the optical intensity. Thereafter, by means of beamforming optics, the optical radiation is collected, collimated, refocused and then propagated through transmission medium which can be any or combination of space, sea or atmosphere to the receiving end [3, 137]. The modulation can

either be internal or external. The most commonly used internal modulation is called intensity/direct modulation where the information data is modulated on the intensity of the optical radiation by varying the driving current of the light source in accordance with the data to be transmitted. This can also be achieved externally by the use of Symmetric Mach-Zehnder interferometer where radiation properties such as amplitude, frequency, phases and state of polarization can also be modulated with information to be transmitted. External modulator can offer a higher data rate than direct modulation at the expense of nonlinear response [138].

In FSO transmitter design, it is very important to condition the optical radiation to be within the safety recommendation so as to prevent issues with human in contact. This is because; optical radiation is highly powerful and can injure both the skin and the eye. Thus, eye safety is the most important factor to be considered due to the ability of the eye to focus and concentrate on the optical energy. It was found that certain wavelength in the near-infrared window have intensity power to penetrate into human eye and cause damage to the retina while other can be absorbed by the other part of the eye [12]. As a result, the front part of eye has higher absorption coefficient for wavelength that is greater than *1400 nm* [139]. In this case, several international bodies have provided guidelines to limit and monitor the transmitted optical power for the safety use of optical beam and a number of standards can be found in [19]. Therefore, various light sources are available for FSO transmitter but the most widely used in optical communication are the Lasers and Light Emitting Diode (LED) in which the operations of both are based on the electronics excitation of semiconductor. Selecting the appropriate light source for the FSO systems depends on the particular application and the key features such as optical power versus current characteristics, speed and the beam profile [139]. Actually, optical communication systems operate within *700-10,000 nm* wavelength bands where there are transmission windows that can offer higher transparent with an attenuation of less than *0.2 dB/km* in clear air transmission [138]. Typically, FSO systems operate in the near-IR wavelength range of *750-1600 nm* and a clear atmosphere is expected to offer high transparent for the system. However, due to the presence of different molecules, certain wavelengths still experience severe absorptions and scattering [3]. In this case, FSO systems are majorly designed to operate with *780-850 nm* and *1520-1600 nm* spectral windows. Owing to the availability and the low cost of devices and components in the *780-850 nm* range, FSO systems are mostly designed within this wavelength range. Moreover, FSO systems operating within *1550 nm* window allows more

power to be transmitted (eye safety) than *750 nm* band. It also reduces solar background noise and scattering effect which make it mostly useful especially in light haze and fog to overcome attenuation. However, the devices in *1550 nm* band are highly expensive and also slightly reduced the detector sensitivity [138].

2.1.2   FSO Receiver System

The FSO receiver functionally helps in detecting and recovering the transmitted information data from the incident optical radiation. The optical field is collected and converted to electrical current by photo-detector and the detected electrical current is then processed to recover the transmitted information from the source. Based on the detection type, FSO systems can be classified into two: the IM/DD systems and coherent systems [138]. In IM/DD systems, the emitted light intensity is used to transmit/send/convey information data and the photo-detector directly detects the variation in the light intensity at the receiver. In coherent systems on the other hand, the amplitude, frequency and phase of optical signal are employed to modulate the information data. At the receiving end, the received optical field is then mixed with the locally generated optical field before being detected by photo-detector. Thus, coherent FSO systems increase the receiver sensitivity and also reject background noise and other inference compared to IM/DD FSO systems [19]. In this case, there are two detection approaches in coherent FSO systems, and these include the Heterodyne and Homodyne detection schemes. The Heterodyne detection is widely used for FSO systems design because accurate phase-locked loop is required in using homodyne detection which is very expensive to achieve [30].

Photo-Detector (PD) is an optoelectronic transducer device in FSO receiver system that obeys square law in generating electrical signal in proportion to the optical filed impinging on it. It has good quantum efficiency for detecting the common light wavelength due to its junction materials such as Silicon (Si), Indium Gallium Arsenide (InGaAs) or Germanium (Ge) which has primary sensitivity to the light wavelength with extremely short transit time. As a result of this, they have high bandwidth and fast speed response. Si and InGaAs Photo-detectors respectively have maximum sensitivity for 850nm and 1550nm wavelength; except the Ge photo-detectors that are rarely found useful in FSO systems due to high level of dark noise [138]. In optical receiver, there are four types of photo-detectors and these include the Positive-Intrinsic Negative (PIN) diode, Avalanche photodiode (APD), photoconductors and metal-semiconductor metal photodiodes. PIN and APD are solid state photo-detectors mostly

used for FSO systems. PIN is widely used for FSO systems over a range of few kilometers but the receiver suffers from thermal noise [19]. APD on the other hand, is suitable for long communication link as it provides current gain through the repeated electron ionization process which increases the device sensitivity. However, this process increases the noise current generated by the APD, and the gain of APD needs to be optimized in order to maximize the received SNR at a particular optical power [11].

2.1.2.1   Direct Detection Scheme

Direct detection can be illustrated as a photon counting optical detection since the photo-detector at the receiver only responds to the change in intensity of optical field impinging on its surface as it is illustrated in Figure 2.2. Thus, the photo-detector then converts the optical incident beam into photocurrent which is further processed for the recovery of information data transmitted from the transmitter.
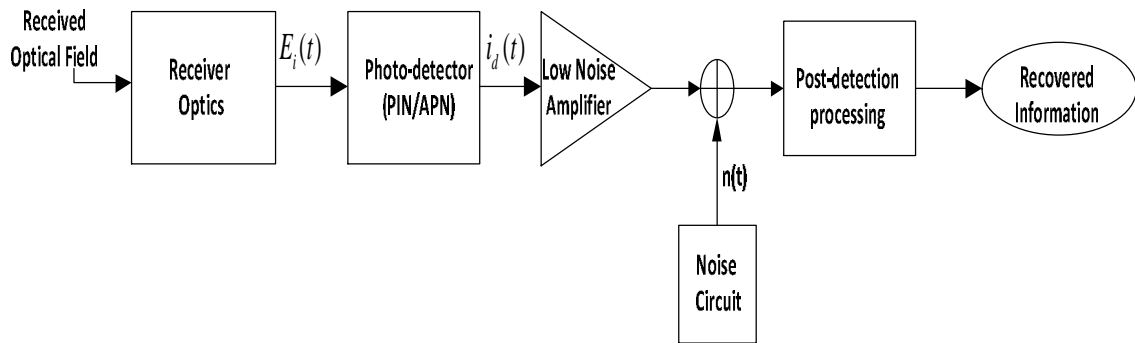
Figure 2.2: Block diagram of direct detection FSO receiver

The beam incident on the photo-detector can therefore be expressed in terms of electrical field as [137]:

$$E_i(t) = \sqrt{2P_tZ_o}\cos(\omega_c t + \phi_h + \phi) \tag{2.1}$$

where P_t is the transmitter laser power, Z_o is the free space impedance, ω_c is the carrier frequency, ϕ_h is the phase noise due to turbulence and ϕ is the phase associated with the modulation order.

In response to the optical field by the photo-detector, the generated output photocurrent can be expressed as [137]:

$$i_d(t) = \frac{R}{Z_o}\left(E_i(t)\right)^2 + n(t)$$

$$\triangleq \frac{R}{Z_o}\left(\sqrt{2P_t Z_o}\cos(\omega_c t + \phi_h + \phi)\right)^2 + n(t) \tag{2.2}$$

where $R = \eta q_e / h v$ is the responsivity of the photo-detector while $q_e = 1.6 \times 10^{-19}\,Cb$ is the electronic charge, $h = 6.6 \times 10^{-34}\,Js$ is the plank constant, η is the photo-detector efficiency and v is the optical central frequency given as $\omega_o/2$ and $n(t)$ is additive noise. The main noise sources in direct detection are the background noise and the circuit noise.

Using trigonometrical identity, the photocurrent in (2.2) can be further simplified but due to low-pass nature of the photo-detector which prevents double frequency term, only average DC term of the output current is obtained as:

$$i_d(t) = RP_t + n(t) \tag{2.3}$$

Hence, it can be deduced from (2.3) that the direct detection technique only responds to the variation in the power of the optical beam received. Therefore, the received instantaneous intensity for direct modulation transmitting laser beam can be expressed as:

$$I(t) = I_a(1 + \rho s(t)) \tag{2.4}$$

where I_a is the average received optical intensity, $s(t)$ is the modulating signal and ρ is the modulation index. Thus, for laser beam to operate within its dynamic range, $|\rho s(t)| \leq 1$ is required since the transmitting optical intensity is non-negative. If the OOK modulating scheme is employed, a digital data bit $s(t) = 0$ is transmitted as "OFF" and data bit $s(t) = 1$ indicate "ON" while $\rho = 1$. Then, the generated photocurrent after detection at the receiver is given as:

$$i_d(t) = RI + n(t) \tag{2.5}$$

where $n(t)$ is the additive noise model as zero mean and variance σ_n^2.

2.1.2.2 Heterodyne Detection Scheme

The configuration of the heterodyne detection is shown in Figure 2.3 where the optical incoming field from the transmitter is mixed with the Local Oscillator (LO) generated optical field resulting into another optical field with intermediate frequency carrier which is then

detected by photo-detector. The mixed optical beam received at the aperture plane of the photo-detector in terms of electrical field can be expressed as [90, 137]:

$$
\begin{aligned}
E_{mixed}(t) &= E_i(t) + E_{LO}(t) \\
&\triangleq \sqrt{2P_t Z_o}\cos(w_c t + \phi_h + \phi) + \sqrt{2P_{LO}Z_o}\cos(\omega_{LO}t)
\end{aligned}
\tag{2.6}
$$

where P_{LO} and Z_o are local oscillator power and free space impedance respectively, $\omega_{LO} = \omega_c + \omega_{IF}$ is the local oscillator frequency while ω_c and ω_{IF} are respectively the carrier frequency and intermediate frequency, ϕ_h is the phase noise due to turbulence and ϕ is the phase associate with the modulation order.

Thus, the generated photocurrent from the output of the photo-detector in response to the received mixed optical beam can be expressed as [140]:

$$
\begin{aligned}
i_d(t) &= \frac{R}{Z_o}\left(E_{mixed}(t)\right)^2 + n(t) \\
&\triangleq i_{DC} + i_{AC}(t) + n(t)
\end{aligned}
\tag{2.7}
$$

where $i_{DC} = R(P_s + P_{LO})$ and $i_{AC}(t) = 2R\sqrt{P_s P_{LO}}\cos(\omega_{IF}t - \phi_h - \phi)$ are the DC and AC terms respectively and $n(t)$ is the zero-mean short noise with variance σ_s^2. Practically, $P_{LO} \gg P_s$, thus, the DC term is dominated by RP_{LO} and the shot noise generated by the LO dominates any other noise sources and its variance can be expressed as [90]:

$$
\sigma_s^2 = 2qRP_{LO}\Delta f
\tag{2.8}
$$

where Δf is the noise equivalent bandwidth of the photo-detector.
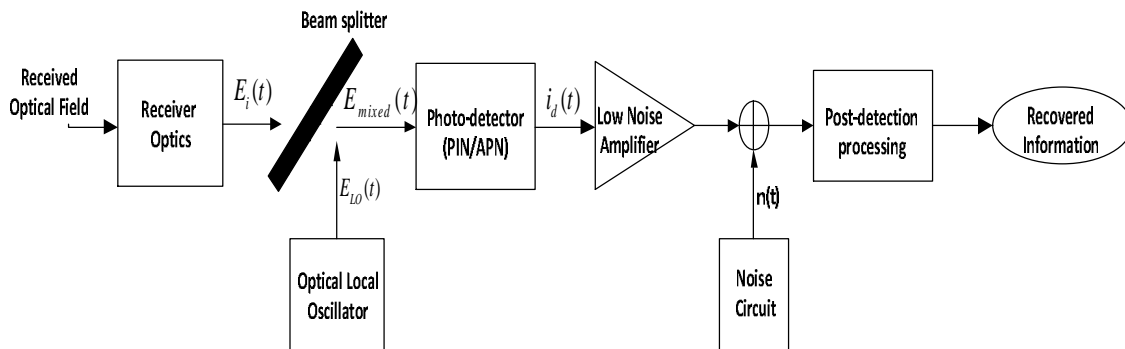
Figure 2.3: Block diagram of heterodyne detection FSO receiver

2.1.3 Additive Noise in FSO Systems

Apart from all channel impairments stated so far, additive noise can also degrade the performance of FSO systems. At the receiver, a photocurrent converts incoming optical field to electrical current and this contained additive noise such as background noise, dark current noise, shot noise and thermal noise [141]. In direct detection, thermal noise is highly pronounced than any other noise while shot noise is highly dominant in heterodyne detection owing to the use of local oscillator. In both cases, background noise and dark current noise are generally considered to be negligible. Therefore, thermal noise and shot noise are the two fundamental noises in FSO systems.

2.1.3.1 Thermal Noise

Thermal noise occurs as a result of random thermal movement of electrons in a resistor at finite temperature which manifests as a fluctuating current even in the absence of applied voltage. This noise is also called Johnson noise or Nyquist noise [141, 142]. The current produced by the thermal noise can be modeled mathematically as a stationary Gaussian process with a frequency independent spectral density defined as [137]:

$$S_T(f) = \frac{2k_B T}{R_l} \tag{2.9}$$

where k_B is the Boltzmann constant, T is the temperature in Kelvin, and R_l is the load resistor.

The spectral density is double-sided and the photocurrent noise variance for the thermal noise can be defined as [137]:

$$\begin{aligned}
\sigma_T^2 &= \int_{-\infty}^{\infty} S_T(f) |H(f)|^2 df \\
&\triangleq \int_{-\Delta f}^{\Delta f} S_T(f) df = \frac{4\Delta f k_B T}{R_l}
\end{aligned} \tag{2.10}$$

where $H(f)$ is assumed to be unity and is called frequency response of the receiver's filter, Δf is the noise equivalent bandwidth of the photo-detector. It is very important to note that both the spectral density and photocurrent noise variance are independent on the received signal.

2.1.3.2 Shot Noise

This was first studied by Schottky in 1918 [143] and since then, it has been widely investigated [144, 145]. It occurs as a result of quantization of photons and electrons in which photons caused quantum noise and electrons caused dark noise [19]. Mathematically, quantum noise can be modeled as a stationary random process following Poisson statistics and normally approximated by Gaussian statistics. Similar to thermal noise, with the spectral density $S_T(f) = qI_q$, the noise variance of the quantum noise can be expressed as [137]:

$$\sigma_q^2 \triangleq \int_{-\infty}^{\infty} S_T(f)df = 2qI_q\Delta f \tag{2.11}$$

where I_q is the received average current of the photo-detector

On the other hand, dark noise current flows in the absence of incident light due to semiconductor nature of photo-detector where electrons and holes carriers overcome band-gap as a result of thermal effect in the semiconductor photo-detector. With the spectral density $S_T(f) = qI_d$, the noise variance of the quantum noise can be expressed as [137]:

$$\sigma_d^2 \triangleq \int_{-\infty}^{\infty} S_T(f)df = 2qI_d\Delta f \tag{2.12}$$

where I_d is the received average current of the photo-detector

Hence, the shot noise variance is the sum of the quantum noise variance and dark noise variance obtained as:

$$\sigma_{sh}^2 = \sigma_q^2 + \sigma_d^2 = 2\Delta f\left(I_q + I_d\right) \tag{2.13}$$

2.1.4   Optical Receive Signal-to-Noise Ratio

In FSO systems, Signal-to-Noise Ratio (SNR) is one of the vital parameters for evaluating the performance of communication systems and it is defined as the ratio of signal power to the total noise power. The instantaneous received SNR for both direct detection system and heterodyne detection FSO system can be obtained from equation (2.5) and (2.7) respectively in the absence of background noise and dark noise. Thus, the instantaneous SNR at the direct detection receiver can then be expressed as the ratio of time-average alternating current (AC) photocurrent power to the noise variance; for $\sigma_T^2 \gg \sigma_{sh}^2$ and is given as [137]:

$$\gamma_{dd} = \frac{\langle i_d(t) \rangle^2}{\sigma_T^2}$$

(2.14)

The instantaneous SNR in the heterodyne receiver, on the other hand, can thus be expressed as the ratio of the RMS magnitude of AC photocurrent power to the total noise variance; for $\sigma_{sh}^2 \gg \sigma_T^2$ and is given as [37, 140]:

$$\gamma_{het} = \frac{\langle i_{AC}(t) \rangle^2}{\sigma_{sh}^2}$$

(2.15)

2.2 Atmospheric Turbulence

As stated earlier in chapter 1, atmospheric turbulence is random effects that occur along the FSO propagation link as a result of inhomogeneities in atmospheric temperature and pressure from one location point to the other along the system link. This random effects form turbulent cells are called eddies of different sizes and refractive indices which cause constructive and destructive interferences of the optical beam intensity. As a result of this, it redistributes the signal energy which leads to fluctuation in both the amplitude and phases of the propagation beam intensity at the receiver and significantly degrades the system performance [146, 147]. In this case, atmospheric turbulence can be characterized by three parameters which include the inner scale l_o, outer scale L_o and the refractive index structure parameter C_n^2. According to Kolmogorov Theory of turbulence, the outer scale is described as the largest cell size before the energy is injected into a region while the inner scale is defined as the smallest cell size before energy is dissipated into heat [3, 146]. In practice, the outer scale has negligible impact on the turbulence since its value is approximated as $L_o \to \infty$. In case of the inner scale, its large value has significant impact on the turbulence resulting in higher irradiance variance especially during strong turbulence [96, 148]. Therefore, the Scintillation Index (SI) is the most useful parameter to estimate the fluctuation resulting from atmospheric turbulence over the FSO links and it can be expressed as [146]:

$$\sigma_{SI}^2 = \frac{E(I^2)}{(E(I))^2} - 1$$

(2.16)

where I is the optical intensity, and the expected value is denoted as $E(.)$.

Moreover, the SI can be defined in terms of Rytov variance and under the assumption of plane wave, the weak turbulent condition can be written as [92]:

$$\sigma_{SI}^2 = \sigma_R^2 = 1.23\, C_n^2 k^{7/6} L^{11/6}$$

and for spherical plane :

(2.17)

$$\sigma_{SI}^2 = 0.4\sigma_R^2 = 0.5\, C_n^2 k^{7/6} L^{11/6}$$

where L is the link distance, $k = 2\pi/\lambda$ is the optical wavenumber and C_n^2 is the refractive index structure parameter.

Based on the values of the Rytov variance, the turbulence conditions can be classified approximately as follows [149-151]: weak turbulence conditions as $\sigma_R^2 \leq 0.3$ moderate to strong turbulence conditions $0.3 \leq \sigma_R^2 \leq 5$ and saturation turbulence conditions $\sigma_R^2 \gg 1$. The refractive index structure parameter C_n^2, on the other hand, measures the strength of the turbulence and its value depends on the altitude and link distance, but is assumed to be constant for a horizontal propagation field. It has large values at lower altitudes due to heat transfer between the air and the earth surface [146]. It is assumed that for homogenous turbulence however C_n^2 is independent on the distance especially for terrestrial FSO systems [94]. Typically, its values range from $10^{-12} m^{-2/3}$ for strong turbulence to $10^{-17} m^{-2/3}$ for the weak turbulence. In the literature, several empirical models of C_n^2 have been proposed based on experimental measurements in different locations, time of the day, wind speeds and terrain type and so on, for the estimation of turbulent strength but Hufnagle-Valley (H-V) model is the most widely used empirical model to characterize C_n^2 [10, 16, 146] and is given as:

$$C_n^2 = 0.000594 \left(\frac{v}{27}\right)^2 (10^{-5}h)^{10} \exp\left(-\frac{h}{1000}\right) + 2.7$$
$$\times\, 10^{-16} \exp\left(-\frac{h}{1500}\right) \hat{A} \exp\left(-\frac{h}{1000}\right)$$

(2.18)

where h is the altitude, v is the root mean square (RMS) of the wind speed, and $\hat{A}$ is the normal value of $C_n^2(0)$ at ground level.

2.2.1 Atmospheric Turbulence Distributions

As mentioned earlier, in FSO systems, atmospheric turbulence induced-fading is one of the most significant channel impairments that degrade the system performance. Actually, it is highly difficult to express the exact PDF that fit the statistics of the optical radiation received through the atmospheric turbulence. To the best of our knowledge, there is no valid universal

statistical model that can be used to study and predict atmospheric turbulence conditions over FSO links due to mathematical complexity involved in its modeling. As a result of this, several researchers have proposed different atmospheric turbulence models based on the turbulence regimes and the most widely accepted ones will be briefly discussed.

2.2.1.1 Lognormal Turbulence Model

Lognormal turbulence model is a suitable statistical distribution to study FSO systems under clear weather condition for short distance propagation [152]. The model is derived based on the Rytov approximation theory, which requires the magnitude of the scattered field wave to be small, compared to the unperturbed phase gradient. Unfortunately, this assumption is only valid in single scattering event characterizing weak turbulence. When multiple scatterings are experienced, especially in longer link ranges, the incident wave becomes increasingly incoherent and lognormal model becomes invalid [70]. The model has Rytov variance of less than unity for the weak turbulence. For a small C_n^2 constant, this model is also valid for long distance propagation since Rytov variance is proportional to the propagation distance [153] as it is stated in (2.18). The detailed derivation of lognormal distribution is given in Appendix B1. Thus, the PDF for the random variable h can be expressed as [146]:

$$f_h(h) = \frac{1}{h\sqrt{2\pi\sigma_h^2}} exp\left(-\frac{(ln(h) + 0.5\sigma_h^2)^2}{2\sigma_h^2}\right) \tag{2.19}$$

where σ_h^2 is the log-amplitude variance, $\sigma_h^2 \approx \sigma_R^2/4 = 0.31\, C_n^2 k^{7/6} L^{11/6}$ and ln is the natural logarithm.

2.2.1.2 Gamma-Gamma Turbulence Model

The Gamma-Gamma is a multiplicative random process which was proposed by Andrew et al as a valid PDF for modeling FSO links over a wide range of turbulence conditions from weak to strong because it offers an excellent fit with the experimental data. The detailed derivation of Gamma-Gamma distribution is given in appendix B2. Thus, the PDF for the random variable h can be expressed as [41, 146]:

$$f_h(h) = \frac{2(\alpha\beta)^{\frac{\alpha+\beta}{2}}}{\Gamma(\alpha)\Gamma(\beta)} h^{\frac{\alpha+\beta}{2}-1} K_{\alpha-\beta}\left(2\sqrt{\alpha\beta h}\right), \qquad h > 0, \alpha > 0, \beta > 0 \tag{2.20}$$

where $\Gamma(.)$ and $K_{(v)}(.)$ are defined as gamma function and v^{th} order modified Bessel function of the second kind respectively, α and β are scintillation parameters which are

defined as the effective number of large scale and small scale eddies respectively, and thus are specified as [42, 146]:

$$
\begin{aligned}
\alpha &= \left[exp\left(\frac{0.49\sigma_R^2}{\left(1 + 1.11\sigma_R^{12/5}\right)^{7/6}} \right) - 1 \right]^{-1} \\
\beta &= \left[exp\left(\frac{0.51\sigma_R^2}{\left(1 + 0.69\sigma_R^{12/5}\right)^{5/6}} \right) - 1 \right]^{-1}
\end{aligned}
\tag{2.21}
$$

where σ_R^2 is the Rytov variance, and the SI to quantify the level of turbulence can be expressed as [146, 154]:

$$
\sigma_{SI}^2 = \frac{1}{\alpha} + \frac{1}{\beta} + \frac{1}{\alpha\beta}
\tag{2.22}
$$

When β is set to unity, the Gamma-Gamma turbulence PDF degenerates to another PDF called K-distribution which is widely used to model strong turbulence condition. Experimental data were used by Andrew and Philip to validate the accuracy of this PDF under strong turbulence conditions [41, 153]. At times, it gives accurate result over a distance of approximate 1km or when the scintillation index is restricted to the range of $(2, 3)$ [146]. Thus, from (2.20), when $\beta = 1$, the K-distribution can then be written as:

$$
f_h(h) = \frac{2(\alpha\beta)^{\frac{\alpha+1}{2}}}{\Gamma(\alpha)} h^{\frac{\alpha}{2}-1} K_{\alpha-\beta}\left(2\sqrt{\alpha h}\right), \qquad h > 0,
\tag{2.23}
$$

Also, from (2.22), the SI can be for K-distribution can therefore be obtained as:

$$
\sigma_{SI}^2 = \frac{2 + \alpha}{\alpha}
\tag{2.24}
$$

2.3 Pointing Error Distribution

Mostly, FSO systems are widely installed on the high building so as to establish a clear LOS required between the transmitter and receiver. However, thermal expansion, dynamic wind loads and weak earthquake resulting in building sway, cause mechanical vibrations of the transmitter beam which lead to a misalignment between the transmitter and the receiver and is known as pointing error [49, 155]. In addition, atmospheric turbulence can also cause

pointing error in FSO systems due to inhomogeneity of large scale atmospheric eddies that result in beam wander leading to random deflection of optical beam from its transmit path and should be taken into consideration over a long distance path [156]. Also, as the distance between the transmitter and receiver increases, the pointing error becomes pronounced, owing to the narrowness of transmitted beam and small receiver FOV [29]. In any of this case, the pointing error affects the power efficiency of the FSO links by a significant amount at the receive photo-detectors resulting in high error. Thus, pointing error effect has three components which include, the beam width, boresight and jitter. The beam width represents the beam waist (radius computed at e^{-2}). Boresight is the fixed displacement between beam center and the center of the detector and mostly affected by thermal expansion of the building. Jitter on the other hand is the random offset of the beam at the detector plane and mostly caused by the building sway and building vibration [61, 157]. The typical range of boresight is $0.0039 - 0.0117\ mrad$, while that of jitter standard variance is $0.0033 - 0.0100\ mrad$ [61].

By considering a circular detection aperture with radius r receiving Gaussian beam propagation through distance z from the transmit laser, and instantaneous radical displacement between the centroid and detector center is assumed to be r, then, the fraction of the collection power by detector can be approximated as [50]:

$$h_p(r,z) \approx A_o exp\left(-\frac{2r^2}{w_{z_{eq}}^2}\right) \qquad (2.25)$$

where A_o is the fraction of the collected power at zero radial distance given as $A_o = [erf(v)]^2$ while $erf(.)$ is the error function. The equivalent beam width/waist $w_{z_{eq}}$ can be written as:

$$w_{z_{eq}} = \frac{w_e^2 \sqrt{\pi} erf(v)}{2v \times exp(-v^2)} \qquad (2.26)$$

where $v = \sqrt{\pi/2}\, r/w_e$ is the ratio between the aperture radius with w_e denoting the beam width/waist at distance z. w_e/r is the normalized beam width/waist by the receiver aperture radius. The beam width can be approximated by $w_e = \theta_z$, where θ is the transmit divergence angle describing the increase in the beam radius with distance from the transmitter.

It is assumed that both the elevation and horizontal displacement (sway) follow an independent identically distributed zero-mean Gaussian distribution. Thus, Rayleigh distribution is used to model the radial displacement r at the receiver and can be expressed as [49, 50]:

$$f_r(r) = -\frac{r}{\sigma_s^2} exp\left(-\frac{r^2}{2\sigma_s^2}\right), \qquad r > 0 \tag{2.27}$$

where σ_s^2 is the jitter variance at the receiver. Hence, by combining (2.25) and (2.27), the pointing error PDF for zero boresight can be obtained as [50, 59]:

$$f_{h_p}(h_p) = \frac{\xi^2}{A_0^{\gamma^2}} h_p^{\gamma^2-1} \tag{2.28}$$

where $\xi^2 = w_{z_{eq}}/2\sigma_s^2$ is the ratio between the equivalent radius at the receiver and the pointing error displacement standard variance at the receiver which measures the degree of pointing error effect.

2.4 Modulation Techniques

In selecting a modulation technique for any communication system, power and bandwidth efficiency are the most prime metrics against which a particular modulation technique may be considered [19]. Transmitted power in FSO systems is the average optical power required to achieve a desired bit error rate at a given data rate. This depends on the factors like eye and skin safety requirement which limits the maximum propagation distance during severe turbulence conditions. Likewise, in some battery power optical wireless system, power consumption needs to be minimized as well in order to improve the battery life [66]. On the other hand, bandwidth determines the maximum data for a given link distance with a particular modulation scheme [147]. Although, the bandwidth of optical communication is "unlimited", however, factors like optoelectronics devices, multipath channel, limit the amount of bandwidth practically available for a distortion-free communication system [158, 159]. There are different modulation schemes for efficient FSO systems operations and these include: OOK modulation which is a baseband modulation mostly used for FSO systems with advantages such as simplicity and cost effectiveness. However, the scheme required adaptive threshold in order to perform optimally [67]. To overcome this short coming, PPM is another baseband modulation which requires no adaptive threshold and has good power efficiency. However, the scheme suffers from poor bandwidth efficiency and requires complex receiver

design due to tight synchronization requirement [66]. The emphasis in this section will be on more powerful modulation techniques which have more advantages than the ones stated above and they include subcarrier intensity modulation and optical spatial modulation which are the major modulation schemes considered in this thesis.

2.4.1   Subcarrier Intensity Modulation

Subcarrier Intensity Modulation is a modulation scheme whose concept is based on multiple carriers RF communication used in many applications such as digital television, local area network , asymmetric digital subscriber line, 4G carrier system and optical fiber carrier [160, 161]. In SIM, a data stream is first modulated onto RF signal which is used to change the intensity of an optical source. Through this, SIM improves the FSO systems error performance as compared to other conventional modulation schemes such as OOK and PPM. It requires no adaptive threshold for optical performance and does not suffers from irreversible error floor like OOK [68]. Also, compared with PPM, it does not suffer from poor bandwidth efficiency. Moreover, it can improve the system capacity/throughput because it allows multiple subcarriers to transmit information signal with minimal inter-symbol interference (ISI). SIM allows seamless integration of FSO systems into present and future networks such as optical fiber cable. However, this modulation scheme requires tight synchronization at the receiving end which will result in a higher receiver complexity. The main drawback of SIM is the poor optical average power efficiency which deteriorates as the number of subcarrier increases. This is as a result of DC bias that is required to be added to multiple subcarrier electrical signals before optical intensity modulation since optical intensity must be non-negative [66]. In this case, different techniques have been proposed in order to improve the poor power problem in SIM [19, 75], but this is not the focus of this thesis.

The block diagram of a FSO SIM system is demonstrated in Figure 2.4 where the serial-to-parallel converter distributes information data $s(t)$ across an N-subcarrier coherent modulator. The RF subcarriers signal $m(t)$ then pre-modulates with the information data which is used to modulate the optical beam intensity $P(t)$ of a continuous wave laser source. Due to positive and negative values of subcarrier signal, a DC bias b_o is applied to the subcarriers before it is used to drive the laser source in order to prevent signal clipping.
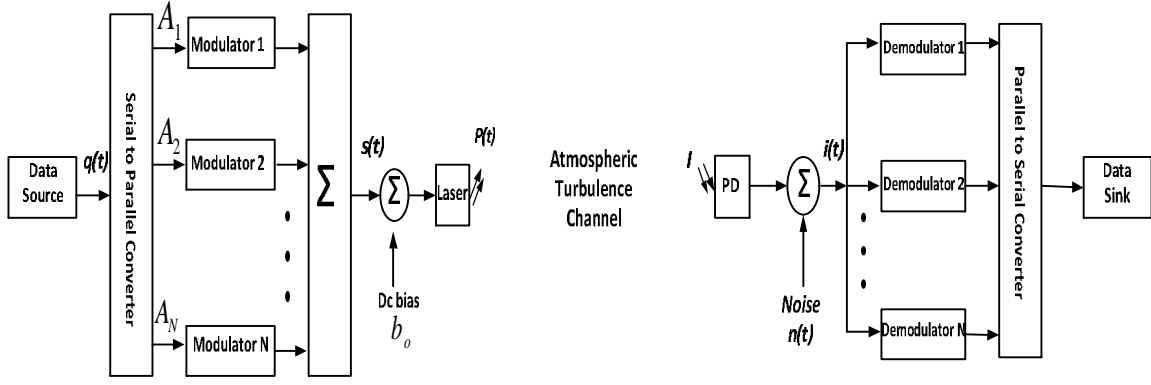
Figure 2.4: Block diagram of a FSO-SIM system

Thus, the general expression for multiple subcarrier modulating signals $s(t)$ can be defined as [104]:

$$s(t) = \Re\left[\left(\sum_{j=1}^{N} A_j exp\left(j\left(2\pi f_j + \theta_j\right)\right)\right)\exp(2\pi f_c)\right] \tag{2.29}$$

where $\Re(z)$ is the real part of z, A_j, f_j and θ_j respectively are the amplitude, frequency and phase of the jth base band equivalent signal and f_c is the carrier frequency. After proper DC biases of subcarrier modulating signal $s(t)$, the transmitted power of the modulated continuous wave laser beam can be expressed as [162]:

$$P_t = P[1 + \rho s(t)] \tag{2.30}$$

where P is the average transmitting optical power. At the receiver, the photo-detector converts the received optical intensity beam into an electrical signal and hence, the photocurrent produced by the photo-detector can be written as [162]:

$$i_r(t) = PRI\left(1 + \rho s(t)\right) + n(t) \tag{2.31}$$

where ρ is the modulation index with conditions $-1 \leq \rho s(t) \leq 1$ in order to avoid over-modulation.

2.4.2   Optical Spatial Modulation

Optical Spatial Modulation (SM) is a promising low-complex energy and bandwidth efficient single carrier transmission technique which effectively operates in diverse MIMO configurations. It employs a simple modulation mechanism in which only active

transmitter(s) propagate signal(s) and this is based on the active laser index to convey information to the receiver. As a result of this, the required energy needed to power the laser sources is drastically reduced [163, 164]. At the receiver, a low-complex detector/decoder is used to estimate the index of active laser through which the transmitted symbol is estimated and the group of information data bit are then retrieved/recovered. Since only one laser is active at an instant, it requires only one transmit chain for data transmission, and inter channel interference (ICI) is completely prevented at the receiver which simplifies the receiver design [79]. Moreover, it offers robustness against channel estimation and correlation compared to other conventional MIMO schemes [165, 166]. As a matter of fact, SM scheme increases the data rate/spectral efficiency of a system by base two logarithms of the number of transmits units without any bandwidth expansion compared to any other conventional MIMO and modulation schemes [82, 84, 90, 167].

A simple optical SM system with transmit lasers N_t, received photo-detectors N_r, and a M constellation size is illustrated in Figure 2.5. The information to be transmitted at the transmitter is grouped into two blocks of $log_2(M\,N_t)$ bits. The first group of $log_2(N_t)$ bits are used to choose the laser that would switch on for data transmission while others are inactive at that instant. Then, the other block of $log_2(M)$ bits are used to select a symbol from the signal constellation diagram. The resultant modulated symbol which is the combination of symbol x_k and the active transmit-laser index l forms a constellation vector defined as [168]:

$$X_{l,k} = \begin{bmatrix} 0 & 0 & \ldots & \underbrace{x_k}_{l^{th}\,laser\,position} & \ldots & 0 & 0 \end{bmatrix}^T \tag{2.32}$$

where k is the symbol from the M-ary constellation and l is the activated laser index.

Hence, the SM signal is transmitted over the MIMO atmospheric turbulence channel H which can be described as a $N_r \times N_t$ dimensional matrix optical MIMO channel and is given as [90]:

$$H(t) = \begin{bmatrix} h_{11}(t) & h_{12}(t) & \cdots & h_{1N_t}(t) \\ h_{12}(t) & h_{12}(t) & \cdots & h_{2N_t}(t) \\ \vdots & \vdots & \ddots & \vdots \\ h_{N_r1}(t) & h_{N_r2}(t) & \ldots & h_{N_rN_t}(t) \end{bmatrix} \tag{2.33}$$

where h_{ij} denotes the channel path gain between the ith transmit laser and the jth receive photo-detector for $i = 1,2,\ldots N_t$ and $j = 1,2,\ldots N_r$. The corresponding received SM signal at the receiver which is a $N_r \times 1$ vector can be expressed as [89]:

$$\begin{aligned} y &= \sqrt{\bar{\gamma}}\, h_l x_k + n(t) \\ &\triangleq \sqrt{\bar{\gamma}} H X_{l,k} + n(t) \end{aligned} \tag{2.34}$$

where $X_{l,k}$ is the transmitted symbol defined in (2.32), $\bar{\gamma}$ is the average received SNR observed at each receiver branch, $n(t)$ is the $N_r \times 1$ channel noise whose elements are modeled as independent identically distributed (I.I.D.) according to $\sim CN(0, \sigma_n^2)$, and h_l denotes the activation of the lth column of channel matrix H for a randomly chosen l during each transmission period and it is given as:

$$h_l = \begin{bmatrix} h_{1l}, h_{2l}, \ldots h_{N_r l} \end{bmatrix}^T \tag{2.35}$$

At the receiver side, the incoming optical radiation is converted to electrical signals by the photo-detectors and the OSM detector is then applied to estimate the Laser transmit index $\hat{l}$ and $\hat{k}$ constellation symbol which are used to decode the transmitted bit stream. Actually, there are three different SM detectors that are mostly used, namely Minimum Mean Square Error (MMSE), Maximum likelihood (ML) and Optimal Detection (OD) [169]. A jointly optimized Maximum likelihood (ML) can thus be employed as a SM demodulator due to its excellent performance compared to the others [170, 171], and can be expressed as:

$$\begin{aligned} [\hat{l}, \hat{k}] &= arg\max_{\hat{l}, \hat{k}} p_Y(y|X_{l,k}, H) \\ &\triangleq arg\min_{\hat{l}, \hat{k}} \sqrt{\bar{\gamma}} \|h_l x_k\|_F^2 - 2Re\{y^H h_l x_k\} \end{aligned} \tag{2.36}$$

where $\hat{l}$ and $\hat{k}$ are the estimated laser and transmitted symbol index, respectively, $\|.\|_F^2$ is the squared Frobenius norm and $p_Y(y|X_{l,k}, H)$ is the PDF of y conditioned on H and $X_{l,k}$ which can be expressed as [171]:

$$p_Y(y|X_{l,k}, H) = \pi^{-N_r} exp\left(-\|y - \sqrt{\bar{\gamma}} H X_{l,k}\|_F^2\right) \tag{2.37}$$
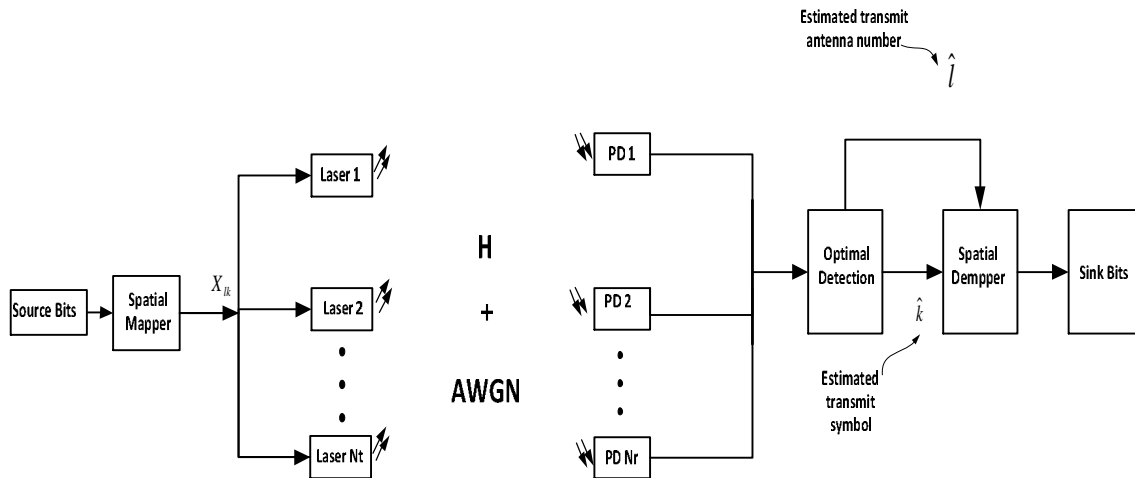
Figure 2.5: Optical spatial modulation system configuration

2.5 Diversity Techniques

Diversity technique involves the use of multiple photo-detectors at the receiver with low probability that all the detectors will simultaneously experience deep fade due to channel impairments. It is one of the efficient and powerful methods employed to mitigate against atmospheric turbulence impairment along the FSO links. With a wide divergence optical source, it combats misalignment between the transmitter and receiver and this circumvents the use of active tracking. Aside this, it also prevents temporary blockage or outage of the link due to obstruction as a result of moving object across the link [147, 172]. To achieve the stated benefits, different diversity techniques have been developed to obtain signal replica at the receiver and these include; wavelength (frequency) diversity, temporal (time) diversity and spatial diversity. In wavelength diversity, information signal is transmitted by composite transmitter onto different carrier wavelengths and each of the receiver only detects the signal at a specific wavelength [173, 174]. However, owing to the atmospheric turbulence which remains unchanged for all wavelengths window; this technique becomes less efficient for FSO systems [175]. Temporal diversity on the other hand, involves transmission of the same signal at different time slots [176-178] and this requires large processing time due to slow nature of the FSO channels [11]. As a consequence, the receiver may require a large memories for storing long data frames that cannot be practically implemented for the system [178, 179]. In spatial diversity, the receiver needs to be provided with redundantly the same transmitted signal through independent fading channels. It then combines these multiple replicas, leading to an increase in the overall received SNR at the receiver and lower the error

performance and outage probability of the system [180]. In order to prevent any correlation in the received signal, the photo-detectors need to be separated by a few centimeters since the spatial coherent length of the atmospheric channel is nearly a few centimeters [70, 146] and the beam footprint covers the whole detectors' field of view at the receiver. Comparing this scheme with the aperture averaging technique, it is easier to provide independent aperture averaging with multiple aperture systems since a single aperture system requires the aperture size to be far greater than spatial coherent length [96, 179]. In this section, we briefly describe three different popular spatial diversity combining techniques which are widely used for FSO systems and they are; Maximum Ratio Combining (MRC), Equal Gain Combining (EGC) and Selection Combining (SC).

2.5.1 Maximum Ratio Combining Scheme

In the MRC combiner technique illustrated in Figure 2.6, the received incoming optical radiation signals on the *N-* receiver branch are co-phased by eliminating the influence of random phases induced from multiple branches and Lasers. Thereafter, the signals are then optimally weighted accordingly by the fading attenuation of each path link before summing so as to maximize the received SNR at the combiner's output. The signal at the output of the MRC combiner can be expressed as [104]:

$$i_T(t) = \sum_{i=1}^{N} a_i \exp(-j\phi_i) i_i(t) \tag{2.38}$$

where a_i is the weighting factor on the ith branch and is proportional to the amplitude of the received electric field while the complex exponential is used for equalizing the channel phase noise ϕ_i on the ith branch. Assuming that each receiver branch has the same average noise power, the instantaneous SNR at the output of the combiner is simply the sum of the SNRs in each branch and can be expressed as [181, 182]:

$$\gamma_{MRC} = \sum_{i=1}^{N} \gamma_i \tag{2.39}$$

where γ_i is the SNR on each receiver branch.

The MRC combiner is the optimal combining technique in the absence of other interferences and result in maximum-likelihood receiver structure. However, the MRC receiver is highly complex because the receiver requires knowledge of all channel fading parameters such as

phase and amplitude and hence, making the scheme very difficult to implement practically [180].
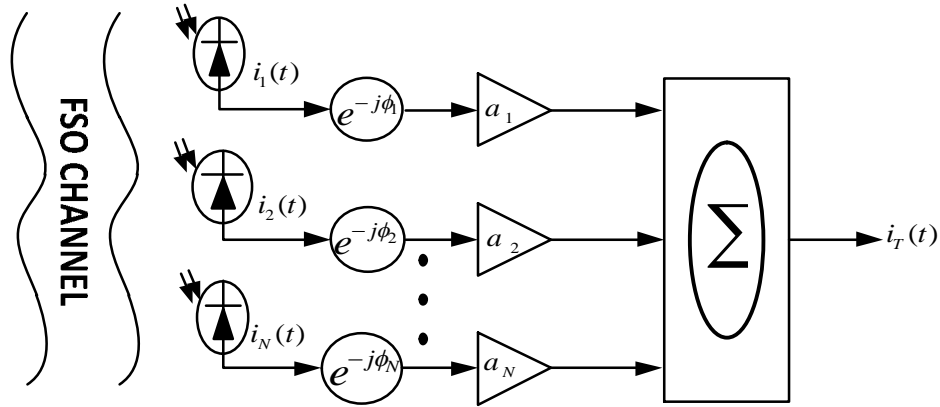
Figure 2.6: Maximum ratio combining Scheme

2.5.2 Equal Gain Combining Scheme

EGC technique is based on the same principle of operation as MRC, except that the weight factor is set to unity as presented in Figure 2.7. In EGC scheme, the combiner co-phases and equally weights all the incoming optical radiation signals on each receiver branch and are then coherently summed. Thus, the instantaneous signal at the EGC combiner output can be expressed as:

$$i_T(t) = \sum_{i=1}^{N} \exp(-j\phi_i) i_i(t) \tag{2.40}$$

Although EGC is suboptimal compared to MRC but it is practically feasible because of its lower receiver complexity scheme since the receiver only requires the estimation of channel fading phase without the knowledge of the channel fading amplitude. Assuming that each branch has the same average noise power, the instantaneous SNR at the output of the combiner can be expressed as [181, 182]:

$$\gamma_{EGC} = \frac{1}{N} \left(\sum_{i=1}^{N} \sqrt{\gamma_i} \right)^2 \tag{2.41}$$

where γ_i is the SNR on each receiver branch.
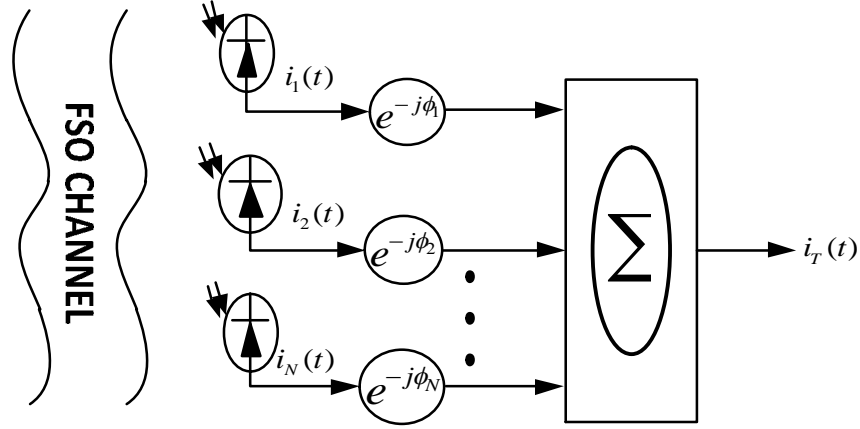
Figure 2.7: Equal gain combining Scheme

2.5.3 Selection Combining Scheme

SC combiner scheme is the simplest receiver among the diversity combiners mentioned earlier and can be referred to as switching technique as it is demonstrated in Figure 2.8. At a given time instant, it only samples all the optical received power level among the receiver branches and selects the link with the maximum signal strength (that is, highest instantaneous SNR) for decoding. The signal at the SC combiner output is equal to the signal on the only one received branch; therefore the coherent sum of the individual branch is not needed as it is in the case of MRC and EGC. Thus, the instantaneous signal at the SC combiner output can be expressed as:

$$i_{SC}(t) = max\left(a_1 i_1(t), a_2 i_2(t), \ldots, a_N i_N(t)\right) \tag{2.42}$$

The simplicity behind the SC combiner scheme is that, it has lower receiver complexity and computation compare to MRC and EGC since it requires no phase estimation and only one received chain is needed. However, it performance is suboptimal compared to MRC and EGC since it only selects from one receiver branch while others information are negligible. Assuming that each branch has the same average noise power, the instantaneous SNR at the output of the combiner can be expressed as [181, 182]:

$$\gamma_{SC} = max\left(\gamma_1, \gamma_2, \ldots, \gamma_N\right) \tag{2.43}$$
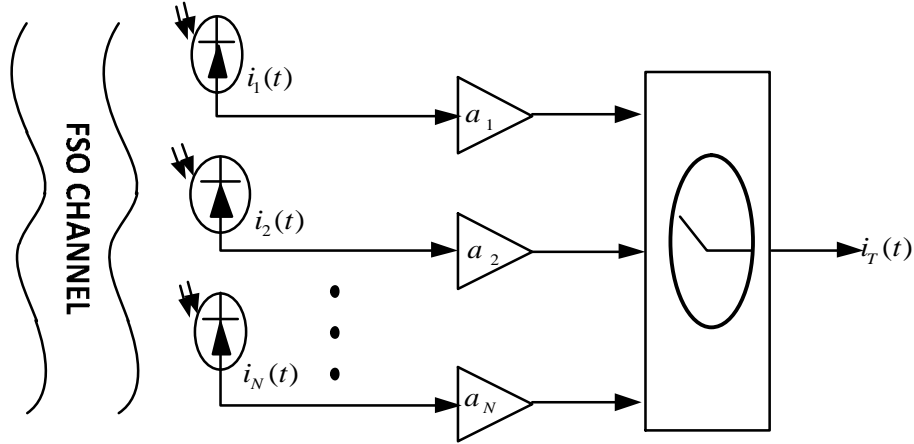
Figure 2.8: Selection combining Scheme

2.6 Relay-Assisted Technology

Relay-assisted technology has been proposed as a promising and viable technique which has the potential to broaden the transmission coverage area and improve the quality of service. Furthermore, it can also enhance gap connectivity and mitigate fading channel with less transmit power in wireless communication systems [183]. It extends the communication network to area where it is either technically or economically impossible to set up full fledge communication system such as desert or offshore. In addition, relay technology can help to reduce interference and improve the overall network performance. The performance of relaying systems can be evaluated under various fading environment. When the fading distributions of relay link are the same, then the channel condition is called Symmetric fading channel and in case of different fading distributions, the channel nature is referred to as Asymmetric fading channel (also called Mixed fading channels) [114]. In relay-assisted systems, the source node (transmitter) propagates data signal to one or more low-cost intermediate nodes (relay) which process the received signals and retransmit the processed signals to the next node. The next node (receiver) may be the destination node in case of dual-hop relaying system or another relay node in case of multi-hop relaying system [184]. Furthermore, the source and relay nodes use orthogonal and non-orthogonal transmission technique to assign signals to the channel.

Orthogonal transmission is the simplest scheme that allows the relay nodes to operate in half-duplex using TDMA or FDMA [185, 186]. Therefore, it prevents inter-signal interference because all source signals are independent during the orthogonal slot and this makes the destination node to receive independent replicas of source signal. On the other hand, non-

orthogonal scheme allows simultaneous transmission of relay signal on the same frequency or time slot which leads to inter-signal interference. As a result of this, the destination node in this scenario requires interference cancellation technique [187] and this increase the design complexity compared to orthogonal scheme. Depending on the method employed by the relay to process the received signal, the relay technology can be classified into major relay protocols, namely, the Amplified-and-Forward (AF) Relaying and Decode-and Forward (DF) Relaying.

2.6.1   Amplify-and-Forward (AF) Relaying

In AF relaying system, the relay amplifies the received signal and retransmits it to the destination without performing any sort of decoding. This is also called non-regenerative or analog relaying system. This kind of relaying protocol has low complexity design and easy to implement since there is no demodulation and decoding of received signal during the transmission phases [188]. However, noise along the transmission path is accumulated and propagated to the destination. AF relaying system can be generally classified into three ways according to availability of the channel state information (CSI) at the relay node: CSI-assisted relaying, fixed or blind relaying and Semi-blind relaying. CSI-assisted relaying is AF relaying system which is based on the optimistic assumption that every relay has perfect knowledge of the channel information. Therefore, it employs the channel state information of the preceding hop (source-to-relay link) to control the gain introduced by the relay leading to power control of the retransmitted signal [189]. As a result of this, it has optimum performance than other AF schemes at the expense of higher complexity. In contrast, the fixed or blind relaying does not employ the channel state information of the previous hop but rather uses the power amplifiers with a constant gain to amplify the received signal leading to signal with variable power at the relay output [190]. Thus, this approach reduces the processing overhead and leads to less complexity in the relay [191]. Semi-blind relaying, on the other hand, depends on the average CSI of the previous hop not the instantaneous CSI as the case of CSI-assisted relaying. Therefore, it exhibits a comparable performance to that of CSI-assisted relaying with lower design complexity.

2.6.2   Decode-and Forward (DF) Relaying

In DF relaying system, the received source signal during the first transmission phase is fully decoded, re-encoded before retransmitting to the destination. This type of relaying protocol is also called regenerative or digital relaying system. It has the advantage of improving the

propagation error, if the relay can successfully decode the source signal, and noise at the relay is eliminated. However, it is very complex to design compared to AF relaying system since it requires demodulation and decoding of the received signal [192]. Thus, DF relaying system can be further sub-categorized into fixed DF relaying and adaptive/selection DF relaying depending on whether relay acquires error detection or not. In fixed DF relaying system, relay detects the source signal and retransmits it to the next node or destination without applying error correcting decoder to correct the possible channel error in the received signal. This scheme depends on the quality of preceding link/hop. Adaptive/selection DF relaying on the other hand, is based on error detection method where it encodes and retransmits the received data only if it can correctly decode the received signal from the source. This is done by checking a cyclic redundancy check (CRC) code of the source signal or using the specific SNR threshold of the preceding hop to determine the accuracy of the decoded source signal [193].

2.7 Relay Network Topologies

Transmission model in relay-assisted systems can be classified as serial relaying model and parallel relaying model[194]. In a serial relaying model, the source node transmits signal information to a relay node and relay detects the signal and retransmits it to the next relay until the source data reaches the destination. This model can be sub-classified into dual-hop relay network and multi-hop relay network [195] which are briefly discussed in a sub-section of this section. Parallel relaying model, also called cooperative relaying, is where the source terminal is equipped with multi-laser transmitter with each of the transmitter pointing out in the direction of corresponding relay terminal. Thus, the source broadcasts the same signal through the use of multiple transmit apertures to relay nodes and each detects and retransmit the signal to the destination only if the received SNR exceeds a given decoding threshold [193]. This model is more cost-free in RF transmission since the propagation angle of the antenna is wide enough for both the relay and destination to receive the source signal. However, the main drawback of parallel relaying scheme in FSO systems is that the transmit laser requires line of sight transmission. Thus, the relay nodes cannot see the source leading to no cooperation within the transmission process. As a result of this, there must be another laser for transmitting source signal to the relay at the expense of extra hardware [109, 193]. Therefore, these results in a difficulty and higher cost to deploy parallel relaying model for FSO transmission compared to serial relaying model. Hence, it is not considered in this thesis. Additionally, the use of multiple relays between the source and the destination suffers

from limitation of power distribution leading to the need of more transmitting power or equally divide the power into all the relays, and this requires strict synchronization at the receiver [196].

2.7.1   Two-hop or Dual-hop Relay Network

In dual-hop relay, the transmission process is in two orthogonal phases. In the first phase, the source transmit its signal to the relay and/or destination while during the second phase, the relay processes the received signal from the source and forward the result to the destination. However, the direct link between the source and the destination depends on the propagation condition and is usually in deep fade; therefore signal is mostly propagated from the source to the destination via the relay node. Considering the dual-hop relaying system illustrated in the Figure 2.9, the received signals during the first transmission phase at the relay can be expressed as:

$$y_{DR}(t) = h_{SR}s(t) + n_R(t) \tag{2.44}$$

where h_{SR} are the channel coefficients of S-to-R link, and $n_R(t)$ is the AWGN at the relay during the first phase. During the second phase, the relay received and processes the signal by using a specific relaying protocol (AF or DF) and then forwards the resulting signal to the destination. Thus, the received signal at the destination in the course of this phase can be expressed as:

$$y_D(t) = h_{RD}f(s, n_R) + n_D(t) \tag{2.45}$$

where $f(.,.)$ is the utilized relaying protocol, h_{RD} is the channel coefficient of R-to-D link and $n_D(t)$ is the AWGN at the destination. Generally, if the relay considered in the system is AF relaying system, then the end-to-end SNR of dual-hop AF system can be expressed as [197]:

$$\gamma_{ed} = \frac{\gamma_{SR}\gamma_{RD}}{a\gamma_{SR} + \gamma_{RD} + b} \tag{2.46}$$

where γ_{SR} and γ_{RD} are the instantaneous SNR on the S-to-R and R-to-D links respectively. Therefore, the expression in (2.46) can be described as end-to-end SNR of dual-hop CSI-assisted AF system if $a = 1$ and $b = 0$ and can be expressed as:

$$\gamma_{ed} = \frac{\gamma_{SR}\gamma_{RD}}{\gamma_{SR} + \gamma_{RD}} \qquad (2.47)$$

In case of fixed gain or semi-blind gain, $a = 0$ such that the end-to-end SNR can be obtained as:

$$\gamma_{ed} = \frac{\gamma_{SR}\gamma_{RD}}{\gamma_{RD} + b} \qquad (2.48)$$

where b is the constant.
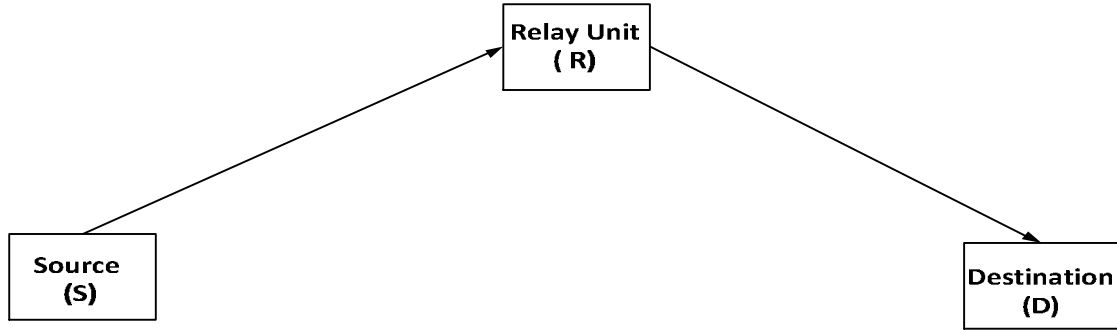
Figure 2.9: Illustration of a dual-hop network

2.7.2   Multi-Hop Relay Network

Topology of multi-hop relay network can be considered as a generalized model for the dual-hop relay system where the source signal can be transverse through multiple intermediate relay nodes. As a result of this, the use of multi-hop relaying transmission can significantly extend the coverage area of wireless system network [109]. As illustrated in Figure 2.10, a general $(L + 1)$-hops relaying system has source S, destination D and relay R nodes where communication span over $L + 1$ hops. During the first hop transmission, the source transmits its signal to the first relay R_1. During the $(L + 1)^{th}$ hop, the Lth relay employs relay protocol (DF or AF) to forward the received signal to the next relay. Considering the multi-hop relaying system illustrated in the Figure 2.10, the received signals at the destination or at each relay node can be generally expressed as [198, 199]:

$$r_D(t) = S(t)\prod_{i=1}^{L} a_i g_{i-1} + \sum_{i=1}^{L} n_{0,i}(t) + \prod_{j=i+1}^{L} a_i g_{j-i} , \quad g_0 = 1 \qquad (2.49)$$

where $S(t)$ is the transmit source signal, a_i is the channel fading amplitude of ith hop, g_{i-1} is the relay gain of $i-1$ node and $n_{0,i}(t)$ is the AWGN signal at the input of ith node.

It is very clear that the dual-hop wireless network can be extended into multi-hop wireless network by merely increasing the number of relay nodes between the source and the destination in order to meet the coverage and reliability when demand arises [114]. However, in multi-hop relay systems, traffic accumulation occurs and tends to grow larger as the number of the relay increases leading to high system complexity. Also, due to unnecessary congestion and rise in media access time, the overall end-to-end packet delay would also increase. Frequent route changes and the resulting route discovery procedures could cause high signaling overhead [200]. Actually, relay assisted multi-hop network has significant advantages by cost-effectively extending the wireless communication system coverage area but by considering the stated limitations, a simple dual-hop relaying system may appear to be better in contrast to multi-hop relaying system. Therefore, in this thesis, innovative techniques are developed for the dual-hop relaying scheme so as to evaluate the performance of the proposed FSO system.
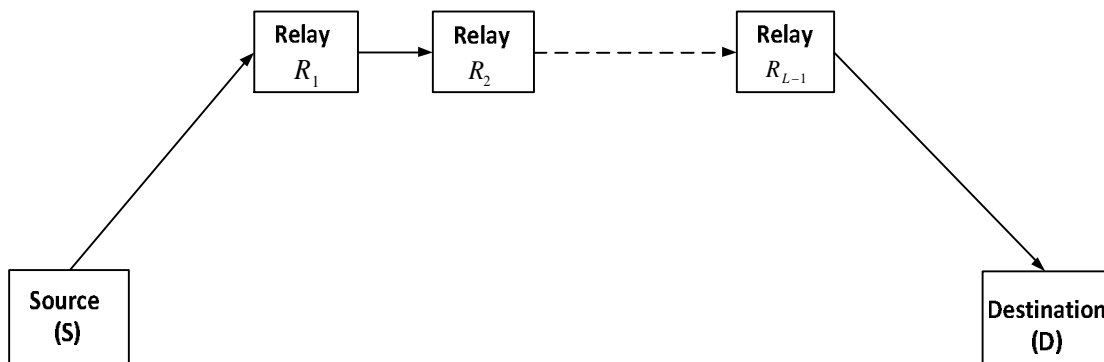
Figure 2.10: Illustration of a multi-hop network

2.8 Mathematical Tools for Analyzing FSO Systems over Gamma-Gamma Turbulence Channel

Owing to difficulty in obtaining fast computational and a traceable closed-form result, Meijer-G function and infinite power series expansion have been considered in many works [51-55, 57, 58, 106, 162, 201, 202] to analyze the performance of the FSO systems over Gamma-Gamma turbulence conditions. In this section, the performance difference between the Meijer-G function and infinite power series expansion as mathematical tools for analyzing the performance of FSO systems over Gamma-Gamma atmospheric turbulence is

presented. This provides a theoretical framework on the benefit of the two approaches and means of adopting them to solve problems in FSO communication systems. The PDF for the Gamma-Gamma channel is obtained in terms of Meijer-G function and infinite power series expansion. Thus, the ABER and outage probability closed-form expressions of a FSO-SIM system that employed BPSK are then derived using the derived channel statistical PDF.

2.8.1 Gamma-Gamma Channel Statistical Models

The probability distribution function of Gamma-Gamma atmospheric turbulence given in (2.20) contains a modified Bessel function $K_v(x)$, hence mathematical complication arises in evaluating the system performance over the channel. Moreover, in some complex system model analyses, the performance metrics may not have closed-form expressions. To avoid this mathematical difficulty, the modified Bessel function $K_v(x)$ in the channel PDF can be expressed in terms of Meijer-G function as [203,equation (14)]:

$$K_v(x) = \frac{1}{2} G_{0,2}^{2,0} \left(\frac{x^2}{4} \middle| \begin{matrix} -, - \\ \frac{v}{2}, \frac{-v}{2} \end{matrix} \right) \tag{2.50}$$

So, substituting (2.50) into (2.20), the PDF of the Gamma-Gamma channel can be defined as:

$$f_{GG}(I) = \frac{(\alpha\beta)^{\frac{\alpha+\beta}{2}}}{\Gamma(\alpha)\Gamma(\beta)} I^{\frac{\alpha+\beta}{2}-1} G_{0,2}^{2,0} \left(\alpha\beta I \middle| \begin{matrix} -, - \\ \frac{\alpha-\beta}{2}, \frac{\beta-\alpha}{2} \end{matrix} \right), \quad I > 0 \tag{2.51}$$

Also, the Gamma-Gamma channel PDF can be defined in terms of generalized power series representation method of the modified Bessel function of the second kind as [204]:

$$K_v(x) = \frac{\pi}{2\sin(\pi v)} \sum_{g=0}^{\infty} \left[\frac{1}{\Gamma(g-v+1)g!} \left(\frac{x}{2}\right)^{2g-v} - \frac{1}{\Gamma(g+v+1)g!} \left(\frac{x}{2}\right)^{2g+v} \right] \tag{2.52}$$

where $v \notin \mathbb{Z}$ and $|x| < \infty$

Thus, putting (2.52) into (2.20), the Gamma-Gamma channel PDF can also be expressed as:

$$f_{GG}(I) = \sum_{p=0}^{\infty} \left[m_g(\alpha,\beta) I^{g+\beta-1} + m_g(\beta,\alpha) I^{g+\alpha-1} \right] \tag{2.53}$$

where

$$m_g(x, y) = \frac{(xy)^{g+y}\Gamma(x - y)\Gamma(1 - x + y)}{\Gamma(x)\Gamma(y)\Gamma(g - x + y + 1)g!}$$

The plot of the Gamma-Gamma PDF in Figure 2.11 shows that the distribution spreads out more over the irradiance I as the turbulent strength (SI) increases from weak to strong turbulence.
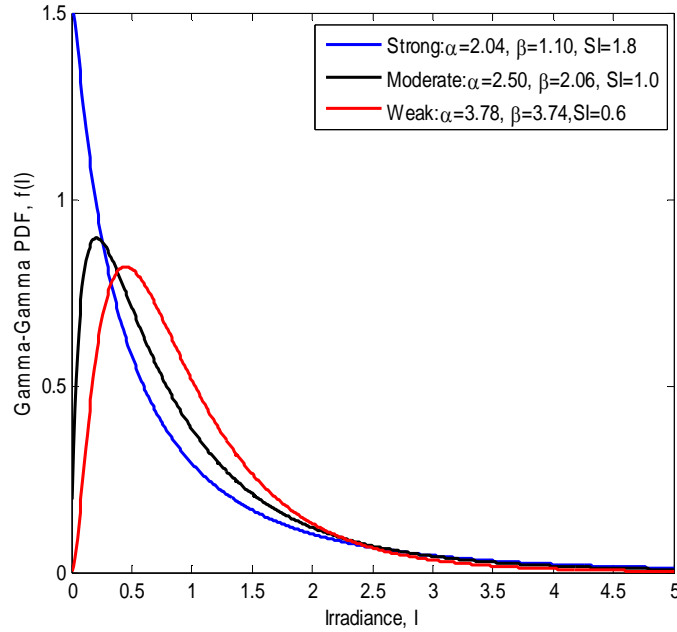
Figure 2.11: Gamma-Gamma PDF under different turbulence conditions

2.8.2 Performance Analysis

The performance of the SIM-BPSK FSO system in terms of average BER and outage probability over the Gamma-Gamma distribution channel is presented in this section. Meijer-G function and infinite Power Series expansion approach are used to obtain the closed-form expression for the two performance metrics. Thus, from (2.31), the instantaneous SNR for the SIM system can be obtained by following (2.14) as:

$$\gamma = \frac{(PR\rho)^2}{\sigma_n^2}I^2 = \bar{\gamma}I^2 \tag{2.54}$$

where $\bar{\gamma} = (PR\rho)^2/\sigma_n^2$ is the average SNR.

2.8.2.1 Average BER using Infinite Power Series Expansion

The average BER of the SIM-BPSK FSO system can be defined as [204]:

$$P_b = \int_0^\infty P_e(I) f_{GG}(I) \, dI \qquad (2.55)$$

where $P_e(I)$ is the conditional probability which is given as $P_e(I) = Q\left(\sqrt{2\bar{\gamma}I^2}\right)$. By using the definition of the Q-function formulated by Craig's as $Q(x) = \frac{1}{\pi}\int_0^\pi exp\left(-\frac{x^2}{2sin^2\theta}\right) d\theta$, the ABER can then be expressed as:

$$
\begin{aligned}
P_e &= \frac{1}{\pi} \int_0^\infty \int_0^{\pi/2} exp\left(-\frac{\bar{\gamma}I^2}{sin^2\theta}\right) f_{GG}(I) \, d\theta dI \\
&\triangleq \frac{1}{\pi} \int_0^{\pi/2} M_Y\left(\frac{\bar{\gamma}}{sin^2\theta}\right) d\theta
\end{aligned}
\qquad (2.56)
$$

where $M_Y(.)$ is the Moment Generating Function (MGF) which can be defined as $M_Y(S) = \int_0^\infty e^{-SI} f_{GG}(I) \, dI$. The MGF of Y can therefore be determined as:

$$M_Y(S) = \frac{1}{2}\sum_{g=0}^\infty \left[m_g(\alpha,\beta) \Gamma\left(\frac{g+\beta}{2}\right) S^{-\frac{g+\beta}{2}} + m_g(\beta,\alpha)\Gamma\left(\frac{g+\alpha}{2}\right) S^{-\frac{g+\alpha}{2}} \right] \qquad (2.57)$$

Substituting (2.56) into (2.57), the ABER for the system can be obtained as:

$$
\begin{aligned}
P_b = \frac{1}{2\pi} \sum_{g=0}^\infty &\left[m_g(\alpha,\beta)\Gamma\left(\frac{g+\beta}{2}\right)(\bar{\gamma})^{-\frac{g+\beta}{2}} \int_0^{\pi/2}(sin\theta)^{g+\beta}d\theta \right. \\
&\left. + m_g(\beta,\alpha)\Gamma\left(\frac{g+\alpha}{2}\right)(\bar{\gamma})^{-\frac{g+\alpha}{2}} \int_0^{\pi/2}(sin\theta)^{g+\alpha}d\theta \right]
\end{aligned}
\qquad (2.58)
$$

Using the integral identity in [205,equation (3.621(1))] (see Appendix A3.2), and the Beta function identity in [205, equation (8.384(4))] (see Appendix A2.6), the integral in (2.58) can be expressed as:

$$\int_0^{2\pi}(sin\theta)^x d\theta = \frac{1}{2}B\left(\frac{1}{2}, \frac{x+1}{2}\right) \qquad (2.59)$$

Thus, the ABER closed-form expression for the system can be obtained by using the integral defined in (2.59) as:

$$P_b \triangleq \frac{1}{4\pi} \sum_{g=0}^{\infty} \left[m_g(\alpha, \beta) \Gamma\left(\frac{g+\beta}{2}\right) (\bar{\gamma})^{-\frac{g+\beta}{2}} B\left(\frac{1}{2}, \frac{g+\beta+1}{2}\right) \right.$$
$$\left. + m_g(\beta, \alpha) \Gamma\left(\frac{g+\alpha}{2}\right) (\bar{\gamma})^{-\frac{g+\alpha}{2}} B\left(\frac{1}{2}, \frac{g+\alpha+1}{2}\right) \right] \tag{2.60}$$

Since ABER is defined in (2.60) in the form of infinite series, the issue of convergence arises. As a result of this, the convergence radius R_1 for the first sub-series in (2.60) is determined using a Cauchy ratio test which states that a series is absolutely convergent if:

$$R_1 = \lim_{g \to \infty} \left| \frac{m_{g+1}(\alpha, \beta)}{m_g(\alpha, \beta)} \right| < 1$$
$$\triangleq \frac{(\alpha\beta) \Gamma\left(\frac{g+\beta+1}{2}\right) B\left(\frac{1}{2}, \frac{g+\beta+2}{2}\right)}{\Gamma\left(\frac{g+\beta}{2}\right) B\left(\frac{1}{2}, \frac{g+\beta+1}{2}\right) (g - \alpha + \beta + 1)(g + 1)} \tag{2.61}$$

Thus, it can be deduced that as the index g increases, (2.60) approaches zero and hence it is absolutely the convergent. Similarly, the second sub-series convergence radius R_2 in (2.60) also tends to zero as g approaches infinity and thus, converges for $\bar{\gamma} < \infty$.

In practices, however, it is necessary to use some finite values of g for the upper limit of the summation in (2.60) which approximate the closed-form expression of the series error rate for the system. In order to evaluate the truncation error caused by eliminating all terms after $K + 1$ term in (2.60), the truncation error is then defined as:

$$\varepsilon_K = \frac{1}{4\pi \Gamma(\alpha)\Gamma(\beta)} \sum_{g=K+1}^{\infty} \frac{1}{g!} \left[\psi_g(\alpha, \beta) + \psi_g(\beta, \alpha) \right] \left(\frac{\alpha\beta}{\sqrt{\bar{\gamma}}}\right)^g \tag{2.62}$$

where

$$\psi_g(x, y) = \frac{\Gamma(1 - x + y) \Gamma\left(\frac{g+y}{2}\right) \Gamma(x - y)}{\Gamma(g - x + y + 1)} B\left(\frac{1}{2}, \frac{g+y+1}{2}\right) \left(\frac{xy}{\sqrt{\bar{\gamma}}}\right)^y \tag{2.6 3}$$

The summation of the term in the (2.62) can be simplified by employing Taylor series expansion of an exponential function and the upper bound of truncation error is obtained as:

$$\varepsilon_K = \frac{1}{4\pi\Gamma(\alpha)\Gamma(\beta)} \max_{g>K}\{\psi_g(\alpha,\beta) + \psi_g(\beta,\alpha)\} exp\left(\frac{\alpha\beta}{\sqrt{\bar{\gamma}}}\right) \tag{2.64}$$

We thus noted that $\psi_g(\alpha,\beta)$ or $\psi_g(\beta,\alpha)$ tends to zero when $g \to \infty$. Therefore, ε_K diminishes as the index g increases. Based on this, (2.63) exists and (2.64) holds. Thus, (2.64) diminishes with an increase in index K.

2.8.2.2 Average BER using Meijer-G Function

The ABER for the SIM-BPSK system can also be determined by using Meijer-G function approach. Thus, using the ABER defined in (2.55), the conditional probability can be expressed as:

$$P_e(I) = Q\left(\sqrt{2\bar{\gamma}I^2}\right) = \frac{1}{2}erfc\left(\sqrt{\bar{\gamma}I^2}\right) \tag{2.65}$$

Substituting (2.51) and (2.65) into (2.55), the $erfc\,(.)$ can be expressed in terms of Meijer-G function defined in [203,equation (12)] (see Appendix A2.2), the ABER can therefore be obtained as:

$$P_b = \int_0^\infty \frac{(\alpha\beta)^{\frac{\alpha+\beta}{2}} I^{\frac{\alpha+\beta}{2}-1}}{2\sqrt{\pi}\Gamma(\alpha)\Gamma(\beta)} G_{0,2}^{2,0}\left(\alpha\beta I \left| \begin{array}{c} -,- \\ \frac{\alpha-\beta}{2}, \frac{\beta-\alpha}{2} \end{array}\right.\right) G_{1,2}^{2,0}\left(\bar{\gamma}I^2 \left| \begin{array}{c} 1 \\ 0, \frac{1}{2} \end{array}\right.\right) \tag{2.66}$$

By applying the integral identity in [203,equation (21)] (see Appendix A3.5) to (2.66), the closed-form solution for the ABER of SIM-BPSK can be expressed as:

$$P_b = \frac{2^{\alpha+\beta-3}}{\sqrt{\pi^3}\Gamma(\alpha)\Gamma(\beta)} G_{5,2}^{2,4}\left(\frac{16\bar{\gamma}}{(\alpha\beta)^2} \left| \begin{array}{c} \frac{1-\alpha}{2}, \frac{2-\alpha}{2}, \frac{1-\beta}{2}, \frac{2-\beta}{2}, 1 \\ 0, \quad \frac{1}{2} \end{array}\right.\right) \tag{2.67}$$

2.8.2.3 Outage Probability using Infinite Power Series Expansion

Outage probability is an alternative performance metric for quantifying the performance of wireless communication systems in the fading channels [179]. This can be interpreted as the probability that the system instantaneous SNR fall below a specific threshold γ_{th} and above which the quality of the channel is satisfactory, and can be mathematically defined as [206]:

$$P_{out}(\gamma_{th}) = \int_0^{\gamma_{th}} f_{GG}(\gamma)d\gamma \tag{2.68}$$

Thus, by power transformation from (2.54), $I = \sqrt{\gamma/\bar{\gamma}}$, the PDF defined in (2.53) can be rewritten as:

$$f_{GG}(\gamma) = \frac{1}{2}\sum_{g=0}^{\infty}\left[\frac{m_g(\alpha,\beta)\gamma^{\frac{g+\beta}{2}-1}}{\bar{\gamma}^{\frac{g+\beta}{2}}} + \frac{m_g(\beta,\alpha)\gamma^{\frac{g+\alpha}{2}-1}}{\bar{\gamma}^{\frac{g+\alpha}{2}}}\right] \tag{2.69}$$

Substitute (2.69) into (2.68), the closed-form expression for the outage probability in terms of infinite power series expansion can be obtained as:

$$
\begin{aligned}
P_{out}(\gamma_{th}) &= \frac{1}{2}\sum_{g=0}^{\infty}\left[m_g(\alpha,\beta)\bar{\gamma}^{-\frac{g+\beta}{2}}\int_0^{\gamma_{th}}\gamma^{\frac{g+\beta}{2}-1}d\gamma + m_g(\beta,\alpha)\bar{\gamma}^{-\frac{g+\alpha}{2}}\int_0^{\gamma_{th}}\gamma^{\frac{g+\alpha}{2}-1}d\gamma\right] \\
&\triangleq \frac{1}{2}\sum_{g=0}^{\infty}\left[\frac{m_g(\alpha,\beta)}{g+\beta}\left(\frac{\gamma_{th}}{\bar{\gamma}}\right)^{\frac{g+\beta}{2}} + \frac{m_g(\beta,\alpha)}{g+\alpha}\left(\frac{\gamma_{th}}{\bar{\gamma}}\right)^{\frac{g+\alpha}{2}}\right]
\end{aligned}
\tag{2.70}
$$

Since (2.70) is in form of infinite series expression, we followed the same truncation error analysis used for ABER expression to evaluate the resulting approximation error. If the outage probability defined in (2.70) is re-written as:

$$
\begin{aligned}
P_{out}(\gamma_{th}) = \frac{1}{2\Gamma(\alpha)\Gamma(\beta)}\sum_{g=0}^{\infty}\frac{1}{g!}&\left[\frac{\Gamma(1-\alpha+\beta)\Gamma(\alpha-\beta)}{\Gamma(g-\alpha+\beta+1)(g+\beta)}\left(\frac{\alpha\beta\sqrt{\gamma_{th}}}{\sqrt{\bar{\gamma}}}\right)^{g+\beta}\right. \\
&\left. + \frac{\Gamma(1-\beta+\alpha)\Gamma(\beta-\alpha)}{\Gamma(g-\beta+\alpha+1)(g+\alpha)}\left(\frac{\alpha\beta\sqrt{\gamma_{th}}}{\sqrt{\bar{\gamma}}}\right)^{g+\alpha}\right]
\end{aligned}
\tag{2.71}
$$

Then, the power series expression in (2.71) is truncated to a finite number of K terms as:

$$\varepsilon_K = \frac{1}{2\Gamma(\alpha)\Gamma(\beta)}\sum_{g=K+1}^{\infty}\frac{1}{g!}[Q_g(\alpha,\beta)+Q_g(\beta,\alpha)]\left(\frac{\alpha\beta\sqrt{\gamma_{th}}}{\sqrt{\bar{\gamma}}}\right)^g \tag{2.72}$$

where

$$Q_g(x,y) = \frac{\Gamma(1-x+y)\Gamma(\alpha-y)}{\Gamma(g-x+y+1)(g+y)}\left(xy\sqrt{\frac{\gamma_{th}}{\bar{\gamma}}}\right)^y \tag{2.73}$$

49

Using Taylor series expansion of an exponential function, the summation of the term in the (2.72) simplified and the upper bound of ε_K is obtained as:

$$\varepsilon_K = \frac{1}{2\Gamma(\alpha)\Gamma(\beta)} \max_{g>K}\{Q_g(\alpha,\beta) + Q_g(\beta,\alpha)\} exp\left(\alpha\beta\sqrt{\frac{\gamma_{th}}{\bar{\gamma}}}\right) \tag{2.74}$$

Thus, it is noted that $Q_g(\alpha,\beta)$ or $Q_g(\beta,\alpha)$ tends to zero when $g \to \infty$, therefore ε_K diminishes as index g increases. Thus, (2.74) diminishes with increase in K.

2.8.2.4 Outage Probability Using Meijer-G Function

The outage probability of the considered system can also be obtained by using Meijer-G function approach. By power transformation, channel PDF defined (2.51) can be rewritten as:

$$f_{GG}(\gamma) = \frac{(\alpha\beta)^{\frac{\alpha+\beta}{2}}\gamma^{\frac{\alpha+\beta}{4}-1}}{\Gamma(\alpha)\Gamma(\beta)\bar{\gamma}^{\frac{\alpha+\beta}{4}}} G_{0,2}^{2,0}\left(\alpha\beta\sqrt{\frac{\gamma}{\bar{\gamma}}}\middle| \begin{matrix} -,- \\ \frac{\alpha-\beta}{2}, \frac{\beta-\alpha}{2} \end{matrix}\right) \tag{2.75}$$

Then, substituting (2.75) into (2.68), the outage probability can be expressed as:

$$P_{out}(\gamma_{th}) = \frac{(\alpha\beta)^{\frac{\alpha+\beta}{2}}}{\Gamma(\alpha)\Gamma(\beta)\bar{\gamma}^{\frac{\alpha+\beta}{4}}} \int_0^{\gamma_{th}} \gamma^{\frac{\alpha+\beta}{4}-1} G_{0,2}^{2,0}\left(\alpha\beta\sqrt{\frac{\gamma}{\bar{\gamma}}}\middle| \begin{matrix} -,- \\ \frac{\alpha-\beta}{2}, \frac{\beta-\alpha}{2} \end{matrix}\right) d\gamma \tag{2.761}$$

By applying the identity defined in [203,equation (26)] (see Appendix A3.4), the closed-form expression for the outage probability in terms of Meijer-G can be expression:

$$P_{out}(\gamma_{th}) = \frac{1}{\Gamma(\alpha)\Gamma(\beta)} G_{1,3}^{2,1}\left(\alpha\beta\sqrt{\frac{\gamma_{th}}{\bar{\gamma}}}\middle| \begin{matrix} 1 \\ \alpha, \beta \end{matrix}\right) \tag{2.77}$$

2.8.3 Numerical Results and Discussions

In this section, the results on the average BER and outage probability of SIM-BPSK FSO system over the Gamma-Gamma channel are presented using the derived expressions of equation (2.60), (2.67), (2.70) and (2.77) for Meijer-G function and infinite power Series expansion method. The approximated error rate and outage probability for the power series expansion approach is obtained by eliminating infinite terms after the first $(K + 1)$ term in our series equations by using the value of $K = 50$. The closed-form expressions are verified by numerical integration of the exact error rate given in equation (2.55) and (2.68). The analysis for the two mathematical tools is based on the influence of the following parameters

such as laser wavelength $\lambda = 1550 \, nm$, index of refractive structure parameter of $C_n^2 = 3 \times 10^{-14} \, m^{2/3}$. Also, the channel atmospheric turbulence levels are considered to be weak ($\alpha = 3.78, \beta = 3.74$), moderate ($\alpha = 2.50, \beta = 2.06$) and strong ($\alpha = 2.04, \beta = 1.10$).

Figure 2.12 illustrates the average BER of the SIM-BPSK system over atmospheric turbulence ranging from weak to strong regime. It can be deduced that as the turbulence increases from weak to strong turbulence, the more system error performance get deteriorated and the two mathematical approaches offer the same performance. For instance, at average SNR of $40 \, dB$, system yields an approximated BER of 10^{-4} over a weak turbulence compared with 10^{-2} BER for strong turbulence.

The outage probability of the system is depicted in Figure 2.13 at threshold SNR of $5 \, dB$. It can also be indicated that both mathematical approaches offer the same outage probability under the turbulence condition. Outage performance is better under the influence of weak turbulence compared to strong turbulence condition. For example, at BER of 10^{-1} the system requires a power of $28 \, dB$ under the weak condition compared to $42 \, dB$ under strong turbulence.
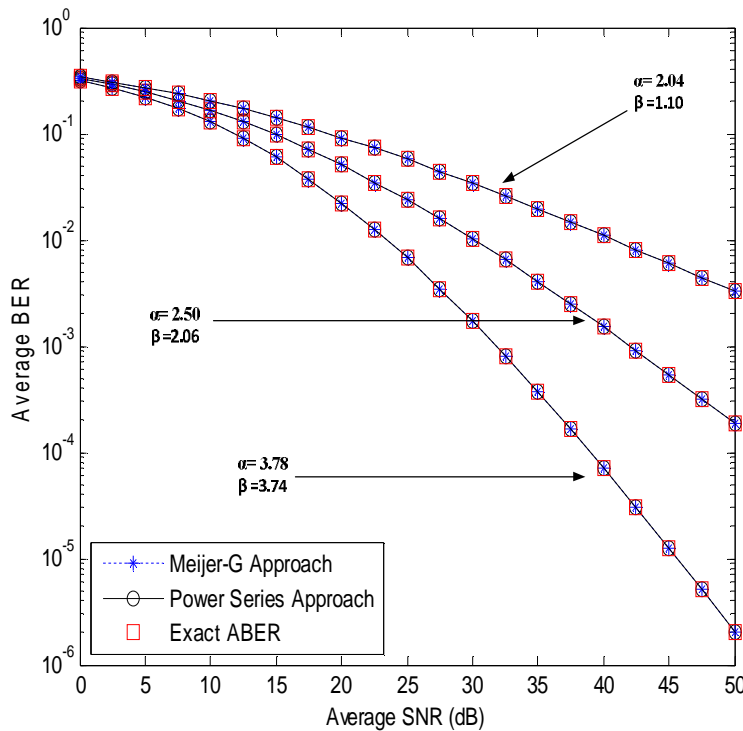
Figure 2.12: Average bit error rate for SIM-BPSK system
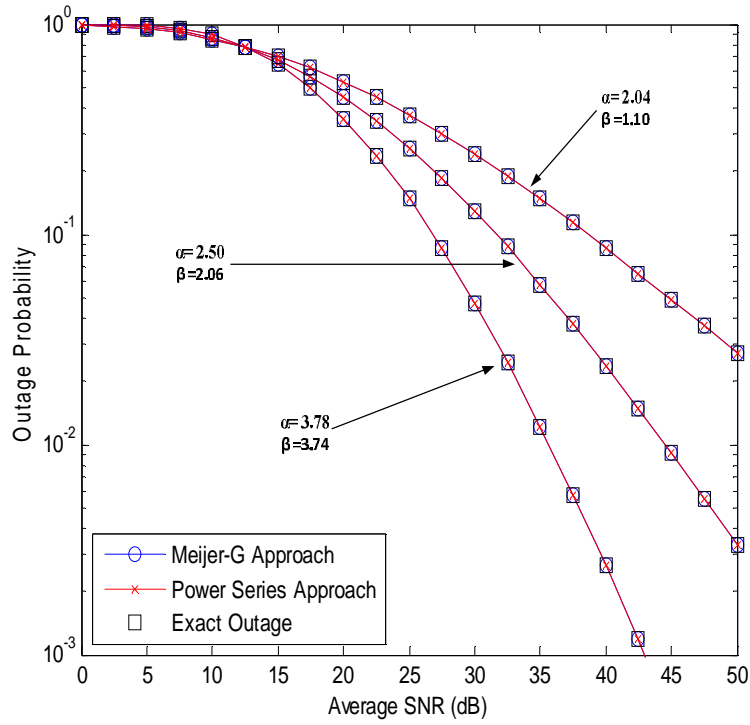
Figure 2.13: Outage probability performance for SIM-BPSK system at threshold of 5 dB

Table 2.1 shows the comparison between the average computational running time of the Meijer-G function and infinite power series expansion for all the performance metric. It can be depicted that in all cases, the computational time taken to evaluate the analytical expressions given by power series expansion method is much lower than that of the Meijer-G approach.

TABLE 2.1: Computational running time comparison between Meijer-G function and power series expansion

PERFORMANCE METRIC	AVERAGE COMPUTATIONAL RUNNING TIME (Seconds)
Power Series (ABER)	0.0510
Meijer-G (ABER)	3.303
Power Series (Outage Probability)	0.0410
Meijer-G (Outage Probability)	3.6710

2.9 Chapter Summary

In this chapter, a general overview concerning the FSO communication systems was provided. Likewise, different statistical atmospheric channel distributions such as lognormal model, Gamma-Gamma model and pointing error distribution for the FSO communication links were also reported. Also, background information on different modulation techniques and mitigation tools such as diversity combiner and relay-assisted technology were presented. The comparison between the Meijer-G function and power series expansion as mathematical tools in analyzing FSO systems over Gamma-Gamma turbulence channel was studied, and FSO SIM-BPSK system was employed as a case study. The analytical results showed that the two methods achieved the same ABER and outage probability under the same turbulence conditions. In addition, the results proved that Meijer-G function approach has higher computational running time than power series expansion. More so, Meijer-G closed-form expressions did not show any insight of the system parameters as compared to the power series closed-form expression, but it offers a traceable result than the power series expansion.

CHAPTER THREE

Free Space Optical Spatial Modulation System with Diversity Combining over different Atmospheric Turbulent Channels

In this chapter, the performance of an heterodyne FSO-SM system with different diversity combining scheme as mitigation techniques over different atmospheric induced-turbulence channels is studied. The diversity combining considered at the receiving end of the proposed system includes; MRC, EGC and SC. A theoretical error performance using APEP and the ABER for each diversity scheme over lognormal and Gamma-Gamma atmospheric turbulence channel is carried out. Under the influence of Gamma-Gamma turbulence, a generalized infinite power series expansion approach is used to obtain the APEP for the system and the proposed system performance is further improved by convolutional coding technique. Under both turbulence scenario, the performance of the proposed system is compared with the well-established FSO systems with diversity combiner and the result proved that the proposed configuration provides better mitigation techniques. Finally, the impact of combined effects of turbulence with pointing error is also carried out on the system performance.

3.1 Heterodyne Optical Spatial Modulation System Model

Consider an FSO-SM link consisting of N_t transmit laser units and N_r heterodyne receivers as illustrated in Figure 3.1. The N_r receive apertures is assumed to be separated sufficiently by more than a coherent length from each other so as to ensure the independency of channel path. Random sequences of independent incoming information bit streams to be transmitted at each time instants are mapped into vectors of $\log_2(N_t M)$ bits with M equal to the constellation size. This is further split into sub-vectors where the first group of $\log_2(N_t)$ bits are used to indicate the active transmit-laser index l while the last $\log_2(M)$ bits are used to choose a kth BPSK symbol from the signal-constellation diagram produce by March-Zehnder Modulator (MZM). At an instant, the information bits are modulated on the electric field of an optical beam as $x_k \exp(j\phi_{x_k})$ and are then emitted from the active transmit-laser index l over the $N_r^k \times N_t^m$ MIMO atmospheric turbulence channel defined as [90]:

$$H(t) = [h_1, h_2, \ldots, h_{N_t}]$$

$$\triangleq \begin{bmatrix} h_{11}(t)\exp(j\phi_{11}) & h_{12}(t)\exp(j\phi_{12}) & \cdots & h_{1N_t}(t)\exp(j\phi_{1N_t}) \\ h_{21}(t)\exp(j\phi_{21}) & h_{22}(t)\exp(j\phi_{22}) & \cdots & h_{2N_t}(t)\exp(j\phi_{2N_t}) \\ \vdots & \vdots & & \vdots \\ h_{N_r1}(t)\exp(j\phi_{N_r1}) & h_{N_r2}(t)\exp(j\phi_{N_r2}) & \cdots & h_{N_rN_t}(t)\exp(j\phi_{N_rN_t}) \end{bmatrix} \quad (3.1)$$

where $h_{l,r}$ and $\phi_{l,r}$ are the real positive fading gain and the phase of channel respectively between the lth activated transmit laser and the nth receiver aperture. Thus, the source transmits the SM signal during this phase over the optical channel as [168]:

$$X_{l,k} = \begin{bmatrix} 0 \ 0 \ \cdots & \underbrace{x_k\exp(j\phi_{x_k})}_{l^{th} \ laser \ position} & \cdots \ 0 \ 0 \end{bmatrix}^T \quad (3.2)$$

At the receiver, the transmitted SM optical field is mixed with a local oscillator field and the photo-detector converts the combined signal into electrical form. The intermediate frequency component is then extracted by using a bandpass filter. Thus, following the derivation of (2.7), the photocurrent generated during the kth symbol interval by the rth receiver in response to the square of the aggregate optical field can be expressed as:

$$i_r(t) = \frac{R}{Z_o}[E_r(t)]^2 + n_r(t) \quad (3.3)$$

where n_r is the $N_r \times 1$ Local Oscillator (LO) noise signal whose elements are modeled as independent and identically distributed (i.i.d.) Additive White Gaussian Noise (AWGN) according to $\sim CN(0, \sigma_n^2)$ and $E_r(t)$ is the received field at the aperture of the rth receiver and this can be expressed following the (2.6) as:

$$E_r(t) = \sqrt{2P_tZ_o}x_kh_{l,r}\cos(\omega_{LO}t + \phi_{l,r} + \phi_{x_k}) + \sqrt{2P_{LO}Z_o}\cos(\omega_{LO}t) \quad (3.4)$$

where ϕ_{x_k} is the phase of the kth transmitted SM symbol.

By substituting (3.4) into (3.3), and solving the expansion with the elimination of double-frequency terms by bandpass filter, the photocurrent can thus be expressed as:

$$i_r(t) = RP_tx_k^2h_{l,r}^2 + RP_{LO} + 2R\sqrt{P_tP_{LO}}x_kh_{l,r}\cos(\omega_{LO}t - \phi_{l,r} - \phi_{x_k}) + n_r(t)$$

$$\triangleq i_{DC}(t) + i_{AC}(t) + n_r(t) \quad (3.5)$$

where $i_{AC}(t) \triangleq 2R\sqrt{P_t P_{LO}} x_k h_{l,r} cos(\omega_{LO} t - \phi_{l,r} - \phi_{x_k})$ is the received photocurrent which contains the information about the frequency and the phase of the received signal that differentiates the heterodyne receiver from direct detection. The term $i_{DC}(t) = R(P_t x_k^2 h_{l,r}^2 + P_{LO})$ is the DC component generated by the signal and the local oscillator respectively. This DC component leads to signal and local oscillator noises with variance $\sigma_{short,s}^2 = 2q_e R P_t x_k^2 h_{l,r}^2 \Delta f$ and $\sigma_{short,L}^2 = 2q_e R P_{LO} \Delta f$ respectively where Δf denotes the noise equivalent bandwidth of the photo-detector. Since it is assumed that the intermediate frequency in heterodyne receiver is said to be non-zero [140, 202], thus the signal power can be expressed as $P_s = 2R^2 P_t P_{LO} x_k^2 h_{l,r}^2$. It is noted that when $P_{LO} \gg P_s$, $\sigma_{short,s}^2$ becomes negligible, and then the DC component can be approximated as $i_{DC}(t) \approx R P_{LO}$. In view of (2.15), the SNR for the heterodyne detection of rth receiver in a given symbol period is given as:

$$\gamma_{Het} = \frac{P_s}{\sigma_{short,L}^2} = \frac{RP_t |x_k h_{l,r}|^2}{q_e \Delta f} \tag{3.6}$$

Thus, the received signal model for the heterodyne detection of rth receiver can be statistically expressed based on the SNR defined in (3.6) as:

$$y_r = \sqrt{\bar{\gamma}} \, h_{l,r} x_k \exp(j\phi_{l,r} + j\phi_{x_k}) + n_r(t)$$
$$\triangleq \sqrt{\bar{\gamma}} h_l x_k + n_r(t) \tag{3.7}$$

where $\bar{\gamma} = RP_t / (q_e \Delta f)$ is the average received SNR, x_k corresponds to electric field $x_k \exp(j\phi_{x_k})$ transmitted over the optical channel and h_l denotes the activation of the ith column of channel matrix H for a randomly chosen l during each transmission period.

It is assumed that the received signal in (3.7) is combined using the spatial diversity combiner such as MRC, EGC and SC combiners. Thereafter, the SM detector is applied to detect the Laser transmit index $\hat{l}$ and $\hat{k}$ constellation symbol which are used to decode the transmitted bit stream following the joint optimum ML spatial modulation detection give in (2.37) as:

$$[\hat{l}, \hat{k}] = arg\max_{\hat{l},\hat{k}} p_Y(y|X_{l,k}, H)$$
$$\triangleq arg\min_{\hat{l},\hat{k}} \sqrt{\bar{\gamma}} \|h_l x_k\|_F^2 - 2Re\{y^H h_l x_k\} \tag{3.8}$$

where

$p_Y\left(y \mid X_{l,k}, H\right)$ is the PDF of y conditioned on H and $x_{l,k}$ which can be expressed as [171]:

$$p_Y\left(y \mid X_{l,k}, H\right) = \pi^{-N_r} exp\left(-\left\|y - \sqrt{\bar{\gamma}}HX_{l,k}\right\|_F^2\right) \qquad (3.9)$$
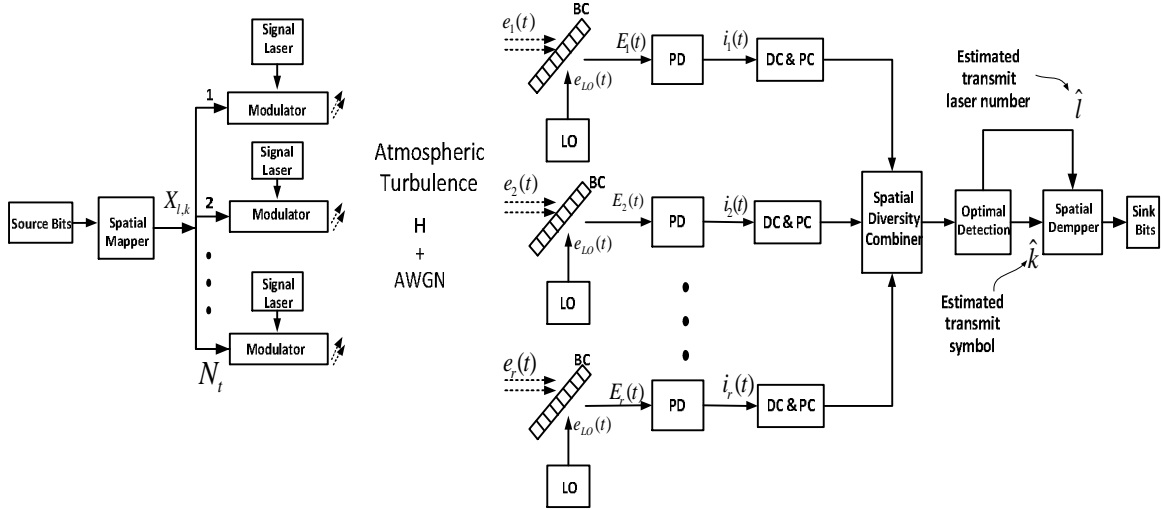
Figure 3.1: Heterodyne FSO-SM system where PD=Photo-detector, BC=Beam Combiner, LO=Local Oscillator, DC=Down Converter and PC= Phase Noise Compensation

3.2 Error Performance Analysis

In this section, the analytical expression for the optical spatial modulation ABER can be obtained using a simple and efficient union bounding technique and thus, the ABER under no turbulence condition is union bounded as [171, 180, 207]:

$$ABER_{SM} \leq \frac{(N_t M)^{-1}}{\log_2(N_t M)} \sum_{l=1}^{N_t} \sum_{k=1}^{M} \sum_{\hat{l}=l+1}^{N_t} \sum_{\hat{k}=k+1}^{M} N\left(k, \hat{k}\right) APEP\left(X_{l,k} \to X_{\hat{l},\hat{k}}\right) \qquad (3.10)$$

where $N\left(k, \hat{k}\right)$ is the number of bit errors when selecting k instead of $\hat{k}$ as the transmit unit index and the $PEP\left(X_{l,k} \to X_{\hat{l},\hat{k}}\right)$ denotes the average pairwise error probability of deciding on the constellation vector $X_{l,k}$ given that $X_{\hat{l},\hat{k}}$ is transmitted and can therefore be expressed as follows [90, 208]:

$$PEP\left(X_{l,k} \rightarrow X_{\hat{l},\hat{k}}\right) = E\left[Q\left(\sqrt{\frac{\bar{\gamma}}{4}}Z\right)\right] \tag{3.11}$$

where $Q(.)$ function is the Craig's formulation function

Thus, it can be deduced that the probability of error in SM systems is determined by the difference between channels associated with the different transmit Lasers rather than actual channel realization [77], and then from (3.11) $Z = \|h_l x_k - h_{\hat{l}} x_{\hat{k}}\|_F^2$

3.3 FSO-SM System with Diversity Combining over Lognormal Atmospheric Turbulence

In this section, MRC, EGC and SC are the spatial diversity schemes considered for the FSO-SM system over the lognormal channel and the average BER are derived for each combining technique.

3.3.1 FSO-SM System with Maximum Ratio Combiner

When considering MRC as diversity combiner for the system, the incoming optical radiation signals on each photo-detector at the receiver are first co-phased. Once the phase distortions are cancelled out, the optical signal in each branch is then weighted by the fading attenuation of each path link and then coherently summed to obtain the combiner output. Therefore, the pairwise error probability conditioned on the channel H is defined for MRC as [209, 210]:

$$PEP_{MRC}\left(X_{l,k} \rightarrow X_{\hat{l},\hat{k}}|H\right) = Q\left(\sqrt{\frac{\bar{\gamma}}{4}\|h_l x_k - h_{\hat{l}} x_{\hat{k}}\|_F^2}\right) \tag{3.12}$$

Since an error in SM systems depends on the difference between channels associated with the different transmit element, then the squared Frobenious norm in (3.12) can be written as [90]:

$$Z = \|h_l x_k - h_{\hat{l}} x_{\hat{k}}\|_F^2 \triangleq \sum_{m=1}^{N_r} |h_l x_k - h_{\hat{l}} x_{\hat{k}}|^2 \tag{3.13}$$

Then,

$$PEP_{MRC}\left(X_{l,k} \rightarrow X_{\hat{l},\hat{k}}|H\right) = Q\left(\sqrt{\frac{\bar{\gamma}}{4}\sum_{m=1}^{N_r} |h_l x_k - h_{\hat{l}} x_{\hat{k}}|^2}\right) \tag{3.14}$$

By letting the $\alpha_m = h_l x_k - h_{\hat{l}} x_{\hat{k}}$ be defined as a complex Gaussian random variable with the real and imaginary parts of the components being a lognormal distribution with equal mean and variance, then the PEP can be further expressed as:

$$PEP_{MRC}(X_{l,k} \rightarrow X_{\hat{l},\hat{k}}|H) = Q\left(\sqrt{\frac{\bar{\gamma}}{4}\sum_{m=1}^{N_r}|\alpha_m|^2}\right) \tag{3.15}$$

Through the definition of the Q-function formulated by Craig's as $Q(x) = \frac{1}{\pi}\int_0^\pi exp\left(-\frac{x^2}{2sin^2\theta}\right)d\theta$ and subsequently integrate over the randomness of the channel coefficients to determine the unconditional PEP as:

$$PEP_{MRC}(X_{l,k} \rightarrow X_{\hat{l},\hat{k}}|H) = \frac{1}{\pi}\int_0^{\frac{\pi}{2}} exp\left(-\frac{\bar{\gamma}\sum_{m=1}^{N_r}|\alpha_m|^2}{8sin^2\theta}\right)d\theta \tag{3.16}$$

The average pairwise error probability of MRC, $APEP_{MRC}$, can therefore be obtained by averaging (3.16) over the fading statistic and it is given as:

$$APEP_{MRC} = \frac{1}{\pi}\int_0^{\pi/2}\int_0^\infty exp\left(-\frac{\bar{\gamma}\sum_{m=1}^{N_r}|\alpha_m|^2}{8sin^2\theta}\right)f_{|\alpha_m|^2}(z)dzd\theta \tag{3.17}$$

where the $|\alpha_m|^2$ lognormal PDF of the fading channel can be expressed following equation (2.19), as:

$$f_{|\alpha_n|^2}(z) = \frac{z^{-1}}{\sigma_h\sqrt{2\pi}}exp\left(-\frac{(\ln(z)+\sigma_h^2/2)^2}{2\sigma_h^2}\right) \tag{3.18}$$

With the aid of the MGF-based method for analyzing the performance of wireless communication systems over fading channel, the average PEP from (3.17) can therefore also be further obtained as:

$$APEP_{MRC} \triangleq \frac{1}{\pi}\int_0^{\frac{\pi}{2}}\prod_{m=1}^{N_r}\left[M_{|\alpha_m|^2}\left(\frac{\bar{\gamma}}{8sin^2\theta}\right)\right]d\theta \tag{3.19}$$

where the integral representation of the MGF of $|\alpha_m|^2$ can be expressed as:

59

$$M_{|\alpha_m|^2}(s) = \int_0^\infty \exp(sz) f_{|\alpha_m|^2}(z) dz$$

$$\triangleq \int_0^\infty \exp(sz) \frac{z^{-1}}{\sigma_h \sqrt{2\pi}} exp\left(-\frac{(\ln(z) + \sigma_h^2/2)^2}{2\sigma_h^2}\right) dz \tag{3.20}$$

Due to the fact that the integral expression presented in (3.19) has no possible solution, it is difficult, if not impossible, to evaluate in closed-form. Therefore, a tight approximation for Gaussian Q-function is obtained using equations (2) and (14) in [211] as $Q(x) \approx \frac{1}{12}\exp\left(-\frac{x^2}{2}\right) + \frac{1}{4}\exp\left(-\frac{2x^2}{3}\right)$. Based on a tight approximation for Gaussian Q-function, (3.15) can the expressed as:

$$PEP_{MRC}\left(X_{l,k} \to X_{\hat{l},\hat{k}}|H\right) = \frac{1}{12}exp\left(-\frac{\bar{\gamma}}{8}\sum_{m=1}^{N_r}|\alpha_m|^2\right) + \frac{1}{4}\exp\left(-\frac{\bar{\gamma}}{6}\sum_{m=1}^{N_r}|\alpha_m|^2\right) \tag{3.21}$$

By letting $R = |\alpha_m|^2$, then the APEP for the approximated MRC can be obtained as:

$$APEP_{MRC} = \frac{1}{12}\prod_{m=1}^{N_r}\int_0^\infty exp\left(-\frac{\bar{\gamma}}{8}R\right)f_R(R)dR + \frac{1}{4}\prod_{m=1}^{N_r}\int_0^\infty exp\left(-\frac{\bar{\gamma}}{6}R\right)f_R(R)dR$$

$$\triangleq \frac{1}{12}\prod_{m=1}^{N_r}\left[M_{|\alpha_m|^2}\left(\frac{\bar{\gamma}}{8}\right)\right] + \frac{1}{4}\prod_{m=1}^{N_r}\left[M_{|\alpha_m|^2}\left(\frac{\bar{\gamma}}{6}\right)\right] \tag{3.22}$$

where $M_{|\alpha_m|^2}(s) = \int_0^\infty exp(-sR) f_{|\alpha_m|^2}(R) dR$.

By numerical integration, (3.22) would actually produce no closed-form solution. As a result of this, the use of Gauss Hermit quadrature integration circumvents this problem and this is expressed as [104]:

$$\int_{-\infty}^\infty f(a)\exp(-a)da \cong \sum_{j=1}^{N_e} w_j f(a_j) \tag{3.23}$$

where N_e^{th} is the order of the Hermite polynomial $He_n(.)$ with its value typically set at 20, gives an excellent accuracy, $\{a_j\}_{j=1}^{N_e}$ and $\{w_j\}_{j=1}^{N_e}$ represent the zeros of the N_e^{th} order Hermit

polynomial $He_n(a)$ and corresponding weight factors, respectively. Thus, w_j can be expressed [212]:

$$w_j = \frac{2^{N_e-1} N_e! \sqrt{\pi}}{N_e^2 \left[He_{N_e-1}(a_j) \right]^2}$$

(3.24)

Using the Gauss-Hermit quadrature integration given in (3.23), then (3.22) can therefore be expressed as:

$$M_{|\alpha_n|^2}(s) = \sum_{j=1}^{N_e} \frac{w_j}{\sqrt{\pi}} exp\left[z exp\left(a_j \sqrt{2} \sigma_h - \sigma_h^2/2 \right) \right]$$

(3.25)

By incorporating (3.25) in (3.22), the improved approximated APEP expression for the MRC can be written as:

$$APEP_{MRC} = \frac{1}{12} \prod_{m=1}^{N_r} \left[\sum_{j=1}^{N_e} \frac{w_j}{\sqrt{\pi}} Q \left[\frac{\bar{\gamma}}{8} exp\left(a_j \sqrt{2} \sigma_{h_m} - \sigma_{h_m}^2/2 \right) \right] \right]$$

$$+ \frac{1}{4} \prod_{m=1}^{N_r} \left[\sum_{j=1}^{N_e} \frac{w_j}{\sqrt{\pi}} Q \left[\frac{\bar{\gamma}}{6} exp\left(a_j \sqrt{2} \sigma_{h_m} - \sigma_{h_m}^2/2 \right) \right] \right]$$

(3.26)

Finally, plugging (3.26) into (3.10), the closed form expression for the average BER for MRC diversity technique in FSO-SM-MRC systems over lognormal fading channel can be obtained as:

$$ABER_{SM(MRC)}$$

$$\leq \frac{(N_t M)^{-1}}{\log_2(N_t M)} \sum_{l=1}^{N_t} \sum_{k=1}^{M} \sum_{\hat{l}=l+1}^{N_t} \sum_{\hat{k}=k+1}^{M} N(k,\hat{k}) \left[\frac{1}{12} \prod_{m=1}^{N_r} \left[\sum_{j=1}^{N_e} \frac{w_j}{\sqrt{\pi}} Q \left[\frac{\bar{\gamma}}{8} exp\left(a_j \sqrt{2} \sigma_{h_m} \right. \right. \right. \right.$$

$$\left. \left. \left. \left. - \frac{\sigma_{h_n}^2}{2} \right) \right] \right] + \frac{1}{4} \prod_{m=1}^{N_r} \left[\sum_{j=1}^{N_e} \frac{w_j}{\sqrt{\pi}} Q \left[\frac{\bar{\gamma}}{6} exp\left(a_j \sqrt{2} \sigma_{h_m} - \frac{\sigma_{h_m}^2}{2} \right) \right] \right] \right]$$

(3.27)

3.3.2 FSO-SM System with Equal Gain Combiner

In EGC, the diversity combiner co-phases and equally weights the incoming optical radiation on each PD and then coherently sums them. The pairwise error probability of EGC can be expressed as [209, 210]:

$$PEP_{EGC}\left(X_{l,k} \rightarrow X_{\hat{l},\hat{k}}|H\right) = Q\left(\sqrt{\frac{\bar{\gamma}}{4N_r}\left(\sum_{m=1}^{N_r}|h_l x_k - h_{\hat{l}}x_{\hat{k}}|\right)^2}\right)$$

$$\triangleq Q\left(\sqrt{\frac{\bar{\gamma}}{4N_r}\left(\sum_{m=1}^{N_r}|\alpha_m|\right)^2}\right) \tag{3.28}$$

Defining $P = \sum_{m=1}^{N_r}|\alpha_m|$ as the sum of N_r lognormal random variables, it can be approximately expressed by a single lognormal variable $P \approx \exp(y)$, where y is normally distributed with mean μ_y and variance σ_y^2. Thus, following the equation (2.19), the PDF for the approximated lognormal random variable P is given as [104]:

$$f_P(P) = \frac{P^{-1}}{\sigma_y\sqrt{2\pi}} exp\left(-\frac{\left(\ln(P) + \mu_y\right)^2}{2\sigma_y^2}\right) \tag{3.29}$$

where its mean and variance can be expressed as $\mu_y = \ln(N_r) - \frac{1}{2}\ln\left(1 + \frac{exp(\sigma_h^2)-1}{N_r}\right)$ and $\sigma_y^2 = \ln\left(1 + \frac{exp(\sigma_h^2)-1}{N_r}\right)$ respectively. By using the Craig's formula for the Gaussian Q-function which is defined as $Q(x) = \frac{1}{\pi}\int_0^{\pi} exp\left(-\frac{x^2}{2sin^2\theta}\right)d\theta$ and the MGF based method, the average PEP can be obtained as:

$$APEP_{EGC} = \int_0^{\infty} Q\left(\sqrt{\frac{\bar{\gamma}}{4N_r}P^2}\right)f_P(P)dP$$

$$\triangleq \frac{1}{\pi}\int_0^{\frac{\pi}{2}}\left[M_p\left(\frac{\bar{\gamma}}{8N_r sin^2\theta}\right)\right]d\theta \tag{3.30}$$

where $M_p(.)$ is the MGF for the random variable P and can be expressed as:

$$M_P(s) = \int_0^{\infty} \exp(sP)\frac{P^{-1}}{\sigma_y\sqrt{2\pi}}exp\left(-\frac{\left(\ln(P) - \mu_y\right)^2}{2\sigma_y^2}\right)dP \tag{3.31}$$

The closed-form expression for (3.31) can therefore be tightly approximated by using the Gaussian-Hermit expression defined in (3.23) as:

$$M_P(s) = \sum_{j=1}^{N_e} \frac{w_j}{\sqrt{\pi}} exp\left[Pexp\left(a_j\sqrt{2}\sigma_y + \mu_y\right)\right] \tag{3.32}$$

The average PEP expression for EGC combining technique can finally be obtained by using (3.32) in (3.30) which can be obtained as:

$$APEP_{EGC} = \sum_{j=1}^{N_e} \frac{w_j}{\sqrt{\pi}} Q\left[\frac{\bar{\gamma}}{4N_r} exp\left(a_j\sqrt{2}\sigma_y + \mu_y\right)\right] \tag{3.33}$$

By substituting (3.33) into (3.10), the closed form expression for the average BER for EGC diversity technique in FSO-SM-EGC system over log-normal fading channel can finally be obtained as:

$$ABER_{SM(EGC)} \leq \frac{(N_tM)^{-1}}{\log_2(N_tM)} \sum_{l=1}^{N_t}\sum_{k=1}^{M}\sum_{\hat{l}=l+1}^{N_t}\sum_{\hat{k}=k+1}^{M} N(k,\hat{k})$$
$$\times \left[\sum_{j=1}^{N_e} \frac{w_j}{\sqrt{\pi}} Q\left[\frac{\bar{\gamma}}{4N_r} exp\left(a_j\sqrt{2}\sigma_y + \mu_y\right)\right]\right] \tag{3.34}$$

3.3.3 FSO-SM System with Selection Combiner

When SC is considered for the system, the combiner samples all the optical radiation from the transmit lasers and selects the link with the maximum signal strength that is $h_{max} = max\left(h_1^2, h_2^2, \ldots, h_{N_r}^2\right)$ without the need of estimating the phase of all incoming radiation. In this case, the pairwise error probability for the selection combiner is given as [210, 213]:

$$PEP_{SC}\left(X_{l,k} \rightarrow X_{\hat{l},\hat{k}}|H\right) = Q\left(\sqrt{\frac{\bar{\gamma}}{4}\left(h|x_{l,k} - x_{\hat{l},\hat{k}}|\right)^2}\right) \tag{3.35}$$

In the (3.35), the $h|x_{l,k} - x_{\hat{l},\hat{k}}|$ can be expressed as random variable Z, thus, by using the Craig's formulation, the PEP for the selection combiner can therefore be written as:

$$PEP_{SC}\left(X_{l,k} \rightarrow X_{\hat{l},\hat{k}}|H\right) = Q\left(\sqrt{\frac{\bar{\gamma}}{4}Z^2}\right)$$
$$\triangleq \frac{1}{\pi}\int_0^{\frac{\pi}{2}} exp\left(-\frac{Z^2\bar{\gamma}}{8sin^2\theta}\right) d\theta \tag{3.36}$$

Now, the average PEP for the receiver can be obtained by averaging the (3.35) with the application of MGF-based method as:

$$APEP_{SC} = \frac{1}{\pi} \int_0^{\frac{\pi}{2}} \int_0^{\infty} exp\left(-\frac{Z^2\bar{\gamma}}{8sin^2\theta}\right) f_z(h_{max})dh_{max}d\theta$$

$$\triangleq \frac{1}{\pi} \int_0^{\frac{\pi}{2}} \left[M_{h_{max}}\left(\frac{\bar{\gamma}}{8sin^2\theta}\right)\right] d\theta$$

(3.37)

The PDF of h_{max}, $f_z(h_{max})$, can be determined by first deriving its cumulative density function and differentiating it with respect to h_{max}, which is given as [104]:

$$f_z(h_{max}) = \frac{2^{1-N_r}N_r exp(-u^2)}{h\sigma_h\sqrt{2\pi}}[1 + erf(u)]^{N_r-1}$$

(3.38)

where $u = \frac{\left(\ln(h)+\frac{\sigma_h^2}{2}\right)}{\sqrt{2}\sigma_h}$

By using the MGF whose solution can be tightly approximated by the Gaussian-Hermit expression defined in (3.23), then (3.37) can be further expressed as:

$$M_{h_{max}}(s) = \int_0^{\infty} \exp(sh)\frac{2^{1-N_r}N_r exp(-u^2)}{h\sigma_h\sqrt{2\pi}}[1 + erf(u)]^{N_r-1}dh_{max}d\theta$$

$$\triangleq \frac{2^{1-N_r}N_r}{\sqrt{\pi}} \sum_{j=1}^{N_e} w_j[1 + erf(a_j)]^{N_r-1}exp\left(hexp\left(\frac{a_j\sqrt{2}\sigma_h - \sigma_h^2}{4sin^2\theta}\right)\right)$$

(3.39)

Using (3.39) in (3.37), the APEP for the system is achieved as:

$$APEP_{SC} = \frac{2^{1-N_r}N_r}{\sqrt{\pi}} \sum_{j=1}^{N_e} w_j[1 + erf(a_j)]^{N_r-1}Q\left(\frac{\bar{\gamma}}{4}exp\left(\frac{a_j\sqrt{2}\sigma_h - \sigma_h^2}{2}\right)\right)$$

(3.40)

Lastly, to obtain the closed form expression for the average BER for SC diversity technique in FSO-SM-SC system over log-normal fading channel, plugging (3.40) into (3.10) results in:

$$ABER_{SM(SC)} \leq \frac{(N_t M)^{-1}}{\log_2 (N_t M)} \sum_{l=1}^{N_t} \sum_{k=1}^{M} \sum_{\hat{l}=l+1}^{N_t} \sum_{\hat{k}=k+1}^{M} N(k,\hat{k}) \left[\frac{2^{1-N_r} N_r}{\sqrt{\pi}} \sum_{j=1}^{N_e} w_j [1 \right. $$

$$ \left. + erf(a_j)]^{N_r-1} Q\left(\frac{\bar{\gamma}}{4} exp\left(\frac{a_j \sqrt{2} \sigma_h - \sigma_h^2}{2} \right) \right) \right] \tag{3.41}$$

3.3.4 Numerical Results and Discussions

The numerical results on the performance error rate of FSO-SM systems over the lognormal channel for different diversity combiners are presented in this section. The derived close form expressions in (3.27), (3.34), and (3.41) are used to study the system error rate. In the simulation, the wavelength of transmitting laser is set to be $\lambda = 1.55 \ \mu m$, $N_t = 2$ transmit lasers, $M = 2$ bits and turbulence strength parameter C_n^2 is fixed at $1.7 \times 10^{-14} \ m^{2/3}$ according to the weak turbulence condition.

The results depicted in Figures 3.2 and 3.3 illustrate the system error performance of the three combiners as a function of link range under different PDs configurations at $SNR = 15 \ dB$. Obviously, it is deduced from the figures that the average bit error rate increases with the increase in the link range. At average link range of $3000 \ m$, it is clearly observed that there is no significant change in error rate despite the fact that the link range increases. This effect demonstrates the saturation scenario of the turbulence strength as the link range increases for all the combiners. As a matter of fact, it proves that the scintillation index (SI) increases as the link range increases since the turbulent strength is a function of link range. Under the same propagation conditions, Figure 3.2 confirmed that EGC outperforms SC in the entire PDs configurations, but yields worse performance when compared with MRC as it is demonstrated in Figure 3.3.

Generally, it is evident that the diversity gain at the receiver can drastically reduce the system error as the link range increases. This is illustrated by Figure 3.4 where the performance of the FSO-SM systems is significantly improved as the number of receive PD increases. For instance, at six PDs, the MRC offers an approximate BER of 10^{-6} compared with EGC and SC respectively yield an approximate BER of 10^{-4} and 10^{-3}.

Moreover, the performance comparison between the diversity combiners for the FSO-SM systems is carried out under the same atmospheric SI of 0.5 as it is illustrated in Figure 3.5 when the receiver is equipped with four PDs. As expected, it is clearly confirmed that MRC

combiner outperforms the other diversity combining schemes because it maximizes the SNR of the combined signal. For instance, at $SNR = 15\ dB$, it is evident that MRC offers error rate of 4.2×10^{-5} compared to EGC and SC with error rate of 4.7×10^{-4} and 1.7×10^{-2} respectively. As a result of this, MRC and EGC diversity combiners can therefore be practically recommended as the best desirable mitigation tools for any optical wireless communication systems but at the expense of receiver complexity. In addition, Figure 3.5 provides the comparison between the simulation results and the analytical results obtained from (3.27), (3.34) and (3.41). It is noted that the analytical results almost agreed with the simulation results, which verified the accuracy of the derived closed form expressions for each diversity combiner.

Looking at Figure 3.6, MRC system is employed to evaluate the performance of FSO-SM under various SI levels with different number of PD at the receiver. The result confirmed that the increase in turbulence level significantly affects the system performance. As earlier mentioned, the increase in the number of PD reduced this effect. For instance, at a BER of 10^{-6}, when $SI = 1.0$ (highest level), the system error performance is enhanced by $6.2\ dB$ when the PDs are four.
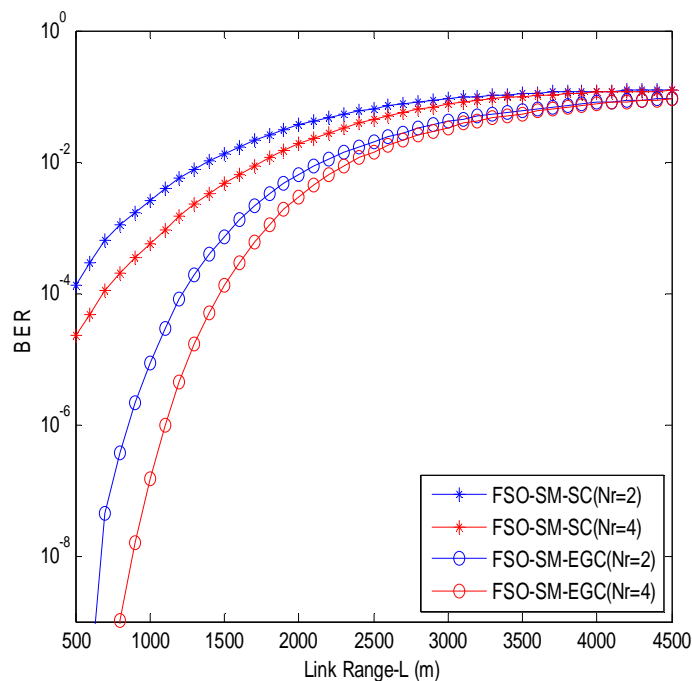
Figure 3.2: ABER with FSO-SM-EGC and FSO-SM-SC against the link range for various number of receive PDs
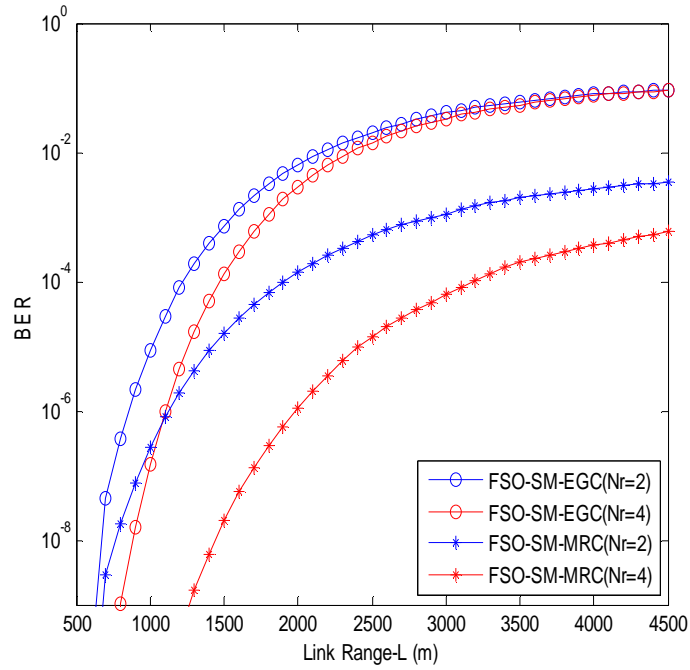
Figure 3.3: ABER with FSO-SM-EGC and FSO-SM-MRC against the link range for various number of receive PDs
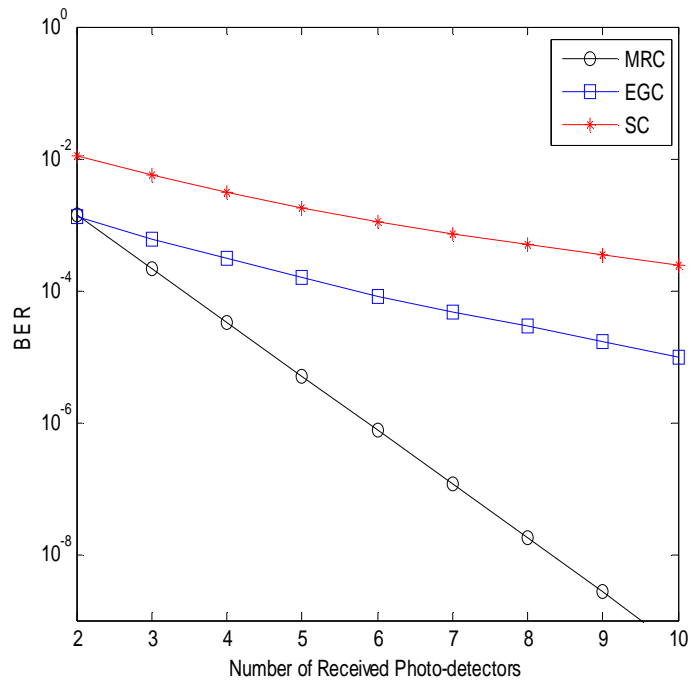
Figure 3.4: Performance of FSO-SM-SD systems for various number of receive PDs at average SNR of $20\ dB$ when SI is 0.7
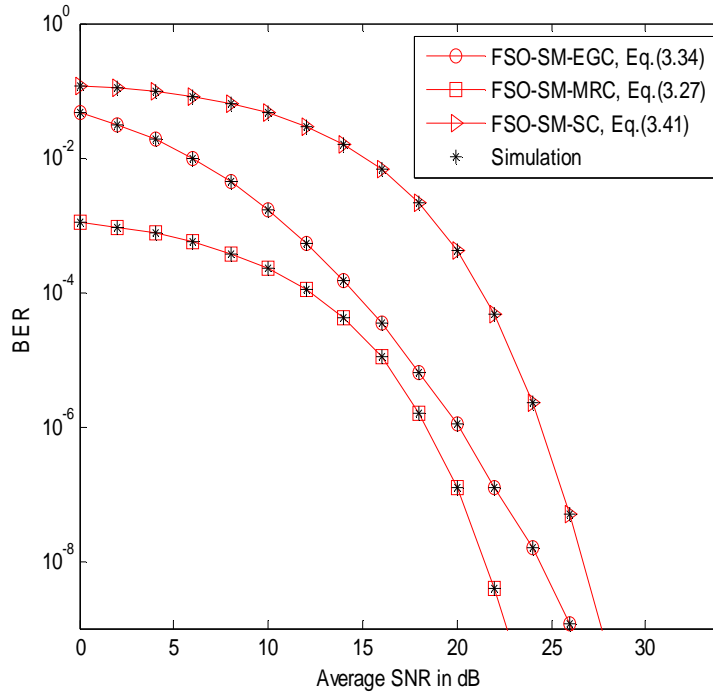
Figure 3.5: Performance comparison between the three diversity combiners for $N_r = 4$ at

$$SI = 0.5$$
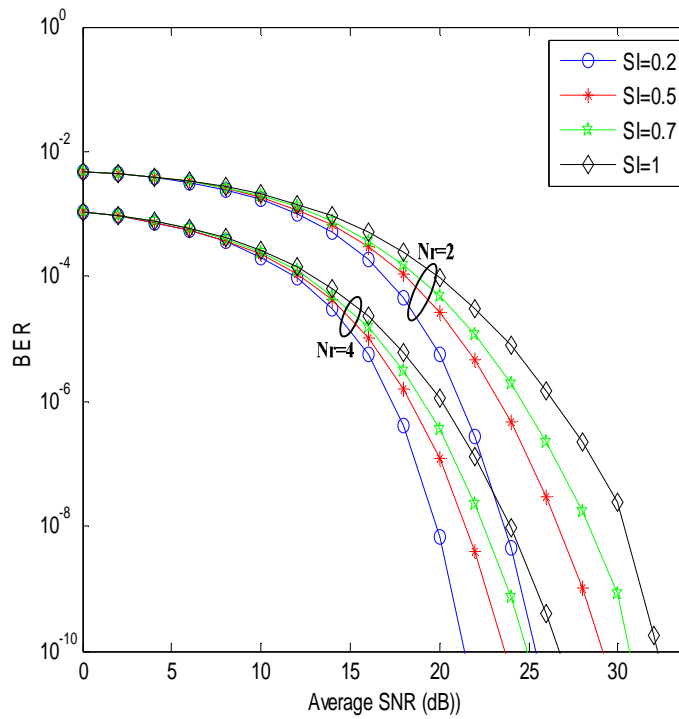
Figure 3.6: Performance of FSO-SM-MRC systems for various scintillation indexes

Finally, because of the simplicity of the EGC and its close performance with MRC, the proposed spatial diversity FSO-SM-EGC system is compared with a well-established spatial diversity FSO-SIM-EGC system in [104]. Therefore, the derived numerical expression in (3.34) is used to compare the proposed system performance with the derived average bit error rate of FSO-SIM-EGC system provided in [104,equation (29)] as:

$$P_{e(EGC-SIM)} = \frac{1}{\sqrt{\pi}} \sum_{i=1}^{m_i} w_i Q\left(Kexp\left(a_j\sqrt{2}\sigma_u + \mu_u\right)\right) \tag{3.42}$$

where $K = RI_oA/\sqrt{2}\sigma N$, σ_u and μ_u are mean and standard deviation, respectively.

Under the same propagation channel condition and receive PDs configuration, it can clearly be observed in Figure 3.7 that the performance of FSO-SM-EGC is much better than FSO-SIM-EGC even when the number of PDs is increased. This is as a result of multiple subcarriers required by FSO-SIM-EGC for the transmission that leads to its poor performance. For instance, the average error rate of FSO-SM-EGC proposed system at $SNR = 20\ dB$ is 29.8% better than FSO-SIM-EGC when $N_r = 4$.
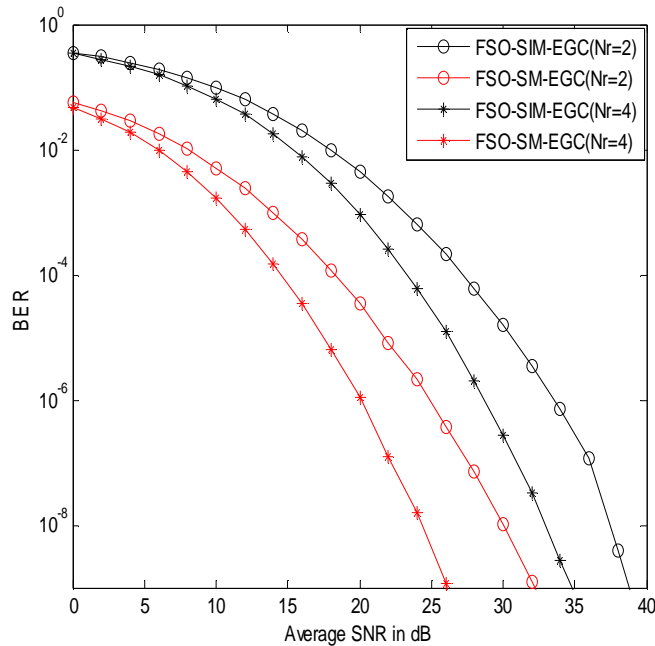
Figure 3.7: Comparison between the FSO-SM-EGC system with FSO-SIM-EGC system under the $SI = 0.5$

3.4 FSO-SM System with Diversity Combining over Gamma-Gamma Atomspheric Turbulence

In this section, the performance of the FSO-SM system over Gamma-Gamma atmospheric turbulence is investigated. Thus, the performance of the under studied combiners are analyzed under the uncoded and coded scenario as follows:

3.4.1 Uncoded FSO-SM System with Maximum Ratio Combiner

When MRC combiner is considered at the system receiving end, the average PEP for the FSO-SM-MRC system can be obtained by using the PEP defined in (3.16) as:

$$APEP_{SM-MRC} \triangleq \frac{1}{\pi} \int_0^{\frac{\pi}{2}} \left[\Phi_Z \left(-\frac{\mu}{8 sin^2\theta} \right) \right] d\theta \qquad (3.43)$$

In order to determine the MGF of random variable G in (3.43), letting $R = |\alpha_m|^2$, then the MGF of random variable R can be defined as:

$$\Phi_R(s) = \mathrm{E}[\exp(-sR)] = \int_0^\infty e^{-sR} f_R(R) dR \qquad (3.44)$$

Substituting (2.53) into (3.44), then the MGF of R can be obtained as:

$$\Phi_R(s) \triangleq \frac{1}{2} \sum_{g=0}^\infty \left[m_g(\alpha, \beta) \Gamma \left(\frac{g+\beta}{2} \right) (-s)^{\frac{g+\beta}{2}} - m_g(\beta, \alpha) \Gamma \left(\frac{g+\alpha}{2} \right) (-s)^{\frac{g+\alpha}{2}} \right] \qquad (3.45)$$

The MGF of the sum of the square Gamma-Gamma distribution of random variable $Z = \sum_{n=1}^{N_r} |\alpha_m|^2$ can be obtained by using binomial expansion as:

$$\Phi_Z(s) = [\Phi_R(s)]^{N_r}$$

$$\triangleq \frac{1}{2^{N_r}} \sum_{q=0}^{N_r} \binom{N_r}{q} \sum_{g=0}^\infty K_g(N_r - q, q)(-s)^{\frac{-g - N_r\beta - q(\alpha - \beta)}{2}} \qquad (3.46)$$

where

$$K_g(N_r - q, q) = \left[m_g(\alpha, \beta) \Gamma \left(\frac{g+\beta}{2} \right) \right]^{[N_r - q]} * \left[m_g(\beta, \alpha) \Gamma \left(\frac{g+\alpha}{2} \right) \right]^{[q]} \qquad (3.47)$$

where

$$\left[m_g(x,y)\Gamma\left(\frac{g+y}{2}\right)\right]^{[n]}$$ implies that $m_g(x,y)\Gamma\left(\frac{g+y}{2}\right)$ is convolved $n-1$ times with itself.

From (3.43), the ABER for the system can be obtained as:

$$APEP_{SM-MRC} = \frac{1}{\pi}\int_0^{\pi/2}\left[\frac{1}{2^{Nr}}\sum_{q=0}^{Nr}\binom{N_r}{q}\sum_{g=0}^{\infty}\mathsf{K}_g(N_r-q,q)\left(\frac{\bar{\gamma}}{8}\right)^{-\frac{\psi}{2}}(sin^2\theta)^{-\frac{\psi}{2}}\right]d\theta \qquad (3.48)$$

where

$$\psi = g + N_r\beta + q(\alpha - \beta)$$

By applying integral identity defined in (2.59) to (3.48), then the ABER for the combiner can be defined as:

$$APEP_{SM-MRC} = \frac{1}{2^{N_r+1}\pi}\sum_{q=0}^{N_r}\binom{N_r}{q}\sum_{g=0}^{\infty}\mathsf{K}_g(N_r-q,q)\left(\frac{\bar{\gamma}}{8}\right)^{-\frac{\psi}{2}}B\left(\frac{1}{2},\frac{\psi+1}{2}\right) \qquad (3.49)$$

where $B(x,y)$ is the Beta function [205].

Finally, the ABER for the system is therefore obtained by substituting equation (3.49) into (3.10) and is obtained as:

$$ABER_{SM-MRC} \leq \frac{(N_tM)^{-1}}{2^{N_r+1}\pi\log_2(N_tM)}\sum_{l=1}^{N_t}\sum_{k=1}^{M}\sum_{\hat{l}=l+1}^{N_t}\sum_{\hat{k}=k+1}^{M}\sum_{q=0}^{N_r}N(k,\hat{k})\binom{N_r}{q}$$

$$\times \sum_{g=0}^{\infty}\left[\mathsf{K}_g(N_r-q,q)\left(\frac{\bar{\gamma}}{8}\right)^{-\frac{\psi}{2}}B\left(\frac{1}{2},\frac{\psi+1}{2}\right)\right] \qquad (3.50)$$

Since (3.50) is in the form of power series expansion, it will be good to truncate the expression to finite number of terms L by eliminating the infinite term after the $L+1$ term in (3.50). Thus, to eliminate the error resulting in series error expansion, the truncation error is expressed as:

$$\varepsilon_L = \frac{(N_t M)^{-1}}{2^{Nr+1}\pi\log_2(N_t M)}\sum_{l=1}^{N_t}\sum_{k=1}^{M}\sum_{\hat{l}=l+1}^{N_t}\sum_{\hat{k}=k+1}^{M}\sum_{q=0}^{N_r}N(k,\hat{k})\binom{N_r}{q}$$

$$\times \sum_{g=L+1}^{\infty}u_g(q,\alpha,\beta)\left(\sqrt{\frac{8}{\bar{\gamma}}}\right)^g \quad (3.51)$$

where

$$u_g(q,\alpha,\beta) = \mathsf{K}_g(N_r - q,q)B\left(\frac{1}{2},\frac{g + N_r\beta + q(\alpha - \beta) + 1}{2}\right)\left(\sqrt{\frac{8}{\bar{\gamma}}}\right)^{N_r\beta+q(\alpha-\beta)} \quad (3.52)$$

Using the Taylor series expansion of $x^n/(1-x)$, then, the summation term in (3.51) can be simplified, and the upper bound of the truncation error can be obtained as:

$$\varepsilon_L = \frac{\sqrt{8}(N_t M)^{-1}}{2^{Nr+1}\pi\log_2(N_t M)\left(\sqrt{\bar{\gamma}}-1\right)\left(\sqrt{\bar{\gamma}}\right)^L}\sum_{l=1}^{N_t}\sum_{k=1}^{M}\sum_{\hat{l}=l+1}^{N_t}\sum_{\hat{k}=k+1}^{M}\sum_{q=0}^{N_r}N(k,\hat{k})$$

$$\times \binom{N_r}{q}\max_{g>L}\{u_L(q,\alpha,\beta)\} \quad (3.53)$$

After examining the first term in (3.52), it was discovered that $u_g(q,\alpha,\beta)$ approaches zero when g tends to infinity, and thus shows that truncation error ε_L reduces with increasing in L.

3.4.2 Uncoded FSO-SM System with Equal Gain Combiner

When EGC is employed for the system, the average PEP for the FSO-SM-EGC system can be obtained by using the PEP defined in (3.30) as:

$$APEP_{SM-EGC} \triangleq \frac{1}{\pi}\int_0^{\frac{\pi}{2}}\left[\Phi_G\left(-\frac{\bar{\gamma}}{N_r 8sin^2\theta}\right)\right]d\theta \quad (3.54)$$

In order to determine the MGF of random variable G in (3.54), letting $G = \left(\sum_{m=1}^{N_r}|\alpha_m|\right)^2$, $Y = |\alpha_m|$ and $U = \sum_{m=1}^{N_r}|\alpha_m|$, then the MGF of random variable Y can be defined as:

$$\Phi_Y(s) = \mathrm{E}[\exp(-sY)] = \int_0^{\infty}e^{-sY}f_Y(Y)dY \quad (3.55)$$

Substituting (2.53) into (3.55), then the MGF of Y can be obtained as:

$$\Phi_Y(s) = \frac{1}{2}\sum_{g=0}^{\infty}\left[m_g(\alpha,\beta)\Gamma(g+\beta)(-s)^{-g+\beta} + m_g(\beta,\alpha)\Gamma(g+\alpha)(-s)^{-g+\alpha}\right] \tag{3.56}$$

Then, the sum of the Gamma-Gamma distribution for the EGC random variable U is derived by binomial expansion as follows:

$$\Phi_U(s) = [\Phi_Y(s)]^{Nr}$$
$$\triangleq \sum_{q=0}^{Nr}\binom{N_r}{q}\left[\left(\sum_{g=0}^{\infty}m_g(\alpha,\beta)\Gamma(g+\beta)(-s)^{-g+\beta}\right)^{N_r-q}\right.$$
$$\left.\times\left(\sum_{g=0}^{\infty}m_g(\beta,\alpha)\Gamma(g+\alpha)(-s)^{-g+\alpha}\right)^{q}\right] \tag{3.57}$$

Thus, the PDF of random variable U can be obtained by the inverse Laplace transform as:

$$f_U(U) = \sum_{q=0}^{N_r}\binom{N_r}{q}\sum_{g=0}^{\infty}\frac{\Lambda_g(\alpha,\beta,N_r-q,q)}{\Gamma(g+N_r\beta+q(\beta-\alpha))}U^{\omega-1} \tag{3.58}$$

where

$$\omega = g + N_r\beta + q(\beta-\alpha)\text{ , and}$$

$$\Lambda_g(\alpha,\beta,N_r-q,q) = [m_g(\alpha,\beta)\Gamma(g+\beta)]^{N_r-q} * [m_g(\beta,\alpha)\Gamma(g+\alpha)]^{q}$$

Integrate (3.58) with respect to U and substitute for $G = U^2$, thereafter differentiate with respect to G. Hence, the PDF of G is expressed as:

$$f_G(G) = \frac{1}{2}\sum_{q=0}^{N_r}\binom{N_r}{q}\sum_{g=0}^{\infty}\frac{\Lambda_g(\alpha,\beta,N_r-q,q)}{\Gamma(g+N_r\beta+q(\beta-\alpha))}U^{\frac{\omega}{2}-1} \tag{3.59}$$

By using binomial expansion, the MGF of G can be obtained as:

$$\Phi_G(s) = \frac{1}{2}\sum_{q=0}^{N_r}\binom{N_r}{q}\sum_{g=0}^{\infty}\frac{\Lambda_g(\alpha,\beta,N_r-q,q)\Gamma\left(\frac{1}{2}\left(g+N_r\beta+q(\beta-\alpha)\right)\right)}{\Gamma(g+N_r\beta+q(\beta-\alpha))}(-s)^{-\frac{\omega}{2}} \tag{3.60}$$

Therefore, the average PEP for the system defined in (3.54) can be expressed as:

$$APEP_{SM-EGC} = \frac{1}{2\pi}\sum_{q=0}^{Nr}\binom{N_r}{q}\sum_{g=0}^{\infty}\frac{\Lambda_g(\alpha,\beta,N_r-q,q)\Gamma\left(\frac{1}{2}(g+N_r\beta+q(\beta-\alpha))\right)}{\Gamma(g+N_r\beta+q(\beta-\alpha))}$$

$$\times\left(\frac{\bar{\gamma}}{8N_r}\right)^{-\frac{\omega}{2}}\int_0^{\pi/2}(\sin^2\theta)^{\frac{-\omega}{2}}d\theta$$

(3.61)

$$\triangleq \frac{1}{2\pi}\sum_{q=0}^{Nr}\binom{N_r}{q}\sum_{g=0}^{\infty}\frac{\Lambda_g(\alpha,\beta,N_r-q,q)\Gamma\left(\frac{1}{2}(g+N_r\beta+q(\beta-\alpha))\right)}{\Gamma(g+N_r\beta+q(\beta-\alpha))}$$

$$\times\left(\frac{\bar{\gamma}}{8N_r}\right)^{-\frac{\omega}{2}}B\left(\frac{1}{2},\frac{\omega}{2}\right)$$

Finally, the ABER for the FSO-SM-EGC can thus be obtained by substituting (3.61) into (3.10) as:

$$ABER_{SM-EGC} \leq \frac{(N_tM)^{-1}}{2\pi\log_2(N_tM)}\sum_{l=1}^{N_t}\sum_{k=1}^{M}\sum_{\hat{l}=l+1}^{N_t}\sum_{\hat{k}=k+1}^{M}\sum_{q=0}^{Nr}N(k,\hat{k})\binom{N_r}{q}$$

$$\times\sum_{g=0}^{\infty}\left[\frac{\Lambda_g(\alpha,\beta,N_r-q,q)\Gamma\left(\frac{1}{2}(g+N_r\beta+q(\beta-\alpha))\right)}{\Gamma(g+N_r\beta+q(\beta-\alpha))}\left(\frac{\bar{\gamma}}{8N_r}\right)^{-\frac{\omega}{2}}B\left(\frac{1}{2},\frac{\omega}{2}\right)\right]$$

(3.62)

It can be deduced that (3.62) is in form of infinite series and to evaluate the truncation error caused by eliminating the infinite term after the $L+1$ term in ABER expression, the truncation error can thus be defined as:

$$\varepsilon_L = \frac{(N_tM)^{-1}}{2\pi\log_2(N_tM)}\sum_{l=1}^{N_t}\sum_{k=1}^{M}\sum_{\hat{l}=l+1}^{N_t}\sum_{\hat{k}=k+1}^{M}\sum_{q=0}^{Nr}N(k,\hat{k})\binom{N_r}{q}\sum_{g=L+1}^{\infty}V_g(q,\alpha,\beta)\left(\sqrt{\frac{8N_r}{\bar{\gamma}}}\right)^g$$

(3.63)

where

$$V_g(q,\alpha,\beta) = \frac{\Lambda_g(\alpha,\beta,N_r-q,q)\Gamma(w/2)}{\Gamma(w)}B\left(\frac{1}{2},\frac{w}{2}\right)\left(\sqrt{\frac{8N_r}{\bar{\gamma}}}\right)^{N_r\beta+q(\alpha-\beta)}$$

(3.64)

Therefore, the summation term in (3.63) can be simplified by using the Taylor series expansion of $x^n/(1-x)$ and the upper bound of truncation error can then be obtained as:

$$\varepsilon_K = \frac{\sqrt{8N_r}(N_tM)^{-1}}{2\pi\log_2(N_tM)\left(\sqrt{\bar{\gamma}}-1\right)\left(\sqrt{\bar{\gamma}}\right)^L}\sum_{l=1}^{N_t}\sum_{k=1}^{M}\sum_{\hat{l}=l+1}^{N_t}\sum_{\hat{k}=k+1}^{M}\sum_{q=0}^{Nr}N\left(k,\hat{k}\right)$$

$$\times \binom{N_r}{q}\max_{g>L}\{V_g(q,\alpha,\beta)\}$$

(3.65)

After examining the first term in (3.64), it was noted that $V_g(q,\alpha,\beta)$ approaches zero when g tends to infinity, thus the truncation error reduces with increasing in index L.

3.4.3 Hard-Coded Technique for Enhancing the Proposed System

In this study, the performance of the systems under the influence of Gamma-Gamma atmospheric turbulence is further enhanced by a convolutional coding technique. Convolutional code was first introduced by *Peter Elias* as one of the error controlling codes alternative to block code for transmission in 1955 [214]. It processes sequence of input bit stream as well as data block in short block lengths. Convolutional encoder for encoding the codes can be considered as a finite state machine with given number of shift register stages and exclusive-OR gates network. It is often denoted as (n,k,M) with k indicates the number of input bits shifted into the encoder at a time, n is the number of encoder output bit corresponding to the k information bit, and M is the constraint length (i.e encoder memory). The rate of the convolutional encoder is a measure of the coding efficiency and can thus be expressed as k/n; and the corresponding output bits stream has the length of $n(M + k)$ successive bits [215, 216]. On the other hand, convolutional decoding involves the process of searching for the best path that an encoder has traversed. Therefore, Viterbi decoder is the most common efficient decoding technique for the convolutional codes. It employs maximum likelihood decoding algorithm which examining all code sequence or code path through trellis and select the one that gives the largest likelihood function or smallest hamming distance [217]. This process starts from an initial state and attempts to determine the maximum likelihood function for each possible path remerging at a specific state (node). In each state, it compares the maximum likelihood (metric) of different paths arriving at that state, preserves the path with the largest metric and discards the rest. This path is called the survivor. The surviving path is stored at each node level together with its metric. The algorithm proceeds through the trellis in an iterative manner and maintains a relatively small list of paths that are always guaranteed to contain the maximum likelihood path [218].

Consequently, a rate ½ encoder of octal representation (5, 7), constraint length of 3 and a free distance of 5 as reported in [214] is employed in this study. Firstly, the input data are

encoded, and then interleaved by a random block interleaver before transmitting via the optical channel by using the established spatial modulation in section 3.1. At the receiving end, (3.8) is used to retrieve and estimate the transmitted bits and the deinterleaved by the random deinterleaver. The ABER for this coded FSO-SM-SD system can be obtained as [219]:

$$ABER_{SM-Coded} \leq \sum_{r=d_{free}}^{\infty} \frac{1}{k} M_r Z_r \qquad (3.66)$$

where d_{free} is the minimum rate free distance of rate k/n convolutional code, r is the Hamming distance, M_r is the weighting coefficient and Z_r is given as:

$$Z_r = \begin{cases} \sum_{e=\frac{r+1}{2}}^{r} \binom{r}{e} p^e (1-p)^{r-e} & ,r\ odd \\ \frac{1}{2}\binom{r}{r/2} p^{r/2}(1-p)^{r/2} + \sum_{e=\frac{r}{2}+1}^{r} \binom{r}{e} p^e (1-p)^{r-e} & ,r\ even \end{cases} \qquad (3.67)$$

where p is the ABER derived in equation (3.50) and (3.62) for uncoded SM-MRC and SM-EGC respectively.

3.4.4 Numerical Results and Discussions

In this section, the numerical results for ABER performance of coded and uncoded FSO-SM-SD system over the Gamma-Gamma atmospheric turbulence channel are presented. This is carried out by using the derived expression obtained with respect to equations (3.50), (3.62) and (3.66). It must be noted that the approximate error rate is obtained by eliminating infinite terms after the first $L + 1$ term in the series equations (3.50) and (3.62). The analysis is based on the influence of the following parameters such as laser wavelength $\lambda = 1550\ nm$, index of refractive structure parameter of $C_n = 3 \times 10^{-14}\ m^{2/3}$. In all the simulation, the value of $L = 50$ and the channel atmospheric turbulence levels is considered to be weak $(\alpha = 3.78, \beta = 3.74)$, moderate $(\alpha = 2.50, \beta = 2.06)$ and strong $(\alpha = 2.04, \beta = 1.10)$.

Figure 3.8 shows the system performance as a function of average SNR for a link range of $3000\ m$ which is equivalent to $(\alpha = 4.15, \beta = 1.41)$. It is confirmed from the result that the increase in the number of PD at the receiving end efficiently reduces the system error that occurs as a result of turbulence fading. It is also evident that MRC technique offers the best

performance as compared to EGC having a relatively close result. At an ABER of 10^{-14} for instant, only approximately $1\,dB$ of average SNR is required for EGC to achieve the same MRC performance. However, the practical implementation of MRC is more complex than the EGC due to the fact that it requires channel knowledge on each link. In consequence, it is practically recommended to employ SM-EGC since it almost offers the same performance as MRC at a lower receiver complexity.

Moreover, the performance comparison between SM-MRC and SM-EGC systems with SISO system under different atmospheric turbulence conditions such as weak, moderate and strong levels is reported in Figure 3.9 where two PDs are considered at the receiving end. At an average SNR of $35\,dB$, when the turbulence is strong, the SM-MRC system has an ABER of 10^{-6}, while the SISO system achieves an error of 10^{-4}. As expected, the increase in turbulence from weak to strong significantly increases the system error rate. It can be confirmed also from the result that MRC combiner outperformed other two systems since it maximizes the output SNR of the combined signal, although with little margin in the case of EGC combiner. Thus, the result proved that the use of combiner with more than one PD at the receiving end improves the system performance by reducing the error rate of the transmitting signal. In addition, Figure 3.9 also confirms that there is precise agreement between the derived series analytical expressions given in (3.50) and (3.62).and the exact ABER obtained by numerical integration through Monte-Carlo simulation and this therefore validates the accuracy of the derived series expressions.

Furthermore, the average BER for the system as a function of link range is presented in the Figure 3.10. The result is computed by considering the link range of using different PD configurations for MRC and EGC combiners at an average $SNR = 40\,dB$. Thus, it clearly shows that the system performance deteriorates with an increase in link range. At an average link range of $5000\,m$, it is observed that there is no significant change in error despite the fact that the link increases as the turbulence strength becomes saturated. However, it is evident that the increase in the number of PDs substantially improves the system error performance and thus, SM-MRC system still offers a better ABER performance than the EGC system irrespective of the link range.
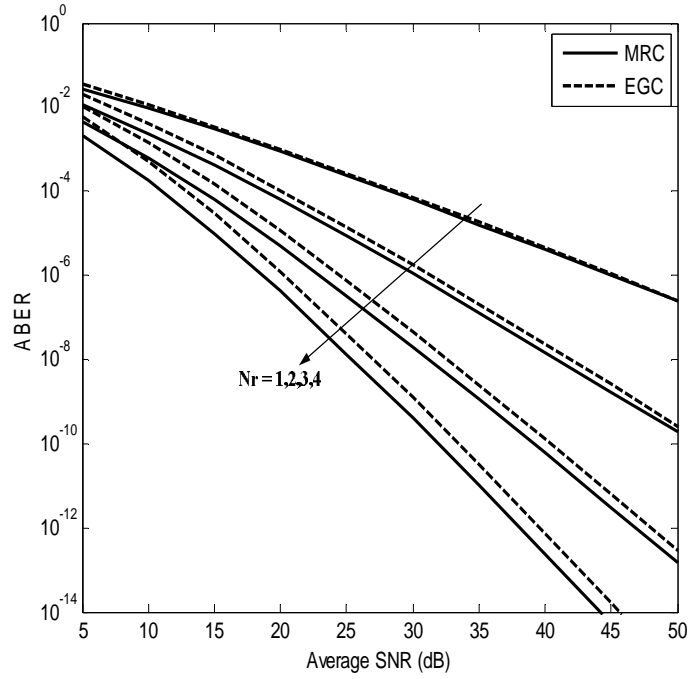
Figure 3.8: ABER of FSO-SM-SD system for various number of receive PDs
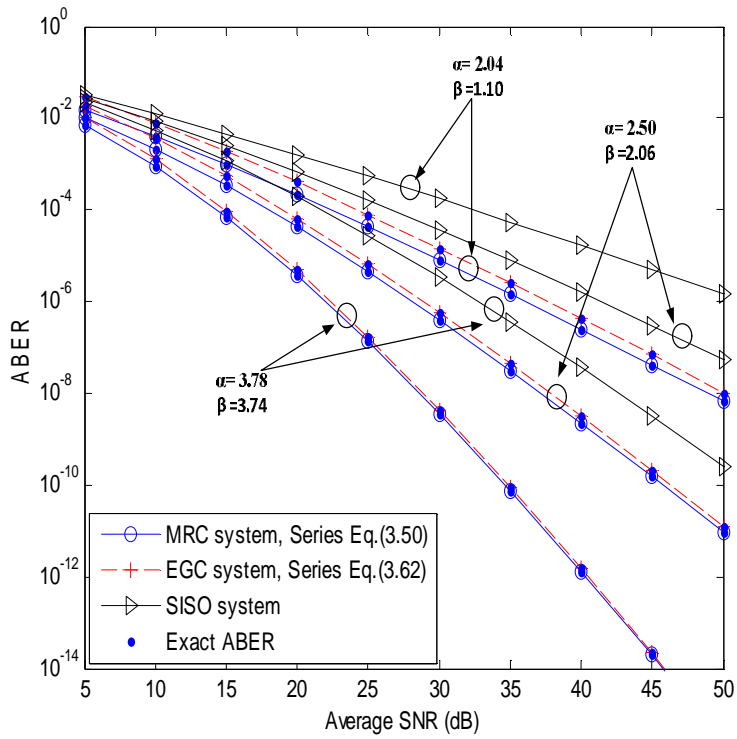
Figure 3.9: Performance comparison of FSO-SM-SD and SISO system under different turbulence levels
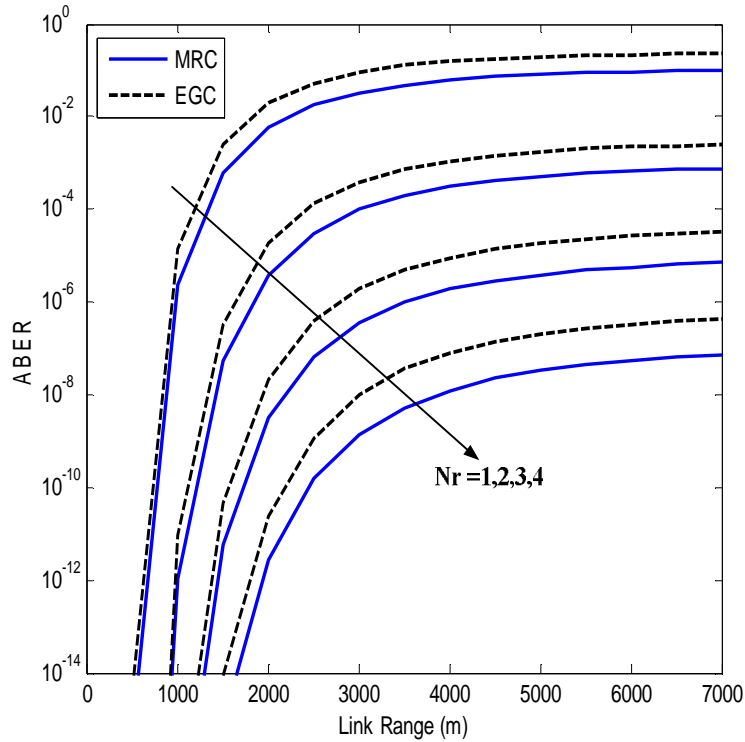
Figure 3.10: Performance of FSO-SM-SD under different link ranges

In Figure 3.11, the effect of increase in SI on the system performance is investigated. The result confirms that as the magnitude of scintillation increases, the system error rate also increases. However, it is noticed here that the performances of SM-MRC and SM-EGC systems do not change significantly by the increase in SI. This shows that the Gamma-Gamma random variable of the channel distribution varies in accordance with the original channel distribution. As a result of this, scintillation only has little effect on the system performance even when the number of PD at the receiving end is varied as it is demonstrated in Figure 3.12 for the SM-EGC system. For instance, it can be deduced from Figure 3.12 that at an average $SNR = 30\,dB$ and $SI = 2.3$, the system with $N_r = 2$ yields an approximate error of 10^{-6} while when $N_r = 4$ offers an approximate error rate of 10^{-10}. It therefore shows that the FSO-SM-SD system has a degree of robustness against the variations in channel turbulence effect especially in the case of scintillation.
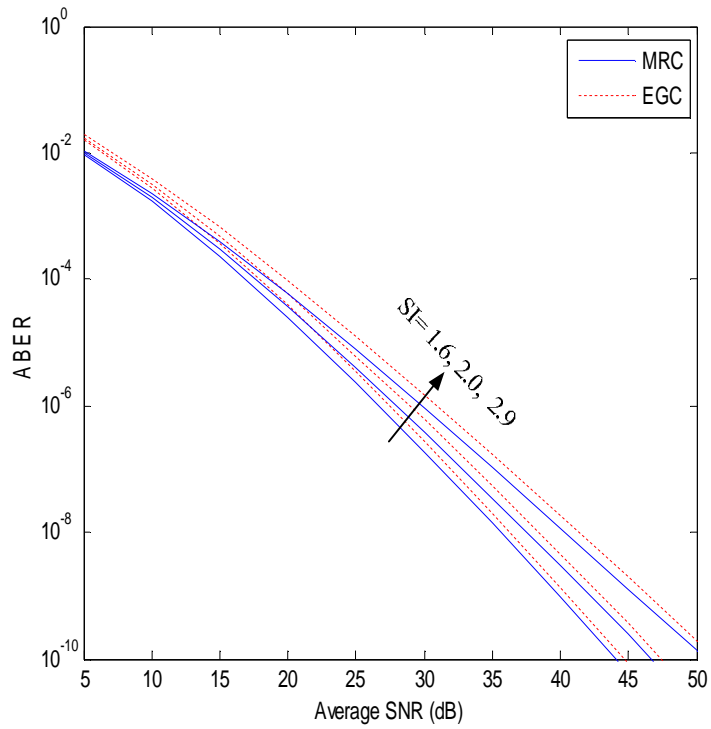
Figure 3.11: Impact of scintillation index on the FSO-SM-SD performance.
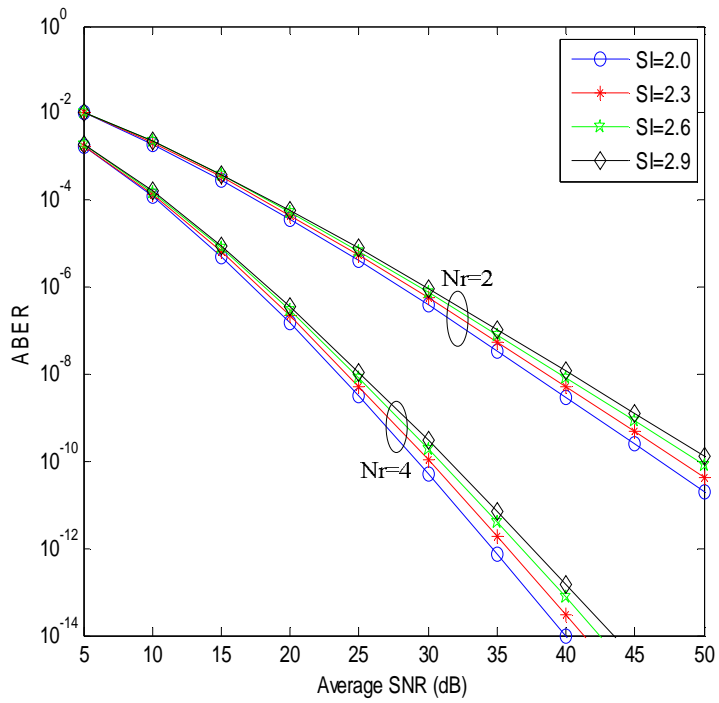
Figure 3.12: Effect on the scintillation index of the EGC-SM

Figure 3.13 presents the comparative studies of FSO-SM-SD with other systems that employ spatial diversity techniques. The two examined systems are SIM-MRC-BPSK and SIM-EGC-DPSK. The comparative studies are done under the condition of $N_r = 4$ or $N_r = 2$ as the receive photo-detectors. It can be seen that the proposed SM-MRC-BPSK offers a better error rate performance than SIM-MRC-BPSK and SIM-EGC-DPSK. For example, to achieve a bit error of 10^{-5} with four transmit lasers, the SM-MRC-BPSK requires an average SNR of $19 \, dB$ compared with SIM-MRC-BPSK and SIM-EGC-DPSK that require $25 \, dB$ and $32 \, dB$ respectively. This generally shows that SM-MRC-BPSK outperforms the other systems even when considering two PDs at the receiving end.

The performance comparison between the uncoded SM-SD system and coded SM-SD system under the strong atmospheric turbulence condition is presented in Figure 3.14. This shows the effect of convolutional coding technique as it enhances the system performance and four receive PDs are considered at the receiving end. It can be depicted from the result that coding scheme significantly improves the systems performance for both SM-MRC and SM-EGC. The technique enhances the performance of SM-MRC system by about $20 \, dB$ while for that SM-EGC system by about $17 \, dB$. Therefore, this illustrates the advantage of using coding technique for the proposed system.
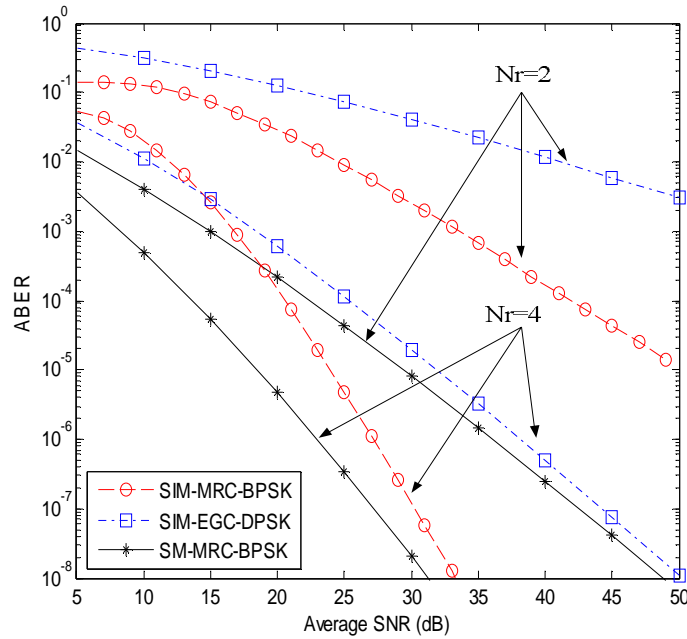
Figure 3.13: Performance comparison of SM-MRC-BPSK with SIM-MRC-BPSK and SIM-EGC-DPSK.
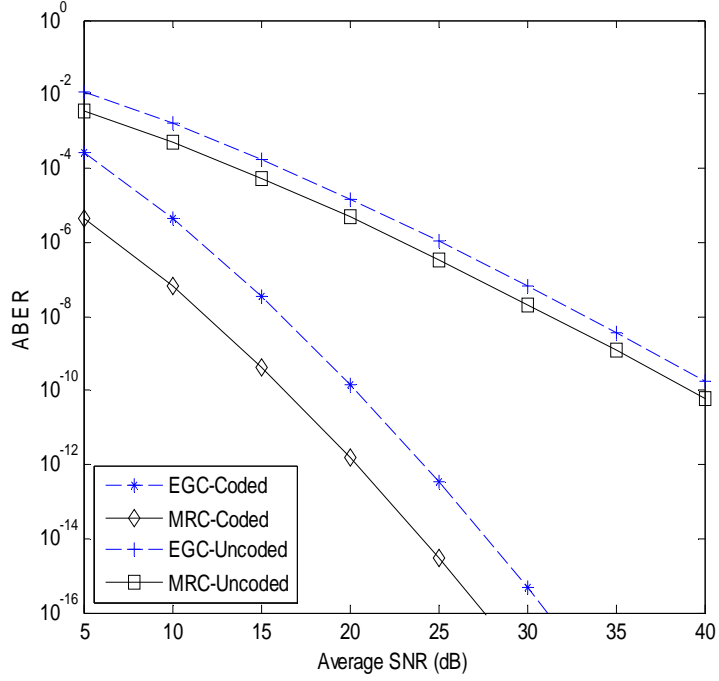
Figure 3.14: Performance comparison between uncoded and coded FSO-SM-SD with four PDs

3.5 Impact of Combined Effects of Atmospheric Turbulence and Pointing Error Impairments on the Performance of Optical Spatial Modulation FSO System

In this section, the report presents the performance error rate of an FSO-SM system under the influence of combined effect of Gamma-Gamma atmospheric turbulence and pointing error. Figure 3.1 is employed as the proposed system model except that a general received diversity is considered at the receiving end.

3.5.1   Statistical Characteristics for the Composite Channel

Since FSO systems is prone to both the effect of Gamma-Gamma atmospheric turbulence fading and pointing error impairments, the channel gain h_l at an instance is defined as the product of two random variables; that is, $h_l = h_l^{(a)} h_l^{(p)}$, where $h_l^{(a)}$ is the atmospheric turbulence attenuation and $h_l^{(p)}$ is the attenuation due to geometric spread and pointing error. Thus, the PDF of the Gamma-Gamma distribution is given in (2.20) as:

$$f_H\left(h_l^{(a)}\right) = \frac{2(\alpha + \beta)^{\frac{\alpha+\beta}{2}}}{\Gamma(\alpha)\Gamma(\beta)} h_l^{(a)\frac{\alpha+\beta}{2}-1} K_{\alpha-\beta}\left(2\sqrt{\alpha\beta h_l^{(a)}}\right) \quad , \quad h_l^{(a)} > 0$$

$$\triangleq \sum_{g=0}^{\infty}\left[m_g(\alpha,\beta)h_l^{(a)g+\beta-1} + m_g(\beta,\alpha)h_l^{(a)g+\alpha-1}\right]$$

(3.68)

Regarding the statistical distribution for the pointing error, the model defined in [50] where the beam waist, jitter variance and detector size were considered is employed in this study and the PDF for the pointing error is defined as:

$$f_H\left(h_l^{(p)}\right) = \frac{\xi^2}{A_o^{\xi^2}} h_l^{(p)\xi^2-1}, \qquad 0 \le h_l^{(p)} \le A_o$$

(3.69)

where $\xi = w_{zeq}/2\sigma_s$ is the ratio between the equivalent beam waist at the receiver and the pointing error displacement standard derivative (jitter) at the receive end, $w_{zeq} = w_e\sqrt{\sqrt{\pi}\mathrm{erf}(v)/2vexp(-v^2)}$, $v = \sqrt{\pi}r/\sqrt{2}w_e$, $A_o = [\mathrm{erf}(v)]^2$ is the fraction of power collected at radical distance zero and $\mathrm{erf}(.)$ is the error function.

Thus, the PDF of the combined channel effect is obtained as [50]:

$$f_H(h_l) = \int_{h/A_o}^{\infty} f_H\left(h_l^{(a)}\right)f_h(h_a)f_{h_l|h_l^{(a)}}\left(h_l\big|h_l^{(a)}\right) dh_l^{(a)}$$

(3.70)

where $f_{h_l|h_l^{(a)}}\left(h_l\big|h_l^{(a)}\right)$ is the conditional probability given a distribution state $h_l^{(a)}$ and can be expressed as:

$$f_{h_l|h_l^{(a)}}\left(h_l\big|h_l^{(a)}\right) = \frac{\xi^2}{A_o^{\xi^2}h_l^{(a)}}\left(\frac{h_l}{h_l^{(a)}}\right)^{\xi^2-1}$$

(3.71)

Putting (3.68), (3.71) into (3.70), then the composite PDF can be expressed as:

$$f_H(h_l) = \frac{C(\alpha,\beta,\xi)h_l^{\xi^2-1}}{A_o^{\xi^2}\Gamma(\alpha)\Gamma(\beta)} \sum_{g=0}^{\infty}\left[\frac{(\alpha\beta)^{g+\beta}\int_{h_l/A_o}^{\infty} h_l^{(a)g+\beta-\xi^2-1} dh_l^{(a)}}{\Gamma(g-\alpha+\beta+1)g!}\right.$$

$$\left.-\frac{(\alpha\beta)^{g+\alpha}\int_{h_l/A_o}^{\infty} h_l^{(a)g+\beta-\xi^2-1} dh_l^{(a)}}{\Gamma(g-\beta+\alpha+1)g!}\right]$$

(3.72)

With the used of the identity $\pi/\sin(\pi v) = \Gamma(v)\Gamma(1-v)$ and $C(\alpha,\beta,\xi) = \frac{\xi^2\Gamma(\alpha-\beta)\Gamma(1-\alpha+\beta)}{\Gamma(\alpha)\Gamma(\beta)}$, then the composite PDF for the combined channel impairments can be rewritten as:

$$f_H(h_l) = C(\alpha,\beta,\xi) \sum_{g=0}^{\infty} \left[\frac{(\alpha\beta)^{g+\beta} U_g(\beta) h_l^{(a)\,g+\beta-1}}{\Gamma(g-\alpha+\beta+1)g!} - \frac{(\alpha\beta)^{g+\beta} U_g(\alpha) h_l^{(a)\,g+\alpha-1}}{\Gamma(g-\beta+\alpha+1)g!} \right] \tag{3.73}$$

where

$$U_g(x) = \int_0^{\infty} exp[(g+x-\xi^2)t]dt$$

3.5.2 Performance Analysis

In determining the ABER for the system; the parameter ξ^2 is assumed to be greater than α and the pairwise error probability for the system is defined by following (3.11) as:

$$PEP\left(X_{l,k} \to X_{\hat{l},\hat{k}}\right) = E\left[Q\left(\sqrt{\frac{\bar{\gamma}}{4}} Z \right) \right] \tag{3.74}$$

By letting the difference channel gain be defined as $\psi_m = h_l x_q - h_{\hat{l}} x_{\hat{q}}$ which is assumed to be i.i.d, then Z becomes $Z = \sum_{m=1}^{N_r} |\psi_m|^2$

By using MGF approach and the Q-function formulated by Craig as $Q(x) = \frac{1}{\pi} \int_0^{\pi} exp\left(-\frac{x^2}{2sin^2\theta} \right) d\theta$, the APEP for the system can then be derived as:

$$APEP_{SM} \triangleq \frac{1}{\pi} \int_0^{\pi/2} \prod_{m=1}^{N_r} \left[M_{|\psi_m|^2}\left(-\frac{\bar{\gamma}}{8sin^2\theta} \right) \right] d\theta \tag{3.75}$$

Then, the analytical expression for the MGF of $|\psi_m|^2$ Gamma-Gamma random variable can be obtained as:

$$M_{|\psi_m|^2}(s) = E[exp(-s|\psi_m|^2)]$$

$$\triangleq \frac{\xi^2}{2} \sum_{g=0}^{\infty} \left[\frac{m_g(\alpha,\beta) U_g(g+\beta)\Gamma\left(\frac{g+\beta}{2}\right)}{A_o^{g+\beta}} (-s)^{-\frac{g+\beta}{2}} \right.$$

$$\left. + \frac{m_g(\beta,\alpha) U_g(g+\alpha)\Gamma\left(\frac{g+\alpha}{2}\right)}{A_o^{g+\alpha}} (-s)^{-\frac{g+\alpha}{2}} \right] \tag{3.76}$$

Thus, (3.75) becomes:

$$APEP_{SM} = \frac{1}{\pi} \int_0^{\frac{\pi}{2}} \prod_{m=1}^{N_r} \left[\frac{\xi^2}{2} \sum_{g=0}^{\infty} \left[a_g(\alpha,\beta,A_o)U_g(g+\beta)\Gamma\left(\frac{g+\beta}{2}\right)\left(\frac{\bar{\gamma}}{8sin^2\theta}\right)^{-\frac{g+\beta}{2}} \right. \right.$$

$$\left. \left. + a_g(\beta,\alpha,A_o)U_g(g+\alpha)\Gamma\left(\frac{g+\alpha}{2}\right)\left(\frac{\bar{\gamma}}{8sin^2\theta}\right)^{-\frac{g+\alpha}{2}} \right] \right] d\theta \qquad (3.77)$$

where

$$a_g(x,y,A_o) = \left(\frac{xy}{A_o}\right)^{g+x} \frac{\Gamma(x-y)\Gamma(1-x+y)}{\Gamma(x)\Gamma(y)\Gamma(g-x+y+1)g!}$$

Thus,

$$APEP_{SM} = \frac{\xi^2}{2\pi} \prod_{m=1}^{N_r} \sum_{g=0}^{\infty} \left[a_g(\alpha,\beta,A_o)U_g(g+\beta)\Gamma\left(\frac{g+\beta}{2}\right)\left(\frac{\bar{\gamma}}{8}\right)^{-\frac{g+\beta}{2}} \int_0^{\pi/2} (sin^2\theta)^{\frac{g+\beta}{2}} d\theta \right.$$

$$\left. + a_g(\beta,\alpha,A_o)U_g(g+\alpha)\Gamma\left(\frac{g+\alpha}{2}\right)\left(\frac{\bar{\gamma}}{8}\right)^{-\frac{g+\alpha}{2}} \int_0^{\pi/2} (sin^2\theta)^{\frac{g+\alpha}{2}} d\theta \right] \qquad (3.78)$$

It is observed that the integral in $U_g(x)$ does not converge when $\xi^2 < g + x$ and (3.78) only converges to zero when $g = 0$. Therefore, (3.78) can be approximated to a finite series which can be obtained by using the integral identity defined in (2.59) as:

$$APEP_{SM} = \frac{\xi^2}{4\pi} \left[\sum_{g=0}^{R} \left[a_g(\alpha,\beta,A_o)\Gamma\left(\frac{g+\beta}{2}\right)\left(\frac{\bar{\gamma}}{8}\right)^{-\frac{g+\beta}{2}} B\left(\frac{1}{2},\frac{g+\beta+1}{2}\right) \right. \right.$$

$$\left. \left. + a_g(\beta,\alpha,A_o)\Gamma\left(\frac{g+\alpha}{2}\right)\left(\frac{\bar{\gamma}}{8}\right)^{-\frac{g+\alpha}{2}} B\left(\frac{1}{2},\frac{g+\alpha+1}{2}\right) \right] \right]^{N_r} \qquad (3.79)$$

where $R = \lfloor \xi^2 - \alpha \rfloor$ and $\lfloor . \rfloor$ is the floor operation.

Finally, by substituting (3.79) into (3.10), the $ABER_{SM}$ is derived as:

$ABER_{SM}$

$$\leq \frac{\xi^2 (N_t M)^{-1}}{4\pi \log_2 (N_t M)} \sum_{l=1}^{N_t} \sum_{k=1}^{M} \sum_{\hat{l}=l+1}^{N_t} \sum_{\hat{k}=k+1}^{M} N(k, \hat{k}) \left[\sum_{g=0}^{R} a_g (\alpha, \beta, A_o) \Gamma \left(\frac{g+\beta}{2} \right) \left(\frac{\bar{\gamma}}{8} \right)^{-\frac{g+\beta}{2}} \right.$$

(3.80)

$$\left. \times B \left(\frac{1}{2}, \frac{g+\beta+1}{2} \right) + a_g (\beta, \alpha, A_o) \Gamma \left(\frac{g+\alpha}{2} \right) \left(\frac{\bar{\gamma}}{8} \right)^{-\frac{g+\alpha}{2}} B \left(\frac{1}{2}, \frac{g+\alpha+1}{2} \right) \right]\right]^{N_r}$$

In order to enhance the performance of the system against the combined channel impairments, then, convolutional coding technique is introduced by substituting (3.80) into (3.66).

3.5.3   Numerical Results and Discussions

In this section, the numerical performance results of FSO-SM system over the Gamma-Gamma atmospheric turbulence with misalignment effect are presented. The following system parameters are considered by setting normalized jitter standard deviation $\sigma_s = 1$, noise standard deviation $\sigma_n = 10^{-7} AHz$, and the lasers wavelength to be $1550\, nm$. According to strong turbulence condition, the structural parameter is fixed to be $3 \times 10^{-14}\, m^{2/3}$. Also, the number of transmit laser is set to be two and the system is subjected to strong atmospheric turbulence with parameters $\alpha = 2.04$ and $\beta = 1.10$ in all the simulations. For the coded FSO-SM system under the combined influence of turbulence and pointing error effect, a rate ½ encoder of octal representation $(5, 7)$, constraint length of 3 and a free distance of 5 is employed as it is stated in (3.66).

Figure 3.15 shows the effect of normalized beam waist on the system performance under the strong atmospheric turbulence condition for different receive PD configurations. It can be deduced that in both configurations, a narrow beam waist offers the system a better ABER performance due to increase in the received signal power. However, the use of narrow beam waist is highly prone to misalignment effect and this may result in loss of LOS which can halt the system link and reduce its reliability. Moreover, the result shows that the received diversity technique prevents this effect of misalignment in LOS as the number of receive PD increases, but still the system error performance deteriorates even with increase in beam waists.

Also, the performance of the SM system as a function of link range at a selected normalized beam waist of 10 with the unity pointing jitter is illustrated in Figure 3.16. The result shows

that as the link range increases, the system error increases and more power is required to achieve a minimum ABER. For instance, to achieve an error rate of 10^{-6} with $N_r = 2$ at a link range of $3000\,m$ and $4000\,m$, a transmitted power of $2\,dBm$ to $4\,dBm$ is required respectively. Thus, at any link range, the error performance of FSO-SM system can be substantially improved with lower transmitted power by increasing the receive PD. For example, when the receiver is equipped with two PDs, a high transmitted power of $2\,dBm$ will achieve an error rate of 1.7×10^{-8} at a link range of $3000\,m$ compared to a lower error rate of 5.7×10^{-12} achieved when the PD is four.

The effect of scintillation index on the system error performance for an FSO-SM system with $N_r = 2$ and $w_e/r = 10$ is reported in Figure 3.17. It is evident here that the increase in scintillation index drastically increases the system ABER and more power is needed to achieve a minimum system error. However, the increase in the number of PD at the receiving end can therefore substantially be used to mitigate this scintillation effect as can be seen in Figure 3.18 with $N_r = 4$ configuration. It can be depicted from the result that the system error reduces when compared with configuration $N_r = 2$ under the same scintillation indices and the required transmitted power drastically reduced. For instance, at a strong scintillation index of 2.9, it requires a low power of $-6\,dBm$ to achieve an error rate of 1.8×10^{-8} with $N_r = 4$ configuration as compared to a configuration of $N_r = 2$ that needs a high power of $8dBm$ to achieve the same ABER.

Figure 3.19 indicates how the increase in link range greatly affects the system performance for different normalized beam waists at power of $15\,dBm$. As expected, it is clearly highlighted that the longer the link range, the more the error rate for the system for any beam waist used at the transmitter. Thus, the use of more PD at the receiving end significantly improves the system error rate. For example, at a link range of $4000\,m$ when transmitter normalized beam waist is 10, the use of four PDs approximately reduce the system error by a difference of 10^{-6}.
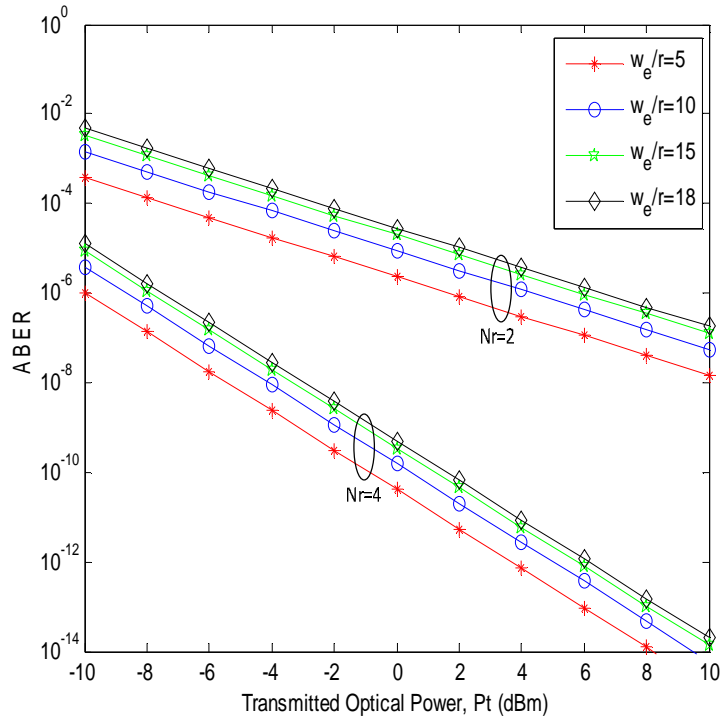
Figure 3.15: Performance of the SM under different normalized beam waist
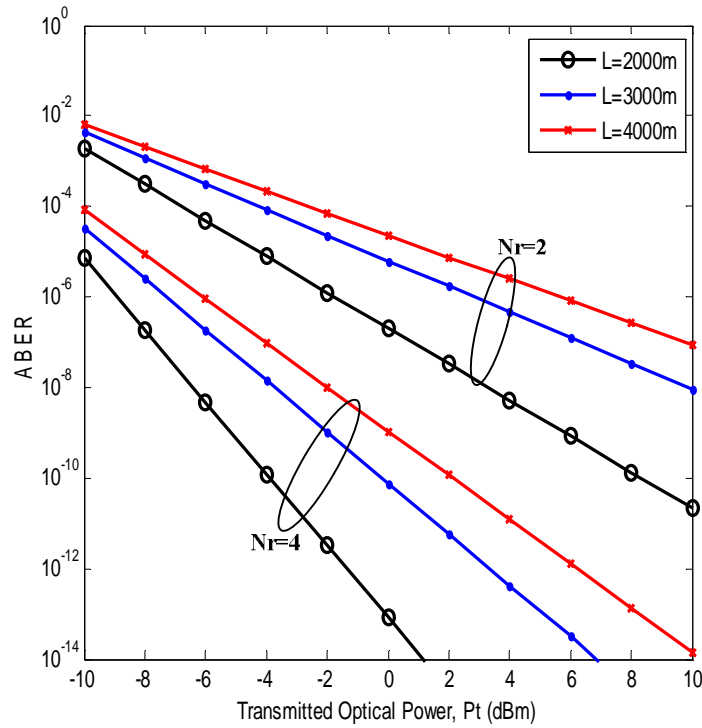
Figure 3.16: ABER vs transmitted optical power for various values of link range
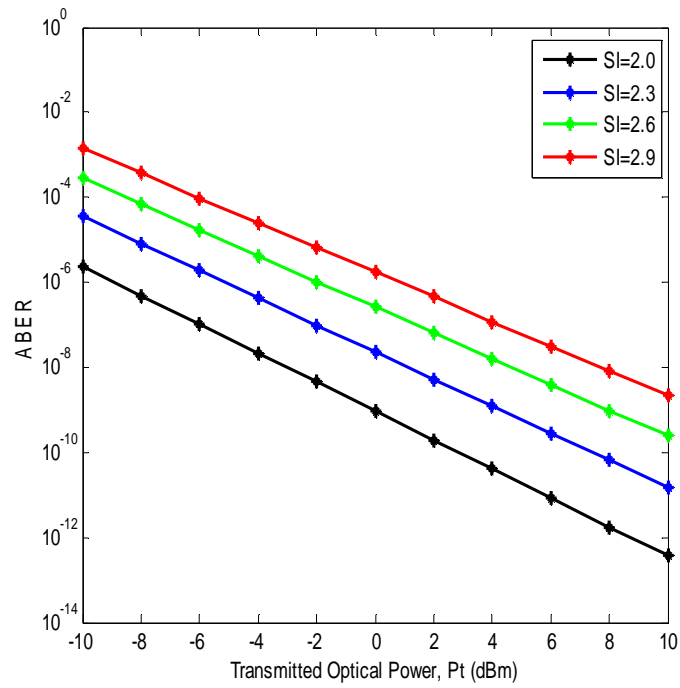
Figure 3.17: Scintillation index effect on the FSO-SM system at $N_r = 2$ configuration
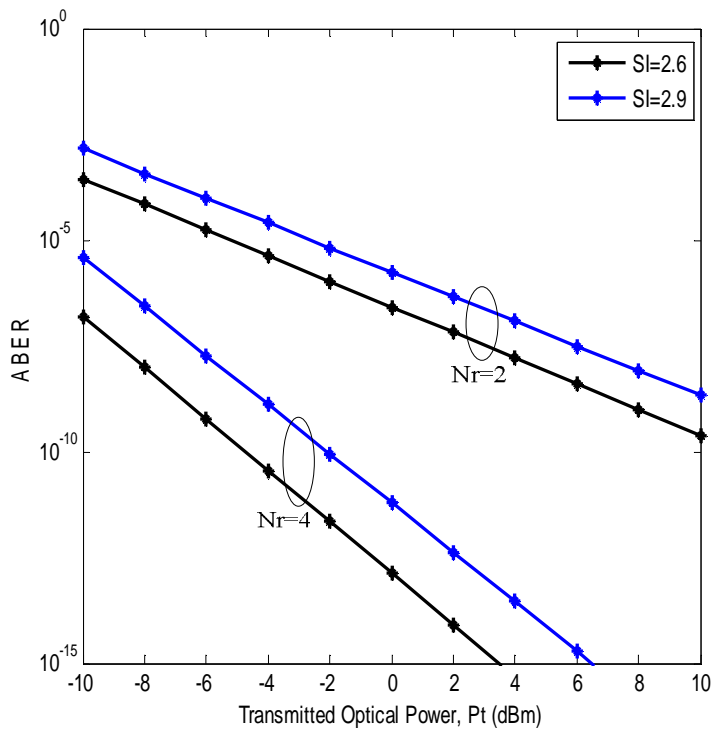
Figure 3.18: Impart of SI on FSO-SM under different MIMO configuration
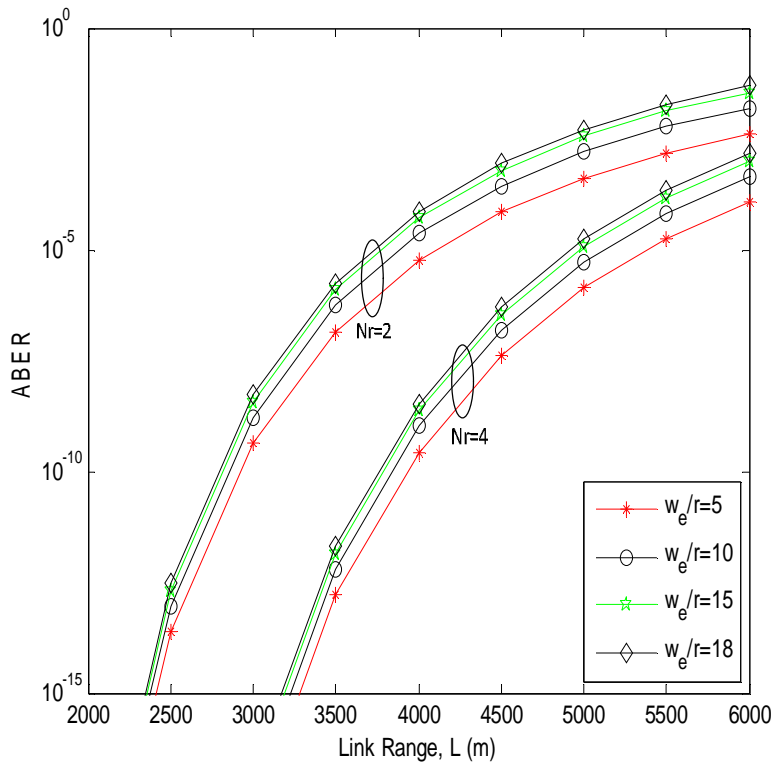
Figure 3.19: Error rate performance of the FSO-SM-SD over link ranges

The performance of convolutional coding technique on the ABER of FSO-SM system is presented in Figure 3.20. The system is considered with two PDs at the receiving end and subjected to the same atmospheric condition. It is clearly illustrated here that coding technique significantly enhances the system performance for any transmitted normalized beam waist without requiring much optical power to achieve a minimum error rate compared with uncoded system. For instance, when considering a normalized beam waist of 5, it requires a power of $2.5\ dBm$ to achieve a minimum ABER of 10^{-14} for coded system compared to a power of $10\ dBm$ that is required to achieve a minimum error rate of 10^{-6} for the uncoded system.
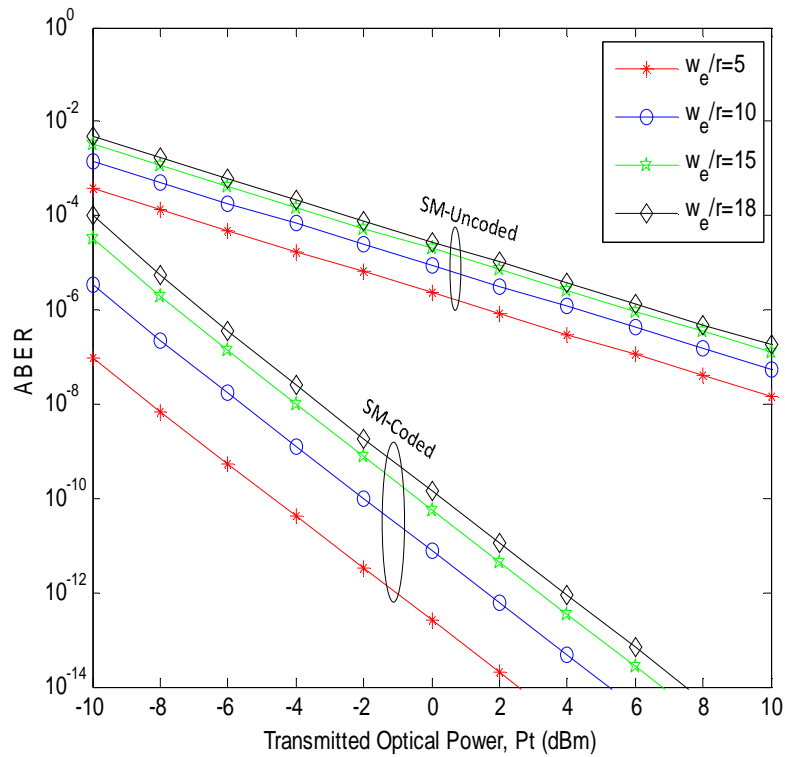
Figure 3.20: Performance of convolutional coded SM system

3.6 Chapter Summary

In this chapter, error performance analysis for FSO-SM communication systems under the lognormal, Gamma-Gamma distributions and pointing error were presented. The error analysis under the influence of Gamma-Gamma turbulence was based on infinite power series approach. It was demonstrated that the ABER of the proposed system under the influence of both distributions can be greatly improved with the aid of spatial diversity techniques such as MRC, EGC and SC. The framework revealed the effect of atmospheric turbulence levels, link range and SI on the overall system performance. Under the same propagation conditions, it was deduced that MRC combiner outperforms other diversity schemes with a tradeoff of system complexity as the number of receive PD increases. Also, the study proved that the longer the link range, the stronger atmospheric turbulence has severity effect on the system performance, and the influence of PD configurations on this effect has been identified. The result also demonstrated the performance comparison between the proposed systems and other conventional systems that employ diversity combiner and the

proposed systems offered the best performance among all of them. Furthermore, the performance of the proposed system over Gamma-Gamma channel was enhanced by employing convolutional coding technique and MRC scheme yielded the best error performance over the EGC scheme. In addition, the performance analysis of optical spatial modulation FSO system under the combined effect of misalignment and Gamma-Gamma turbulence fading was also analyzed. The derived ABER for this system was also based on power series expansion. The result revealed that the narrow beam waist offers the system a better performance than the wide beam waist. Therefore, an increase in the transmitter beam waist strongly affects the system error rate with higher transmitter optical power, but improve the system robustness against loss of LOS due to misalignment.

CHAPTER FOUR

Relay Assisted Dual-Hop Heterodyne Free Space Optical Spatial Modulation System with Diversity Combining over Induced Fading Channel

In this chapter, the performance analysis of relay-assisted dual-hop heterodyne FSO-SM systems in-conjunction with diversity combiners over a Gamma-Gamma atmospheric turbulence channel is presented. DF relay and AF relay protocols are considered for the proposed system. Under DF dual-hop FSO system, power series expansion of modified Bessel function is used to obtain the closed-form expressions for the end-to-end APEP for each of the combiners under study over Gamma-Gamma channel and a tight upper bound on the ABER per hop is given. Thus, the overall end-to-end ABER for the dual-hop FSO system is then evaluated. Thus, it is confirmed that the dual-hop transmission systems outperformed the direct link systems and the combination of dual-hop transmission with spatial modulation and diversity combiner significantly improves the systems error rate. Under AF dual-hop FSO system, the statistical characteristics of AF relay in terms of MGF, PDF and CDF are derived for the combined Gamma-Gamma turbulence and/or pointing error distributions channel. Based on these expressions, the APEP for each of the under study combiner is determined in terms of Meijer-G function and the ABER for the system is given by using union bounding technique. By utilizing the derived ABER expressions, the effective capacity for the considered system is then obtained. The effect of turbulence strength ranging from weak to strong levels and pointing errors in terms of beam width and jitter displacement are studied.

4.1 Optical Spatial Modulation with Diversity Combiner in Dual-Hop Decode-and-Forward Relay Systems over Atmospheric Turbulence

In this section, the performance analysis of DF dual-hop FSO systems in-conjunction with optical SM and diversity combiners over a Gamma-Gamma atmospheric turbulence channel using heterodyne detection is presented. MRC, EGC and SC are considered at the relay and destination as mitigation tools to improve the system error performance.

4.1.1   System Model

In this study, dual-hop heterodyne FSO relaying system consisting of a Source (S), Relay (R) and Destination (D) is considered and illustrated in Figure 4.1. A comprehensive description

of each unit is shown in Figure 4.1 (a), (b) and (c). Since optical SM is considered for the transmission, the scheme requires that the transmitter should have more than one laser. In this case, source and relay systems are considered as transmitting node, that is, $m \in \{S, R\}$, and at the same time provided with N_t^m transmit lasers in which only one is active at any transmitting instant to convey SM signals. Also, the relay and the destination are regarded as receiving nodes that is $k \in \{R, D\}$ and equipped with N_r^k receive photo-detector diodes $(N_r^k \geq 1)$ for heterodyne detection. In this system, the transmission of SM signal occurs in two phases. In the first phase, a block of B bits that is, $B = log_2(N_t^s M)$ is mapped into a constellation vector $X = [x_1, x_2, x_3 \dots x_{N_t^s}]^T$ at the source and M is the constellation size. The first group of these bits $log_2(N_t^s)$ is used to identify the active transmit laser index l^{th}, while the remaining $log_2(M)$ bits are employed to indicate the BPSK modulation symbol x_p from the pth signal constellation generated by the March-Zehnder Modulator (MZM) for the transmission. At an instant, the information bits are modulated on the electric field of an optical beam as $x_p^s \exp(j\phi_{x_p})$ and are then emitted from the active transmit-laser index l over the $N_r^k \times N_t^m$ MIMO atmospheric turbulence channel defined as [90]:

$$
\begin{aligned}
H_{mk}(t) &= [h_1, h_2, \dots, h_{N_t}] \\
&\triangleq \begin{bmatrix}
h_{11}(t)\exp(j\phi_{11}) & h_{12}(t)\exp(j\phi_{12}) & \cdots & h_{1N_t}(t)\exp(j\phi_{1N_t}) \\
h_{21}(t)\exp(j\phi_{21}) & h_{22}(t)\exp(j\phi_{22}) & \cdots & h_{2N_t}(t)\exp(j\phi_{2N_t}) \\
\vdots & \vdots & & \vdots \\
h_{N_r1}(t)\exp(j\phi_{N_r1}) & h_{N_r2}(t)\exp(j\phi_{N_r2}) & \cdots & h_{N_rN_t}(t)\exp(j\phi_{N_rN_t})
\end{bmatrix}
\end{aligned} \quad (4.1)
$$

where $h_{l,n}^m$ and $\phi_{l,n}^m$ are the real positive fading gain and the phase of channel respectively between the lth activated transmit laser and the nth receiver aperture. Thus, the source transmits the SM signal during this phase over the optical channel as [168]:

$$
X_{lp}^m = \left[0\ 0\ \cdots\ \underbrace{x_p^m \exp(j\phi_{x_p})}_{l^{th}\ laser\ position}\ \cdots\ 0\ 0 \right]^T \quad (4.2)
$$

At the relay, the incoming optical field is combined with the optical LO field and the process produces another optical field at intermediate frequency (ω_{IF}). The resulted field is then converted to electrical signal by the photo-detector. Due to slow nature of optical channel, the phase noise from the turbulence is then fully compensated with a carrier phase estimator circuit. Finally, the signals from each branch of the receiver are then combined using

diversity combiner and maximum-likelihood based optimum detection. This is used to retrieve the active transmit-laser index which result in estimating the sequence of data bit B emitted from the transmitter.

In analyzing the aforementioned detection process, the received optical field $E_n(t)$ at the aperture plane of the relay photo-detector is obtained as the sum of transmitted optical field $e_{s,n}(t)$ from the source and the locally generated optical field $e_{LO,n}(t)$ at the relay following the equation (2.6) as:

$$
\begin{aligned}
E_n(t) &= e_{s,n}(t) + e_{LO,n}(t) \\
&\triangleq \sqrt{2P_t Z_o}\, x_p^S h_{l,n}^S \cos\left(\omega_{LO} t + \phi_{l,n}^S + \phi_{x_p}\right) + \sqrt{2P_{LO} Z_o}\cos(\omega_{LO} t)
\end{aligned}
\tag{4.3}
$$

Thus, the generated photocurrent from the output of the photo-detector in response to the received mixed optical beam $E_n(t)$ can then be expressed, following the (2.7), as:

$$
\begin{aligned}
i_n(t) &= \frac{R}{Z_o}[E_n(t)]^2 + n_{SR}(t) \\
&\triangleq i_{R,n}(t) + n_{SR}(t)
\end{aligned}
\tag{4.4}
$$

where n_{SR} is the additive noise vector at the relay input which is modeled as AWGN and is assumed to be dominated by LO shot noise with zero-mean and variance $\sigma_{shot,LO}^2 = 2q_e R P_{LO} B_e$, and $i_{R,n}(t)$ is the information-carrying current at the relay which can be defined as:

$$
\begin{aligned}
i_{R,n}(t) &= R P_t \left|x_p^S h_{l,n}^S\right|^2 + R P_{LO} + 2R\sqrt{P_t P_{LO}}\, x_p^S h_{l,n}^S \cos\left(\omega_{LO} t - \phi_{l,n}^S - \phi_{x_p}\right) \\
&\triangleq i_{DC,n} + i_{AC,n}(t)
\end{aligned}
\tag{4.5}
$$

where $i_{DC,n} = R\left(P_t\left|x_p^S h_{l,n}^S\right|^2 + P_{LO}\right)$ is the DC component generated by the transmitted signal and the LO fields at the relay and $i_{AC,n}(t) \triangleq 2R\sqrt{P_t P_{LO}}\, x_p^S h_{l,n}^S \cos\left(\omega_{LO} t - \phi_{l,n}^S - \phi_{x_p}\right)$ is the received photocurrent which contains the information about the frequency and the phase of the received signal. Therefore, the SNR of the optical receiver can be defined as the ratio of the time-average AC photocurrent and the total noise. In view of equation (2.15), the SNR for the nth heterodyne receiver can be expressed as:

$$\gamma_{Het} = \frac{RP_t|x_p^S h_{l,n}^S|^2}{q_e B_e} \tag{4.6}$$

Based on the γ_{Het}, the sufficient statistics at the nth heterodyne receiver at the relay can be modeled as [90, 140]:

$$y_{SR} = \sqrt{\mu_{SR}} h_{l,n}^S x_p^S \exp(j\phi_{l,n}^S + j\phi_{x_p}) + n_{SR}(t)$$
$$\triangleq \sqrt{\mu_{SR}} H_{SR} X_{lp}^S + n_{SR}(t) \tag{4.7}$$

where $\mu_{SR} = RP_t / (q_e \Delta f)$ is the average received SNR at the relay system, x_p^S corresponds to the SM signal transmitted over the optical channel from the transmitter. H_{SR} is the channel matrix between source and relay with dimension $N_r^R \times N_t^S$ whose elements are modeled as i.i.d with distribution $CN(0, \sigma_{SR}^2)$ which is defined in (4.1).

During the second transmission phase, the relay node first combines the entire FSO radiation signal from the source during the first phase using MRC, EGC or SC; it then decodes the SM symbol, and re-transmits the decoded SM signal vector X_{lp}^R to the destination. At the destination, following the same heterodyne detection process at the relay, the received signal can be modeled as:

$$y_{RD} = \sqrt{\mu_{RD}} h_{l,n}^R x_p^R \exp(j\phi_{l,n}^R + j\phi_{x_p}) + n_{RD}(t)$$
$$\triangleq \sqrt{\mu_{RD}} H_{RD} X_{lp}^R + n_{RD}(t) \tag{4.8}$$

where μ_{RD} is the average SNR at the destination and is assumed to be equal to μ_{SR}, H_{RD} is the channel matrix between relay and destination with dimension $N_r^D \times N_t^R$ whose elements are modeled as IID with distribution $CN(0, \sigma_{RD}^2)$ and n_{RD} is the additive noise vector at the input of the destination which is also assumed to be dominated by LO shot noise and is modeled as AWGN.

In order to detect the SM signal vector X_{lp}^m transmitted from the S-to-R and R-to-D respectively, after the signal has been combined by spatial diversity combiner, a jointly optimum ML detection is applied to estimate the transmit laser index $\hat{l}^{(m)}$ and the transmitted constellation symbol index $\hat{p}^{(m)}$ at the R and D following (2.36) as:

$$\left[\hat{l}^{(m)} , \hat{p}^{(m)} \right] = \underset{\hat{l}^{(m)} , \hat{p}^{(m)}}{argmax} \ p_Y\left(y \middle| X_{lp}^m , H_{mk}\right)$$

$$\triangleq \underset{\hat{l}^{(m)} , \hat{p}^{(m)}}{argmin} \ \sqrt{\mu_{mk}} \left\| h_l^m x_p^m \right\|_F^2 - 2Re\left\{ y_{mk}^H h_l^m x_p^m \right\}$$

(4.9)
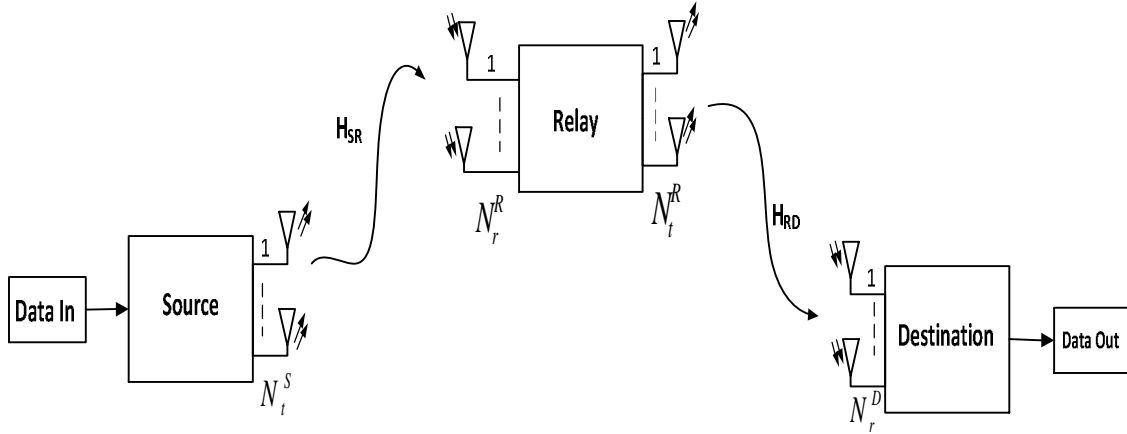
Figure 4.1: Dual-hop relaying FSO system with SM and SD where PD: Photo-detector, LO: Local Oscillator, BC: Beam Combiner, DC: Down Converter, PC: Phase Compensator
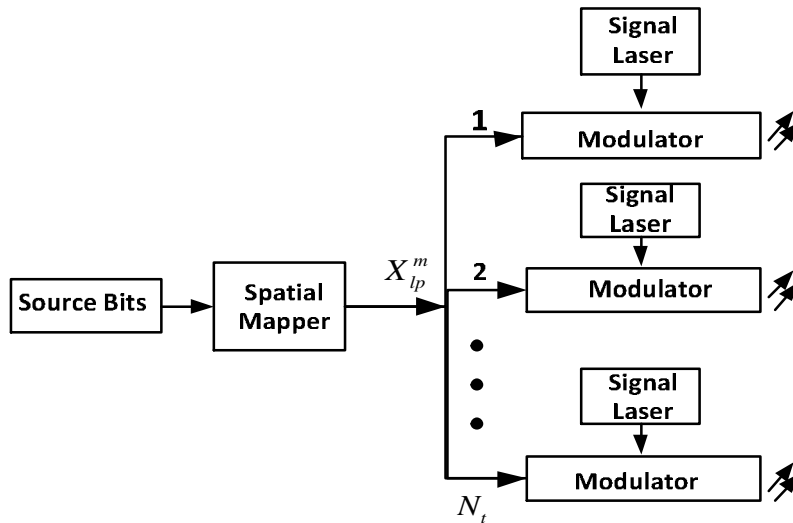
Figure 4.1(a): Source Unit
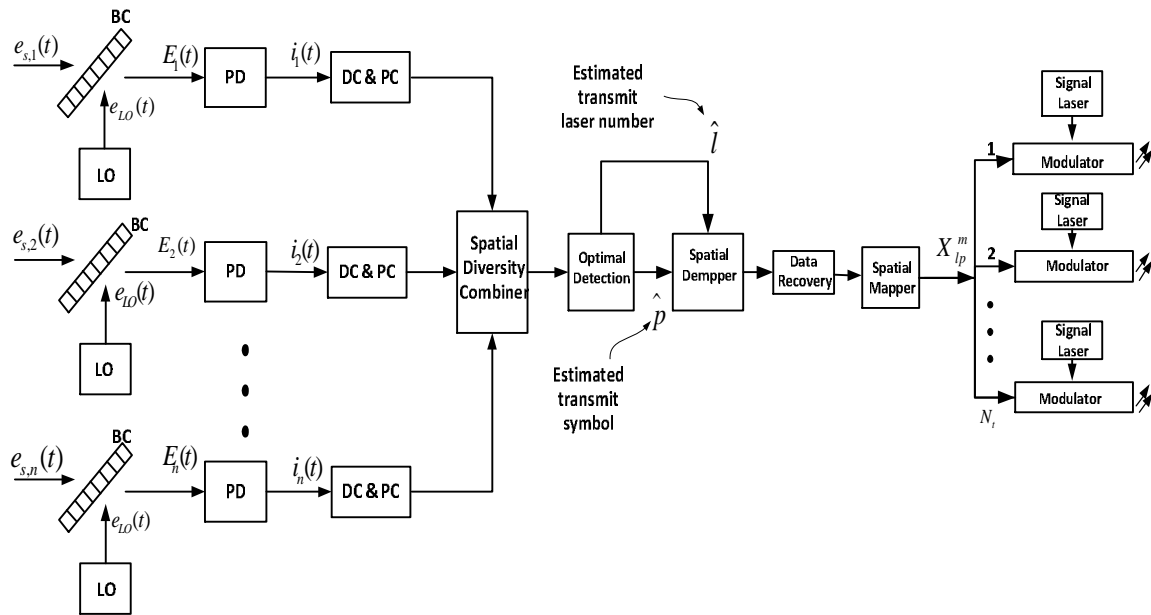
Figure 4.1(b): Relay Unit
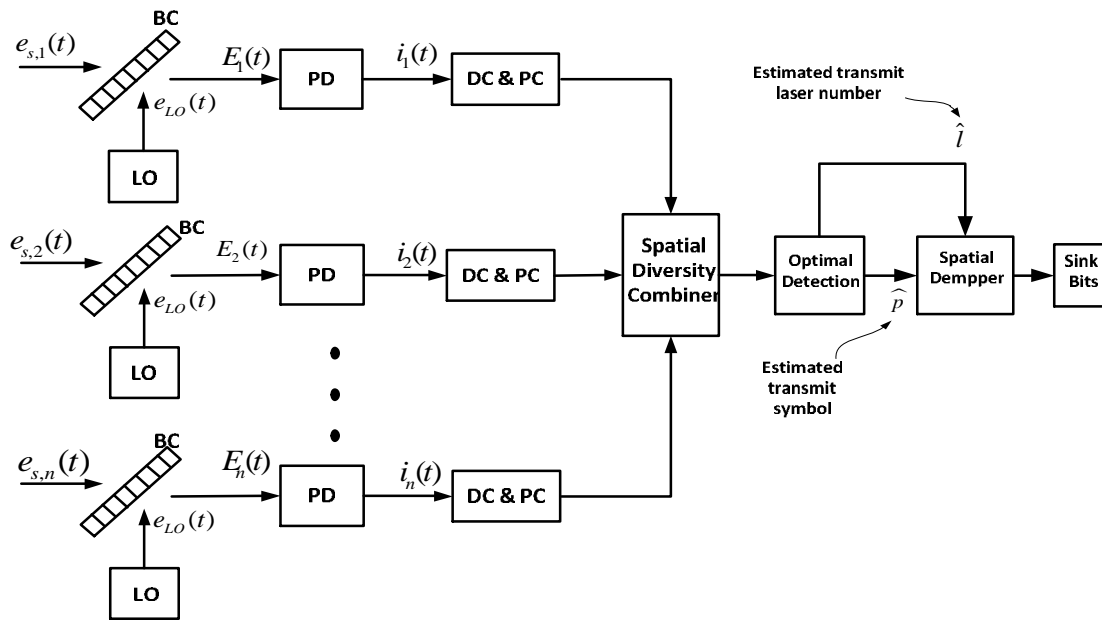
Figure 4.1(c): Destination Unit

4.1.2 Performance Analysis of End-to-End ABER

The end-to-end bit error rate for the dual-hop FSO system over the independent channel SNRs is presented in this section. Hence, the overall bit error rate for the dual-hop system using DF relay protocol is a function of the individual average BER SM links and this can be expressed as [220]:

$$P_b^{overall}(E_{SD}) = P_b(E_{SR}) + P_b(E_{RD}) - 2P_b(E_{SR})P_b(E_{RD}) \tag{4.10}$$

where $P_b(.)$ is the ABER per hop with the energy E_{mk} between the node m and k

In order to determine the average BER per hop over the Gamma-Gamma atmospheric turbulence channel, union bounding technique is adopted following (3.10) and the ABER per hop can be defined as [171]:

$$ABER_{SM}(E_{mk}) \leq \frac{(N_t^m M)^{-1}}{\log_2(N_t^m M)} \sum_{l=1}^{N_t^m} \sum_{p=1}^{M} \sum_{\hat{l}=l+1}^{N_t^m} \sum_{\hat{p}=p+1}^{M} N(p,\hat{p}) APEP\left(X_{l,p}^m \to X_{\hat{l},\hat{p}}^m\right) \tag{4.11}$$

where $N(p,\hat{p})$ is the number of bit error when selecting p instead of $\hat{p}$ as the transmit unit index

4.1.2.1 Maximum Ratio Combiner

The $PEP\left(X_{l,p}^m \to X_{\hat{l},\hat{p}}^m\right)$ for the MRC scheme can therefore be expressed by following the (3.15):

$$PEP_{SM-MRC}\left(X_{l,p}^m \to X_{\hat{l},\hat{p}}^m | H_{mk}\right) = Q\left(\sqrt{\frac{\mu_{mk}}{4} \sum_{n=1}^{N_r^k} |\alpha_n|^2}\right) \tag{4.12}$$

By applying a tight approximation for Gaussian Q-function obtained in [211] as $Q(x) \approx \frac{1}{12}\exp\left(-\frac{x^2}{2}\right) + \frac{1}{4}\exp\left(-\frac{2x^2}{3}\right)$, equation (4.12) can be expressed as:

$$PEP_{SM-MRC}\left(X_{l,p}^m \to X_{\hat{l},\hat{p}}^m | H_{mk}\right) = \frac{1}{12}exp\left(-\frac{\mu_{mk}}{8}\sum_{n=1}^{N_r^k}|\alpha_n|^2\right) + \frac{1}{4}exp\left(-\frac{\mu_{mk}}{6}\sum_{n=1}^{N_r^k}|\alpha_n|^2\right) \tag{4.13}$$

If we let $Y = |\alpha_n|^2$, then the average PEP for the approximated MRC can be obtained as:

$$APEP_{SM-MRC} = \frac{1}{12}\prod_{n=1}^{N_r^k}\int_0^\infty exp\left(-\frac{\mu_{mk}}{8}Y\right)f_Y(Y)dY + \frac{1}{4}\prod_{n=1}^{N_r^k}\int_0^\infty exp\left(-\frac{\mu_{mk}}{6}Y\right)f_Y(Y)dY$$

$$\triangleq \frac{1}{12}\prod_{n=1}^{N_r^k}\left[M_{|\alpha_n|^2}\left(\frac{\mu_{mk}}{8}\right)\right] + \frac{1}{4}\prod_{n=1}^{N_r^k}\left[M_{|\alpha_n|^2}\left(\frac{\mu_{mk}}{6}\right)\right] \qquad (4.14)$$

where $M_{|\alpha_n|^2}(.)$ is the Moment Generating Function (MGF) of $|\alpha_n|^2$ which can be obtained as:

$$M_{|\alpha_n|^2}(s) = \int_0^\infty exp(-sY)f_{|\alpha_n|^2}(Y)dY$$

$$\triangleq \frac{1}{2}\sum_{g=0}^\infty\left[m_g(\alpha,\beta)\Gamma\left(\frac{g+\beta}{2}\right)(-s)^{\frac{g+\beta}{2}} + m_g(\beta,\alpha)\Gamma\left(\frac{g+\alpha}{2}\right)(-s)^{\frac{g+\alpha}{2}}\right] \qquad (4.15)$$

Thus,

$$APEP_{SM-MRC} \triangleq \frac{1}{24}\prod_{n=1}^{N_r^k}[A_1] + \frac{1}{8}\prod_{n=1}^{N_r^k}[A_2] \qquad (4.16)$$

where

$$A_1 = \sum_{g=0}^\infty\left[m_g(\alpha,\beta)\Gamma\left(\frac{g+\beta}{2}\right)\left(\frac{\mu_{mk}}{8}\right)^{(g+\beta)/2} + m_g(\beta,\alpha)\Gamma\left(\frac{g+\alpha}{2}\right)\left(\frac{\mu_{mk}}{8}\right)^{(g+\alpha)/2}\right]$$

$$A_2 = \sum_{g=0}^\infty\left[m_g(\alpha,\beta)\Gamma\left(\frac{g+\beta}{2}\right)\left(\frac{\mu_{mk}}{6}\right)^{(g+\beta)/2} + m_g(\beta,\alpha)\Gamma\left(\frac{g+\alpha}{2}\right)\left(\frac{\mu_{mk}}{6}\right)^{(g+\alpha)/2}\right]$$

Consequently, the average BER per hop can be expressed by substituting (4.16) into (4.11) as:

$$ABER_{SM-MRC}(E_{mk})$$

$$\leq \frac{(N_t^m M)^{-1}}{\log_2(N_t^m M)}\sum_{l=1}^{N_t^m}\sum_{p=1}^{M}\sum_{\hat{l}=l+1}^{N_t^m}\sum_{\hat{p}=p+1}^{M}N(p,\hat{p})\left[\frac{1}{24}\prod_{n=1}^{N_r^k}[A_1] + \frac{1}{8}\prod_{n=1}^{N_r^k}[A_2]\right] \qquad (4.17)$$

The overall average BER for the dual-hop MRC system can therefore be determined by substituting the $ABER_{MRC-SM}(E_{mk})$ in (4.17) into the (4.10).

4.1.2.2 Equal Gain Combiner

The $PEP\left(X_{l,p}^m \to X_{\hat{l},\hat{p}}^m\right)$ for the EGC combiner scheme can therefore be expressed, following (3.28), as:

$$PEP_{SM-EGC}\left(X_{l,p}^m \to X_{\hat{l},\hat{p}}^m | H_{mk}\right) = Q\left(\sqrt{\frac{\mu_{mk}}{4N_r^k}\left(\sum_{n=1}^{N_r^k} |\alpha_n|\right)^2}\right) \tag{4.18}$$

By letting $P = \left(\sum_{n=1}^{N_r^k} |\alpha_n|\right)^2$, then (4.18) can be expressed as:

$$PEP_{SM-EGC}\left(X_{l,p}^m \to X_{\hat{l},\hat{p}}^m | H_{mk}\right) = Q\left(\sqrt{\frac{\mu_{mk}}{4N_r^k} P}\right) \tag{4.19}$$

By using the definition of the Q-function formulated by Craig's as $Q(x) = \frac{1}{\pi}\int_0^\pi exp\left(-\frac{x^2}{2sin^2\theta}\right)d\theta$, then the average PEP for the EGC can be written as:

$$APEP_{SM-EGC} = \frac{1}{\pi}\int_0^{\pi/2}\int_0^\infty exp\left(-\frac{\mu_{mk}P}{8N_r^k sin^2\theta}\right)f_P(P)dPd\theta \tag{4.20}$$

Through MGF, the squared sum of the random variable P is obtained, and this can be expressed by letting $T = \sum_{n=1}^{N_r^k} |\alpha_n|$ and $Z = |\alpha_n|$, the $P = (R)^2$. Cast in this way,

$$
\begin{aligned}
M_Z(s) &= \int_0^\infty exp(-sZ)f_{|\alpha_n|^2}(Z)dZ \\
&\triangleq \frac{1}{2}\sum_{g=0}^\infty \left[m_g(\alpha,\beta)\Gamma(g+\beta)(-S)^{(g+\beta)} + m_g(\beta,\alpha)\Gamma(g+\alpha)(-s)^{(g+\alpha)}\right]
\end{aligned}
\tag{4.21}
$$

By using binomial expansion, the MGF of the sum of T can be expressed as:

$$
\begin{aligned}
M_T(s) &= [M_Z(s)]^{N_r^k} \\
&\triangleq \sum_{q=0}^{N_r^k} \binom{N_r^k}{q}\left[\left(m_g(\alpha,\beta)\Gamma(g+\beta)(-s)^{(g+\beta)}\right)^{N_r^k-q}\left(m_g(\beta,\alpha)\Gamma(g+\alpha)(-s)^{(g+\alpha)}\right)^q\right]
\end{aligned}
\tag{4.22}
$$

The PDF of the T can be determined by applying the Laplace transform to its MGF obtained in (4.22):

$$f_T(T) = \sum_{q=0}^{N_r^k} \binom{N_r^k}{q} \sum_{g=0}^{\infty} \frac{e_g(\alpha, \beta, N_r^k - q, q)}{\Gamma\left(g + N_r^k \beta + q(\beta - \alpha)\right)} R^{\Psi - 1} \tag{4.23}$$

where

$$\Psi = g + N_r^k \beta + q(\beta - \alpha) \text{ , and}$$

$$e_g(\alpha, \beta, N_r^k - q, q) = \left[\xi_g(\alpha, \beta)\Gamma(g + \beta)\right]^{N_r^k - q} * \left[\xi_g(\beta, \alpha)\Gamma(g + \alpha)\right]^q$$

where $\left[m_g(\alpha, \beta)\Gamma(g + \beta)\right]^{[x]}$ implies that $m_g(\alpha, \beta)\Gamma(g + \beta)$ is convolved $x - 1$ times with itself.

By integrating (4.23) with respect to T and substituting $P = T^2$ thereafter, then differentiate with respect to P, then the PDF of P is expressed as:

$$f_P(P) = \frac{1}{2}\sum_{q=0}^{N_r^k} \binom{N_r^k}{q} \sum_{g=0}^{\infty} \frac{e_g(\alpha, \beta, N_r^k - q, q)}{\Gamma\left(g + N_r^k \beta + q(\beta - \alpha)\right)} P^{\frac{\Psi}{2} - 1} \tag{4.24}$$

That being so, the $APEP_{SM-EGC}$ in (4.20) can be further expressed as:

$$APEP_{SM-EGC}$$

$$= \frac{1}{2\pi} \int_0^{\frac{\pi}{2}} \int_0^{\infty} exp\left(-\frac{\mu_{mk} P}{8 N_r^k \sin^2\theta}\right) \sum_{q=0}^{N_r^k} \binom{N_r^k}{q} \sum_{g=0}^{\infty} \frac{e_g(\alpha, \beta, N_r^k - q, q)}{\Gamma\left(g + N_r^k \beta + q(\beta - \alpha)\right)} P^{\frac{\Psi}{2} - 1} dP d\theta$$

$$\triangleq \frac{1}{2\pi} \sum_{q=0}^{N_r^k} \sum_{g=0}^{\infty} \binom{N_r^k}{q} \frac{e_g(\alpha, \beta, N_r^k - q, q)}{\Gamma\left(g + N_r^k \beta + q(\beta - \alpha)\right)} \int_0^{\frac{\pi}{2}} \int_0^{\infty} exp\left(-\frac{\mu_{mk} P}{8 N_r^k \sin^2\theta}\right) P^{\frac{\Psi}{2} - 1} dP d\theta \tag{4.25}$$

Applying the integral identities in (2.59) to the (4.25), the average PEP for the EGC can be expressed as:

$$APEP_{SM-EGC} = \frac{1}{2\pi} \sum_{q=0}^{N_r^k} \sum_{g=0}^{\infty} \binom{N_r^k}{q} \frac{e_g(\alpha, \beta, N_r^k - q, q)}{\Gamma\left(g + N_r^k \beta + q(\beta - \alpha)\right)}$$

$$\times \Gamma\left(\frac{g + N_r^k \beta + q(\beta - \alpha)}{2}\right) \left(\frac{\mu_{mk}}{8 N_r^k}\right)^{-\frac{\Psi}{2}} B\left(\frac{1}{2}, \frac{\Psi}{2}\right) \tag{4.26}$$

Consequently, the average BER per hop can be expressed by substituting (4.26) into (4.11) as:

$$
\begin{aligned}
ABER_{SM-EGC}(E_{mk}) \;\leq\; &\frac{(N_t^m M)^{-1}}{\log_2(N_t^m M)} \sum_{l=1}^{N_t^m} \sum_{p=1}^{M} \sum_{\hat{l}=l+1}^{N_t^m} \sum_{\hat{p}=p+1}^{M} N(p,\hat{p}) \left[\frac{1}{2\pi} \sum_{q=0}^{N_r^k} \sum_{g=0}^{\infty} \binom{N_r^k}{q} \right. \\
&\left. \times \frac{e_g(\alpha,\beta,N_r^k-q,q)}{\Gamma\!\left(g+N_r^k\beta+q(\beta-\alpha)\right)} \Gamma\!\left(\frac{g+N_r^k\beta+q(\beta-\alpha)}{2}\right)\left(\frac{\mu_{mk}}{8N_r^k}\right)^{-\frac{\Psi}{2}} B\!\left(\frac{1}{2},\frac{\Psi}{2}\right) \right]
\end{aligned}
\tag{4.27}
$$

Substitute the $ABER_{SM-EGC}(E_{mk})$ in (4.27) into the (4.10) to determine the overall average BER for the dual hop EGC system.

4.1.2.3 Selection Combiner

The pairwise error probability for the selection combiner is given by following the (3.35) as:

$$
PEP_{SM-SC}\!\left(X_{l,p}^m \to X_{\hat{l},\hat{p}}^m \middle| H_{mk}\right) = Q\!\left(\sqrt{\frac{\mu_{mk}}{4}\left(h_l^m \middle| x_p^m - x_{\hat{p}}^m \middle|\right)^2}\right)
\tag{4.28}
$$

In the (4.28), the $h_l^m \middle| x_p^m - x_{\hat{p}}^m \middle|$ can be expressed as random variable U and since selection is made according to $h_{l(max)}^m = max\left(h_1^m, h_2^m, \ldots, h_{N_r^k}^m\right)$, then the average PEP for the SC combiner can be expressed as:

$$
\begin{aligned}
APEP_{SM-SC} &= \int_0^{\infty} Q\!\left(\sqrt{\frac{\mu_{mk}}{4}U^2}\right) f_{h_{l(max)}^m}(U)\,dU \\
&\triangleq -\int_0^{\infty} F_{h_{l(max)}^m}^{sel}(U)\, Q'\!\left(\sqrt{\frac{\mu_{mk}}{4}U^2}\right) dU
\end{aligned}
\tag{4.29}
$$

where $Q'(.)$ is the derivative of Q-function which is defined in [124] as $Q'(x) = \frac{1}{2\sqrt{\pi}}\exp(-x^2/2)$ and $F_{h_{l(max)}^m}^{sel}(U)$ is the CDF of random variable U for the SC combiner and can be expressed as [221]:

$$
F_{h_{l(max)}^m}^{sel}(U) = \prod_{n=1}^{N_r^k} F_{h_n^m}(U)
\tag{4.30}
$$

Thus, the CDF of the channel is then obtained by using the series expression for the PDF of the Gamma-Gamma turbulence channel given in (2.53) as:

$$f_{h_l^m}(h) = \sum_{g=0}^{\infty} \left[m_g(\alpha, \beta) h^{g+\beta-1} + m_g(\beta, \alpha) h^{g+\alpha-1} \right] \qquad (4.31)$$

Then, the Cumulative Distribution Function (CDF) for the Gamma-Gamma distribution for the system channel can be obtained from (4.13) as:

$$
\begin{aligned}
F_{h_l^m}(h) &= \int_0^{\infty} f_{h_l^m}(h) dh \\
&\triangleq \sum_{g=0}^{\infty} \left[\frac{m_g(\alpha, \beta)}{g+\beta} h^{g+\beta} + \frac{m_g(\beta, \alpha)}{g+\alpha} h^{g+\alpha} \right]
\end{aligned} \qquad (4.32)
$$

So, the average conditional PEP for the SC can therefore be expressed as:

$$
\begin{aligned}
APEP_{SM-SC} &= \frac{\sqrt{\mu_{mk}}}{2\sqrt{2\pi}} \prod_{n=1}^{N_r^k} \left[\sum_{g=0}^{\infty} \left[\frac{m_g(\alpha, \beta)}{g+\beta} \int_0^{\infty} exp\left(\frac{-\mu_{mk}}{8} U^2 \right) U^{g+\beta} dU \right. \right. \\
&\quad \left. \left. + \frac{m_g(\beta, \alpha)}{g+\alpha} \int_0^{\infty} exp\left(\frac{-\mu_{mk}}{8} U^2 \right) U^{g+\alpha} dU \right] \right]
\end{aligned} \qquad (4.33)
$$

The integration in the (4.33) can then be solved by applying integral identity defined in [205, equation (3.326(2))] (see Appendix A3.1), and the $APEP_{SM-SC}$ can be expressed as:

$$
\begin{aligned}
APEP_{SM-SC} &= \frac{1}{4} \sqrt{\frac{\mu_{mk}}{2\pi}} \prod_{n=1}^{N_r^k} \left[\sum_{g=0}^{\infty} \left[\frac{m_g(\alpha,\beta)\Gamma\left(\frac{g+\beta+1}{2}\right)}{(g+\beta)\left(\frac{\mu_{mk}}{8}\right)^{\frac{g+\beta+1}{2}}} + \frac{m_g(\beta,\alpha)\Gamma\left(\frac{g+\alpha+1}{2}\right)}{(g+\alpha)\left(\frac{\mu_{mk}}{8}\right)^{\frac{g+\alpha+1}{2}}} \right] \right] \\
&\triangleq \left[\frac{1}{4} \sqrt{\frac{\mu_{mk}}{2\pi}} \left[\sum_{g=0}^{\infty} \left[\frac{m_g(\alpha,\beta)\Gamma\left(\frac{g+\beta+1}{2}\right)}{(g+\beta)\left(\frac{\mu_{mk}}{8}\right)^{\frac{g+\beta+1}{2}}} + \frac{m_g(\beta,\alpha)\Gamma\left(\frac{g+\alpha+1}{2}\right)}{(g+\alpha)\left(\frac{\mu_{mk}}{8}\right)^{\frac{g+\alpha+1}{2}}} \right] \right] \right]^{N_r^k}
\end{aligned} \qquad (4.34)
$$

Substituting the average PEP in (4.34) into (4.11) to determine the ABER per hop for the SC combiner as:

$$ABER_{SC-SM}(E_{mk}) \leq \frac{(N_t^m M)^{-1}}{\log_2(N_t^m M)} \sum_{l=1}^{N_t^m} \sum_{p=1}^{M} \sum_{\hat{l}=l+1}^{N_t^m} \sum_{\hat{p}=p+1}^{M} N(p,\hat{p})$$

$$\times \left[\frac{1}{4}\sqrt{\frac{\mu_{mk}}{2\pi}} \left[\sum_{g=0}^{\infty} \left[\frac{m_g(\alpha,\beta)\Gamma\left(\frac{g+\beta+1}{2}\right)}{(g+\beta)\left(\frac{\mu_{mk}}{8}\right)^{\frac{g+\beta+1}{2}}} + \frac{m_g(\beta,\alpha)\Gamma\left(\frac{g+\alpha+1}{2}\right)}{(g+\alpha)\left(\frac{\mu_{mk}}{8}\right)^{\frac{g+\alpha+1}{2}}} \right] \right] \right]^{N_r^k} \quad (4.35)$$

Thus, the overall average BER for the system can be obtained by substituting the $ABER_{SM-SC}(E_{mk})$ in (4.35) into the (4.10).

4.1.3 Numerical Results and Discussions

In this section, the numerical results on the average BER of the dual-hop system over the Gamma-Gamma channel are presented using the derived expression of equations (4.17), (4.27) and (4.35) in (4.10) for the overall system ABER. Generally, the relay and destination terminals are assumed to employ MRC, EGC, SC for combining the SM signal during each transmission phase. The analysis in this study is based on the influence of the following parameters such as laser wavelength $\lambda = 1550\ nm$, index of refractive structure parameter of $C_n^2 = 3 \times 10^{-14} m^{-2/3}$. Also, we considered the channel atmospheric turbulence levels to be weak $(\alpha = 3.78, \beta = 3.74)$, moderate $(\alpha = 2.50, \beta = 2.06)$ and strong $(\alpha = 2.04, \beta = 1.10)$. Moreover, the values of N_t^m and M are set to be 2 in all cases; both at the source and relay, except otherwise stated in the simulations. The results presented illustrate the different behaviours of the proposed system when varying the atmospheric turbulence conditions, average SNR at the relay and destination, the link range, the receive photo-detector at the relay and destination. It should be noted here for instance that, a MRC-with-MRC (MRC-MRC) dual-hop system describes that either R or D has MRC combiner. Likewise strong-to-moderate channel condition for example implies that S-to-R link is subjected to strong turbulence condition and R-to-D link experiences moderate turbulence condition.

Looking at Figure 4.2, the performance comparison between the direct link system without relay with a dual-hop systems is presented. The relay and destination terminal possess the same combiner for SM signal combination over a link range of $6\ km$ with both terminals having four photodetectors. It is depicted that the dual-hop system equiped with MRC on both R and D outperformed other systems snice it maximazes its output SNR of the combined signal while SC-direct link offers the least preformance because it depends on only the the

highest SNR of the combined signal. In all cases, the EGC has a very close performance relative to MRC. However, both MRC and EGC direct link performed better than dual-hop with SC on both R and D since the system makes use of channels with the maxium SNR. For instance, in comparing the dual hops with direct link systems, it is clear that at an average received SNR of 30 dB, MRC-MRC system offers an ABER of 3.26×10^{-11} compared with MRC without relay which gives 3.75×10^{-9} over the same link range. Also, the SC-SC dual hop system produces an ABER of 8.87×10^{-7} compare with 1.62×10^{-5} by SC direct link system. This generally shows that relay unit actually increases the FSO systems coverage area.

In considering different combiners at the R and D over link range of $6\ km$ as it is shown in Figure 4.3, it is confirmed that when MRC and EGC either at R or D, the dual-hop systems offer the best performance than other sytems as compared with direct link with MRC and EGC. Nevertheless, dual-hop systems with MRC-SC and EGC-SC yield the same error peformance of 4.43×10^{-7} and outperform the SC direct link system with ABER of 1.62×10^{-5}. It is also discovered that direct link system with the MRC and EGC outperforms the two sytems (that is, MRC-SC and EGC-SC) due to the fact that SC combiner within the systems cause degration in the hops of the transmission phase. This is because, SC combiner requires only the highest SNR which might have suffered from the turbulence.

The effect of different levels of atmospheric turbulence on the performance of dual-hop systems when the relay is equipped with one receive PD and the destination with two receive PDs is presented in Figure 4.4. As expected, the increase in turbulence level from weak to strong severely degrades the systems error performance with MRC outperforming the other systems. For instance, at average SNR of 35 dB, MRC system yields an approximate ABER of 10^{-5} and 10^{-3} respectively over a weak and strong turbulence as compared with SC of 10^{-2} and 10^{-1} respectively under the channel conditions. Based on the numerical integration through Monte-Carlo simulation, the exact error rate is determined to validate the accuracy of the analytical series expressions derived in (4.17), (4.27) and (4.35). It can thus be deduced from the Figure 4.4 that there is excellent agreement between series expressions and the exact ABER of the systems.

When different and identical combiners are considered for the dual-hop systems, the performance behaviour of the system over different turbulence levels is presented in Figure 4.5. It is shown that dual-hop system with MRC-MRC at R and D offers the best performance

while the EGC-EGC and MRC-EGC systems performance are the same and very close to MRC-MRC system. Over a strong turbulence condition, it is indicated that they offer a BER of approximately 10^{-4} at the average received SNR of $25\ dB$. Also, it is indicated that dual-hop systems with SC-SC, EGC-SC and MRC-SC at either R or D produce the same performance for all the turbulence levels but with poor ABER of 10^{-2} at the same SNR as compared with the other systems under strong turbulence.
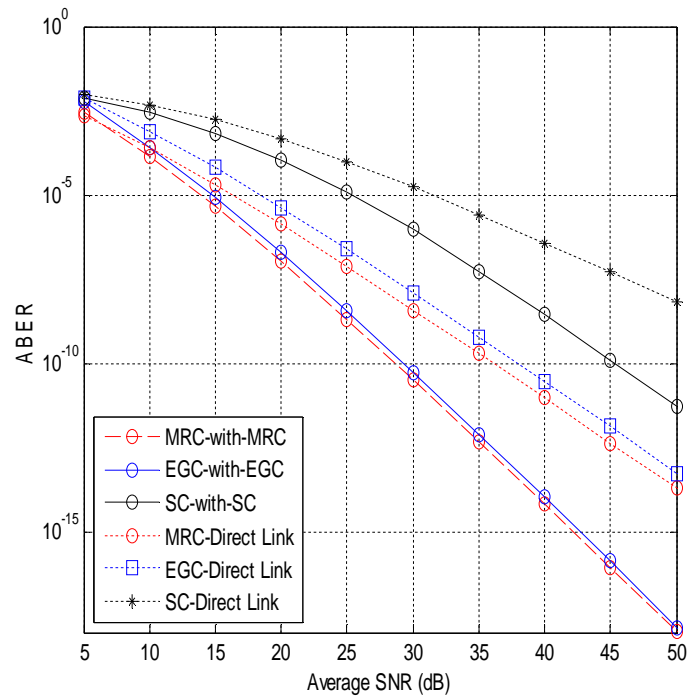
Figure 4.2: Comparison between direct link and dual-hop systems with same combiners at the relay and destination for $N_r^R = 4$ and $N_r^D = 4$ over $6\ km$ link range
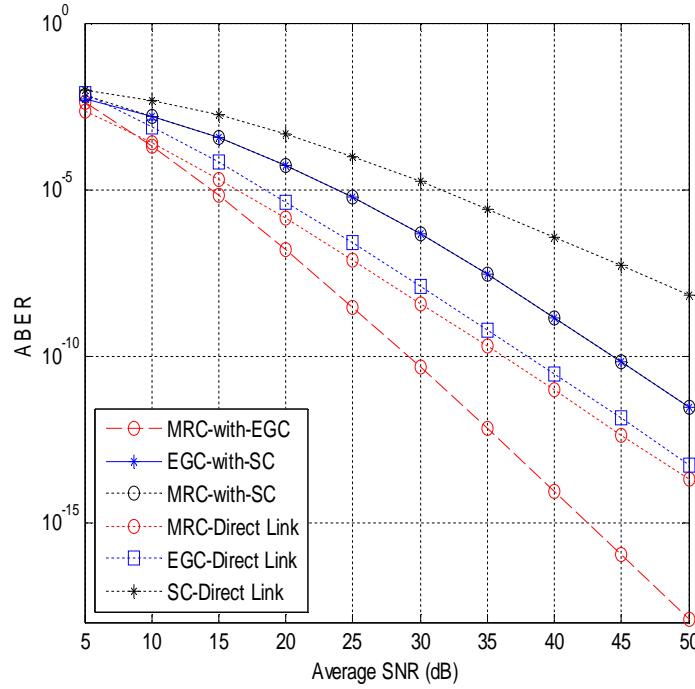
Figure 4.3: Comparison between direct link and dual-hop systems with different combiners at the relay and destination for $N_r^R = 4$ and $N_r^D = 4$ over $6\ km$ link range
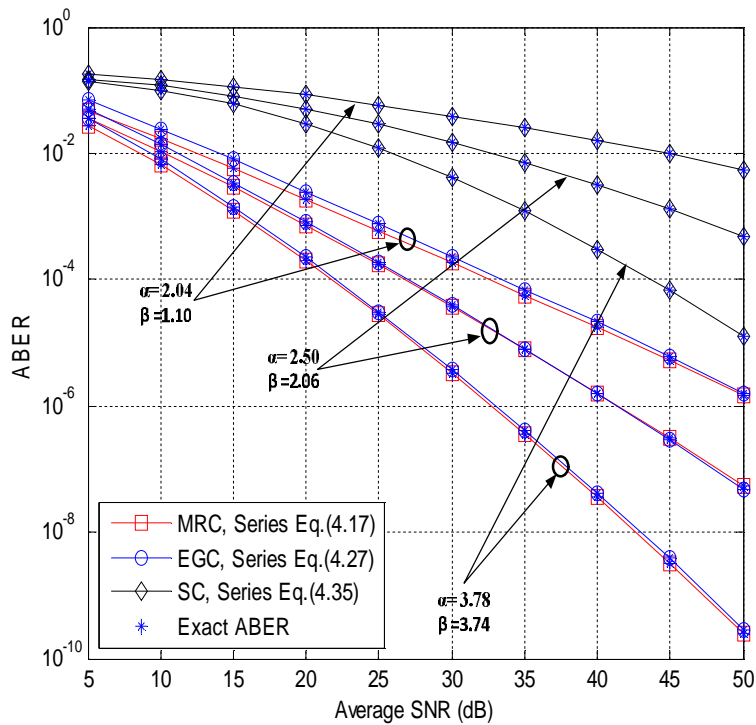
Figure 4.4: Effect of turbulence conditions on the dual-hop system with $N_r^R = 1$ and $N_r^D = 2$
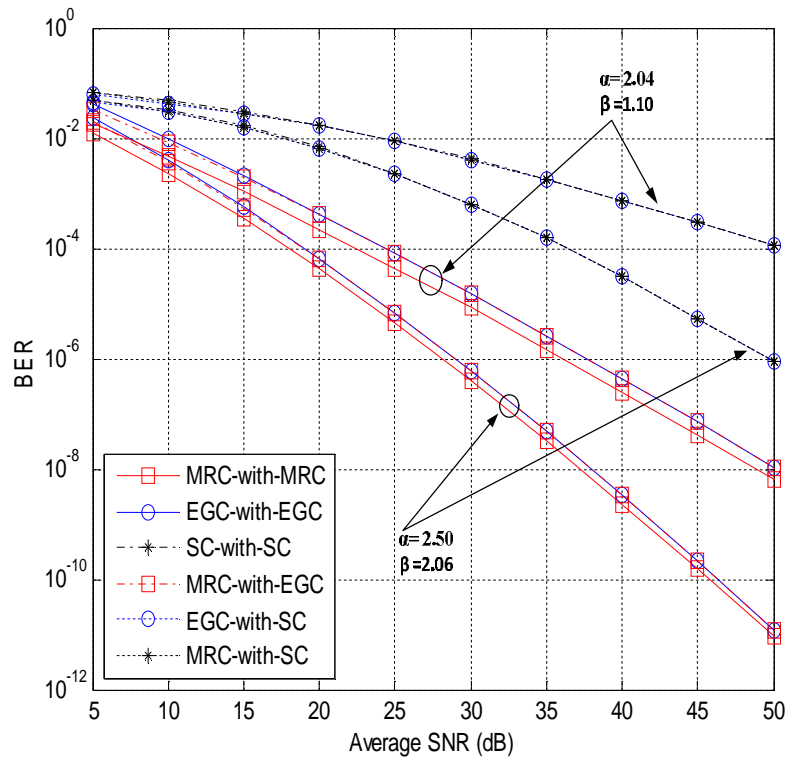
Figure 4.5: Comparison between dual-hop system with the same and different combiners at the relay and destination under different turbulence conditions when $N_r^R = 2$ and $N_r^D = 4$

Dual-hop technology introduces two channels between the source and the destination. As a result of this, the effect of having symetrical and non-symeterical channel conditions between S and D is illustrated in Figure 4.6 with the same combiner at the R and D. It can be clearly shown that symetrical channel significantly degrades the system peformance as compared with non-symetrical channel conditions. Thus, in all cases, MRC-MRC systems yield the best performance compared with other systems. For instance, at a SNR of $30\ dB$ over a strong symmetric channel, MRC-MRC system offers an ABER of 10^{-5} as compared with SC-SC system of 10^{-2}. It can also be deduced that there is an improvement of $5\ dB$ for MRC-MRC system over symetrical and non-symeterical channel system at ABER of 10^{-6}.
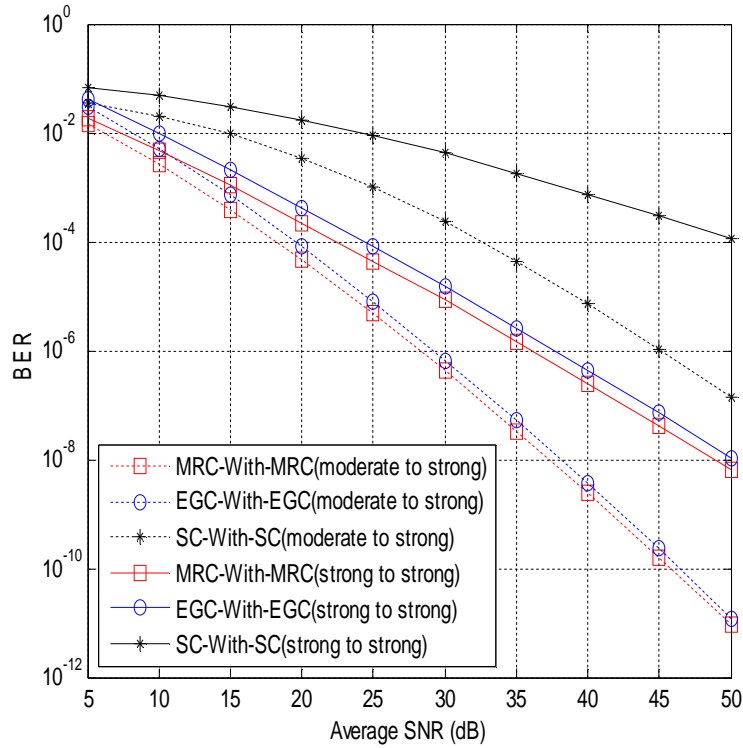
Figure 4.6: Performance of dual-hop system over symmeteric and non-symeteric turbulence channel when $N_r^R = 2$ and $N_r^D = 4$

In Figure 4.7, it is illustrated that the increase in the number of receive photo-detectors at the R and D significantly improves the dual-hop error performance against the atmospheric turbulence. The increment effect in the receive photo-detector caused the MRC-MRC dual-hop system to have the best performance among other systems in all channel cases. For example, MRC-MRC achieved an ABER of 10^{-9} when both the R and D are equipped with six received photo-detectors as compared with MRC-SC and SC-SC of ABER value of 10^{-7} over a non-symmetric channel. It should be noted that the change in channel condition does not affect the performance of MRC-SC system.

The effect of average SNR on the dual-hop systems error performance is illustrated in Figure 4.8 over a strong atmospheric turbulence. It is clearly shown that when the average received SNR on the S-to-R link is less than the average received SNR on the R-to-D link; there is upward shift in the error performance for the entire system. For instance, at ABER of 10^{-5}, the condition caused the performance of the MRC-MRC system to reduce by $5\,dB$ as compared to EGC-EGC of $5.4\,dB$ and the worst performance is observed in the case of SC with the SNR value of $15\,dB$. Generally, it is observed that as the average received SNR on

110

the S-to-R link is increasing more than the average received SNR on the R-to-D link, then the more the system error performance improves. This is clearly illustrated in Figure 4.9 where the EGC is considered at the relay and destination terminals with the system performance shift inward. By the way of illustration, at average SNR of $35\ dB$, the dual-hop systems with EGC at both R and D achieve an ABER of 10^{-8}, 10^{-7} and 10^{-9} respectively when the received SNR of S-to-R link is increased by the order of $1/5, 1$, and 5 magnitude of the average received SNR of R-to-D link.

Also, the comparison between the effect of symmetric and non-systematic average received SNR on the systems performance are illustrated in Figure 4.10 when the same and different combiners are considered at the R and D terminals. As it is mentioned earlier, the increase in average received SNR on the S-to-R link significantly improves the system performance with EGC-EGC dual-hop system having the best performance compared with MRC-SC in all cases. For instance, at an ABER of 10^{-6}, EGC-EGC yields an improvement of $6\ dB$ when the average received SNR of S-to-D is increased by $5\ dB$, while the MRC-SC offers $8\ dB$.
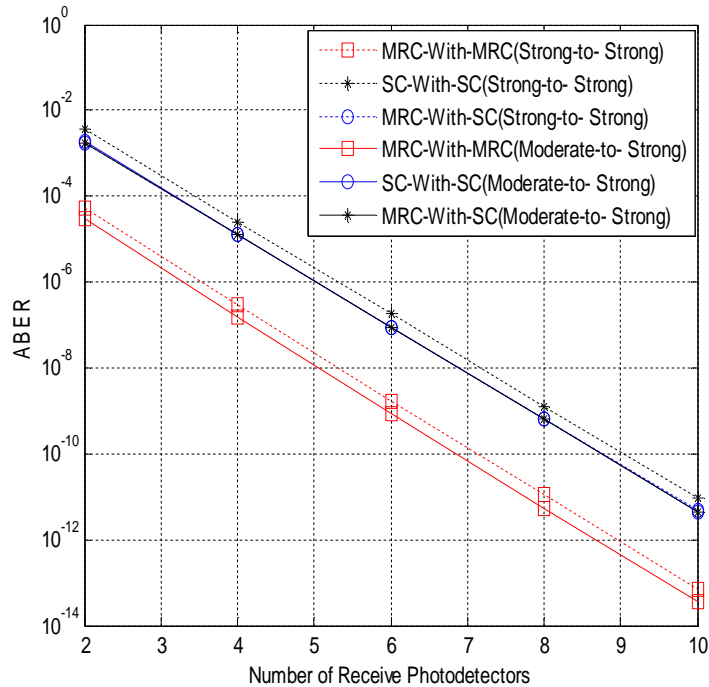
Figure 4.7: Effect of receive photo-detector on the system over symmetric and non-symmetric turbulence channel
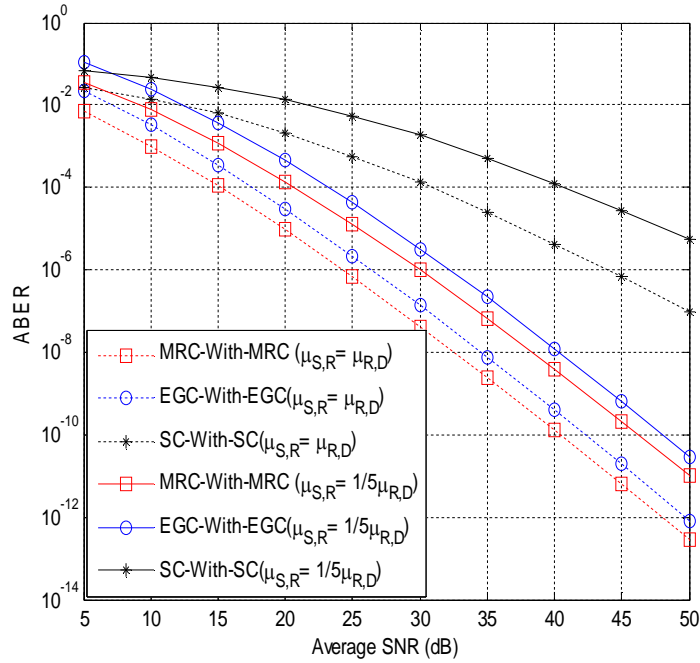
Figure 4.8: Performance comparison between when $\mu_{SR} = \mu_{RD}$ and $\mu_{SR} = 1/5\mu_{RD}$ over strong turbulence for $N_r^R = 4$ and $N_r^D = 4$ with same combiner
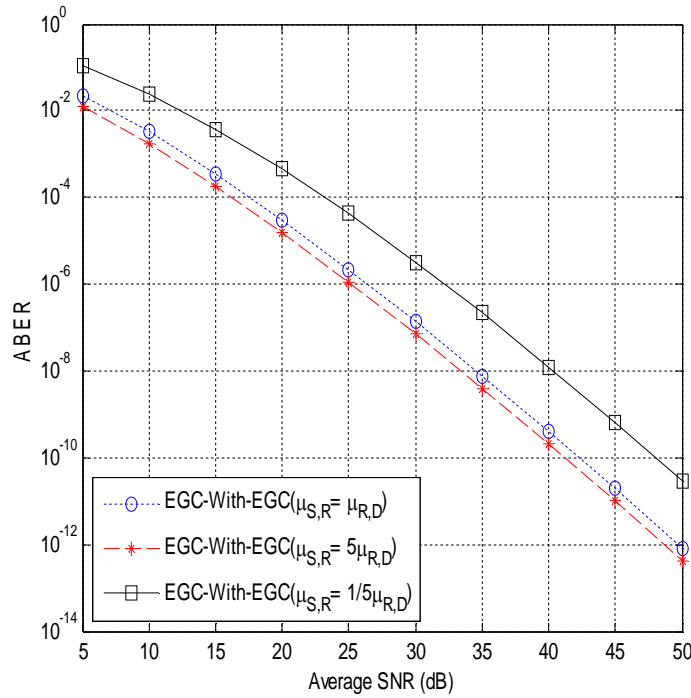
Figure 4.9: ABER Performance comparis at the different values of average SNR at the destination
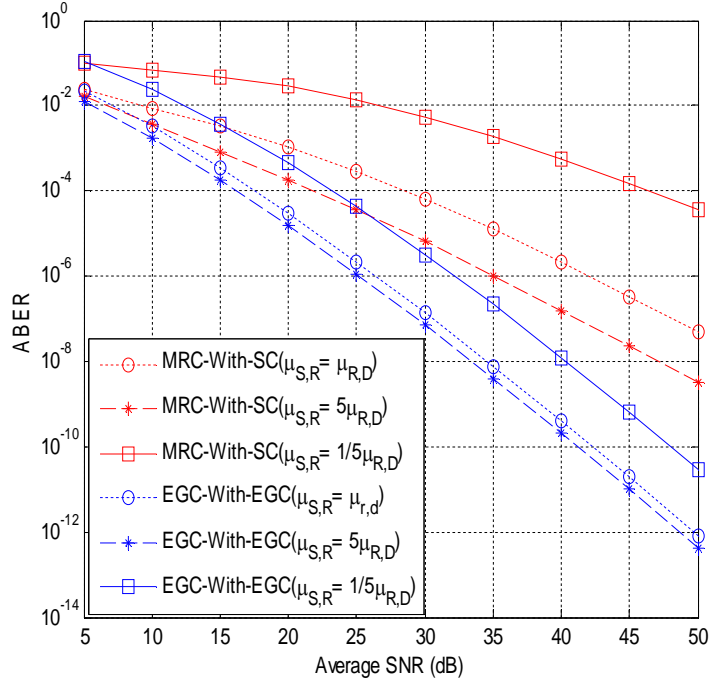
Figure 4.10: ABER Performance comparison between dual-hop system with different and identical combiners over strong turbulence for different values of average SNR

4.2 Optical Spatial Modulation with Diversity Combiner in Dual-Hop Amplify-and-Forward Relay Systems over Atmospheric Impairments

In this section, the analysis of average BER and effective capacity of a dual-hop FSO-SM CSI-assisted AF relay system with diversity combiner over atmospheric turbulence and/or pointing error is reported. MRC and EGC are the two combining techniques considered as mitigation tools against the channel impairments.

4.2.1   System Model

Figure 4.11 illustrates a dual-hop SM-based relay FSO system with the Source (S) as transmitter, Destination (D) as receiver and Relay (R). The S-to-R and R-to-D links are assumed to be independent, non-identical channel and heterodyne detection is considered at D. The Source and the Destination are respectively equipped with N_t^S transmit lasers and N_r^D photo-detectors. The relay (R) in the system operates as Channel State Information (CSI)-assisted AF protocol and the destination employed spatial diversity combiner such MRC and EGC. The system conducts transmission in two time slots. In the first phase, at the source, random sequence of bits stream to be transmitted are mapped into block of q-bits that is

$q = log_2(N_tM)$ of $X = [x_1, x_2, x_3 \ldots \ldots x_{N_t}]^T$. The first group of these bits $log_2(N_t)$ are used to represent the transmit laser index j^{th} with the laser array while the remaining $log_2(M)$ bits identify the BPSK modulation symbol x_p in the signal constellation produced by MZM. During this phase, the information bits are modulated on the electric field of an optical beam as $x_p = x_p \exp(j\phi_{x_p})$ and are then emitted from the active transmit-laser index j at an instance over the optical atmospheric channel as:

$$X_{jp} = \begin{bmatrix} 0 & 0 \cdots & \overbrace{x_p e^{j\phi_{x_p}}}^{j^{th}\,laser\,position} & \cdots 0 & 0 \end{bmatrix}^T \tag{4.36}$$

At any instance of time, the received electric field at the aperture plane of the relay is the sum of the optical field from the transmitter and the Local oscillator at the relay which can be expressed by following (2.6) as:

$$E_R(t) = E_s(t) + E_L(t)$$
$$\triangleq \sqrt{2P_tZ_o}|X_{jp}H_{SR}|cos\left(\omega_{0,S}t + \phi_{h,S} + \phi_{x_p}\right) + \sqrt{2P_{LO}Z_o}cos(\omega_{LO,R}t) \tag{4.37}$$

where

$E_s(t) = \sqrt{2P_{t,S}Z_o}|X_{jp}H_{SR}|cos\left(\omega_{0,S}t + \phi_{h,S} + \phi_{x_p}\right)$ is the optical field from the transmitter and $E_L(t) = \sqrt{2P_{LO,R}Z_o}cos(\omega_{LO,R}t)$ is the LO field. $H_{SR} = |h_{SR}|e^{j\phi_{h,S}}$ denotes the fading factor with the h_{SR} and $\phi_{h,S}$ are the fading gain and the link phase between the source and the relay.

Thus, the photocurrent at the relay photo-detector output can be obtained, following (2.7), as:

$$i_R(t) = RP_{t,S}|X_{jp}H_{SR}|^2 + RP_{L,R} + 2R\sqrt{P_tP_{LO,R}}|X_{jp}H_{SR}|cos\left(\omega_{IF,R}t - \phi_{h,S} - \phi_{x_p}\right) \tag{4.38}$$

where $I_{DC,S} \triangleq RP_{t,S}|X_{jp}H_{SR}|^2$ and $I_{DC,L} \triangleq RP_{L,R}$ is the DC current generated due to signal and LO electric field respectively. $I_{AC} \triangleq 2R\sqrt{P_{t,S}P_{L,R}}|X_{jp}H_{SR}|cos\left(\omega_{IF,R}t - \phi_{h,S} - \phi_{x_p}\right)$ is the AC current which contains the useful information about the frequency and the phase of the received signal at the relay. The total output of DC current at the photo-detector can be approximately equal to $RP_{L,R}$. Therefore, the shot noise impairment during the photo-

detection process at this stage is dominated by LO shot noise with variance of $\sigma_{short,L,R}^2 = 2q_e R P_{LO} B_e$. In other words, the instantaneous SNR of the optical receiver can be defined as the ratio of time-average AC photocurrent and the total noise [37] and thus the SNR for the heterodyne relay receiver can be expressed, following the (2.15), as:

$$\gamma_{SR} = \frac{RP_t |X_{jp} H_{SR}|^2}{q_e B_e} \triangleq \bar{\gamma}_{SR} |X_{jp} H_{SR}|^2 \tag{4.39}$$

Based on the $SNR_{(Het),SR}$, the sufficient statistics at the relay can be modeled as [90, 140]:

$$y_R(t) = \sqrt{\bar{\gamma}_{SR}} H_{SR} X_{jp} + n_R(t) \tag{4.40}$$

where $\bar{\gamma}_{SR} = RP_t / (q_e \Delta f)$ is the average received SNR at the relay system and $n_R(t)$ is the noise term at the relay dominated by LO shot noise modeled as AWGN with zero-mean and $\sigma_{short,L,R}^2$.

During the second phase, the photocurrent $i_R(t)$ at the relay photo-detector output is then amplified by the relay gain *G,* converted to optical signal and retransmitted to the destination. At the destination, using the same approach at the relay, the received optical signal at the nth heterodyne receiver at the destination can be expressed as:

$$E_{D,n}(t) = \sqrt{2P_{t,R} Z_o} |y_R(t) G H_{RD}| cos(\omega_{O,R} t + \phi_{h,R}) + \sqrt{2P_{L,D}} cos(\omega_{LO,D} t) \tag{4.41}$$

where $E_s(t) \triangleq \sqrt{2P_t Z_o} |y_R(t) G H_{RD}| cos(\omega_{LO} t + \phi_{h,R})$ is the electric field transmitted by relay and $E_{L,D}(t) \triangleq \sqrt{2P_{L,D} Z_o} cos(\omega_{LO,D} t)$ is the LO electric field at the destination. $H_{RD} \triangleq |h_{RD}| e^{j\phi_{h,R}}$ is the fading factor having the h_{RD} and $\phi_{h,R}$ as the fading gain and the link phase respectively between the relay and the destination.

The photocurrent at the nth photo-detector at the destination can be similarly obtained as:

$$i_{D,n}(t) = \frac{R}{Z_o} [E_s(t) + E_L(t)]^2$$
$$\triangleq RP_{t,R} |y_R(t) G H_{RD}|^2 + RP_{L,R} G H_{RD} + 2R\sqrt{P_{t,R} P_{L,R}} |y_R(t) G H_{RD}| cos(\omega_{IF} t - \phi_{h,R}) \tag{4.42}$$

where $I_{DC,s} \triangleq RP_{t,R} |y_R(t) G H_{RD}|^2$ and $I_{DC,L} \triangleq RP_{L,R} G H_{RD}$ are the DC current generated due to signal and LO electric field respectively at the nth heterodyne receiver at the

destination. $I_{AC,D} \triangleq 2R\sqrt{P_t P_{L,R}}|y_R(t)GH_{RD}|\cos(\omega_{IF}t - \phi_{h,R})$ is the AC current which contains the useful information about the frequency and the phase of the received signal at the destination. The shot noise impaired during the photo-detection process at this stage is also dominated by destination LO short noise with variance of $\sigma_{short,L,D}^2 = 2q_e R P_{L,D} B_e$. The SNR on the R-to-D link for the nth heterodyne receiver can therefore be expressed as:

$$\gamma_{RD} = \frac{RP_t|sH_{RD}|^2}{q_e B_e} \triangleq \bar{\gamma}_{RD}|sH_{RD}|^2 \tag{4.43}$$

where $s = y_R(t)G$ is the amplified signal transmitted from the relay unit to the destination.

The received signal at the nth heterodyne receiver can be statistically obtained as:

$$y_D(t) = \sqrt{\bar{\gamma}_{RD}}GH_{RD}y_R(t) + n_D(t)$$

$$\triangleq \sqrt{\bar{\gamma}_{RD}}GH_{RD}\left(\sqrt{\bar{\gamma}_{SR}}H_{SR}X_{jp} + n_R(t)\right) + n_D(t) \tag{4.44}$$

$$\triangleq \underbrace{\sqrt{\bar{\gamma}_{RD}\bar{\gamma}_{SR}}GH_{RD}H_{SR}X_{jp}}_{signal\ part} + \underbrace{\sqrt{\bar{\gamma}_{RD}}GH_{RD}n_R(t) + n_D(t)}_{Noise\ part}$$

In this study, the receiver is assumed to have full CSI and therefore after the normalization of the noise, the received signal at the nth heterodyne receiver at the destination can be further simplified as:

$$y_D(t) = \sqrt{K}H_{RD}X_{jp} + \hat{n}(t) \tag{4.45}$$

where $K = \frac{G^2 H_{RD}^2 \bar{\gamma}_{RD}\bar{\gamma}_{SR}}{\bar{\gamma}_{RD}G^2 H_{RD}^2 + 1}$ with G denotes the amplification factor at the relay and $\hat{n}(t)$ is the complex additive with Gaussian noise (AWGN) at the input of the destination having similar statistical characteristic as $n_R(t)$.

At destination, an optimum ML detection is considered to detect the transmitted SM signal vector X_{jp} from the Source after the signal is combined by spatial diversity combiner. When the detector is applied, the estimated laser index $\hat{j}$ and the transmitted constellation symbol index $\hat{p}$ at a specific time instance can be expressed following (2.36) as [171]:

$$[\hat{j}, \hat{p}] = \underset{\hat{j}, \hat{p}}{argmax} \; p_Y\left(y_D \middle| X_{jp}, H_{RD}\right)$$

$$\triangleq \underset{\hat{j}, \hat{p}}{argmin} \; \sqrt{K}\left\|h_l^D x_p\right\|_F^2 - 2Re\left\{y_D^H h_{RD} x_p\right\}$$

(4.46)

In view of (2.47), the equivalent end-to-end SNR that is, the instantaneous received SNR at the destination can be obtained as [71, 116, 222]:

$$\gamma_{eq} = \frac{\gamma_1 \gamma_2}{\gamma_1 + \gamma_2} \triangleq \left(\sum_{i=1}^{2}\frac{1}{\gamma_i}\right)^{-1}, i\epsilon \; (1,2)$$

(4.47)

where γ_1 and γ_2 are the instantaneous SNR at S-to-R and R-to-S links respectively which are define in equations (4.39) and (4.43). It is assumed that both links have the same average SNR obtained as $\bar{\gamma}_1 = \bar{\gamma}_2 = RP_t / (q_e \Delta f)$. Thus, the upper bound for the end-to-end SNR γ_{eq} can be derived by using the well-known inequality between geometric and harmonic means for the random variable $\bar{\gamma}_1$ and $\bar{\gamma}_2$ which is given as [71, 116]:

$$\gamma_{eq} \leq \gamma_a = \frac{1}{2}\prod_{i=1}^{2}\gamma_i$$

(4.48)
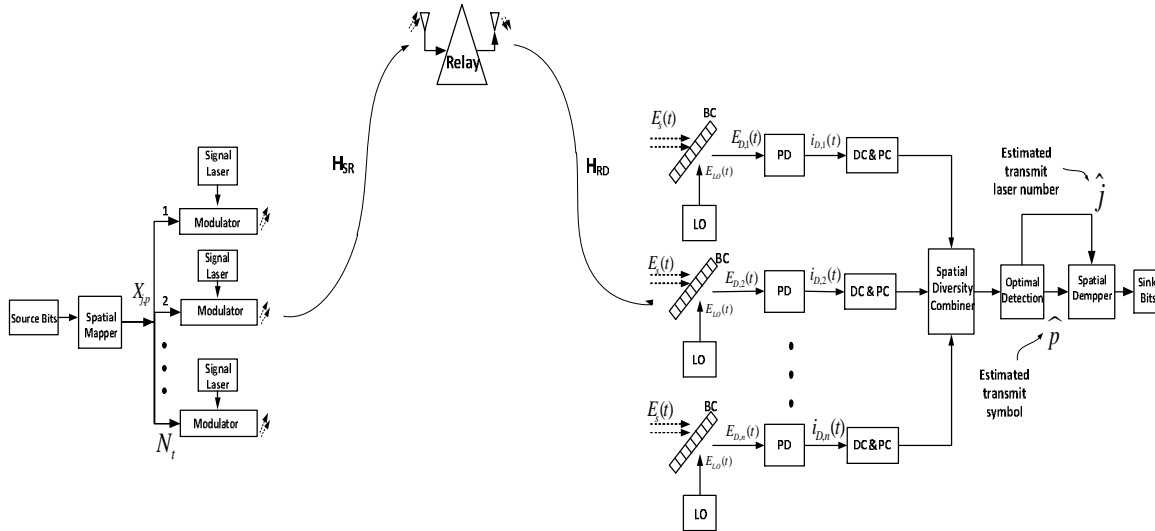
Figure 4.11: Dual-hop FSO-SM AF relay FSO system where PD: Photo-detector, LO: Local Oscillator, BC: Beam Combiner, DC: Down Converter, and PC: Phase Compensator

4.2.2   Statistical Characteristics of End-to-End SNR

The channel statistical model of Gamma-Gamma atmospheric turbulence for modeling FSO link with the conditions from weak to strong turbulence has been stated in (2.20) and the model PDF can be expressed as:

$$f_{H_{mk}}(h_a) = \frac{2(\alpha\beta)^{\frac{\alpha+\beta}{2}}}{\Gamma(\alpha)\Gamma(\beta)} h_a^{\frac{\alpha+\beta}{2}-1} K_{\alpha-\beta}\big(2\sqrt{\alpha\beta h_a}\big), \qquad h_a > 0 \tag{4.49}$$

Expressing $K_v(x)$ in terms of Meijer-G function, the PDF of the Gamma-Gamma channel has been defined in (2.51) as:

$$f_{H_{mk}}(h_a) = \frac{(\alpha\beta)^{\frac{\alpha+\beta}{2}}}{\Gamma(\alpha)\Gamma(\beta)} h_a^{\frac{\alpha+\beta}{2}-1} G_{0,2}^{2,0}\left(\alpha\beta h_a \left| \frac{-,-}{\frac{\alpha-\beta}{2}, \frac{\beta-\alpha}{2}}\right.\right), \qquad h_a > 0 \tag{4.50}$$

Also, the Gamma-Gamma channel PDF can be defined in terms of generalized power series representation method of the modified Bessel function of the second kind as is it defined in (2.53):

$$f_{H_{mk}}(h_a) = \sum_{g=0}^{\infty}\left[m_g(\alpha,\beta)h_a^{g+\beta-1} + m_g(\beta,\alpha)h_a^{g+\alpha-1}\right] \tag{4.51}$$

4.2.3   Under the Influence of Atmospheric Turbulence without Pointing Error

In this section, the MGF, PDF and CDF of the end-to-end SNR γ_a defined in (4.48) are derived, by assuming that independent non-identical distribution Gamma-Gamma turbulence channel.

4.2.3.1 MGF of the End-to-End SNR γ_a

The MGF of the end-to-end SNR γ_a can be derived in closed form as:

$$M_{\gamma_a}(-s) = \int_0^{\infty}\int_0^{\infty}\left[exp-\left(s\prod_{i=1}^{2}\gamma_i^{1/2}\right)\right]\left[\prod_{i=1}^{2} f_{\gamma_i}(\gamma_i)\right] d\gamma_i$$

$$\triangleq \int_0^{\infty}\int_0^{\infty} exp\left(-s\gamma_1^{\frac{1}{2}}\gamma_2^{\frac{1}{2}}\right) f_{\gamma_1}(\gamma_1) f_{\gamma_2}(\gamma_2) d\gamma_1 d\gamma_2 \tag{4.52}$$

It should be noted here that the Gamma-Gamma PDF defined in (4.50) and (4.51) may be used to evaluate the MGF defined in (4.52). However, the integrals of the equation will yield infinite and untraceable result if (4.51) is applied to compute these integrals and therefore the exact closed-form expression for the end-to-end SNR cannot be obtained. As a result of this, PDF defined in (4.50) is applied to determine the MGF as follows:

Utilizing a random variable transformation through (4.39) or (4.43), the PDF in terms of end-to-end SNR for the Gamma-Gamma distribution can be expressed as:

$$f_{\gamma_i}(\gamma_i) = \frac{(\alpha_i\beta_i)^{\frac{\alpha_i+\beta_i}{2}}\gamma_i^{\frac{\alpha_i+\beta_i}{4}-1}}{2\Gamma(\alpha_i)\Gamma(\beta_i)\bar{\gamma}_i^{\frac{\alpha_i+\beta_i}{4}}} G_{0,2}^{2,0}\left(\frac{\alpha\beta}{\sqrt{\bar{\gamma}_i}}\sqrt{\gamma_i}\,\middle|\,\frac{-,-}{\frac{\alpha_i-\beta_i}{2},\frac{\beta_i-\alpha_i}{2}}\right) \tag{4.53}$$

By letting $\Xi_i = \frac{\alpha\beta}{\sqrt{\bar{\gamma}_i}}$ and applying the Meijer-G identity defined in [205,equation (9.31.5)], then the PDF can be expressed as:

$$f_{\gamma_i}(\gamma_i) = \frac{\left(\Xi_i\sqrt{\gamma_i}\right)^{\frac{\alpha_i+\beta_i}{2}}}{2\Gamma(\alpha_i)\Gamma(\beta_i)}\gamma_i^{-1} G_{0,2}^{2,0}\left(\Xi_i\sqrt{\gamma_i}\,\middle|\,\frac{-,-}{\frac{\alpha_i-\beta_i}{2},\frac{\beta_i-\alpha_i}{2}}\right)$$
$$\triangleq \frac{1}{2\Gamma(\alpha_i)\Gamma(\beta_i)}\gamma_i^{-1} G_{0,2}^{2,0}\left(\Xi_i\sqrt{\gamma_i}\,\middle|\,\frac{-,-}{\frac{\alpha_i}{2},\frac{\beta_i}{2}}\right) \tag{4.54}$$

The first integration in (4.52), that is the one on γ_1, is of the form:

$$\mathfrak{T}_1(s) = \frac{1}{2\Gamma(\alpha_1)\Gamma(\beta_1)}\int_0^\infty \gamma_1^{-1} G_{0,2}^{2,0}\left(\Xi_1\sqrt{\gamma_1}\,\middle|\,\frac{-,-}{\frac{\alpha_1}{2},\frac{\beta_1}{2}}\right) exp\left(-sV\gamma_1^{1/2}\right)d\gamma_1 \tag{4.55}$$

where $V = \frac{\sqrt{\gamma_2}}{2}$

Using a Meijer-G identity of the exponential function in [203,equation (11)] (see Appendix A2.4) to the (4.55), then,

$$\mathfrak{T}_1(s) = \frac{1}{2\Gamma(\alpha_1)\Gamma(\beta_1)}\int_0^\infty \gamma_1^{-1} G_{0,2}^{2,0}\left(\Xi_1\sqrt{\gamma_1}\,\middle|\,\frac{-,-}{\frac{\alpha_1}{2},\frac{\beta_1}{2}}\right) G_{0,1}^{1,0}\left(sV\gamma_1^{1/2}\,\middle|\,\frac{-}{0}\right)d\gamma_1 \tag{4.56}$$

Let $Z = \gamma_1^{1/2}$, $Z^2 = \gamma_1$, $\frac{d\gamma_1}{dZ} = 2Z$ and $d\gamma_1 = 2ZdZ$, then apply the integral identity in [203, equation (21)] (see Appendix A3.5) to (4.56), then,

$$\mathfrak{T}_1(s) = \frac{1}{2\Gamma(\alpha_1)\Gamma(\beta_1)} \int_0^\infty Z^{-1} G_{0,2}^{2,0}\left(\Xi_1 Z \left|\begin{matrix} -, & - \\ \frac{\alpha_1}{2}, \frac{\beta_1}{2} \end{matrix}\right.\right) G_{0,1}^{1,0}\left(sVZ \left|\begin{matrix} - \\ 0 \end{matrix}\right.\right) dZ$$

(4.57)

$$\triangleq \frac{1}{\Gamma(\alpha_1)\Gamma(\beta_1)} G_{2,1}^{1,2}\left(\frac{sV}{\Xi_1} \left|\begin{matrix} 1 - \alpha_1, 1 - \beta_1 \\ 0 \end{matrix}\right.\right)$$

Using the similar method, the integration on γ_2 can be obtained by substituting (4.57) into (4.52) and apply the same integral identity, then $\mathfrak{T}_2(s)$ can be obtained as:

$$\mathfrak{T}_2(s)$$
$$= \frac{1}{\Gamma(\alpha_1)\Gamma(\beta_1)} \frac{1}{2\Gamma(\alpha_2)\Gamma(\beta_2)} \int_0^\infty \gamma_2^{-1} G_{0,2}^{2,0}\left(\Xi_2 \sqrt{\gamma_2} \left|\begin{matrix} -, & - \\ \alpha_2, \beta_2 \end{matrix}\right.\right) G_{2,1}^{1,2}\left(\frac{sV}{\Xi_1} \sqrt{\gamma_2} \left|\begin{matrix} 1 - \alpha_1, 1 - \beta_1 \\ 0 \end{matrix}\right.\right) d\gamma_2$$

(4.58)

$$\triangleq \frac{1}{\Gamma(\alpha_1)\Gamma(\beta_1)} \frac{1}{\Gamma(\alpha_2)\Gamma(\beta_2)} G_{4,1}^{1,4}\left(\frac{sV}{\Xi_1 \Xi_2} \left|\begin{matrix} 1 - \alpha_1, 1 - \beta_1, 1 - \alpha_2, 1 - \beta_2 \\ 0 \end{matrix}\right.\right)$$

Thus, by substituting (4.57) and (4.58) into (4.52), then the MGF can be obtained as:

$$M_{\gamma_b}(s) = \prod_{i=1}^{2} \frac{1}{\Gamma(\alpha_i)\Gamma(\beta_i)} G_{4,1}^{1,4}\left(\frac{s}{2\Xi_1 \Xi_2} \left|\begin{matrix} 1 - \alpha_1, 1 - \beta_1, 1 - \alpha_2, 1 - \beta_2 \\ 0 \end{matrix}\right.\right)$$

(4.59)

4.2.3.2   PDF of End-to-End SNR γ_a

The PDF of γ_b can be determined by applying the inversed Laplace Transform $\mathcal{L}^{-1}$ to the MGF in (4.59), and this can be expressed as $f_{\gamma_a}(\gamma) = \mathcal{L}^{-1}\{M_{\gamma_a}(s), \gamma\}$. Applying the identity [223, equation (3.40.1.1)] (see Appendix A4.1) for the inverse Laplace transform of the Meijer-G function, the PDF of γ_b in closed form can be obtained as:

$$f_{\gamma_a}(\gamma) = \gamma^{-1} \prod_{i=1}^{2} \frac{1}{\Gamma(\alpha_i)\Gamma(\beta_i)} G_{4,1}^{1,4}\left(2\gamma \prod_{i=1}^{2} \Xi_i \left|\begin{matrix} - \\ \alpha_1, \beta_1, \alpha_2, \beta_2 \end{matrix}\right.\right)$$

(4.60)

4.2.3.3   CDF of End-to-End SNR γ_a

The CDF of the γ_a can be defined as $F_{\gamma_a}(\gamma) = \int_0^\gamma f_{\gamma_a}(\gamma) d\gamma$. Applying the integral identity stated in [203, equation (26)] (see Appendix A3.4), the CDF can therefore be obtained as follows:

$$F_{\gamma_b}(\gamma) = \prod_{i=1}^{2} \frac{1}{\Gamma(\alpha_i)\Gamma(\beta_i)} \int_0^\gamma \gamma^{-1} \prod_{i=1}^{2} \frac{1}{\Gamma(\alpha_i)\Gamma(\beta_i)} G_{4,1}^{1,4}\left(2\gamma \prod_{i=1}^{2} \Xi_i \left|\begin{matrix} - \\ \alpha_1, \beta_1, \alpha_2, \beta_2 \end{matrix}\right.\right)$$

$$\triangleq \prod_{i=1}^{2} \frac{1}{\Gamma(\alpha_i)\Gamma(\beta_i)} G_{1,5}^{4,1}\left(2\gamma \prod_{i=1}^{2} \Xi_i \left|\begin{matrix} 1 \\ \alpha_1, \beta_1, \alpha_2, \beta_2, 0 \end{matrix}\right.\right)$$

(4.61)

4.2.4 Under the Combined Influence of Atmospheric Turbulence and Pointing Error

The PDF of the misalignment fading due to pointing error (h_p) loss can be expressed by considering the Raleigh distributions for both the horizontal and vertical displacement (sway) at the receiver as is it given in (2.28):

$$f_{H_{mk}}(h_p) = \frac{\xi^2}{A_o^{\xi^2}} h_p \xi^2 - 1 \,, 0 \leq h_p \leq A_o$$

(4.62)

The combined distributions of $h = h_a h_p$ can be obtained as:

$$f_{H_{mk}}(h) = \int_{h/A_o}^{\infty} f_h(h_a) f_{h|h_a}(h|h_a) dh_a$$

(4.63)

where $f_{h|h_a}(h|h_a)$ is the conditional probability given a distribution state h_a and can be expressed as:

$$f_{h|h_a}(h|h_a) = \frac{\xi^2}{A_o^{\xi^2} h_a} \left(\frac{h}{h_a}\right)^{\xi^2 - 1}$$

(4.64)

Considering the impact of pointing error impairment, the PDF of the combined channel can therefore be expressed by substituting (4.50) and (4.64) into (4.63) as:

$$f_{H_{mk}}(h) = \frac{\alpha\beta\xi^2}{A_o\Gamma(\alpha)\Gamma(\beta)} G_{4,1}^{1,4}\left(\frac{\alpha\beta}{A_o}h \left|\begin{matrix} \xi^2 \\ \xi^2 - 1, \alpha - 1, \beta - 1 \end{matrix}\right.\right)$$

(4.65)

The PDF of γ_i is obtained by using simple random variable transformation of the (4.50) and is expressed as:

$$f_{\gamma_i}(\gamma_i) = \frac{\xi_i^2}{2\gamma_i \Gamma(\alpha_i)\Gamma(\beta_i)} G_{1,3}^{3,0}\left(\alpha_i\beta_i \sqrt{\frac{\gamma_i}{\bar{\gamma}_i}} \left|\begin{matrix} \xi_i^2 + 1 \\ \xi_i^2, \alpha_i, \beta_i \end{matrix}\right.\right)$$

(4.66)

4.2.4.1 MGF of End-to-End SNR γ_a for the Pointing Error

Following the same approach used in obtaining the MGF of end-to-end SNR without pointing error, the MGF of end-to-end SNR with pointing error can thus be obtained by using (4.54), and the first integral on γ_1 is expressed as:

$$\mathfrak{I}_1(s) = \frac{\xi_1^2}{2\Gamma(\alpha_1)\Gamma(\beta_1)} \int_0^\infty \gamma_1^{-1} G_{1,3}^{3,0}\left(\alpha_1\beta_1\sqrt{\frac{\gamma_1}{\bar{\gamma}_1}} \,\middle|\, \begin{matrix} \xi_1^2 + 1 \\ \xi_1^2, \alpha_1, \beta_1 \end{matrix}\right) G_{0,1}^{1,0}\left(sV\gamma_1^{1/2} \,\middle|\, \begin{matrix} - \\ 0 \end{matrix}\right) d\gamma_1 \tag{4.67}$$

By letting $Z = \gamma_1^{1/2}$, $Z^2 = \gamma_1$, $\frac{d\gamma_1}{dZ} = 2Z$ and $d\gamma_1 = 2ZdZ$, then the integration of $\mathfrak{I}_1(S)$ can be solved using [203,equation (21)] (see Appendix A3.5) as:

$$\mathfrak{I}_1(s) = \frac{\xi_1^2}{2\Gamma(\alpha_1)\Gamma(\beta_1)} \int_0^\infty Z^{-1} G_{1,3}^{3,0}\left(\alpha_1\beta_1\sqrt{\frac{\gamma_1}{\bar{\gamma}_1}} \,\middle|\, \begin{matrix} \xi_1^2 + 1 \\ \xi_1^2, \alpha_1, \beta_1 \end{matrix}\right) G_{0,1}^{1,0}\left(sVZ \,\middle|\, \begin{matrix} - \\ 0 \end{matrix}\right) dZ$$

$$\triangleq \frac{\xi_1^2}{\Gamma(\alpha_1)\Gamma(\beta_1)} G_{2,3}^{3,1}\left(\frac{\alpha_1\beta_1}{sV\sqrt{\bar{\gamma}_1}} \,\middle|\, \begin{matrix} 1, \xi_1^2 + 1 \\ \xi_1^2, \alpha_1, \beta_1 \end{matrix}\right) \tag{4.68}$$

To solve the second integral in (4.54), substitute for $\mathfrak{I}_1(s)$ and follow the same approach by applying the integral identity given in [203, equation (21)], then the MGF is therefore obtained as:

$$M_{\gamma_a}(s) = \prod_{i=1}^{2}\left[\frac{\xi_i^2}{\Gamma(\alpha_i)\Gamma(\beta_i)}\right] G_{3,6}^{6,1}\left(\frac{2}{s}\prod_{i=1}^{2}\Xi_i \,\middle|\, \begin{matrix} 1, \psi_3 \\ \psi_1, \psi_2 \end{matrix}\right) \tag{4.69}$$

where $\psi_1 = \alpha_1, \beta_1\alpha_2, \beta_2$, $\psi_2 = \xi_1^2, \xi_2^2$ and $\psi_3 = \xi_1^2 + 1, \xi_2^2 + 1$

4.2.4.2 PDF of End-to-End SNR γ_a for the Pointing Error

To determine the PDF of the end-to-end SNR, $f_{\gamma_a}(\gamma)$, the inverse Laplace transform is applied to (4.69) using the identity given in [223,equation (30.40.1.1)] (see Appendix A4.1) as:

$$f_{\gamma_a}(\gamma) = \gamma^{-1}\prod_{i=1}^{2}\left[\frac{\xi_i^2}{\Gamma(\alpha_i)\Gamma(\beta_i)}\right] G_{3,6}^{6,1}\left(2\gamma\prod_{i=1}^{2}\Xi_i \,\middle|\, \begin{matrix} \psi_3 \\ \psi_1, \psi_2 \end{matrix}\right) \tag{4.70}$$

4.2.4.3 CDF of End-to-End SNR γ_a for the Pointing Error

The CDF for the end-to-end SNR can be obtained as $F_{\gamma_a}(\gamma) = \int_0^{\gamma} f_{\gamma_a}(\gamma) d\gamma$. Applying the integral identity stated in [203,equation (26)] (see Appendix A3.4), the CDF can therefore be obtained as follows:

$$
\begin{aligned}
F_{\gamma_a}(\gamma) &= \int_0^{\gamma} \gamma^{-1} \prod_{i=1}^{2} \left[\frac{\xi_i^2}{\Gamma(\alpha_i)\Gamma(\beta_i)} \right] G_{2,6}^{6,0} \left(2\gamma \prod_{i=1}^{2} \Xi_i \left| \begin{matrix} \psi_3 \\ \psi_1, \psi_2 \end{matrix} \right. \right) d\gamma \\
&\triangleq \prod_{i=1}^{2} \left[\frac{\xi_i^2}{\Gamma(\alpha_i)\Gamma(\beta_i)} \right] G_{3,6}^{6,1} \left(2\gamma \prod_{i=1}^{2} \Xi_i \left| \begin{matrix} 1, \psi_3 \\ \psi_1, \psi_2 \end{matrix} \right. \right)
\end{aligned}
\tag{4.71}
$$

4.2.5 Performance Analysis

At the destination, the receiver combines the amplified SM signal transmitted from the relay through the use of MRC and EGC. Thus, to determine the ABER for the proposed FSO-SM dual-hop AF relay system, a well-known boundary technique, adopted in (4.11) is used to evaluate the ABER under the fading condition. The ABER can be bounded as given in [171] by:

$$
ABER_{SM-SD} \leq \frac{(N_t^s M)^{-1}}{\log_2(N_t^s M)} \sum_{j=1}^{N_t^s} \sum_{p=1}^{M} \sum_{\hat{j}=j+1}^{N_t^s} \sum_{\hat{p}=p+1}^{M} N(p, \hat{p}) APEP(X_{j,p} \to X_{\hat{j},\hat{p}})
\tag{4.72}
$$

4.2.5.1 Average Pairwise Error Probability for the MRC Combiner

By following (2.39), the instantaneous SNR at the output of MRC is defined as:

$$
\gamma_t^{MRC} = \sum_{n=1}^{N_r^D} \gamma_{a_n}
\tag{4.73}
$$

where γ_{a_n} is the end-to-end SNR received at the nth heterodyne receiver defined in (4.47). Thus, the PEP can be expressed in terms of instantaneous SNR as [77]:

$$
\begin{aligned}
PEP_{MRC}(X_{j,p} \to X_{\hat{j},\hat{p}}) &= Q\left(\sqrt{2\gamma_t^{MRC}} \right) \\
&\triangleq Q\left(\sqrt{2 \sum_{n=1}^{N_r^D} \gamma_{a_n}} \right)
\end{aligned}
\tag{4.74}
$$

Thus, by averaging the (4.74), the average PEP for the SM-MRC system can be obtained as:

$$APEP_{MRC}\left(X_{j,p} \to X_{\hat{j},\hat{p}}\right) = \int_0^\infty \left(\sqrt{2 \sum_{n=1}^{N_r^D} \gamma_{a_n}} \right) f_{\gamma_{a_n}}(\gamma) d\gamma \qquad (4.75)$$

Using the upper bound of Craig's Q-function defined as $Q(x) \leq 1/2 exp(-x^2/2)$ [181], then the average PEP can be expressed as:

$$APEP_{MRC}\left(X_{j,p} \to X_{\hat{j},\hat{p}}\right) = \frac{1}{2} \int_0^\infty exp\left(-\sum_{n=1}^{N_r^D} \gamma_{a_n} \right) f_{\gamma_a}(\gamma) d\gamma$$

$$\triangleq \frac{1}{2} \prod_{n=1}^{N_r^D} M_{\gamma_{a_n}}(s) \qquad (4.76)$$

To determine the average PEP for the SM-MRC system under the influence of atmospheric turbulence without pointing error, substitute (4.59) into (4.76) as:

$$APEP_{MRC}\left(X_{j,p} \to X_{\hat{j},\hat{p}}\right)$$

$$= \frac{1}{2} \left[\prod_{i=1}^2 \frac{1}{\Gamma(\alpha_i)\Gamma(\beta_i)} G_{4,1}^{1,4} \left(\frac{1}{2\Xi_1\Xi_2} \middle| \begin{matrix} 1-\alpha_1, 1-\beta_1, 1-\alpha_2, 1-\beta_2 \\ 0 \end{matrix} \right) \right]^{N_r^D} \qquad (4.77)$$

Similarly, for the average PEP for the SM-MRC system under the influence of atmospheric turbulence with pointing error, substitute (4.69) into (4.76) as:

$$APEP_{MRC}\left(X_{j,p} \to X_{\hat{j},\hat{p}}\right) = \frac{1}{2} \left[\prod_{i=1}^2 \left[\frac{\xi_i^2}{\Gamma(\alpha_i)\Gamma(\beta_i)} \right] G_{3,6}^{6,1} \left(2 \prod_{i=1}^2 \Xi_i \middle| \begin{matrix} 1, \psi_3 \\ \psi_1, \psi_2 \end{matrix} \right) \right]^{N_r^D} \qquad (4.78)$$

Thus, the average BER for the SM-MRC dual-hop relay system without and with pointing error can therefore be respectively obtained by substituting (4.77) and (4.78) into (4.72) to give:

$$ABER_{MRC(without\ pointing\ error)} \leq \frac{(N_t M)^{-1}}{2\log_2(N_t M)} \sum_{j=1}^{N_t} \sum_{p=1}^{M} \sum_{\hat{j}=j+1}^{N_t} \sum_{\hat{p}=p+1}^{M} N(p,\hat{p})$$

$$\times \left[\prod_{i=1}^{2} \frac{1}{\Gamma(\alpha_i)\Gamma(\beta_i)} G_{4,1}^{1,4}\left(\frac{1}{2\Xi_1\Xi_2}\middle|\begin{array}{c}1-\alpha_1, 1-\beta_1, 1-\alpha_2, 1-\beta_2\\0\end{array}\right)\right]^{N_r^D} \tag{4.79}$$

$$ABER_{MRC(with\ pointing\ error)} \leq \frac{(N_t M)^{-1}}{2\log_2(N_t M)} \sum_{j=1}^{N_t} \sum_{p=1}^{M} \sum_{\hat{j}=j+1}^{N_t} \sum_{\hat{p}=p+1}^{M} N(p,\hat{p})$$

$$\times \left[\prod_{i=1}^{2} \left[\frac{\xi_i^2}{\Gamma(\alpha_i)\Gamma(\beta_i)}\right] G_{3,6}^{6,1}\left(2\prod_{i=1}^{2} \Xi_i \middle|\begin{array}{c}1, \psi_3\\\psi_1, \psi_2\end{array}\right)\right]^{N_r^D} \tag{4.80}$$

4.2.5.2   Average Pairwise Error Probability for the EGC Combiner

In view of (2.14), the instantaneous SNR at the output of EGC is defined as [224]:

$$\gamma_t^{EGC} = \frac{1}{N_r^D}\left(\sum_{n=1}^{N_r^D} \sqrt{\gamma_{a_n}}\right)^2 \tag{4.81}$$

Following the approach detailed in [179, 225], where $\gamma_T = \left(\sum_{n=1}^{N_r^D} \sqrt{\gamma_{a_n}}\right)^2$ represents the sum of N_r^D Gamma-Gamma random variable with mean $\bar{\gamma}_T = N_r^D \bar{\gamma}$, and parameters $\alpha_{\gamma_T} = N_r^D \alpha + \varepsilon_\gamma$ and $\beta_{\gamma_T} = N_r^D \beta$ which contain ε_γ as adjustment parameter for the improvement on the accuracy of the proposed approximation [225] and it is defined as:

$$\varepsilon_\gamma = \left(\frac{1}{N_r^D} - 1\right)\frac{-0.127 - 0.95\alpha - 0.0058\beta}{1 + 0.00124\alpha + 0.98\beta} \tag{4.82}$$

The average PEP for the SM-EGC system can be expressed as:

$$APEP_{EGC}(X_{j,p} \rightarrow X_{\hat{j},\hat{p}}) = \int_0^\infty \left(\sqrt{2\gamma_t^{EGC}}\right) f_{\gamma_a}(\gamma)d\gamma$$

$$\triangleq -\int_0^\infty Q'\left(\sqrt{2\gamma_t^{EGC}}\right) F_{\gamma_a}(\gamma)d\gamma \tag{4.83}$$

where $Q'(.)$ is the derivative of Q-function which is defined in [124] as $Q'(x) = \frac{1}{2\sqrt{\pi}}\exp(-x^2/2)$. Thus, the APEP for the system can then be expressed as:

$$APEP_{EGC}\left(X_{j,p} \to X_{\hat{j},\hat{p}}\right) = \frac{1}{2\sqrt{\pi}} \int_0^\infty \frac{1}{\sqrt{\gamma_T}} \exp\left(-\frac{\gamma_T}{N_r^D}\right) F_{\gamma_a}(\gamma_T) d\gamma_T \tag{4.84}$$

To determine the APER for the SM-EGC dual-hop AF system under the influence of atmospheric turbulence without pointing error, substitute for the CDF defined in (4.61) into (4.84), then average PEP for the system can be expressed as:

$$APEP_{EGC}\left(X_{j,p} \to X_{\hat{j},\hat{p}}\right) \triangleq \frac{1}{2\sqrt{\pi}} \prod_{i=1}^{2} \left[\frac{1}{\Gamma\left(\alpha_{\gamma T_i}\right)\Gamma\left(\beta_{\gamma T_i}\right)}\right] \int_0^\infty \gamma_T^{-\frac{1}{2}}$$
$$\times \exp\left(-\frac{\gamma_T}{N_r^D}\right) G_{4,1}^{1,4}\left(2\gamma_T \prod_{i=1}^{2} \Xi_i \,\middle|\, \begin{matrix} 1 \\ \alpha_{\gamma T 1}, \beta_{\gamma T 1}, \alpha_{\gamma T 2}, \beta_{\gamma T 2}, 0 \end{matrix}\right) d\gamma_T \tag{4.85}$$

Applying the integral identity defined in [205,equation (7.813.1)] (see Appendix A3.3), the APER for the SM-EGC dual-hop AF system under the influence of atmospheric turbulence without pointing error can be expressed as:

$$APEP_{EGC}\left(X_{j,p} \to X_{\hat{j},\hat{p}}\right) \triangleq \frac{1}{2}\sqrt{\frac{N_r^D}{\pi}} \prod_{i=1}^{2} \left[\frac{1}{\Gamma\left(\alpha_{\gamma T_i}\right)\Gamma\left(\beta_{\gamma T_i}\right)}\right]$$
$$\times G_{2,5}^{4,2}\left(2N_r^D \prod_{i=1}^{2} \Xi_i \,\middle|\, \begin{matrix} \frac{1}{2}, 1 \\ \alpha_{\gamma T 1}, \beta_{\gamma T 1}, \alpha_{\gamma T 2}, \beta_{\gamma T 2}, 0 \end{matrix}\right) \tag{4.86}$$

Under the influence of pointing error, using (4.71) in (4.83), the average PEP for the system can be expressed as:

$$APEP_{EGC}\left(X_{j,p} \to X_{\hat{j},\hat{p}}\right) = \frac{1}{2\sqrt{\pi}} \prod_{i=1}^{2} \left[\frac{\xi_i^2}{\Gamma\left(\alpha_{\gamma T_i}\right)\Gamma\left(\beta_{\gamma T_i}\right)}\right] \int_0^\infty \gamma_T^{-1/2} \exp\left(-\frac{\gamma_T}{N_r^D}\right)$$
$$\times G_{3,6}^{6,1}\left(2\gamma_T \prod_{i=1}^{2} \Xi_i \,\middle|\, \begin{matrix} 1, \psi_3 \\ \psi_1, \psi_2 \end{matrix}\right) d\gamma_T \tag{4.87}$$

Apply the integral identity defined in [205,equation (7.813.1)] (see Appendix A3.3), the APER for the SM-EGC dual-hop AF system under the influence of atmospheric turbulence without pointing error can be expressed as:

$$APEP_{EGC}\left(X_{j,p} \rightarrow X_{\hat{j},\hat{p}}\right) = \frac{1}{2}\sqrt{\frac{N_r^D}{\pi}}\prod_{i=1}^{2}\left[\frac{\xi_i^2}{\Gamma\left(\alpha_{\gamma_{T_i}}\right)\Gamma\left(\beta_{\gamma_{T_i}}\right)}\right]G_{4,6}^{6,2}\left(2N_r^D\prod_{i=1}^{2}\Xi_i \left|\begin{array}{c} \frac{1}{2},1,\psi_3 \\ \psi_1,\psi_2 \end{array}\right.\right) \quad (4.88)$$

Thus, the average BER for the SM-EGC dual hop relay system without and with pointing error can therefore be respectively be obtained by substituting (4.86) and (4.88) into (4.72):

$$ABER_{EGC(with\ poning\ error)} \leq \frac{(N_t^S M)^{-1}}{2\log_2(N_t^S M)}\sqrt{\frac{N_r^D}{\pi}}\prod_{i=1}^{2}\left[\frac{\xi_i^2}{\Gamma\left(\alpha_{\gamma_{T_i}}\right)\Gamma\left(\beta_{\gamma_{T_i}}\right)}\right]$$

$$\times \sum_{j=1}^{N_t^S}\sum_{p=1}^{M}\sum_{\hat{j}=j+1}^{N_t^S}\sum_{\hat{p}=p+1}^{M}N(p,\hat{p})\ G_{2,5}^{4,2}\left(2N_r^D\prod_{i=1}^{2}\Xi_i \left|\begin{array}{c} \frac{1}{2},1 \\ \alpha_{\gamma_{T_1}},\beta_{\gamma_{T_1}},\alpha_{\gamma_{T_2}},\beta_{\gamma_{T_2}},0 \end{array}\right.\right) \quad (4.89)$$

$$ABER_{EGC(with\ pointing\ error)} \leq \frac{(N_t^S M)^{-1}}{2\log_2(N_t^S M)}\sqrt{\frac{N_r^D}{\pi}}\prod_{i=1}^{2}\left[\frac{\xi_i^2}{\Gamma\left(\alpha_{\gamma_{T_i}}\right)\Gamma\left(\beta_{\gamma_{T_i}}\right)}\right]$$

$$\times \sum_{j=1}^{N_t^S}\sum_{p=1}^{M}\sum_{\hat{j}=j+1}^{N_t^S}\sum_{\hat{p}=p+1}^{M}N(p,\hat{p})\ G_{4,6}^{6,2}\left(2N_r^D\prod_{i=1}^{2}\Xi_i \left|\begin{array}{c} \frac{1}{2},1,\psi_3 \\ \psi_1,\psi_2 \end{array}\right.\right) \quad (4.90)$$

4.2.6   Effective Capacity for the Systems

The capacity of spatial modulation systems as stated in [169, 226, 227] cannot be determined in the same way it is done in MIMO communication systems. This is because, the number of transmitting antenna represents the added information, and the antenna index signifies the spatial constellation not as the information source as in other MIMO systems. Therefore, using the conventional approach stated in [226], the capacity for the dual-hop spatial modulation with combiners can be expressed as:

$$C_{SM} = log_2(N_t^S M)[1 + P_e log_2(P_e) + P_c log_2(P_c)] \quad (4.91)$$

where, P_e is the overall probability of error defined in (4.72) which has been obtained for the systems and $P_c = 1 - P_e$ represents the probability of correct detection and $log_2(N_t^S M)$ define the total bits convey by the system.

4.2.7   Numerical Results and Discussions

In this section, using the derived expression of equations (4.79), (4.80), (4.89), (4.90) and (4.91), the effect of atmospheric turbulence and pointing error on the average BER and the effective capacity performance of optical SM-SD dual-hop CSI-assisted relay are presented. Generally, the link between the S-R and R-D are assumed to be symmetric atmospheric turbulence channel with weak $(\alpha = 3.78, \beta = 3.74)$, moderate $(\alpha = 2.50, \beta = 2.06)$ and strong $(\alpha = 2.04, \beta = 1.10)$ conditions.

Figure 4.12 shows the effect of atmospheric turbulence conditions on the average BER on the system performance under different PD configurations when MRC is considered at the receiver. This result confirmed that the change in turbulence condition from weak to strong level significantly degrades the system performance. For instance, at average SNR of $25\ dB$ when considering two PDs at the receiver, it is discovered that atmospheric turbulence greatly degraded the system error by 99.76% between the weak and strong turbulence condition. However, this performance can be improved by increasing the number of PD. Thus, at average BER of 10^{-4}, it is shown that the MRC system with four PDs offers a gain of $5\ dB$ when compared with two PDs system under the same weak turbulence.

The performance comparison between the MRC and EGC is presented in Figure 4.13. It is clearly shown that the MRC yields an optimal performance than EGC under the same conditions as it is maximized the output SNR of the combined signal. For instance, at average SNR of $20\ dB$ under moderate turbulence conditions, MRC offers an error rate of 1.32×10^{-5} compared with EGC of 6.20×10^{-4}. Moreover, it can be observed from the Figure 4.13 that the derived analytical expressions provide a perfect match with the simulation result obtained through Monte-Carlo simulation and this therefore validates the accuracy of the presented analytical framework.

The impact of beam width on the system error rate is also illustrated in Figure 4.14. It is depicted in Figure 4.14(a) that as the beam width increases the better the system error performance for the MRC system over a strong atmospheric turbulence for both PD configurations and is least with no pointing error. It can be deduced that with four PDs, there is less error compared with two PDs. For instance, when considering four PDs at the MRC system, at average SNR of $20\ dB$, the system offers an error improvement of 97% by producing an error of 3.03×10^{-5} compared to 1.5×10^{-3} average errors produced when using two PDs. Moreover, the performance of the MRC dual-hop AF relay system is also

compared with the EGC in Figure 4.14(b) when using two PDs at the receiving end. Under the strong turbulence condition, it is clearly shown that MRC offers a $2\ dB$ diversity gain compared to EGC at the average BER of 10^{-2}.
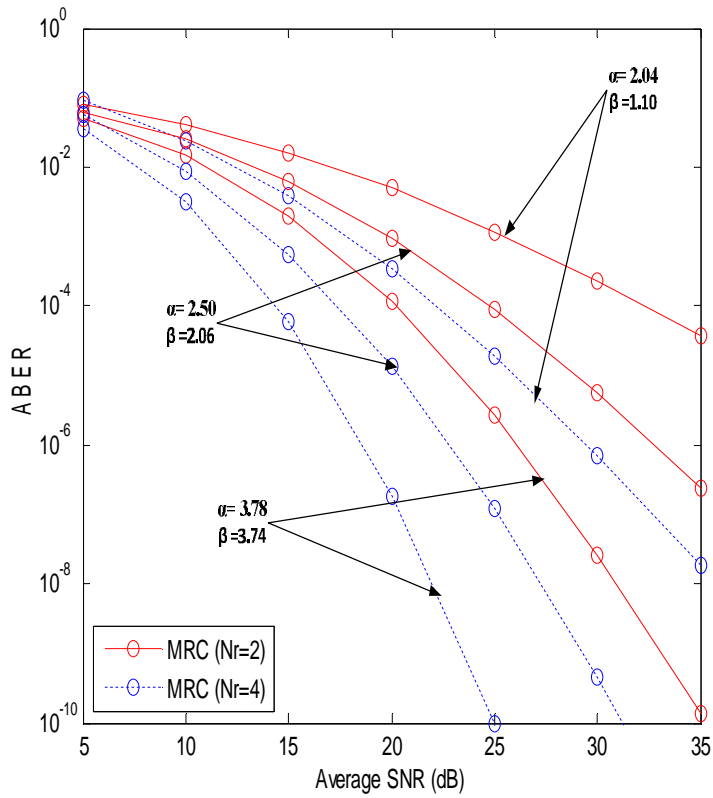
Figure 4.12: Performance of dual-hop AF FSO-SM-MRC system under different atmospheric turbulence without pointing error when the $N_r^D = 2$ and $N_r^D = 4$
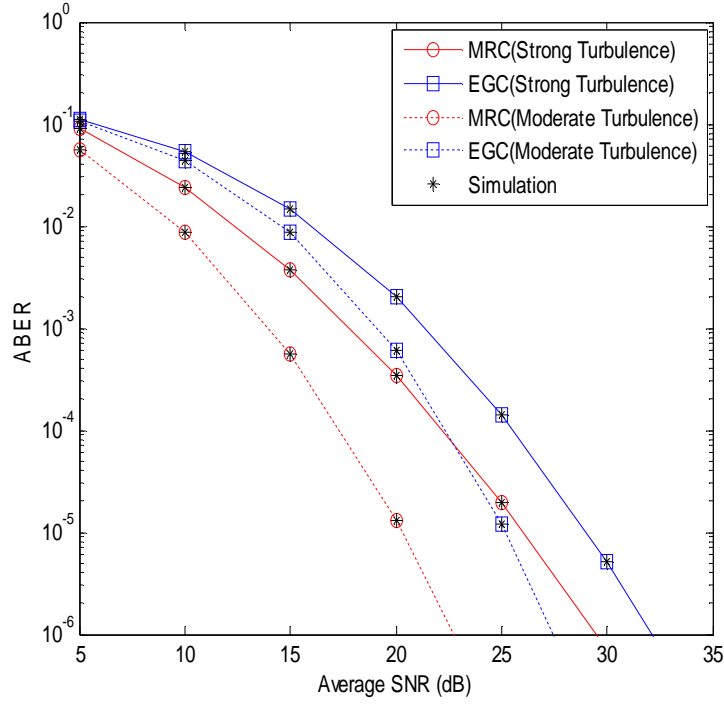
Figure 4.13: Performance comparison between the SM EGC and MRC dual-hop AF system under different atmospheric turbulence without pointing error when the $N_r^D = 4$
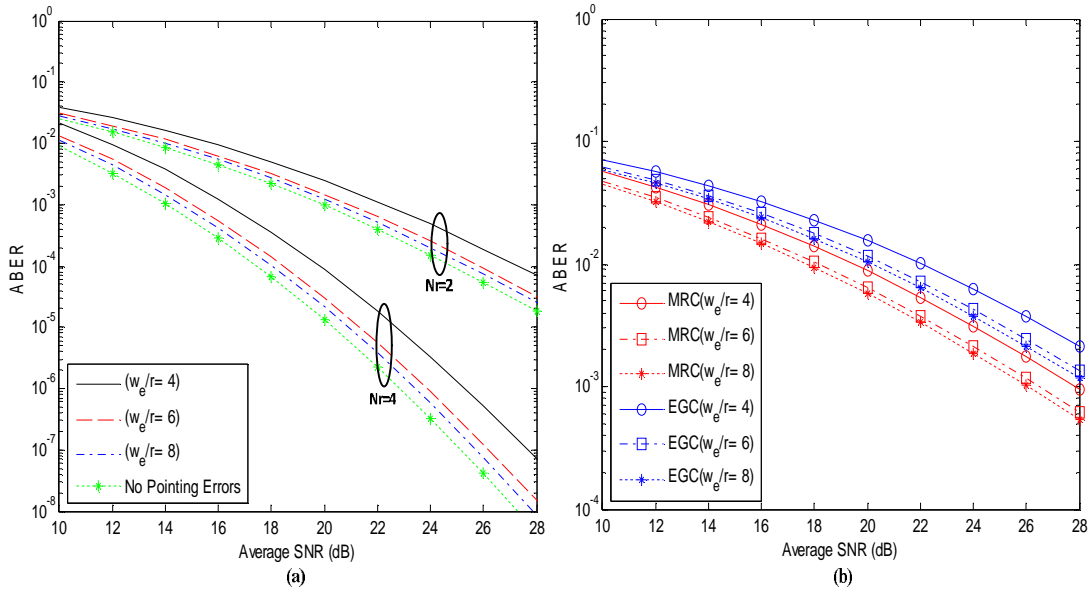
Figure 4.14: (a) Impact of normalized beam width on the SM-MRC dual-hop AF system with different receive photo-detector at the destination (b) Performance comparison between the SM-MRC and SM-EGC dual-hop AF system under influence of normalized beam width at $N_r^D = 2$
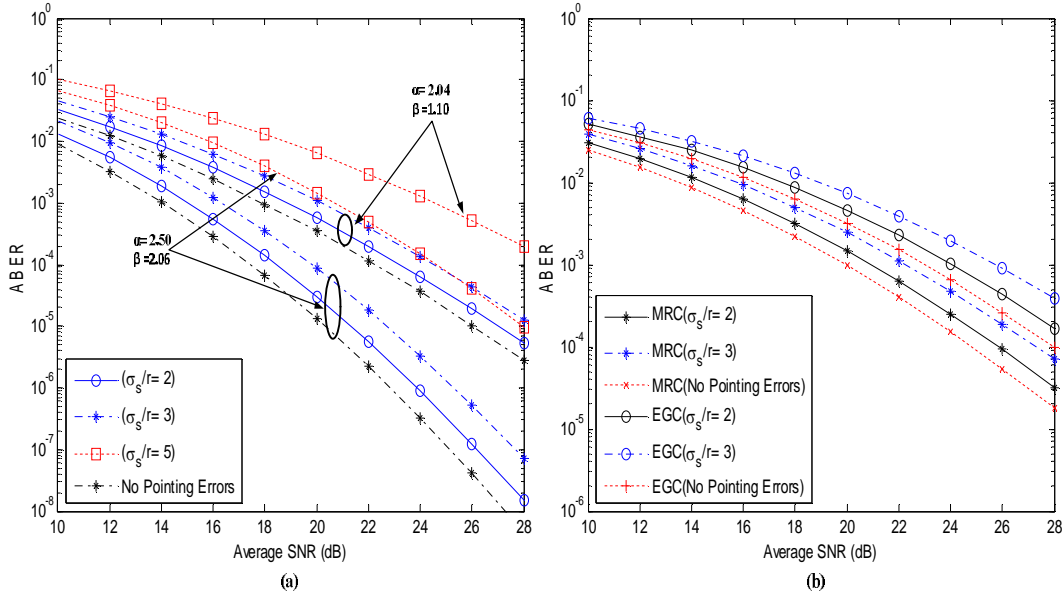
Figure 4.15: (a) Impact of pointing error on the SM-MRC dual-hop AF system with different receive photo-detector at the destination (b) Performance comparison between the SM-MRC and SM-EGC dual-hop AF system under the influence of strong turbulence and pointing error at $N_r^D = 2$

Furthermore, the impart of pointing error on the dual-hop MRC AF relay system is demonstrated in figure 4.15(a) under different turbulence conditions. It clearly shows that as the pointing error increases from values 2 to 5, the more the system error rate deteriorates. For instance, under the strong turbulence condition, the pointing error value of 5 causes the MRC system to offer an average error of 9.5×10^{-3} compared to when no pointing error is considered with error 2.25×10^{-4}. Under the same turbulence condition and pointing error, comparison between the performance of MRC and EGC systems are presented in Figure 5(b). As expected, the MRC system offers the best performance compared to the EGC system for various values of pointing error. For instance, to achieve an average BER of 10^{-3} when pointing error value is set to 2, the MRC system requires only a power of 21 dB compared to EGC of 24 dB when the receiver is equipped with two PDs.

In addition, the average error performance of the dual-hop MRC AF relay system is presented in Figure 4.16(a) under different values of ξ and atmospheric turbulence ranging from weak to strong levels. It can be clearly depicted that the higher the value of ξ, the lower the system error rate and also the system performance deteriorates as the atmospheric turbulence

condition gets worst. For instance, at an average SNR of $20\ dB$ under weak turbulence, there is a margin error of 3.93×10^{-4} between the two ξ values, and this shows that there is 74% error improvement when $\xi = 6.5$ under the same average SNR. Comparing the MRC with EGC as it is demonstrated in Figure 4.16(b) at a high value of $\xi = 6.5$, it is found that at average BER of 10^{-3}, the MRC required a power of $20\ dB$ compared to $25\ dB$ for EGC.

The capacity performance of the dual-hop AF relay system is illustrated in Figure 4.17 under different turbulence conditions without pointing error when considering both the MRC and EGC at the receiver. It is clearly confirmed that as the turbulence gets severe, the more the capacity of the system deteriorates. It is also indicated in the result that the number of lasers at the transmitter significantly improved the system capacity. For instance, at the average SNR of $14\ dB$, it is shown that MRC offers an effective capacity of $1.72\ bits/s/Hz$ compared to $1.60\ bits/s/Hz$ offered by EGC and the use of four lasers caused 32% increment in capacity for MRC under the same conditions.
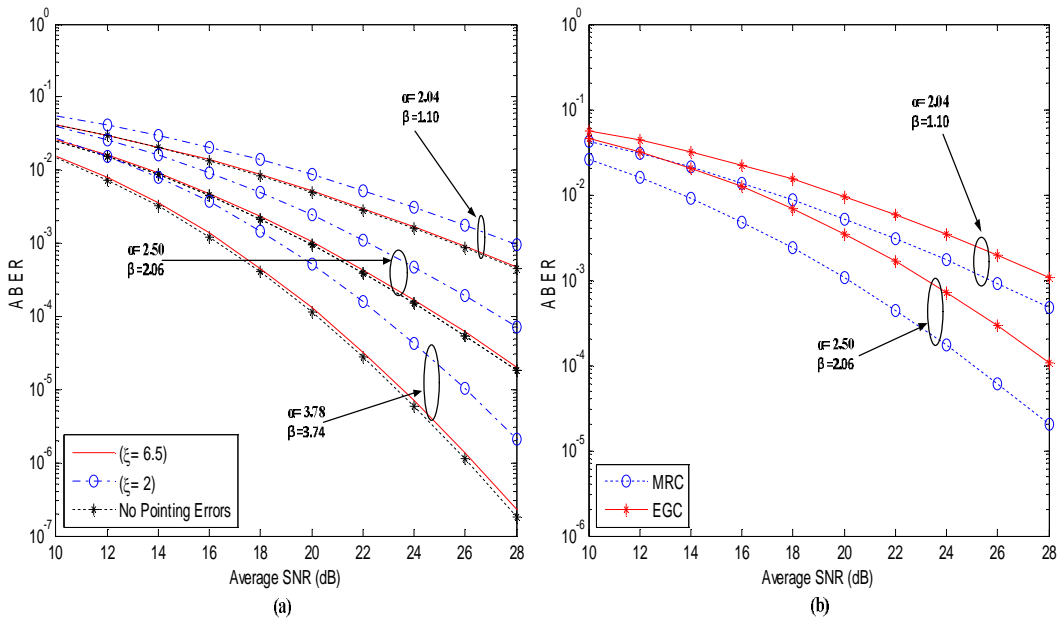
Figure 4.16: Average error performance of SM-MRC dual-hop AF system under different values of ξ and atmospheric turbulence (b) Performance comparison between SM-MRC and SM-EGC dual-hop AF systems at $\xi = 6.5$

Figure 4.18 illustrates the influence of both pointing error and turbulence on the MRC dual-hop AF system capacity. It is clearly shown that as the pointing error increases, the system capacity performance deteriorates for both when the transmit laser is two and four as against when there is no pointing error. It is also confirmed that for a given turbulence condition and pointing error, the capacity of MRC with four lasers is higher compared to when the transmitter is equipped with two lasers. This proved that the higher the laser at the transmitter, the more the system capacity which is an advantage of MIMO scheme specially SM with lower system complexity.

The impact of beam width on the system capacity is presented in Figure 4.19. The transmitter is equipped with two lasers and the receiver makes use of MRC and EGC under a strong turbulence condition. It can be deduced that the system capacity increases with the increase in the beam width. Thus, the MRC offers the best performance. For example, at beam width of 8, the MRC system offers capacity of $1.87\ bits/s/Hz$ compared with $1.85\ bits/s/Hz$ at the same average SNR of $18\ dB$.
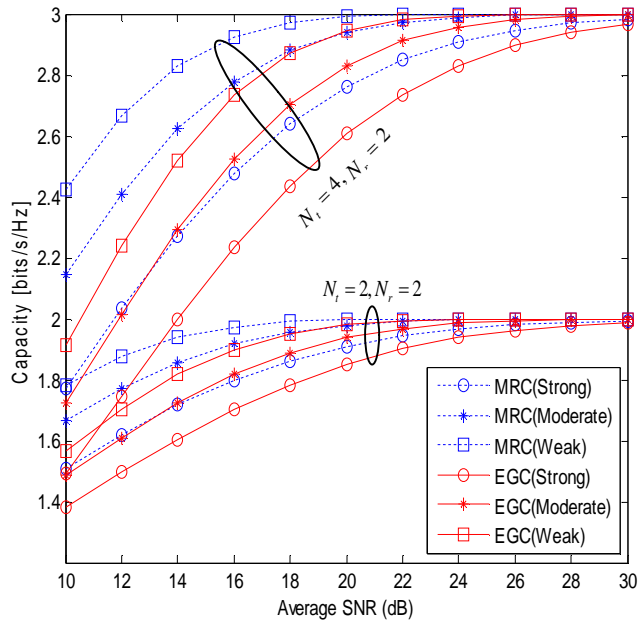
Figure 4.17: Comparison between the capacity of MRC and EGC systems under various turbulence conditions without pointing error
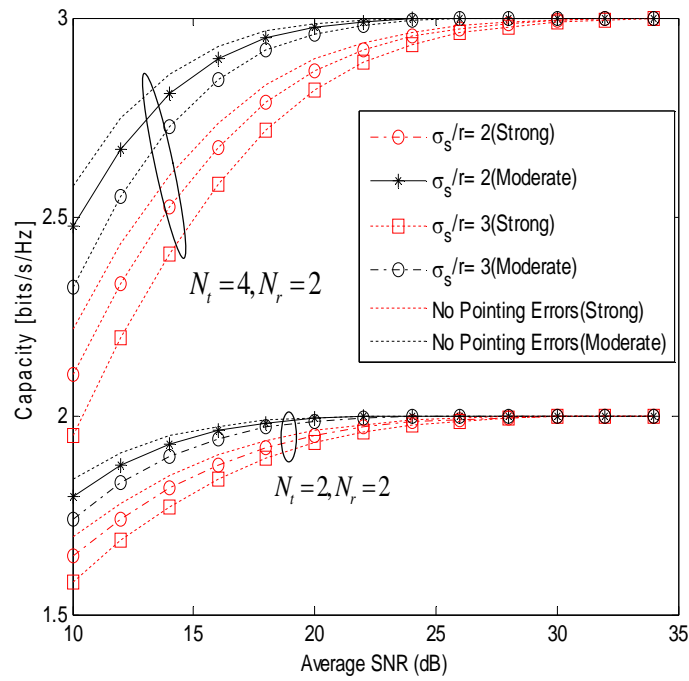
Figure 4.18: Influence of pointing error on capacity of the SM-MRC dual hop AF system under different atmospheric turbulence conditions
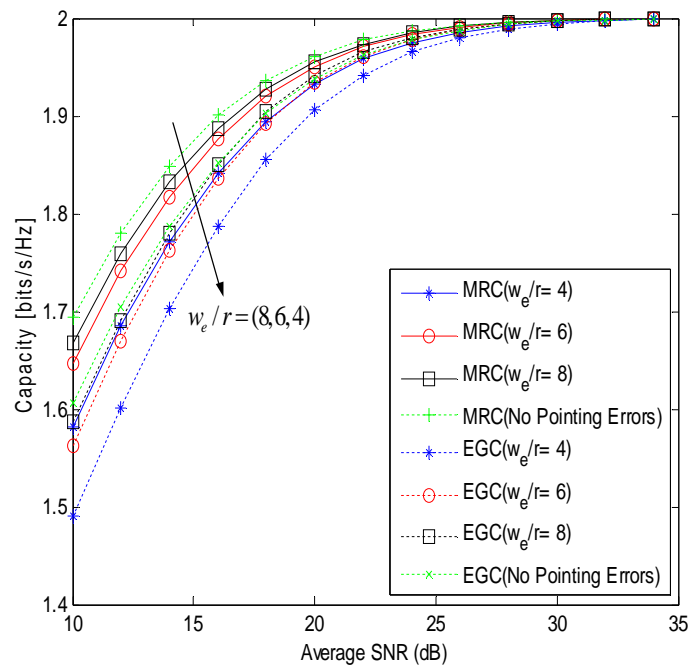
Figure 4.19: Impact of normalized beam width on the SM-MRC and SM-EGC dual-hop AF system under strong turbulence with pointing error for $N_t^S = 2$ and $N_r^D = 2$

4.3 Chapter Summary

In this chapter, a DF dual-hop FSO system using spatial modulation inconjunction with diversity combiners at the relay and destination was proposed. Power series expansion of modified Bessel function was employed to determine the system end-to-end average BER per hop for the systems. The results showed that the dual-hop actually increased the system coverage area with lower error performance when compared with the direct link. Also, the impact of having the same and different combiners at the relay and destination was presented. Additionally, the performance analysis and evaluation of optical spatial modulation heterodyne dual-hop CSI-assisted relay system with MRC and EGC combiners at the destination over Gamma-Gamma turbulence induced fading with and without pointing error were reported. The statistical characteristics of the equivalent end-to-end SNR were derived and utilized to determine the average PEP for each combiner in terms of Meijer-G function. The average BER closed-form express for the system was then determined. The results showed the significant effect of atmospheric turbulence and/or pointing error conditions on the system average BER and the effective system capacity.

CHAPTER FIVE

**Dual-Hop Free Space Optical Spatial Modulation Relaying System with Spatial
Diversity over Asymmetric Channels**

In this chapter, the performance of a dual-hop spatial modulation asymmetric RF/FSO relaying system with MRC as mitigation tools at the destination is investigated. The RF link experiences Nakagami-m distribution and FSO links subjected to Gamma-Gamma distribution with and/or without pointing error. The MGF of the system equivalent SNR is derived using the CDF of the system equivalent SNR. Utilizing the MGF, the APEP for the system was then obtained. Through this, the ABER for the system is determined using the union bounding technique. The analytical results showed that fading and turbulence induced on the RF and FSO links respectively and pointing error strongly degraded the system error performance.

5.1 System Model

The asymmetric RF/FSO communication system that consist of multiple antennas Source (S), a Relay (R), and a multi-PDs Destination (D) units is illustrated in Figure 5.1. The S-R link is assumed to be Nakagami-m distribution while the R-D link is modeled as Gamma-Gamma distribution with and/or without pointing error. Moreover, AF scheme is considered at the relay units which amplify the received signal by fixed gain; converting the electrical signal to optical signal and retransmits it to destination. At the destination, a heterodyne receiver is employed to detect the optical signals before being combined by MRC. Time Division Multiple Access is assumed for transmission over both links, and the orthogonal half-duplex operation is implemented to avoid inter-signal interference. Therefore, the overall systems communication is established in two different phases.

In the first phase, the random sequences of independent incoming information bit streams to be transmitted at the source are mapped into a constellation vector $X = \left[x_1, x_2, x_3 \dots \dots x_{N_t^s}\right]^T$. The first group of these bits $log_2(N_t^s)$ is used to identify the active transmit antenna index k^{th} while the remaining $log_2(M)$ bits are employed to indicate the BPSK modulation symbol x_q from the qth signal constellation for transmission. At any instance, the information bits are then transmitted from the active antenna index k over the Nakagami-m RF link as:

$$\overset{q^{th}\,antenna\,position}{X_{k,q} = [0\ 0\ldots\quad \widehat{x_q}\quad \ldots 0\ 0]^T} \tag{5.1}$$

Thus, the received signal at the relay unit at an instant can therefore be expressed as [18]:

$$y_R = \sqrt{\bar{\gamma}_{SR}} h_{SR}^k\, x_q + n_R(t)$$

$$\triangleq \sqrt{\bar{\gamma}_{SR}} H_{SR} X_{k,q} + n_R(t) \tag{5.2}$$

where $\bar{\gamma}_{SR}$ is the average SNR of the S-to-R link, n_R is the relay noise signal whose elements are modeled as independent identically distributed (i.i.d.) Additive White Gaussian Noise (AWGN) according to $\sim CN(0, \sigma_{n_R}^2)$ and h_{SR}^k denotes the activation of the kth column of channel matrix H_{SR} for a randomly chosen k during each transmission period.

During the second phase, at an instant, the relay unit detects and coverts the transmitted SM signal into optical signal. The photo-detector current $i_R(t)$ at the relay photo-detector is amplified by the fixed relay gain and then retransmitted to the destination. At the destination, the received optical signal at the rth heterodyne receiver is expressed as the sum of the signal electric field $E_s(t)$ transmitted by relay and LO electric field $E_{LO}(t)$ at the destination which can be defined, following the (2.6), as:

$$E_r(t) = E_s(t) + E_{LO}(t)$$

$$\triangleq \sqrt{2P_t Z_o} |y_R(t) G H_{RD}| \cos(\omega_o t + \phi_{h,R}) \quad + \sqrt{2P_{LO}} \cos(\omega_{LO} t) \tag{5.3}$$

where $H_{RD} = |h_{RD}| e^{j\phi_h}$ denotes the fading factor while h_{SR} and ϕ_h are the fading gain and the link phase between the source and the relay respectively.

Thus, the photo-current at the output of each rth photo-detector at the destination can be expressed as [90, 171]:

$$i_D(t) = \frac{R}{Z_o}[E_S(t) + E_{LO}(t)]^2 \triangleq I_{DC,s} + I_{DC,LO} + I_{AC,D}$$

$$\triangleq RP_t |y_R(t) G H_{RD}|^2 + RP_t G H_{RD} + 2R\sqrt{P_t P_{LO}}|y_R(t) G H_{RD}| \cos(\omega_{IF} t - \phi_h) \tag{5.4}$$

where $I_{DC,s}$ and $I_{DC,LO}$ are the DC current generated due to signal and LO electric field respectively at the rth heterodyne receiver at the destination while $I_{AC,D}$ is the AC current which contains the useful information about the frequency and the phase of the received

signal at the destination. The short noise impairment during the photo-detection process at this stage is dominated by destination LO short noise with variance of $\sigma_{short,L,D}^2 = 2q_eRP_{L,D}B_e$. The SNR on the R-to-D link for the rth heterodyne receiver can therefore be expressed following (2.15) as:

$$\gamma_{RD} = \frac{RP_t|sH_{RD}|^2}{q_eB_e} \triangleq \bar{\gamma}_{RD}|sH_{RD}|^2 \tag{5.5}$$

The received signal at the rth heterodyne receiver can be statistically obtained as:

$$y_D(t) = \underbrace{\sqrt{\bar{\gamma}_{RD}\bar{\gamma}_{SR}}GH_{RD}H_{SR}X_{kq}}_{signal\ part} + \underbrace{\sqrt{\bar{\gamma}_{RD}}GH_{RD}n_R(t) + n_D(t)}_{Noise\ part} \tag{5.6}$$

where $\bar{\gamma}_{RD} = RP_t/q_eB_e$ is the average SNR of the R-to-D link and $n_D(t)$ is the noise term at the input of the relay unit modeled as a zero-mean unit variance complex Gaussian random variable.
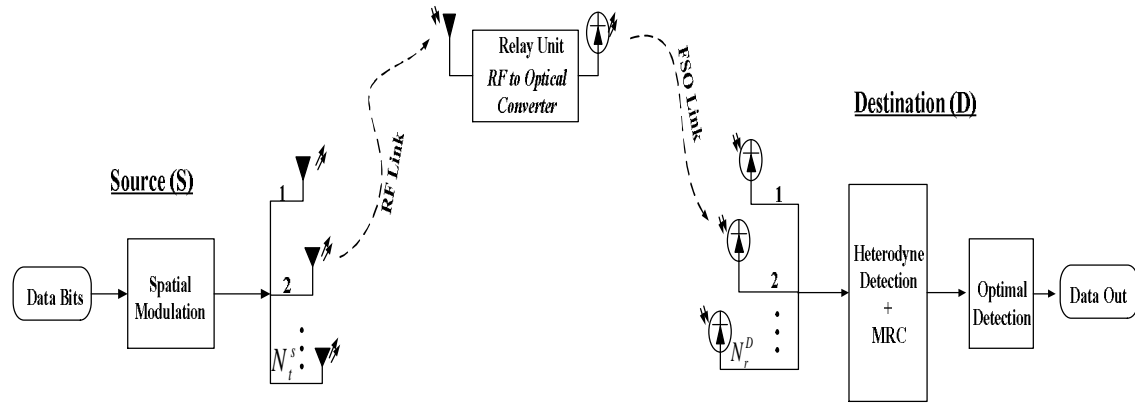
Figure 5.1: A dual-hop spatial modulation asymmetric RF/FSO relaying system

In this study, the receiver is assumed to have full channel state information. Therefore, after the normalization of the noise, the received signal at the rth heterodyne receiver at the destination can be further simplified as:

$$y_D(t) = \sqrt{A}H_{SR}X_{kq} + \hat{n}(t) \tag{5.7}$$

where $A = \frac{G^2H_{RD}^2\bar{\gamma}_{RD}\bar{\gamma}_{SR}}{\bar{\gamma}_{RD}G^2H_{RD}^2+1}$ with G denoting the amplification factor at the relay and $\hat{n}(t)$ is the complex AWGN at the input of the destination having similar statistical characteristic as $n_R(t)$.

Considering an optimal decoder at the destination, the estimated laser index $\hat{k}$ and the transmitted constellation symbol index $\hat{q}$ from the transmitted SM signal vector X_{kq} at a specific time instant can then be obtained, following the (2.36), as:

$$\begin{aligned}
\left[\,\hat{k}\,,\hat{q}\right] &= \underset{\hat{k},\ \hat{q}}{argmax}\ p_Y\left(y_D\middle|X_{kq},H_{SR}\right) \\
&\triangleq \underset{\hat{k},\ \hat{q}}{argmin}\ \sqrt{A}\left\|h_{SR}^k x_q\right\|_F^2 - 2Re\{y_D^H h_{SR}^k x_q\}
\end{aligned}$$
(5.8)

From (5.6), using the similar analysis in [121], the equivalent instantaneous SNR at the destination in a fixed gain relay system can be expressed as:

$$\gamma_{eq} = \frac{\gamma_{RD}\gamma_{SR}}{\gamma_{RD} + C}$$
(5.9)

where $C \geq 0$ is the fixed relay gain, γ_{SR} is the instantaneous SNR of the S-to-R link and γ_{RD} is the instantaneous SNR of the R-to-D link.

5.2 Statistical Channel Models

Since the S-to-R link is assumed to experience Nakagami-m fading, the channel PDF can therefore be expressed as [125]:

$$f_{\gamma_{SR}}(\gamma_{SR}) = \frac{m^m \gamma_{SR}^{m-1}}{\Gamma(m)\bar{\gamma}_{SR}^{\,m}} exp\left(-\frac{m\gamma_{SR}}{\bar{\gamma}_{SR}}\right)$$
(5.10)

where m is the Nakagami fading parameter ($m \geq 1/2$) and $\Gamma(.)$ is the Gamma function.

The turbulence in the R-to-D link is considered to undergo Gamma-Gamma distribution and the PDF for this channel without pointing error can be defined by following the (4.53), as:

$$f_{\gamma_{RD}}(\gamma_{RD}) = \frac{(\alpha\beta)^{\frac{\alpha+\beta}{2}}\bar{\gamma}_{RD}^{-\left(\frac{\alpha+\beta}{4}\right)}}{2\Gamma(\alpha)\Gamma(\beta)}\gamma_{RD}^{\frac{\alpha+\beta}{4}-1}G_{0,2}^{2,0}\left(\alpha\beta\sqrt{\frac{\gamma_{RD}}{\bar{\gamma}_{RD}}}\,\middle|\,\frac{-,\,-}{\frac{\alpha-\beta}{2},\frac{\beta-\alpha}{2}}\right)$$
(5.11)

Considering the impact of pointing error impairment, the PDF of the combined atmospheric turbulence with pointing error can therefore be expressed by following (4.66) and further simplified using Meijer-G identity in [205, equation (9.31.5)] (see Appendix A2.5) as:

$$f_{\gamma_{RD}}(\gamma_{RD}) = \frac{\alpha\beta\xi^2}{2\sqrt{\bar{\gamma}_{RD}}\Gamma(\alpha)\Gamma(\beta)}\gamma_{RD}^{-1/2}G_{1,3}^{3,0}\left(\alpha\beta\sqrt{\frac{\gamma_{RD}}{\bar{\gamma}_{RD}}}\,\middle|\,\frac{\xi^2}{\xi^2 - 1,\alpha - 1,\beta - 1}\right)$$
(5.12)

5.3 Statistical Characteristics

The mathematical expression for the CDF and MGF is presented for the proposed system when the link between the relay and the destination experienced Gamma-Gamma induced-fading with or without pointing error.

5.3.1   CDF for the Equivalent SNR

The S-to-R link experiences Nakagami-m fading and R-to-D undergoes Gamma-Gamma distributions, the CDF can therefore be obtained as [125]:

$$
F_{\gamma_{eq}}(\gamma) = P_r \left[\frac{\gamma_{RD}\gamma_{SR}}{\gamma_{RD} + C} \le \gamma \right]
$$

$$
\triangleq \int_0^\infty P_r \left[\gamma_{SR} \le \frac{\gamma_{RD} + C}{\gamma_{SR}} \right] f_{\gamma_{RD}}(\gamma_{RD}) d\gamma_{RD}
$$

(5.13)

The CDF of the equivalent SNR under the influence of atmospheric turbulence without pointing error can be determined by substituting (5.11) into (5.13), and the CDF of γ_{eq} can be expressed as:

$$
F_{\gamma_{eq}}(\gamma) = 1 - \frac{(\alpha\beta)^{\frac{\alpha+\beta}{2}}}{\Gamma(m)\Gamma(\alpha)\Gamma(\beta)\bar{\gamma}_{RD}^{\frac{\alpha+\beta}{4}}} \int_0^\infty \gamma_{RD}^{\frac{\alpha+\beta}{4}-1} \Gamma\left(m, \frac{m\gamma(\gamma_{RD} + C)}{\bar{\gamma}_{SR}\gamma_{RD}}\right) d\gamma_{RD}
$$

$$
\times G_{0,2}^{2,0}\left(\frac{\alpha\beta}{\sqrt{\bar{\gamma}_{RD}}}\gamma_{RD}^{1/2} \,\middle|\, \frac{\overline{},\overline{}}{\frac{\alpha - \beta}{2}, \frac{\beta - \alpha}{2}}\right)
$$

(5.14)

where $\Gamma(m, y)$ is the upper incomplete Gamma function and its finite power series form can be expressed as [205, equation (8.352(7))]:

$$
\Gamma(m, y) = (m - 1)! \left(\exp(-y) \sum_{j=0}^{m-1} \frac{y^j}{j!} \right)
$$

(5.15)

Thus, the Gamma function in (5.14) can then be expressed as:

$$
\Gamma\left(m, \frac{m\gamma(\gamma_{RD} + C)}{\bar{\gamma}_{SR}\gamma_{RD}}\right) = (m - 1)! \left[\exp\left(-\frac{m\gamma(\gamma_{RD} + C)}{\bar{\gamma}_{SR}\gamma_{RD}}\right) \sum_{j=0}^{m-1} \frac{1}{j!} \left(\frac{m\gamma(\gamma_{RD} + C)}{\bar{\gamma}_{SR}\gamma_{RD}}\right)^j \right]
$$

$$
\triangleq (m - 1)! \left[\exp\left(-\frac{m\gamma}{\bar{\gamma}_{SR}}\right) \exp\left(-\frac{mC\gamma}{\bar{\gamma}_{SR}\gamma_{RD}}\right) \sum_{j=0}^{m-1} \frac{1}{j!} \left(\frac{m\gamma}{\bar{\gamma}_{SR}}\right)^j \left(1 + \frac{C}{\gamma_{RD}}\right)^j \right]
$$

(5.16)

Using binomial expansion, $\left(1 + \frac{C}{\gamma_{RD}}\right)^{k} = \Sigma_{p=0}^{j} \binom{j}{p}\left(\frac{C}{\gamma_{RD}}\right)^{p}$

Substitute (5.16) into (5.14) and express $exp\left(-\frac{mC\gamma}{\bar{\gamma}_{SR}\gamma_{RD}}\right)$ in terms of Meijer-G representation using identity in [203, equation (11)] (see Appendix A2.4), then (5.14) can be expressed as:

$$F_{\gamma_{eq}}(\gamma) = 1 - \frac{(\alpha\beta)^{\frac{\alpha+\beta}{2}}}{\Gamma(\alpha)\Gamma(\beta)\bar{\gamma}_{RD}^{\frac{\alpha+\beta}{4}}} exp\left(-\frac{m\gamma}{\bar{\gamma}_{SR}}\right) \sum_{j=0}^{m-1} \frac{1}{j!}\left(\frac{m\gamma}{\bar{\gamma}_{SR}}\right)^{j} \sum_{p=0}^{j}\binom{j}{p}C^{p}$$

$$\times \int_{0}^{\infty} \gamma_{RD}^{\frac{\alpha+\beta}{4}-j-1} G_{1,0}^{0,1}\left(\frac{\bar{\gamma}_{SR}\gamma_{RD}}{mC\gamma}\middle|\begin{matrix}0\\1,\end{matrix}\right) G_{0,2}^{2,0}\left(\frac{\alpha\beta}{\sqrt{\bar{\gamma}_{RD}}}\gamma_{RD}^{1/2}\middle|\begin{matrix}-,-\\\frac{\alpha-\beta}{2},\frac{\beta-\alpha}{2}\end{matrix}\right) d\gamma_{RD}$$

(5.17)

Using the integral identity [203, equation (21)] (see Appendix A3.5), CDF of γ_{eq} can be derived as:

$$F_{\gamma_{eq}}(\gamma) = 1 - \sum_{j=0}^{m}\sum_{p=0}^{j} \Psi_{1}\gamma^{\frac{\alpha+\beta}{4}+p} exp\left(-\frac{m\gamma}{\bar{\gamma}_{SR}}\right) G_{0,5}^{5,0}\left(\frac{m(\alpha\beta)^2 C\gamma}{16\bar{\gamma}_{SR}\bar{\gamma}_{RD}}\middle|\begin{matrix}-\\\Xi_{1}\end{matrix}\right)$$

(5.18)

where

$$\Psi_{1} = \frac{(\alpha\beta)^{\frac{\alpha+\beta}{2}}j!\,(C)^{\frac{\alpha+\beta}{4}}(m)^{\frac{\alpha+\beta}{4}+p}}{4\pi p!\,(j-p)!\,\Gamma(\alpha)\Gamma(\beta)\Gamma(j+1)\bar{\gamma}_{SR}^{\frac{\alpha+\beta}{4}+p}\bar{\gamma}_{RD}^{\frac{\alpha+\beta}{4}}}$$

$$\Xi_{1} = \left[\frac{\alpha-\beta}{4},\frac{\alpha-\beta+2}{4},\frac{\beta-\alpha}{4},\frac{\beta-\alpha+2}{4},\frac{-\alpha-\beta}{4}-p+j\right]$$

Similarly, obtained by substituting (5.12) into (5.13), the CDF for the turbulence with pointing error can be expressed as:

$$F_{\gamma_{eq}}(\gamma) = 1 - \frac{\alpha\beta\xi^2}{2\Gamma(\alpha)\Gamma(\beta)\Gamma(m)}\int_{0}^{\infty}\frac{1}{\gamma_{RD}}\Gamma\left(m,\frac{m\gamma(\gamma_{RD}+C)}{\bar{\gamma}_{SR}\gamma_{RD}}\right)$$

$$\times G_{1,3}^{3,0}\left(\alpha\beta\sqrt{\frac{\gamma_{RD}}{\bar{\gamma}_{RD}}}\middle|\begin{matrix}\xi^2\\\xi^2-1,\alpha-1,\beta-1\end{matrix}\right)d\gamma_{RD}$$

(5.19)

Following the same analysis of CDF for the turbulence without pointing error, the CDF of γ_{eq} for the turbulence with pointing error can be derived as:

$$F_{\gamma_{eq}}(\gamma) = 1 - \sum_{j=0}^{m} \sum_{p=0}^{j} \Psi_2 \gamma^{\frac{1}{2}+p} \exp\left(-\frac{m\gamma}{\bar{\gamma}_{SR}}\right) G_{2,7}^{7,0}\left(\frac{m(\alpha\beta)^2 C\gamma}{16\bar{\gamma}_{SR}\bar{\gamma}_{RD}} \middle| \begin{array}{c} \frac{\xi^2}{2}, \frac{\xi^2+1}{2} \\ \Xi_2 \end{array}\right) \tag{5.20}$$

where

$$\Psi_2 = \frac{2^{\alpha+\beta-3}(\alpha\beta)\xi^2 j! \, (C)^{\frac{1}{2}}(m)^{p+\frac{1}{2}}\bar{\gamma}_{RD}^{-\frac{1}{2}}}{4\pi p! \, (j-p)! \, \Gamma(\alpha)\Gamma(\beta)\Gamma(j+1)\bar{\gamma}_{SR}^{p+\frac{1}{2}}}$$

$$\Xi_2 = \left[\frac{\xi^2-1}{2}, \frac{\xi^2}{2}, \frac{\alpha-1}{2}, \frac{\alpha}{2}, \frac{\beta-1}{2}, \frac{\beta}{2}, \frac{1}{2} - p + j\right]$$

5.3.2 MGF for the Equivalent SNR

The MGF equivalent SNR under the influence of atmospheric turbulence with and without pointing error can be expressed as:

$$M_{\gamma_{eq_r}}(S) = S \int_0^{\infty} e^{-S\gamma} F_{\gamma_{eq}}(\gamma) d\gamma \tag{5.21}$$

By substituting (5.18) into (5.21) and applying the integral identity in [205, equation. (7.813.1)] (see Appendix A3.3), the MGF under the influence of turbulence without pointing error can be obtained as:

$$M_{\gamma_{eq_r}}(S) = 1 - S\Psi_1 \sum_{j=0}^{m} \sum_{p=0}^{j} \left(\frac{S\bar{\gamma}_{SR}+m}{\bar{\gamma}_{SR}}\right)^{-\left(\frac{\alpha+\beta}{4}\right)-p-1}$$

$$\times G_{1,5}^{5,1}\left(\frac{m(\alpha\beta)^2 C\bar{\gamma}_{SR}}{16\bar{\gamma}_{SR}\bar{\gamma}_{RD}S(\bar{\gamma}_{SR}+m)} \middle| \begin{array}{c} \frac{-\alpha-\beta}{4}-p \\ \Xi_1 \end{array}\right) \tag{5.22}$$

Similarly, by substituting (5.20) into (5.21) and applying the integral identity in [205, equation (7.813.1)] (see Appendix A3.3), the MGF under the influence of turbulence with pointing error is obtained as:

$$M_{\gamma_{eq_r}}(S) = 1 - S\Psi_2 \sum_{j=0}^{m} \sum_{p=0}^{j} \left(\frac{S\bar{\gamma}_{SR}+m}{\bar{\gamma}_{SR}}\right)^{-\left(\frac{\alpha+\beta}{4}\right)-p-1}$$

$$\times G_{3,7}^{7,1}\left(\frac{m(\alpha\beta)^2 C\bar{\gamma}_{SR}}{16\bar{\gamma}_{SR}\bar{\gamma}_{RD}S(\bar{\gamma}_{SR}+m)} \middle| \begin{array}{c} -p-\frac{1}{2}, \frac{\xi^2}{2}, \frac{\xi^2+1}{2} \\ \Xi_2 \end{array}\right) \tag{5.23}$$

5.4 Performance Analysis

At the system destination, the amplified SM signal from the relay is combined using MRC combining technique. Thus, to determine the ABER for the proposed asymmetric RF/FSO dual-hop AF relay system, a well-known boundary technique is adopted to evaluate the ABER under the fading condition, following (3.10), as:

$$ABER_{SM} \leq \frac{(N_t^S M)^{-1}}{\log_2(N_t^S M)} \sum_{k=1}^{N_t^S} \sum_{q=1}^{M} \sum_{\hat{k}=k+1}^{N_t^S} \sum_{\hat{q}=q+1}^{M} N(q,\hat{q}) APEP\left(X_{k,q} \to X_{\hat{k},\hat{q}}\right) \qquad (5.24)$$

To determine the APEP for the system with MRC combiner, the instantaneous SNR at the output of MRC is defined following the (2.39) as:

$$\gamma_t^{MRC} = \sum_{r=1}^{N_r^D} \gamma_{eq_r} \qquad (5.25)$$

where γ_{eq_r} is the equivalent SNR received at the rth heterodyne receiver defined in (5.9). Thus, the PEP can be expressed, by following (4.74), as:

$$PEP\left(X_{k,q} \to X_{\hat{k},\hat{q}}\right) = Q\left(\sqrt{2\gamma_t^{MRC}}\right)$$

$$\triangleq Q\left(\sqrt{2 \sum_{r=1}^{N_r^D} \gamma_{eq_r}}\right) \qquad (5.26)$$

Thus, using the upper bound of Craig's Q-function defined as $Q(x) \leq 1/2exp(-x^2/2)$ [124], the average PEP for the system can be expressed as:

$$APEP\left(X_{k,q} \to X_{\hat{k},\hat{q}}\right) = \frac{1}{2} \int_0^{\infty} exp\left(-\sum_{r=1}^{N_r^D} \gamma_{eq_r}\right) f_{\gamma_{eq}}(\gamma) d\gamma$$

$$\triangleq \frac{1}{2} \prod_{r=1}^{N_r^D} M_{\gamma_{eq_r}}(S) \qquad (5.27)$$

By substituting (5.22) and (5.23) into (5.27), the APEP for the system under the influence of atmospheric turbulence without and with pointing error can be obtained as it is defined in (5.28) and (5.29) respectively.

$$APEP_{without\ Pointing\ Error} = \frac{1}{2}\prod_{r=1}^{N_r^D}\left[1 - \Psi_1 \sum_{j=0}^{m}\sum_{p=0}^{j}\left(\frac{\bar{\gamma}_{SR} + m}{\bar{\gamma}_{SR}}\right)^{-\left(\frac{\alpha+\beta}{4}\right)-p-1}\right.$$
$$\left. \times\ G_{1,5}^{5,1}\left(\frac{m(\alpha\beta)^2 C\bar{\gamma}_{SR}}{16\bar{\gamma}_{SR}\bar{\gamma}_{RD}(\bar{\gamma}_{SR} + m)}\left|\begin{array}{c}\frac{-\alpha-\beta}{4}-p\\ \Xi_1\end{array}\right.\right)\right] \tag{5.28}$$

$$APEP_{with\ Pointing\ Error} = \frac{1}{2}\prod_{r=1}^{N_r^D}\left[1 - \Psi_2 \sum_{j=0}^{m}\sum_{p=0}^{j}\left(\frac{\bar{\gamma}_{SR} + m}{\bar{\gamma}_{SR}}\right)^{-\left(\frac{\alpha+\beta}{4}\right)-p-1}\right.$$
$$\left. \times\ G_{3,7}^{7,1}\left(\frac{m(\alpha\beta)^2 C\bar{\gamma}_{SR}}{16\bar{\gamma}_{SR}\bar{\gamma}_{RD}(\bar{\gamma}_{SR} + m)}\left|\begin{array}{c}-p-\frac{1}{2},\frac{\xi^2}{2},\frac{\xi^2+1}{2}\\ \Xi_2\end{array}\right.\right)\right] \tag{5.29}$$

The ABER for the system under the influence of atmospheric turbulence with and without pointing error can therefore be determined by substituting (5.28) and (5.29) respectively into (5.24).

5.5 Numerical Results and Discussions

In this section, the analytical results on the asymmetric RF/FSO system under the influence of atmospheric channel with and/or without pointing error are presented using the derived average BER expression through equations (5.28) and (5.29). The value of the fixed relay gain is set in such a way that $C = 0.75$. Moreover, the link between the relay and destination is assumed to be atmospheric turbulence channel with weak $(\alpha = 3.78, \beta = 3.74)$, moderate $(\alpha = 2.50, \beta = 2.06)$ and strong $(\alpha = 2.04, \beta = 1.10)$ turbulence conditions.

Figure 5.2 illustrates the performance of the system under the varying effect of different values of fading parameters and turbulence conditions without pointing error effect. As expected, the increase in the fading and turbulence, the more the system performance deteriorates. This explains that the ABER for the system becomes poorer with the unified effect of fading and turbulence at the S-to-R and R-to-D links respectively. For instance, at $SNR = 20\ dB$, when $m = 3$ under weak turbulence condition, the ABER produced by the system is 2.13×10^{-10} and it increases to 8.24×10^{-8} and 1.01×10^{-5} respectively under moderate and strong conditions. In addition, the accuracy of the derived analytical

expressions and their computational realizations are compared with the Monte-Carlo simulation in Figure 5.2. It can be observed from the result that the derived expressions agreed with the simulation and thus validate their accuracy.

The performance comparison between the proposed system and the well-established SIM asymmetric system is presented in Figure 5.3. It is clearly shown that the use of MRC at the receiving end significantly improves the proposed system performance. Expectedly, as the number of the PD at the destination increases the better the ABER for the system. For example, at $SNR = 15\,dB$ when $N_r^D = 1$, the system offers ABER of 0.54×10^{-2} and this is reduced to 3.09×10^{-4} and 7.66×10^{-7} when $N_r^D = 2$ and $N_r^D = 4$ respectively. Additionally, it can be observed that the proposed system outperformed the well-established SIM system with different modulation schemes under the same conditions. For instance, at $SNR = 20\,dB$, the SM-BPSK system offers error of 2.58×10^{-5} when $N_r^D = 2$ as compared to 0.44×10^{-2} produced by SIM-CBPSK system.
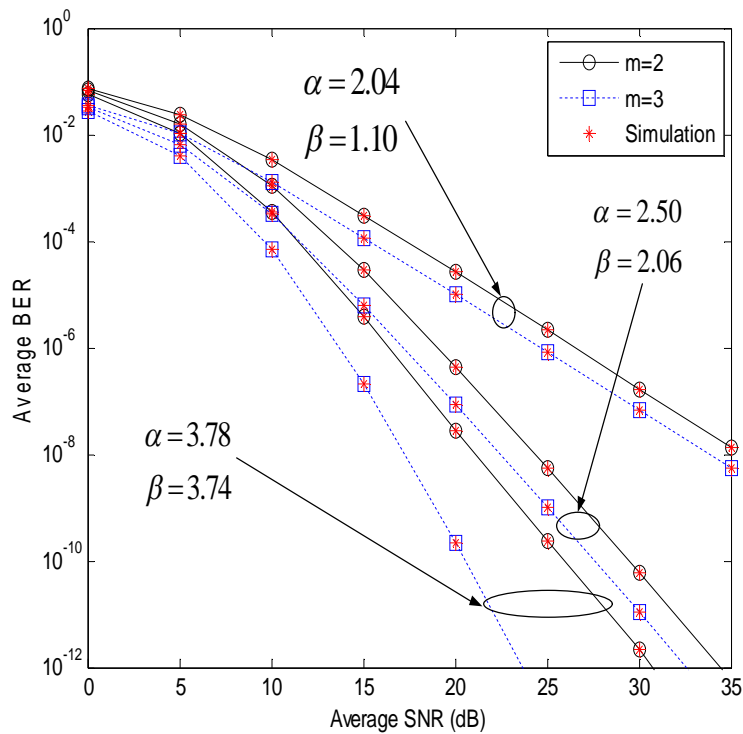
Figure 5.2: Performance of the system under different fading and turbulence conditions without pointing error when $N_r^D = 2$

The effect of pointing error on the system performance is depicted in Figure 5.4 for different values of beam waist at $m = 3$. As it is clearly shown, the system performance gets degraded as the turbulence conditions become more severe on the FSO link. Moreover, it is confirmed that large beam waist reduces the system error because the value for ξ results in lower pointing error. Thus, as the beam waist increases, the better the system performance becomes. For instance, when $SNR = 20\ dB$ at moderate turbulence, the normalized beam waist of 8 radius offers the system ABER of 5.2×10^{-7} as compared to 9.68×10^{-4} produced when $w_e/r = 4$.

The performance of the proposed system is compared with well-established SIM-CBPSK system presented in [124] under the influence of pointing error as it is depicted in Figure 5.5. Generally, it is deduced that large value of normalized jitter caused low value in ξ and this results in stronger effect of pointing error. Therefore, as the normalized jitter increases, the more the performance of the both systems deteriorate, with SM-BPSK offering the best performance compared with SIM-CBPSK under the same turbulence condition. For instance, at $SNR = 20\ dB$ when $\sigma_s/r = 4$, the SM-BPSK yields error of 1.50×10^{-6} compared to 1.69×10^{-2} produced by SIM-CBPSK.
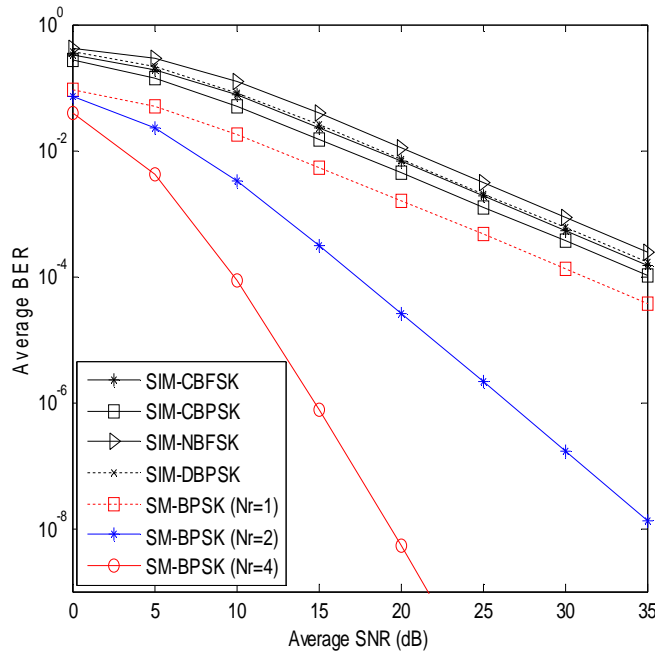
Figure 5.3: Performance comparison between SM-BPSK-MRC and the SIM with different binary modulations at $m = 2$ over a strong turbulence
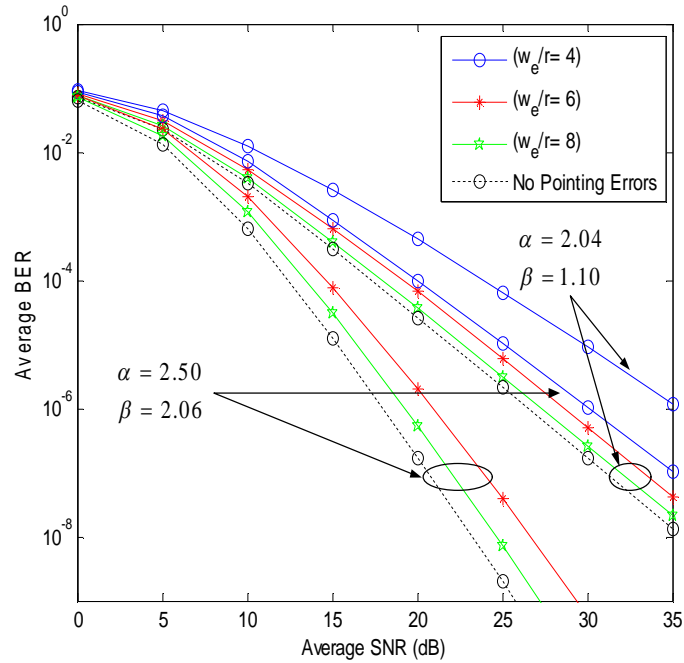
Figure 5.4: Effect of normalized beam waist on the SM-BPSK at $m = 3$ and $N_r^D = 2$ over the moderate and strong turbulence at $\sigma_s/r = 2$
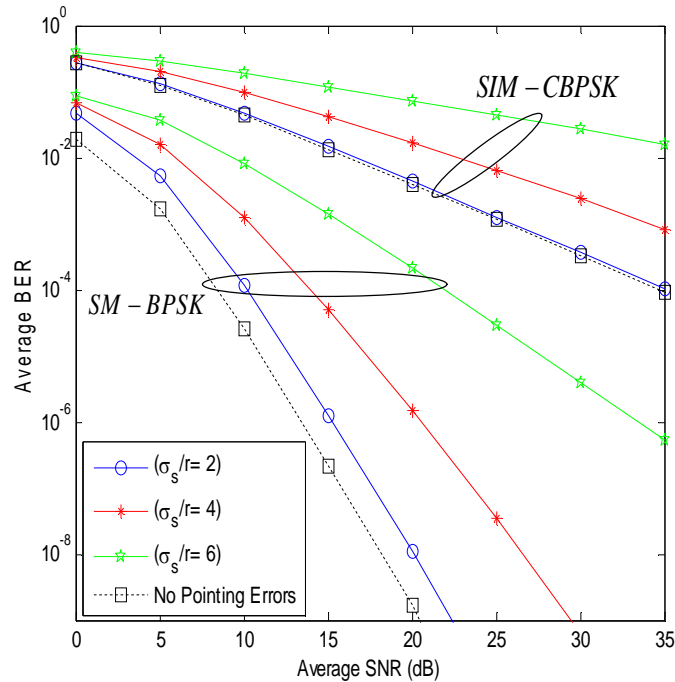
Figure 5.5: Comparison between the SIM-CBPSK and SM-BPSK under the effect of normalized sigma at $m = 2$, $w_e/r = 8$ and $N_r^D = 4$ over a strong turbulence

5.6 Chapter Summary

In this chapter, the performance analysis of a dual-hop spatial modulation relaying system over asymmetric RF/FSO with heterodyne detection and MRC combiner at the destination was presented. The S-to-R and R-to-D links were respectively considered to be Nakagami-m fading and Gamma-Gamma turbulence with and/or without pointing error. For this asymmetric channel system, a mathematical closed form expression for the CDF, PDF and MGF was derived. Thus, the finite power series approach was then used to determine the ABER for the system under study in term of Meijer-G function. The effect of pointing error and atmospheric turbulence on the system was investigated. Finally, the results proved that the performance of the proposed system was better than the well-established systems under the same conditions.

Block Error Rate Performance of Subcarrier Intensity Modulation FSO Link with Spatial Diversity over Atmospheric Channel Impairments.

When transmitting data in block of N bits in a communication system, the probability $P(M, N)$ of more than M bits error in a block can be estimated by average BLER. This is based on the fact that the optical channel is slow in nature and causes the received signal strength to be constant over the duration of a block of N bits. Due to the rigorous mathematical complexity and untraceable closed-form expression that may result from using spatial modulation scheme, the BLER performance of the FSO system was carried by considering subcarrier intensity modulation scheme. In this chapter, block error rate performance of SIM-BPSK FSO system with spatial diversity combiners over Gamma-Gamma atmospheric turbulence with and without pointing error is reported. The channel PDF for MRC and EGC by using power series expansion of the modified Bessel function is derived. Through this, the BLER closed-form expressions for the combiners are obtained. Under the same atmospheric conditions, BLER performance of the proposed FSO-SIM system with diversity combiners is compared with the well-established FSO-SIM system without combiner. Convolutional error control coding technique was also introduced to further enhance the system performance.

6.1 System Model

At the transmitter of the FSO-SIM system, pre-modulated RF signal $s(t)$ is used to modulate a continuous wave optical laser beam and the transmitted power of the modulated optical beam is given following equation (2.30) as:

$$P_T(t) = P[1 + \rho s(t)]$$

(6.1)

At the receiving end, the laser optical beam is converted into electrical signal through direct detection. The photocurrent at the photo-detector (PD) can therefore be expressed following equation (2.31) as:

$$i(t) = PR[1 + \rho s(t)]I(t) + n(t)$$

(6.2)

where $n(t)$ is the AWGN with zero-mean and variance defined as $\sim\mathbb{N}(0, \sigma_n^2)$. The instantaneous SNR at the input of the electrical demodulator of an optical receiver can be derived from equation (6.2) as:

$$\gamma = \frac{(PR\rho)^2}{\sigma_n^2}I^2 = \bar{\gamma}I^2 \tag{6.3}$$

In this study, the BPSK binary modulation FSO system is considered for the transmission and $P(t)$ is normalized to unity. The two combiners considered at the receiver are the MRC and EGC having identical PDs on each channel link. The receiver converts the optical beam into electrical signals and N_r- detectors PD combine the signal before being demodulated coherently. For S number of subcarriers, the $s(t)$ over one symbol duration can be given following (2.29) as:

$$s(t) = \sum_{j=1}^{S} A_j g(t) \cos(w_c t) + \theta_j \tag{6.4}$$

Thus, the output from the combiner can be expressed as [75]:

$$r_i(t) = \frac{R}{N_r}I_i\left(1 + \sum_{j=1}^{S} A_j g(t) \cos(w_c t) + \theta_j\right) + n_i(t), \qquad j = 1,2,3\ldots, N_r \tag{6.5}$$

6.2 Performance Analysis of FSO-SIM System with Diversity Combiner under the Influence of Gamma-Gamma Turbulence

The average BLER for the FSO-SIM system with spatial diversity combiner over a slow fading channel can be expressed as [127, 130, 131]:

$$P(M, N) = \int_0^\infty \sum_{m=M+1}^{N} \binom{N}{m} P^m (1 - P)^{N-m} f_I(I) dI \tag{6.6}$$

where P is the probability of bit error, M is the number of bit errors within a block length , N is the number of blocks of bits and $f_I(I)$ denotes the PDF of the Gamma-Gamma distribution defined in (2.53).

Since the BPSK modulation is considered on each subcarrier, the conditional probability of bit error for the modulation is obtained as [228]:

$$P(I) = Q\left(\sqrt{2\bar{\gamma}I^2}\right) \tag{6.7}$$

Therefore, the Q-function in (6.7) can be expressed through of used the Q-function derived in [130] as:

$$Q(x) = \frac{5}{24}\exp(-2x^2) + \frac{4}{24}\left(-\frac{11}{20}x^2\right) + \frac{1}{24}exp\left(-\frac{1}{2}x^2\right) \tag{6.8}$$

Thus, from (6.8), the conditional probability can be expressed as:

$$P(I) = \frac{5}{24}\exp(-4\bar{\gamma}I^2) + \frac{1}{6}\left(-\frac{11}{10}\bar{\gamma}I^2\right) + \frac{1}{24}exp(-\bar{\gamma}I^2) \tag{6.9}$$

By substituting for probability of bit error into the (6.9), then the BLER, defined as (6.6), can be rewritten as:

$$P(M,N) = \int\limits_0^\infty \sum_{m=M+1}^{N} \sum_{q=0}^{N-m} \binom{N}{m}\binom{N-m}{q}(-1)^q Q\left(\sqrt{2\bar{\gamma}I^2}\right)^{m+q} f_I(I)\, dI \tag{6.10}$$

To expand the Q-function in (6.10), multinomial expansion approach is applied and this is obtained as:

$$\left(\frac{5}{24}\exp(-4\bar{\gamma}I^2) + \frac{1}{6}\left(-\frac{11}{10}\bar{\gamma}I^2\right) + \frac{1}{24}exp(-\bar{\gamma}I^2)\right)^{m+q}$$
$$= \sum_{b=0}^{m+q}\sum_{l=0}^{b}\binom{m+q}{b}\binom{b}{l}\left(\frac{1}{24}\right)^{m+q-1}\left(\frac{5}{24}\right)^{b-l}\left(\frac{1}{6}\right)^{l}\exp\left(-\bar{\gamma}I^2\left(m+3b-\frac{29}{10}l\right)\right) \tag{6.11}$$

6.2.1 BLER for SIM-BPSK System with MRC over Gamma-Gamma Channel

When MRC is considered at the receiver, the combiner weights the transmitted optical beam from each link. Following the instantaneous SNR for the MRC combiner defined in (2.39) as:

$$\gamma_s = \bar{\gamma}\sum_{i=1}^{N_r} I_i^2 \tag{6.12}$$

The PDF of the MRC combiner channel is determined through the use of MGF. From (6.12), $Y = \sum_{i=1}^{N_r} I^2$ and $I_X = I^2$, the MGF of I is obtained as:

$$\Phi_I(s) = E[\exp(-sI_X)] = \int_0^\infty e^{-sI} f_{I_X}(I_X) dI_X$$

$$\triangleq \frac{1}{2} \sum_{g=0}^{\infty} \left[m_g(\alpha,\beta)\Gamma\left(\frac{g+\beta}{2}\right)(-s)^{\frac{g+\beta}{2}} - m_g(\beta,\alpha)\Gamma\left(\frac{g+\alpha}{2}\right)(-s)^{\frac{g+\alpha}{2}} \right] \tag{6.13}$$

Thus, the summation of the MGF of Y can be obtained through binomial expansion as:

$$\Phi_Y(s) = [\Phi_I(s)]^{N_r}$$

$$\triangleq \frac{1}{2^{Nr}} \sum_{j=0}^{N_r} \binom{N_r}{j} \sum_{g=0}^{\infty} d_g(N_r - j,j)(-s)^{\frac{-g-N_r\beta-j(\alpha-\beta)}{2}} \tag{6.14}$$

where;

$$d_g(N_r - j,j) = \left[m_g(\alpha,\beta)\Gamma\left(\frac{g+\beta}{2}\right) \right]^{[N_r-j]} * \left[m_g(\beta,\alpha)\Gamma\left(\frac{g+\alpha}{2}\right) \right]^{[j]}$$

for $\left[m_g(x,y)\Gamma\left(\frac{g+y}{2}\right) \right]^{[n]}$ implies that $m_g(x,y)\Gamma\left(\frac{g+y}{2}\right)$ is convolved by $n-1$ times with itself.

By applying the inverse Laplace transform to the (6.14), the PDF of $f_Y(Y) = f_{MRC}(I)$ can be expressed as:

$$f_{MRC}(I) = \frac{1}{2^{Nr}} \sum_{j=0}^{N_r} \binom{N_r}{j} \sum_{g=0}^{\infty} \frac{d_g(N_r - j,j)}{\Gamma(\Delta)} I^{\Delta-1} \tag{6.15}$$

where

$$\Delta = \frac{-g - N_r\beta - j(\alpha-\beta)}{2}$$

To determine the BLER for the considered combiner, the derived combiner channel PDF (6.15) is substituted into (6.10), and the BLER of the MRC receiver can then be obtained as:

$$P_{MRC}(M, N)$$

$$= \left(\frac{1}{2}\right)^{N_r} \sum_{m=M+1}^{N} \sum_{q=0}^{N-m} \sum_{b=0}^{m+q} \sum_{l=0}^{b} \sum_{j=0}^{N_r} \sum_{g=0}^{\infty} \binom{N}{m}\binom{N-m}{q}\binom{m+q}{b}\binom{b}{l}\binom{N_r}{j}(-1)^q \times$$

$$\left(\frac{1}{24}\right)^{m+q-1}\left(\frac{5}{24}\right)^{b-l}\left(\frac{1}{6}\right)^l \frac{d_g(N_r - j, j)}{\Gamma(\Delta)} \left[\left[\int_0^\infty \exp\left(-\bar{\gamma}I^2\left(m + 3b - \frac{29}{10}l\right)\right) I^{\Delta-1} \right] dI \right]$$

(6.16)

Then, by applying the integral identity defined in [205,equation 3.326(2)] (see Appendix A3.1), the BLER for the system can be expressed as:

$$P_{MRC}(M, N) = \frac{1}{2^{N_r+1}} \sum_{m=M+1}^{N} \sum_{q=0}^{N-m} \sum_{b=0}^{m+q} \sum_{l=0}^{b} \sum_{j=0}^{N_r} \sum_{g=0}^{\infty} \binom{N}{m}\binom{N-m}{q}\binom{m+q}{b}\binom{b}{l}\binom{N_r}{j}$$

(6.17)

$$\times (-1)^q \left(\frac{1}{24}\right)^{m+q-1}\left(\frac{5}{24}\right)^{b-l}\left(\frac{1}{6}\right)^l \frac{d_g(N_r - j, j)}{\Gamma(\Delta)} \Gamma\left(\frac{\Delta}{2}\right)\left[m + 3b - \frac{29}{10}l\right]^{-\frac{\Delta}{2}} \bar{\gamma}^{-\frac{\Delta}{2}}$$

6.2.2 BLER for SIM-BPSK System with EGC over Gamma-Gamma Channel

When considering EGC at the receiver, the combiner gathers all the transmitted optical beam, estimates and sums them coherently with equal weights of one. The instantaneous SNR for the EGC can be defined by following the (2.41) as:

$$\gamma_s = \frac{\bar{\gamma}}{N_r}\left(\sum_{i=1}^{N_r} I_i\right)^2$$

(6.18)

Therefore, the combiner channel PDF for the system is then determined through the MGF. From (6.18), then, $R = \left(\sum_{i=1}^{N_r} I_i\right)^2$ and $P = I_i$ and $Z = \sum_{i=1}^{N_r} I_i$, then the MGF of P is obtained as:

$$\Phi_P(s) = E[\exp(-sP)] = \int_0^\infty e^{-sP} f_P(P) dP$$

$$\triangleq \frac{1}{2}\sum_{g=0}^{\infty}\left[m_g(\alpha, \beta)\Gamma(g + \beta)(-s)^{-g+\beta} + m_g(\beta, \alpha)\Gamma(g + \alpha)(-s)^{-g+\alpha}\right]$$

(6.19)

Then, by binomial expansion, the sum of the Gamma-Gamma distribution for the EGC random variable Z is derived as follows:

$$\Phi_Z(s) = [\Phi_P(s)]^{Nr}$$

$$\triangleq \sum_{j=0}^{Nr} \binom{N_r}{j} \left[\left(\sum_{k=0}^{\infty} m_g(\alpha,\beta)\Gamma(g+\beta)(-s)^{-g+\beta} \right)^{Nr-j} \times \left(\sum_{k=0}^{\infty} m_g(\beta,\alpha)\Gamma(g+\alpha)(-s)^{-g+\alpha} \right)^{j} \right] \tag{6.20}$$

By applying inverse Laplace transform to (6.20), the PDF of Z can be obtained as:

$$f_Z(Z) = \sum_{j=0}^{N_r} \binom{N_r}{j} \sum_{g=0}^{\infty} \frac{\varsigma_g(\alpha,\beta,Nr-j,j)}{\Gamma(\mu)} Z^{\mu-1} \tag{6.21}$$

where

$$\mu = k + N_r\beta + j(\beta - \alpha) \text{, and}$$

$$\varsigma_g(\alpha,\beta,Nr-j,j) = [m_g(\alpha,\beta)\Gamma(g+\beta)]^{Nr-j} * [m_g(\beta,\alpha)\Gamma(g+\alpha)]^{j}$$

In order to obtain the channel PDF for the EGC combiner, the (6.21) is integrated with respect to Z and $R = Z^2$ is substituted. Then, by differentiating with respect to R, the PDF of R, that is, $f_R(R) = f_{EGC}(I)$ is obtained as:

$$f_{EGC}(I) = \frac{1}{2} \sum_{j=0}^{N_r} \binom{N_r}{j} \sum_{g=0}^{\infty} \frac{\varsigma_g(\alpha,\beta,N_r-j,j)}{\Gamma(\mu)} I^{\frac{\mu}{2}-1} \tag{6.22}$$

Following the same approach in MRC, the BLER of the EGC receiver can then be obtained by substituting for combiner channel PDF into equation (6.10) as:

$$P_{EGC}(M,N)$$
$$= \frac{1}{2} \sum_{m=M+1}^{N} \sum_{q=0}^{N-m} \sum_{b=0}^{m+q} \sum_{l=0}^{b} \sum_{j=0}^{N_r} \sum_{k=0}^{\infty} \binom{N}{m}\binom{N-m}{q}\binom{m+q}{b}\binom{b}{l}\binom{N_r}{j}(-1)^q \left(\frac{1}{24}\right)^{m+q-1}$$
$$\times \left(\frac{5}{24}\right)^{b-l} \left(\frac{1}{6}\right)^l \frac{\varsigma_k(\alpha,\beta,N_r-j,j)}{\Gamma(\mu)} \left[\left[\int_0^{\infty} \exp\left(-\bar{\gamma}I^2\left(m+3b-\frac{29}{10}l\right)\right) I^{\frac{\mu}{2}-1} \right] dI \right] \tag{6.23}$$

Then, by applying the integral identity defined in [205,equation 3.326(2)] (see Appendix A3.1), the BLER for EGC can be expressed as:

$$P_{EGC}(M,N) = \frac{1}{4} \sum_{m=M+1}^{N} \sum_{q=0}^{N-m} \sum_{b=0}^{m+q} \sum_{l=0}^{b} \sum_{j=0}^{N_r} \sum_{g=0}^{\infty} \binom{N}{m} \binom{N-m}{q} \binom{m+q}{b} \binom{b}{l} \binom{N_r}{j} \times$$

$$(-1)^q \left(\frac{1}{24}\right)^{m+q-1} \left(\frac{5}{24}\right)^{b-l} \left(\frac{1}{6}\right)^l \frac{\varsigma_g(\alpha,\beta,N_r-j,j)}{\Gamma(\mu)} \Gamma\left(\frac{\mu}{4}\right) \left[m+3b-\frac{29}{10}l\right]^{-\frac{\mu}{4}} \bar{\gamma}^{-\frac{\mu}{4}}$$

(6.24)

It should be noted that both the (6.17) and (6.24) are in form of infinite series and this needs to be truncated to finite terms for evaluation purpose. Based on this, it is necessary to evaluate the approximate error resulting from the elimination of all term after $K+1$ in the BLER rate series expression. Thus, average BLER for MRC in (6.17) is used as illustration, since the EGC follows similar procedure and thus, the truncation error is defined as:

$$\varepsilon_K = \frac{1}{2^{N_r+1}} \sum_{m=M+1}^{N} \sum_{q=0}^{N-m} \sum_{b=0}^{m+q} \sum_{l=0}^{b} \sum_{j=0}^{N_r} \sum_{g=K+1}^{\infty} \binom{N}{m} \binom{N-m}{q} \binom{m+q}{b} \binom{b}{l} \binom{N_r}{j}$$

$$\times (-1)^q \left(\frac{1}{24}\right)^{m+q-1} \left(\frac{5}{24}\right)^{b-l} \left(\frac{1}{6}\right)^l \left(\frac{1}{\sqrt{\bar{\gamma}\left(m+3b-\frac{29}{10}l\right)}}\right)^g$$

(6.25)

where

$$\psi_g(\alpha,\beta) = \frac{d_g(N_r-j,j)\Gamma(\Delta/2)}{\Gamma(\Delta)\left(\sqrt{\bar{\gamma}\left(m+3b-\frac{29}{10}l\right)}\right)^{N_r\beta-j(\alpha-\beta)}}$$

(6.26)

The summation in (6.25) can therefore be simplified using the Taylor series expansion of $x^n/(1-x)$, and the upper bound of truncation error can then be obtained as:

$$\varepsilon_K = \frac{1}{2^{N_r+1}\left(\sqrt{\bar{\gamma}\varrho_A}-1\right)(\bar{\gamma}\varrho_A)^L} \sum_{m=M+1}^{N} \sum_{q=0}^{N-m} \sum_{b=0}^{m+q} \sum_{l=0}^{b} \sum_{j=0}^{N_r} \binom{N}{m} \binom{N-m}{q} \binom{m+q}{b}$$

$$\times \binom{b}{l} \binom{N_r}{j} (-1)^q \left(\frac{1}{24}\right)^{m+q-1} \left(\frac{5}{24}\right)^{b-l} \left(\frac{1}{6}\right)^l \max_{g>K}\{\psi_g(\alpha,\beta)\}$$

(6.27)

where

$$\varrho_A = m + 3b - \frac{29}{10}l$$

It is evident that as g tends to infinity, the (6.26) approaches zero and thus the ε_K in (6.27) reduces with increase in index g.

6.2.3   Hard-Coded Technique for SIM-BPSK FSO System

In this study, the error control coding technique called convolutional coding is adopted to further improve the BLER of the system due to its performance over a slow channel fading like FSO link. A ½ rate encoder of octal representation (5, 7), constraint length of 3 and a free distance of 5 as presented in [214] is considered. The BLER for this coded SIM-BPSK system can be obtained following equation (3.66).

6.2.4   Numerical Results and Discussions

In this section, the results on BLER performance of the SIM with MRC and EGC over Gamma-Gamma turbulence channel are presented. The approximate error rate is obtained by eliminating the infinite term after the $K + 1$ term of the derived series solutions and the K term is set to be 50. This is verified by numerical integration of the exact error rate given in equation (6.10). In the simulation, the number of bit errors in a block length of N is denoted as $M = 2$, except otherwise stated. Since Gamma-Gamma turbulence channel was considered, the following turbulence levels are employed and these include, weak $(\alpha = 3.78, \beta = 3.74)$, moderate $(\alpha = 2.50, \beta = 2.06)$ and strong $(\alpha = 2.04, \beta = 1.10)$.

The performance of the system with both MRC and EGC are compared under different PD configurations over the link range of $3000\, m$, and are illustrated in Figure 6.1. It can be depicted here that MRC has superior BLER improvement at an expense of system complexity than EGC for different PDs since the MRC receiver complexity is directly proportional to the number of branch signal present at it receiver. For instance, at SNR of $20\, dB$, the MRC yields an approximate BLER of 10^{-2}, while EGC produces 10^{-1} with PDs of two. This is further enhanced by increasing the system PDs to four, and the MRC offers an improved BLER of approximate 10^{-5}, while EGC gives 10^{-3} error rate at the same SNR. Also, the result demonstrated clearly that the series solution at $L = 50$ has a perfect agreement with the exact BLER calculated by the numerical integration.

The systems error performance over Gamma-Gamma turbulence is illustrated in Figure 6.2 for 15 block lengths with two PDs at the receiver. This clearly showed that as the turbulence increases, the error rate for the system also increased. As expected, MRC offers better performance in all the turbulence levels than EGC system. For instance, at weak turbulence

condition, the BLER performance for the two systems is better; with MRC and EGC offers approximate error rate of 10^{-6} and 10^{-5} respectively at SNR of $35\ dB$. This degrades to $\cong 10^{-1}$ and $\cong 10^{-2}$ respectively for MRC and EGC over the strong turbulence. Moreover, it can be observed from the Figure 6.2 that the derived analytical expressions in (6.17) and (6.24) provide a perfect match with the exact BLER result obtained through Monte-Carlo simulation and this therefore validates the accuracy of the numerical expressions.

The increase in the number of block bits transmitted at the transmitter also has influence on the systems error rate. It can be depicted in Figure 6.3 that as the block length increases from $5\ to\ 20$, the more the system error rate increases. However, a point is reached where the effect becomes less pronounced due to lack of independence between the successive bit errors in a block under the slow fading channel. Nevertheless, the increase in the number of PDs employed at the receiving end therefore improves the system error performance as can be seen when $N_r = 4$.
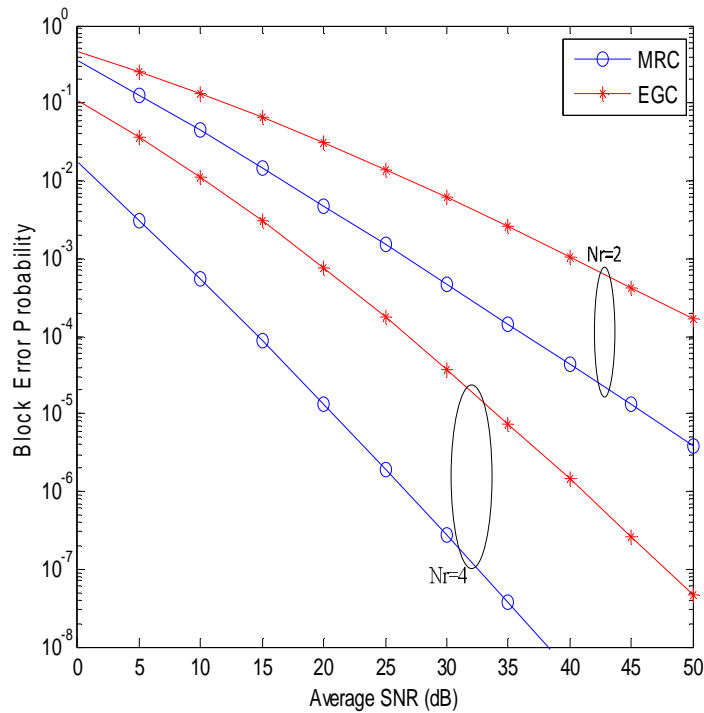
Figure 6.1: Performance comparison between MRC-SIM and EGC-SIM for 20 block lengths
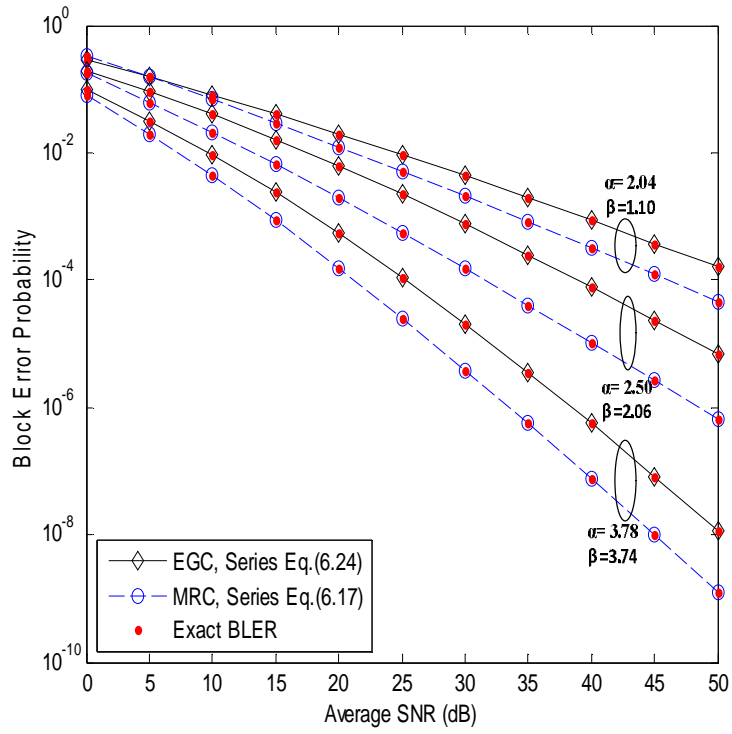
Figure 6.2: Performance comparison between MRC and EGC under different turbulence strengths at $N_r = 2$ for 15 block lengths
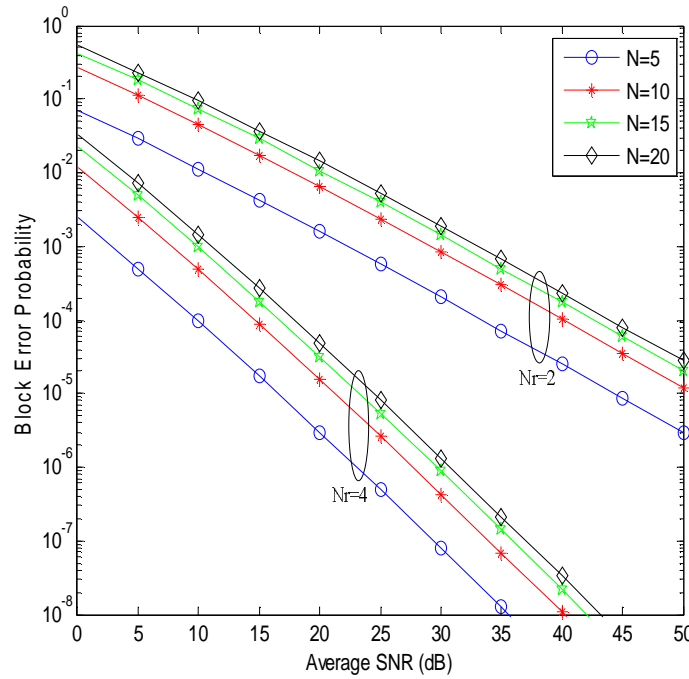
Figure 6.3: Performance of MRC under different block lengths

The impact of link range on the system BLER is demonstrated by EGC system in Figure 6.4. It is clearly shown that the increase in link range increases the BLER for the system. This effect can be significantly reduced by increasing the number of PD at the receiving end. For instance, at link range of $2500\,m$, the system produces approximate BLER of 10^{-2} and 10^{-6} when $N_r = 2$ and 4 respectively at SNR of $35\,dB$. This degrades when considering a link range of $3500\,m$ at the same SNR, as the system offers approximate BLER of 10^{-1} when $N_r = 2$ and 10^{-5} when $N_r = 4$. However, it is noticed that as the link range increases the system performance deteriorated in terms of block error due to Gamma-Gamma random variable whose variation is in parallel with the original channel.
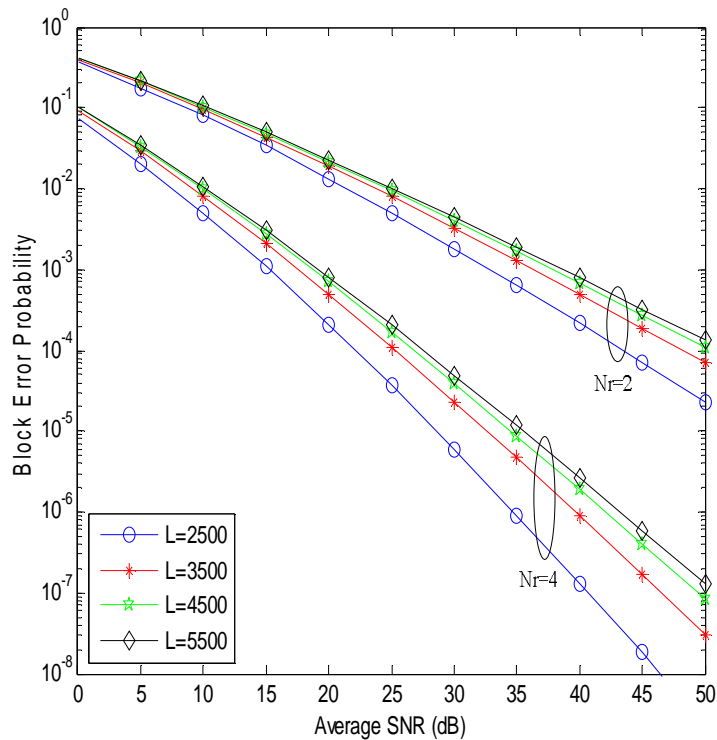
Figure 6.4: Performance of BLER EGC system under different link range for 20 block lengths

To validate the performance of the proposed system, the impact of diversity combiner on the FSO-SIM system is illustrated in Figure 6.5, where the proposed system is compared with other well-established systems presented in [130] under the same channel condition. In order to have a fair comparison, the systems were subjected to the same atmospheric condition with the SIM-BPSK-MRC and SIM-BPSK-EGC systems having four PDs at the receiving end. As it can be observed, the SIM-DPSK and SIM-NCFSK offer a poor BLER performance while MRC-BPSK system yields the best performance among all the systems. For instance, it can be depicted that at a BLER of 10^{-4}, MRC combiner enhances the BLER performance of BPSK system by $10\ dB$ as compared with the case of EGC with the value of $5\ dB$.
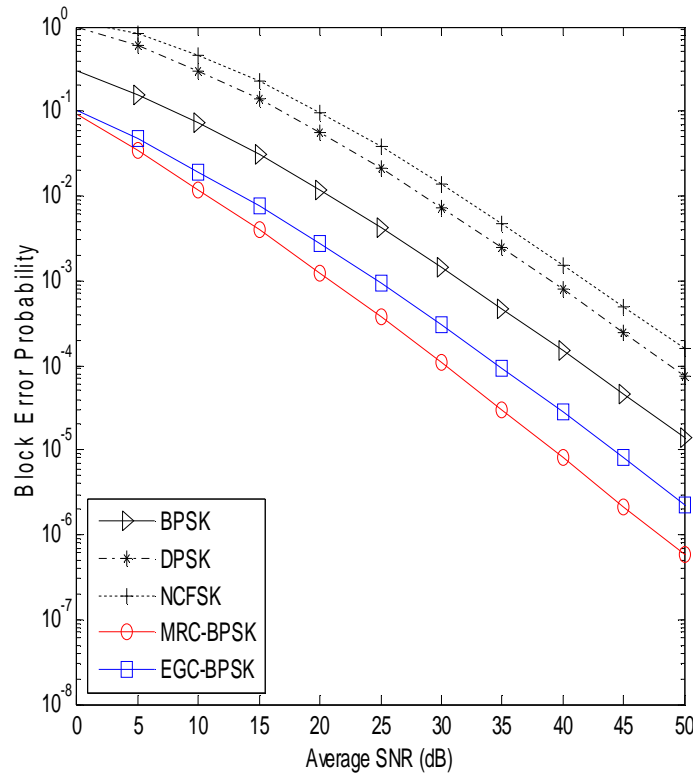
Figure 6.5: Comparison between the proposed FSO-SIM systems with well-established FSO-SIM for 10 block lengths when $N_r = 4$ over the strong turbulence

The performance of the convolutional coding technique on the BLER of MRC-BPSK and its EGC counterpart is presented in Figure 6.6. The two systems are subjected to a strong turbulence with the transmission of 10 block lengths of bits over the link. It can be deduced that the coding technique greatly enhanced the systems BLER, and the MRC-BPSK is found to produce the best performance than the EGC. For instance, at a system of four PDs, the

coding technique enhances the system performance by about $32\,dB$ in SNR at a BLER of 10^{-6} as compared with EGC system of $35\,dB$. At the same BLER, the coding gain between $N_r = 2$ and $N_r = 4$ is around 6dB and $8\,dB$ respectively for MRC and EGC combiners.
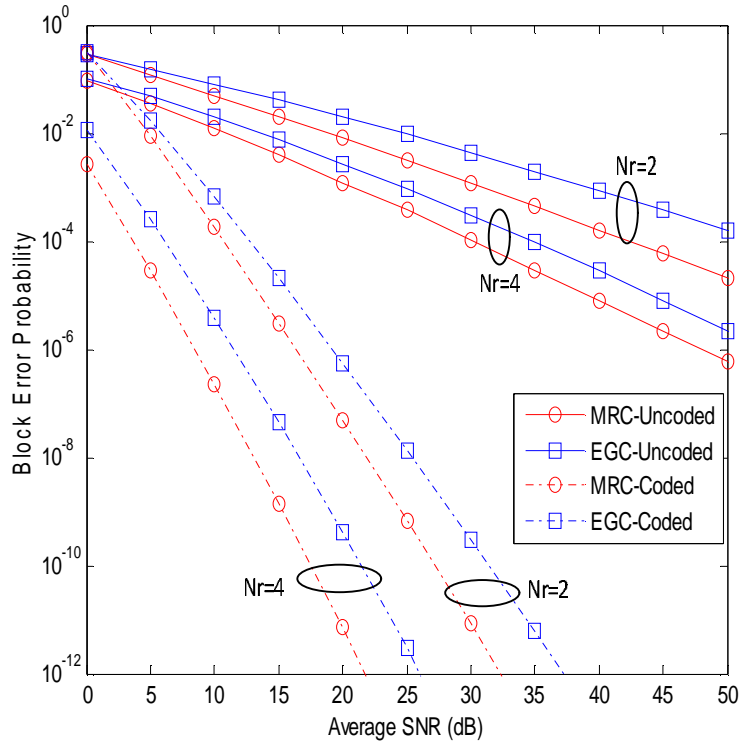
Figure 6.6: Performance of convolutional coding on SIM BPSK-SD systems for 10 block lengths over the strong turbulence

6.3 Performance Analysis of Block Error Rate for SIM-FSO System with Diversity Combiner under the combined influence of Gamma-Gamma Fading and Pointing Error Channel

In this study, the combined effect of Gamma-Gamma atmospheric turbulence fading with pointing error are considered since of FSO systems is susceptible to either conditions. Following the (3.72), the PDF of the combined impairments can therefore be expressed through infinite power series expansion as:

$$f_I(I) = \Xi(\alpha, \beta, \xi) \sum_{i=0}^{\infty} \left[\psi_g(\alpha, \beta, A_0) R_g(\beta) I^{g+\beta-1} - \psi_g(\beta, \alpha, A_0) R_g(\alpha) I^{g+\alpha-1} \right] \qquad (6.28)$$

161

where

$$\Xi(\alpha, \beta, \xi) = \frac{\xi^2 \Gamma(\alpha - \beta)\Gamma(1 - \alpha + \beta)}{\Gamma(\alpha)\Gamma(\beta)}$$

$$\psi_g(x, y, A_0) = \frac{\left(\frac{xy}{A_o}\right)^{g+y}}{\Gamma(g - x + y + 1)g!}$$

$$R_g(y) = \int\limits_0^\infty exp[(g + y - \xi^2)t]dt$$

6.3.1   BLER for SIM-BPSK System with MRC over Combined Distributions

When MRC is considered at the system receiving end, the channel PDF can then be obtained following the same approach given in (6.13). Thus, the MGF of Y under the influence of pointing error is obtained as:

$$\begin{aligned}
\mathrm{M}_I(s) &\triangleq \frac{\Xi(\alpha, \beta, \xi)}{2} \sum_{g=0}^{\infty} \left[\psi_g(\alpha, \beta, A_0)R_g(\beta)\Gamma\left(\frac{g + \beta}{2}\right)(-s)^{\frac{g+\beta}{2}} \right. \\
&\quad \left. - \psi_g(\beta, \alpha, A_0)R_g(\alpha)\Gamma\left(\frac{g + \alpha}{2}\right)(-s)^{\frac{g+\alpha}{2}} \right]
\end{aligned} \tag{6.29}$$

It is deduced from the $R_g(y)$ defined in (6.28) that when $\xi^2 < k + y$, the integral does not converge. Also, it is noticed from (6.29) that the infinite series equation converges to zero when $g = 0$. Thus, the MGF of the sum of N_r link can be approximated as a finite series and expressed through binomial expansion as:

$$\begin{aligned}
\mathrm{M}_Y(s) &= [\mathrm{M}_I(s)]^{N_r} \\
&\triangleq \left(\frac{\Xi(\alpha, \beta, \xi)}{2}\right)^{N_r} \sum_{p=0}^{N_r} \binom{N_r}{p} \sum_{g=0}^{W} c_g(N_r - p, p, Ao)(-s)^{\frac{-g-N_r\beta-p(\alpha-\beta)}{2}}
\end{aligned} \tag{6.30}$$

where $W = \lfloor \xi^2 - \alpha \rfloor$ with $\lfloor . \rfloor$ is the floor operator and

$$c_g(\alpha, \beta, N_r - p, p, A_0) = \left[\frac{\psi_g(\alpha,\beta,A_0)\Gamma\left(\frac{g+\beta}{2}\right)}{(\xi^2-g-\beta)} \right]^{[N_r-p]} * \left[\frac{\psi_g(\beta,\alpha,A_0)\Gamma\left(\frac{g+\alpha}{2}\right)}{(\xi^2-g-\alpha)} \right]^{[p]} \text{ with}$$

$\left[\frac{\psi_g(x,y,A_0)\Gamma\left(\frac{g+y}{2}\right)}{(\xi^2-g-y)} \right]^{[n]}$ denotes that $\frac{\psi_g(x,y,A_0)\Gamma\left(\frac{g+y}{2}\right)}{(\xi^2-g-y)}$ is convolved by $n - 1$ times with itself.

By applying the inverse Laplace transform to the equation (6.30), the PDF of $f_Y(Y) = f_{MRC}(I)$, and can be expressed as:

$$f_{MRC}(I) = \left(\frac{\Xi(\alpha, \beta, \xi)}{2}\right)^{N_r} \sum_{p=0}^{N_r} \binom{N_r}{p} \sum_{g=0}^{W} \frac{c_g(\alpha, \beta, N_r - p, p, A_0)}{\Gamma(\Delta)} I^{\Delta - 1} \qquad (6.31)$$

By substituting (6.28) and (6.11) into (6.10) and applying integral identity in [205, equation 3.326(2)] (see Appendix A3.1), then the average BLER for the SIM-BPSK system with MRC can be expressed as:

$$P_{MRC}(M, N) = \frac{\left(\Xi(\alpha, \beta, \xi)\right)^{N_r}}{2^{N_r+1}} \sum_{m=M+1}^{N} \sum_{q=0}^{N-m} \sum_{b=0}^{m+q} \sum_{l=0}^{b} \sum_{p=0}^{N_r} \sum_{g=0}^{W} \eta \frac{c_g(\alpha, \beta, N_r - p, p, A_0)}{\Gamma(\Delta)}$$

$$\times \Gamma\left(\frac{\Delta}{2}\right) \left[m + 3b - \frac{29}{10}l\right]^{-\frac{\Delta}{2}} \bar{\gamma}^{-\frac{\Delta}{2}} \qquad (6.32)$$

where

$$\eta = \binom{N}{m}\binom{N-m}{q}\binom{m+q}{b}\binom{b}{l}\binom{N_r}{j}(-1)^q \left(\frac{1}{24}\right)^{m+q-1} \left(\frac{5}{24}\right)^{b-l} \left(\frac{1}{6}\right)^l$$

6.3.2   BLER for SIM-BPSK System with EGC over Combined Distributions

When the system employs EGC combiner, following the approach in (6.19), the MGF of Z under the influence of pointing error is obtained as:

$$M_G(s) = E[\exp(-sG)] = \int_0^\infty e^{-sG} f_G(G) dG$$

$$\triangleq \Xi(\alpha, \beta, \xi) \sum_{g=0}^\infty \left[\psi_g(\alpha, \beta, A_0) R_g(\beta) \Gamma(g + \beta)(-s)^{-g+\beta} \qquad (6.33)\right.$$

$$\left. + \psi_g(\beta, \alpha, A_0) R_g(\alpha) \Gamma(g + \alpha)(-s)^{-g+\alpha}\right]$$

As mentioned earlier, the integral in $R_g(y)$ does not converge when $\xi^2 < g + y$. Thus, the sum of the Gamma-Gamma distribution for the EGC random variable can then be approximated as a finite series and derived as:

$$M_Z(s) = [M_G(s)]^{N_r}$$

$$\triangleq \left(\Xi(\alpha,\beta,\xi)\right)^{N_r} \sum_{p=0}^{N_r} \binom{N_r}{p} \sum_{g=0}^{W} \frac{\mathrm{d}_g(\alpha,\beta,Nr-p,p,A_0)}{\Gamma\left(g + N_r\beta + p(\beta-\alpha)\right)} S^{\mu-1} \tag{6.34}$$

where

$$\mathrm{d}_g(\alpha,\beta,Nr-p,p,A_0) = \left[\frac{\psi_g(\alpha,\beta,A_0)\Gamma(g+\beta)}{(\xi^2-g-\beta)}\right]^{N_r-p} * \left[\frac{\psi_g(\beta,\alpha,A_0)\Gamma(g+\alpha)}{(\xi^2-g-\alpha)}\right]^{p}$$

Then, from (6.34), the PDF of Z can then be obtained by the inverse Laplace transform as:

$$f_Z(Z) = \left(\Xi(\alpha,\beta,\xi)\right)^{N_r} \sum_{p=0}^{N_r} \binom{N_r}{p} \sum_{g=0}^{W} \frac{\mathrm{d}_g(\alpha,\beta,Nr-p,p,A_0)}{\Gamma\left(g + N_r\beta + p(\beta-\alpha)\right)} Z^{\mu-1} \tag{6.35}$$

By integrating (6.35) with respect to Z and substitute for $R = Z^2$, and thereafter, differentiate with respect to R, the PDF of R, that is, $f_R(R) = f_{EGC}(I)$ is obtained as:

$$f_{EGC}(I) = \frac{\left(\Xi(\alpha,\beta,\xi)\right)^{N_r}}{2} \sum_{p=0}^{N_r} \binom{N_r}{p} \sum_{g=0}^{W} \frac{\mathrm{d}_g(\alpha,\beta,Nr-p,p,A_0)}{\Gamma(\mu)} I^{\frac{\mu}{2}-1} \tag{6.36}$$

By substituting (6.36) and (6.11) into (6.10) and applying integral identity in [205, equation 3.326(2)] (see Appendix A3.1), the average BLER for the SIM-BPSK with EGC can be obtained as:

$$P_{EGC}(M,N)$$
$$= \frac{\left(\Xi(\alpha,\beta,\xi)\right)^{N_r}}{4} \sum_{m=M+1}^{N} \sum_{q=0}^{N-m} \sum_{b=0}^{m+q} \sum_{l=0}^{b} \sum_{j=0}^{N_r} \sum_{g=0}^{W} \eta \frac{\mathrm{d}_g(\alpha,\beta,Nr-p,p,A_0)}{\Gamma(\mu)}$$
$$\times \Gamma\left(\frac{\mu}{4}\right)\left[m + 3b - \frac{29}{10}l\right]^{-\frac{\mu}{4}} \bar{\gamma}^{-\frac{\mu}{4}} \tag{6.37}$$

6.3.3 Numerical Results and Discussions

In this section, the analytical BLER results of FSO SIM-BPSK over Gamma-Gamma atmospheric turbulence and pointing error with assumption that $\xi^2 > \alpha$ is presented. The BLER for the system with MRC and EGC at the receiving end is presented using the derived closed form expressions in (6.32) and (6.37). The Gamma-Gamma turbulence channel is described by the following turbulence levels which include, weak $(\alpha = 3.78, \beta = 3.74)$,

moderate $(\alpha = 2.50, \beta = 2.06)$ and strong $(\alpha = 2.04, \beta = 1.10)$. Also, the pointing error parameters are characterized as follows; the normalized Jitter standard deviation and noise standard deviation to be $\sigma_s/r = 1$ and $\sigma_n = 10^{-7} A/Hz$ respectively, normalized beam waist is varied accordingly and the number of bit errors in a block length of N is set to $M = 2$.

Figure 6.7 illustrates the performance of MRC and EGC systems over different normalized beam waist when the block length is 10 and number of the photo-detector is 2. It is confirmed from Figure 6.7 (a) that a very narrow beam waist of 5 offers the MRC system a better error performance compared to others. For instance, at optical power of $5 \, dBm$, the system beam waist of 5 offers error of 1.87×10^{-8} compared 2.32×10^{-5} produced when $w_e/r = 8$. However, the effect of narrow beam waist may cause the system to lose its LOS in the direction of the receiver due to misalignment. The performance comparison between MRC and EGC systems are illustrated in Figure 6.7(b) where MRC offers the best performance compared to EGC under different beam waists.

The BLER performance of the MRC and EGC under different turbulence conditions is demonstrated in Figure 6.8 where 10 block lengths of bits are transmitted with the beam waist and the photo-detector are set to 15 and 2 respectively. It is noted from the result that the turbulence significantly degrades the system performance. For instance, at optical power of $10 \, dBm$ under weak turbulent, the MRC offers 7.21×10^{-5} error and this is increased to 1.71×10^{-2} and 3.11×10^{-1} respectively under the moderate and strong turbulence. Under the same turbulence condition, it is confirmed that the MRC produces better error with 4.01×10^{-3} compared with 2.01×10^{-3} for EGC at optical power of $20 \, dBm$ under moderate condition. Furthermore, the Figure 6.8 is employed to verify the accuracy of the derived analytical expressions in (6.32) and (6.37). It is observed that the derived expressions coincided with simulation and this validate the accuracy of the analytical expressions obtained for the proposed FSO system.
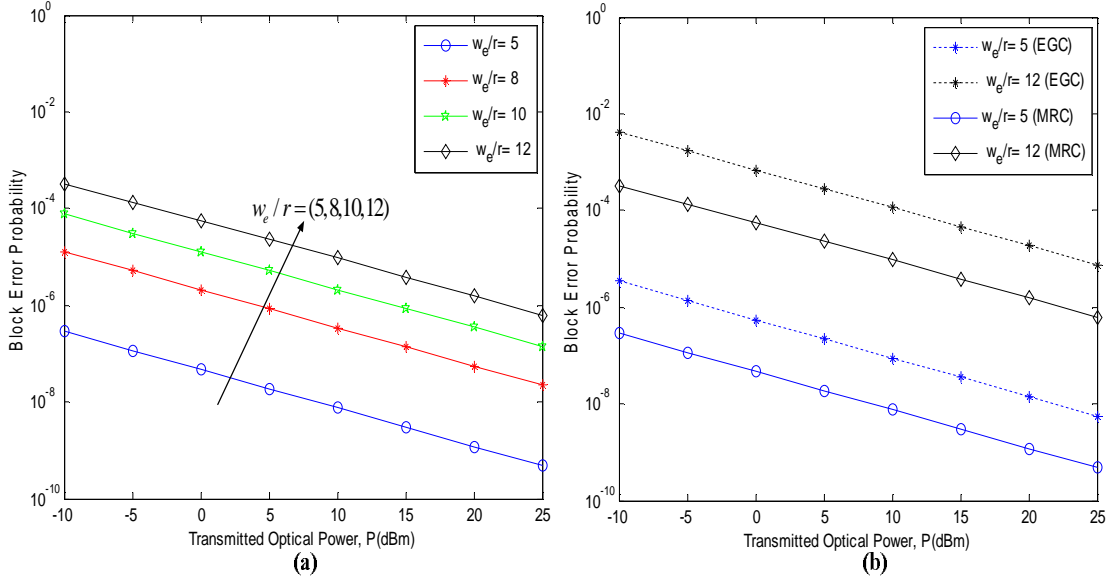
Figure 6.7: (a) Effect of beam waist on the MRC at $N = 10$ when $N_r = 2$ over strong turbulence **(b)** Performance comparison between the MRC and EGC under different beam waist
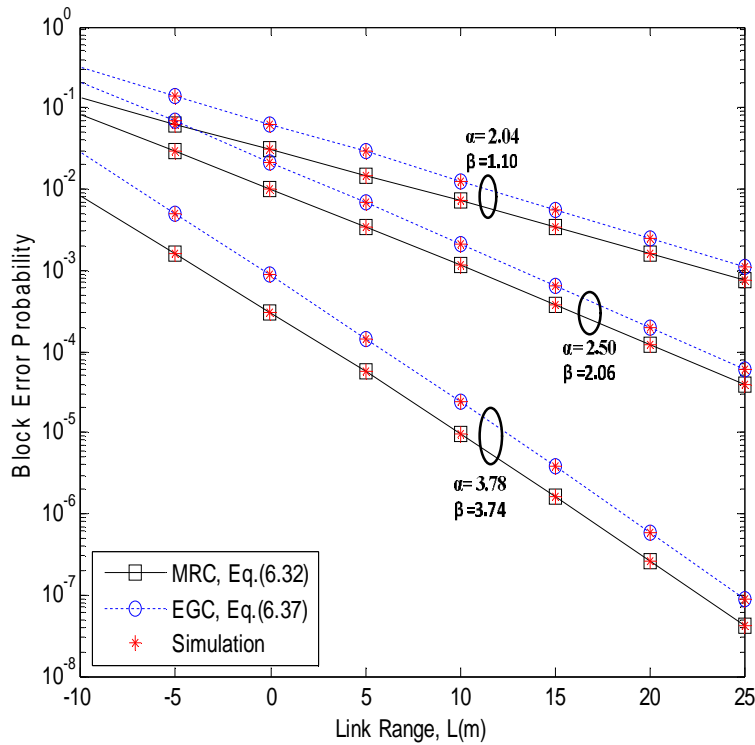
Figure 6.8: BLER Performance of MRC and EGC SIM system over difference turbulence when $N_r = 2$ and $w_e/r = 15$ and $N = 10$

In Figure 6.9, the performance of the proposed system over several link ranges is presented. Obviously, it is deduced from the result that the BLER increases with the increase in the link range but this can be reduced with the increase in the number of PDs at the receiving end. For example, at a link range of $3500\,m$, the MRC yields 2.21×10^{-4} error when $N_r = 2$ and this is reduced to 6.15×10^{-7} when $N_r = 4$. Expectedly, the MRC outperformed the EGC by 9.2% over the link range of $4500\,m$ when $N_r = 4$.

The effect of an increase in the number of block lengths over the channel impairment is demonstrated in Figure 6.10. It is confirmed from the result that as the number of block lengths increases the more the system performance got deteriorated. It is noticed however that a point is reached where the effect became less pronounced due to lack of independence between the successive bit errors in a block under the slow fading channel. Notwithstanding, the MRC technique offered the system better performance in all cases compared to EGC combining.
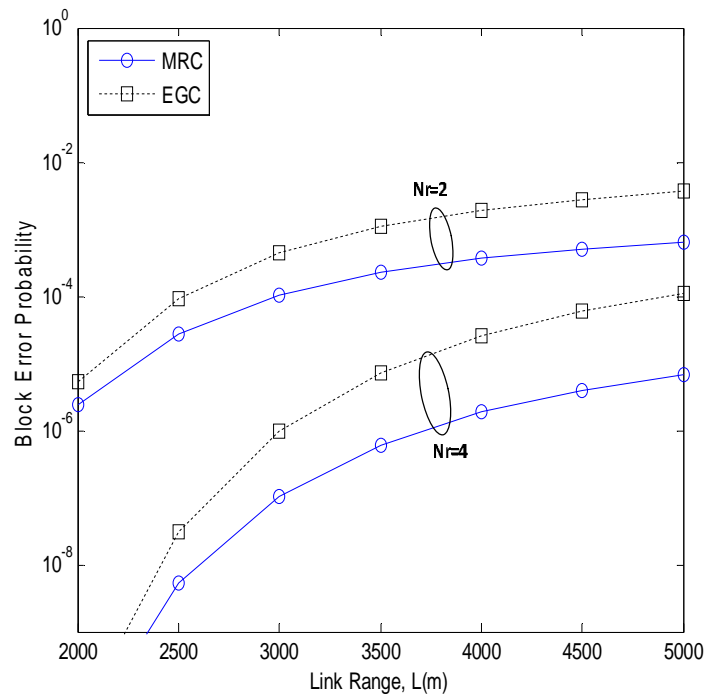
Figure 6.9: BLER performance between the MRC and EGC over the link range when
$w_e/r = 12$ and $N = 10$
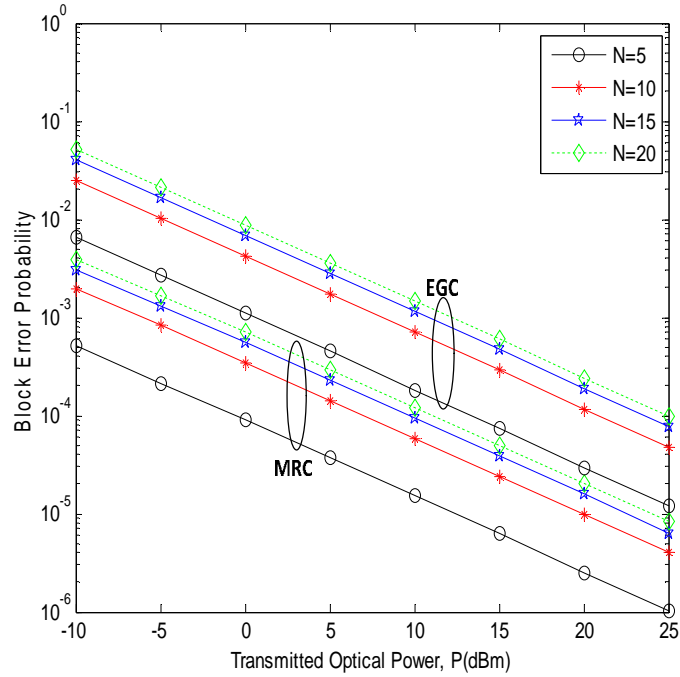
Figure 6.10: Performance of MRC and EGC at $N_r = 2$ and $w_e/r = 10$

6.4 Chapter Summary

In this chapter, the analysis of BLER performance of FSO-SIM system with diversity combiners was presented under the Gamma-Gamma atmospheric turbulence channel and/or pointing error. In both cases, the channel PDF for MRC and EGC was derived by using power series expansion of the modified Bessel function. Then, the BLER closed-form expressions for the combiners were obtained. The effect of Gamma-Gamma induced fading channel on the block transmissions in FSO systems was evaluated. The results confirmed that atmospheric turbulence has severe effects on the systems BLER. The impact of pointing error on the system performance was presented with narrow beam waist offering the system good performance but highly prone to loss of LOS. Moreover, it was also shown that as the data block length and link range increased; the more the system performance deteriorated.

CHAPTER SEVEN

Conclusions and Future Research

In this chapter, the results obtained in this thesis are summarized and potential recommendations relating to our accomplished work are suggested for future research.

7.1 Summary of Results

In this thesis, spatial diversity combining and relay-assisted technique were introduced to address the challenges facing the performance of FSO communication systems. Firstly, the performance comparison between the Meijer-G function and infinite power series expansion as mathematical tools in analyzing FSO systems over Gamma-Gamma turbulence channel was investigated with the two methods offer the same performance under the same turbulence condition. Thus, the performance of the FSO optical spatial modulation system with diversity combiner under the influence of lognormal and Gamma-Gamma atmospheric turbulence which describes the channel conditions of FSO link from weak to strong turbulence was investigated. Moreover, the influence of pointing error on the proposed system was also carried out. Thereafter, the performance of dual-hop relay-assisted technique on the FSO optical spatial modulation system in-conjunction with the combiner was demonstrated in order to improve the system error rate and capacity as well as coverage area. Furthermore, the system under study was also subjected to asymmetric channel environment. Due to the slow nature of the FSO channel, the performance of BLER on the FSO system over Gamma-Gamma atmospheric turbulence with and without pointing error was also presented using SIM modulation scheme. Thus, the accomplished works in this thesis are summarized as follows:

In chapter three, the error performance analysis for FSO-SM communication systems under the lognormal and Gamma-Gamma distributions were presented. The error analysis under the influence of Gamma-Gamma turbulence was based on power series approach. It was demonstrated that the ABER of the proposed system can be greatly improved with the aid of spatial diversity techniques such as MRC, EGC and SC. The theoretical framework revealed the effect of atmospheric turbulence levels and link range on the overall system performance. It was shown that the increase in the SI degrades the system performance for each diversity scheme and the results confirmed that MRC yields better error performance than the other diversity schemes. Also, the study proves that the longer the link range, the stronger the

atmospheric turbulence has severe effect on the system performance and the influence of PD configurations on this effect has been identified. In both channel distributions, the simulation results therefore showed that EGC has yielded lower average BER performance than MRC, but it is very simple to implement practically. Thus, it can be recommended that as spatial diversity technique for FSO-SM to mitigate atmospheric turbulence. The performance of the proposed FSO-SM system was also compared with other conventional systems that employ diversity combiner and the proposed system offered the best performance among all of them. Furthermore, the performance of the proposed system over Gamma-Gamma channel was also enhanced by employing convolutional coding technique, and MRC scheme yielded the best error performance compared with the EGC scheme. In addition, under the joint influence of both Gamma-Gamma turbulence and pointing error effect, the result revealed that FSO system with narrow beam waist offers a better performance than the wide beam waist. Thus, increase in the transmitter beam waist strongly affects the system error rate with higher transmitter optical power, but improves the system robustness against loss of LOS due to misalignment.

In chapter four, a dual-hop DF relaying FSO spatial modulation system using diversity combiners at the relay and destination was proposed. The power series expansion of modified Bessel function was employed for the considered turbulence channel to determine the system end-to-end average BER per hop for the system. The results showed that the dual-hop actually increased the system coverage area with lower error performance when compared with the direct link. In all cases, it was demonstrated that MRC combiner offers an optimal error performance than any other combiners. It was also inferred from the results that considering two identical optimal combiners (MRC or EGC) for a dual-hop system, the better the error performance, except when the optimal combiner is inconjunction with the SC combiner that the system performance degraded. This is a result of maximum channel gain upon which SC combiner depends. Furthermore, it was shown in this study that the higher the average received SNR on the S-to-R link, the more improvement on the BER for the dual-hop system. The results also depicted that a dual hop FSO system under non-symmetric turbulence channel performs better than when subjected to symmetric turbulence channel. From this, it was noticed that providing substantial received photo-detectors at the relay and destination of the system, the better the error performance of dual-hop FSO system. Additionally, analysis and evaluation for the performance of heterodyne optical spatial modulation dual-hop AF CSI-assisted relay systems with MRC and EGC combiners at the

destination over Gamma-Gamma turbulence induced fading with and without pointing error were carried out. The statistical characteristics of the equivalent end-to-end SNR were derived and this was utilized to determine the APEP for each combiner. The ABER closed-form expression for the system was then determined. The results illustrated in this thesis show the significant effect of atmospheric turbulence and/or pointing error conditions on the SM-SD dual hop system. It is therefore proved that as atmospheric turbulence varies from weak to strong levels, the more the ABER and the effective system capacity performance degraded. Also, the result further confirmed that as the pointing error increases the worst the system error and capacity becomes, but large beam width offers the system better performance, while the MRC yields the best performance compared with EGC.

In chapter five, the performance analysis of a dual-hop spatial modulation relaying system over asymmetric RF/FSO with heterodyne detection and MRC combiner at the destination was presented. The S-to-R and R-to-D links were respectively considered to be Nakagami-m fading and Gamma-Gamma turbulence with and/or without pointing error. According to our results, the system clearly showed worse performance in ABER as the fading and turbulence induced on the RF and FSO links increased respectively. Also, the result of the effect of normalized jitter and beam waist on FSO link confirmed that pointing error significantly deteriorates the system ABER. It was also depicted from the results that the MRC combiner improved the system performance as the number of PDs at the destination increases. Finally, the results proved that the performance of the proposed system is better than the well-established systems under the same conditions.

In chapter six, the analysis of BLER performance of SIM with diversity combiners was presented under the Gamma-Gamma atmospheric turbulence channel with and without pointing error. Under the influence of Gamma-Gamma atmospheric turbulence, the effect of Gamma-Gamma induced fading channel on the data block transmissions in FSO systems was evaluated. The results confirmed that atmospheric turbulence has severe effects on the systems BLER. Moreover, it also showed that as the data block length and link range increases, the more the system performance deteriorates. It was also inferred that the systems BLER can be improved by increasing the number of PDs at the receiving end for both MRC and EGC systems. The performance analysis results of using these combiners were compared with other well-established FSO-SIM systems and the results showed the importance of using diversity combiner to mitigate atmospheric turbulence impairment in the FSO communication channel. In addition, the performance of the FSO SIM system was also enhanced through the

use of convolutional coding technique, and the MRC scheme yielded the best BLER performance over the EGC scheme. Under the influence of pointing error, it was confirmed from the result that the impairments greatly degraded the system error performance as the pointing error made the system power inefficient. It was also revealed that narrow beam waist offered the system good performance but highly prone to loss of LOS. The impact of using high number photo-detectors at the receiver over large link range showed that the system with MRC offers the best BLER performance compare to EGC.

7.2 Suggestions for Future Research

In this thesis, the performance of FSO-SM system over lognormal and Gamma-Gamma atmospheric channel with diversity combiners at the receiving end was presented. It will be very interesting to evaluate the performance of the proposed system over other channel distributions which can also be used to express the conditions of the FSO links. Also, in this thesis the distance between the diversity branches was assumed to be greater than the spatial coherent distance which results in each branch receiving independent signals. In practical scenario, this may not be valid as the correlation between the branches will deteriorate the system performance. Thus, it will be useful to evaluate the effect of correlation on the proposed system performance over the lognormal and Gamma-Gamma channel. Moreover, the impact of pointing error on the performance of the FSO systems was considered and the boresight component of the pointing error was assumed to be zero, that is, zero-boresight pointing error. As a result, the random radical displacements (jitter) in both vertical and horizontal directions are assumed to be the same and modeled as Rayleigh distribution. Thus, it will be very important to evaluate the impact of nonzero-boresight pointing error where jitter is taken into consideration in both vertical and horizontal direction and can be modeled using different statistical distributions. In addition, a serial dual-hop relay model using the AF and DF relay protocol was considered for the proposed system. Therefore, it will be very interesting to evaluate the performance of parallel relay model between the transmitter and receiver for which there can be possibility of improving the system error performance. At the same time, other possible mitigation techniques are open for study to improve the performance of the proposed system such as Radio on FSO where RF signals are transmitted through FSO link can also be investigated for this proposed systems over different turbulence conditions.

Finally, thorough analytical performance of FSO-SM system using diversity combiner and relay-assisted scheme over atmospheric turbulence channel was reported in this thesis. Also, it is well known that spatial modulation scheme offers less complexity and better error performance as compared to other modulation techniques. Therefore, this makes its implementation a promising system for the next generation FSO systems. As a result of this, it is very important to carry out the experimental verification for this type of modulation scheme using empirical data through which theoretical and experimental investigation research may lead to adoption of spatial modulation for future FSO systems.

References

[1]   M. Awan, P. Brandl, E. Leitgeb, F. Nadeem, T. Plank, and C. Capsoni, "Results of an optical wireless ground link experiment in continental fog and dry snow conditions," In *Proceedings of IEEE International Conference on Telecommunications*, Zagreb, Croatia, June 2009, pp. 45-49.

[2]   A. K. Majumdar and J. C. Ricklin, *Free-space laser communications: principles and advances* vol. 2: Springer Science & Business Media, 2010.

[3]   M. A. Khalighi and M. Uysal, "Survey on free space optical communication: A communication theory perspective," *IEEE Communications Surveys & Tutorials,* vol. 16, no. 4, pp. 2231-2258, November 2014.

[4]   A. G. Bell, "On the production and reproduction of sound by light," *American Journal of Science,* no. 118, pp. 305-324, October 1880.

[5]   D. Hutt, K. Snell, and P. Belanger, "Alexander Graham Bell's Photophone," *Optics and Photonics News,* vol. 4, no. 6, pp. 20-25, June 1993.

[6]   M. Uysal and H. Nouri, "Optical wireless communications—An emerging technology," In *Proceedings of International Conference onTransparent Optical Networks (ICTON)*, Graz, Austria, July 2014, pp. 1-7.

[7]   J. Hecht, *City of light: the story of fiber optics*: Oxford University Press on Demand, 2004.

[8]   F. E. Goodwin, "A review of operational laser communication systems," *Proceedings of the IEEE,* vol. 58, no. 10, pp. 1746-1752, October 1970.

[9]   L. Hanzo, H. Haas, S. Imre, D. O'Brien, M. Rupp, and L. Gyongyosi, "Wireless myths, realities, and futures: from 3G/4G to optical and quantum wireless," *Proceedings of the IEEE,* vol. 100, no. Special Centennial Issue, pp. 1853-1888, May 2012.

[10]   Z. Ghassemlooy and W. O. Popoola, *Terrestrial free-space optical communications*: InTech, 2010.

[11]   M. Z. Hassan, M. J. Hossain, J. Cheng, and V. C. Leung, "Subcarrier Intensity Modulated Optical Wireless Communications: A Survey from Communication Theory Perspective," *ZTE Communications,* vol. 2, p. 002, 2016.

[12]   S. Hranilovic, *Wireless optical communication systems*: Springer Science & Business Media, 2006.

[13]   H. Willebrand and B. S. Ghuman, *Free space optics: enabling optical connectivity in today's networks*: SAMS publishing, 2002.

[14]   Z. Ghassemlooy, S. Arnon, M. Uysal, Z. Xu, and J. Cheng, "Emerging optical wireless communications-advances and challenges," *IEEE Journal on Selected Areas in Communications,* vol. 33, no. 9, pp. 1738-1749, September 2015.

[15]   Alamy.com, "Alexander Graham Bell's photo phone" [Online]. Available: http://www.alamy.com/stock-photo-alexander-graham-bells-photo-phone-131277080.html, [Accessed: 15, August 2017].

[16]   A. G. Alkholidi and K. S. Altowij, "Free Space Optical Communications—Theory and Practices," in *Contemporary Issues in Wireless Communications*, ed: InTech, 2014.

[17]   H. Henniger and O. Wilfert, "An Introduction to Free-space Optical Communications," *Radioengineering,* vol. 19, no. 2, pp. 203-212, June 2010.

[18]   D. Kedar and S. Arnon, "Urban optical wireless communication networks: the main challenges and possible solutions," *IEEE Communications Magazine,* vol. 42, no. 5, pp. S2-S7, May 2004.

[19]   Z. Ghassemlooy, W. Popoola, and S. Rajbhandari, *Optical wireless communications: system and channel modelling with Matlab®*: CRC press, 2012.

[20]   I. I. Kim and E. Korevaar, "Availability of free space optics (FSO) and hybrid FSO/RF systems," In *Proceedings of SPIE Conference*, August 2001, pp. 84-95.

[21]   A. Bekkali, C. B. Naila, K. Kazaura, K. Wakamori, and M. Matsumoto, "Transmission analysis of OFDM-based wireless services over turbulent radio-on-FSO links modeled by gamma–gamma distribution," *IEEE Photonics Journal,* vol. 2, no. 3, pp. 510-520, June 2010.

[22]   F. Demers, H. Yanikomeroglu, and M. St-Hilaire, "A survey of opportunities for free space optics in next generation cellular networks," In *Proceedings of IEEE Communication Networks and Services Research Conference (CNSR)*, Ontario, Canada, May 2011, pp. 210-216.

[23]   I. I. Kim and E. Korevaar, "Availability of free space optics (FSO) and hybrid FSO/RF systems," In *Proceedings of International Symposium on the Convergence of IT and Communications*, Denver, USA, November 2001, pp. 84-95.

[24]   G. P. Anderson, A. Berk, P. K. Acharya, M. W. Matthew, L. S. Bernstein, J. Chetwynd, *et al.*, "MODTRAN4: Radiative transfer modeling for remote sensing," In *Proceedings of Society of Photo-Optical Instrumentation Engineers (SPIE) series*, Orlando, USA, August 2000, pp. 176-183.

[25]   S. Clough, F. Kneizys, E. Shettle, and G. Anderson, "Atmospheric radiance and transmittance-FASCOD2," In *Proceedings of 6th Conference on Atmospheric Radiation*, 1986, pp. 141-144.

[26]   T. A. Tsiftsis, H. G. Sandalidis, G. K. Karagiannidis, and M. Uysal, "Optical wireless links with spatial diversity over strong atmospheric turbulence channels," *IEEE Transactions on Wireless Communications,* vol. 8, no. 2, pp. 951-957, February 2009.

[27]   X. Zhu and J. M. Kahn, "Free-space optical communication through atmospheric turbulence channels," *IEEE Transactions on Communications,* vol. 50, no. 8, pp. 1293-1300, August 2002.

[28]   R. Boluda-Ruiz, A. García-Zambrana, B. Castillo-Vázquez, and C. Castillo-Vázquez, "On the capacity of MISO FSO systems over gamma-gamma and misalignment fading channels," *Optics Express,* vol. 23, no. 17, pp. 22371-22385, August 2015.

[29]   A. García-Zambrana, B. Castillo-Vázquez, and C. Castillo-Vázquez, "Asymptotic error-rate analysis of FSO links using transmit laser selection over gamma-gamma atmospheric turbulence channels with pointing errors," *Optics Express,* vol. 20, no. 3, pp. 2096-2109, January 2012.

[30]   D. L. Fried, "Optical heterodyne detection of an atmospherically distorted signal wave front," *Proceedings of the IEEE,* vol. 55, no. 1, pp. 57-77, January 1967.

[31]   E. J. Lee and V. W. Chan, "Part 1: Optical communication over the clear turbulent atmospheric channel using diversity," *IEEE Journal on Selected Areas in Communications,* vol. 22, no. 9, pp. 1896-1906, November 2004.

[32]   S. G. Wilson, M. Brandt-Pearce, Q. Cao, and J. H. Leveque, "Free-space optical MIMO transmission with Q-ary PPM," *IEEE Transactions on Communications,* vol. 53, no. 8, pp. 1402-1412, August 2005.

[33]   X. Zhu and J. M. Kahn, "Performance bounds for coded free-space optical communications through atmospheric turbulence channels," *IEEE Transactions on Communications,* vol. 51, no. 8, pp. 1233-1239, August 2003.

[34]   X. Zhu, J. M. Kahn, and J. Wang, "Mitigation of turbulence-induced scintillation noise in free-space optical links using temporal-domain detection techniques," *IEEE Photonics Technology Letters,* vol. 15, no. 4, pp. 623-625, April 2003.

[35]   E. Jakeman, "On the statistics of K-distributed noise," *Journal of Physics A: Mathematical and General,* vol. 13, no. 1, p. 31, 1980.

[36]   E. Jakeman and P. Pusey, "Significance of K distributions in scattering experiments," *Physical Review Letters,* vol. 40, no. 9, p. 546, February 1978.

[37]   M. Niu, J. Cheng, and J. F. Holzman, "Error rate analysis of M-ary coherent free-space optical communication systems with K-distributed turbulence," *IEEE Transactions on Communications,* vol. 59, no. 3, pp. 664-668, March 2011.

[38]   G. Parry, "Measurement of atmospheric turbulence induced intensity fluctuations in a laser beam," *Journal of Modern Optics,* vol. 28, no. 5, pp. 715-728, May 1981.

[39]   G. R. Osche, "Optical detection theory for laser applications," *Optical Detection Theory for Laser Applications, by Gregory R. Osche, pp. 424. ISBN 0-471-22411-1. Wiley-VCH, July 2002.,* p. 424, July 2002.

[40]   K. P. Peppas, F. Lazarakis, A. Alexandridis, and K. Dangakis, "Simple, accurate formula for the average bit error probability of multiple-input multiple-output free-space optical links over negative exponential turbulence channels," *Optics Letters,* vol. 37, no. 15, pp. 3243-3245, August 2012.

[41]   L. C. Andrews, R. L. Phillips, C. Y. Hopen, and M. Al-Habash, "Theory of optical scintillation," *Journal of the Optical Society of America* vol. 16, no. 6, pp. 1417-1429, June 1999.

[42]   M. Al-Habash, L. C. Andrews, and R. L. Phillips, "Mathematical model for the irradiance probability density function of a laser beam propagating through turbulent media," *Optical Engineering,* vol. 40, no. 8, pp. 1554-1562, August 2001.

[43]   L. C. Andrews and R. L. Phillips, "I–K distribution as a universal propagation model of laser beams in atmospheric turbulence," *Journal of the Optical Society of America* vol. 2, no. 2, pp. 160-163, February 1985.

[44]   J. H. Churnside and R. Frehlich, "Experimental evaluation of log-normally modulated Rician and IK models of optical scintillation in the atmosphere," *Journal of the Optical Society of America* vol. 6, no. 11, pp. 1760-1766, November 1989.

[45]   R. Barrios and F. Dios, "Exponentiated Weibull distribution family under aperture averaging for Gaussian beam waves," *Optics Express,* vol. 20, no. 12, pp. 13055-13064, June 2012.

[46]   J. H. Churnside and S. F. Clifford, "Log-normal Rician probability-density function of optical scintillations in the turbulent atmosphere," *Journal of the Optical Society of America* vol. 4, no. 10, pp. 1923-1930, October 1987.

[47]   R. J. Hill and R. G. Frehlich, "Probability distribution of irradiance for the onset of strong scintillation," *Journal of the Optical Society of America* vol. 14, no. 7, pp. 1530-1540, July 1997.

[48]   S. Arnon, "Effects of atmospheric turbulence and building sway on optical wireless-communication systems," *Optics Letters,* vol. 28, no. 2, pp. 129-131, January 2003.

[49]   S. Arnon, "Optimization of urban optical wireless communication systems," *IEEE Transactions on Wireless Communications,* vol. 2, no. 4, pp. 626-629, July 2003.

[50]   A. A. Farid and S. Hranilovic, "Outage capacity optimization for free-space optical links with pointing errors," *Journal of Lightwave technology,* vol. 25, no. 7, pp. 1702-1710, July 2007.

[51]   H. G. Sandalidis, T. A. Tsiftsis, and G. K. Karagiannidis, "Optical wireless communications with heterodyne detection over turbulence channels with pointing errors," *Journal of lightwave technology,* vol. 27, no. 20, pp. 4440-4445, October 2009.

[52]   H. G. Sandalidis, T. A. Tsiftsis, G. K. Karagiannidis, and M. Uysal, "BER performance of FSO links over strong atmospheric turbulence channels with pointing errors," *IEEE Communications Letters,* vol. 12, no. 1, pp. 44-46, January 2008.

[53]   M. R. Bhatnagar and S. Anees, "On the performance of Alamouti scheme in Gamma-Gamma fading FSO links with pointing errors," *IEEE Wireless Communications Letters,* vol. 4, no. 1, pp. 94-97, February 2015.

[54]   O. Hasan and M. Taha, "Optimized FSO System Performance over Atmospheric Turbulence Channels with Pointing Error and Weather Conditions," *Radioengineering,* vol. 25, no. 4, p. 659, December 2016.

[55]   M. Z. Hassan, M. J. Hossain, J. Cheng, and V. C. Leung, "Effective Capacity of Coherent POLMUX OWC Impaired by Atmospheric Turbulence and Pointing Errors," *Journal of Lightwave Technology,* vol. 34, no. 21, pp. 5007-5022, November 2016.

[56]   P. Krishnan and D. S. Kumar, "Performance analysis of free-space optical systems employing binary polarization shift keying signaling over gamma-gamma channel with pointing errors," *Optical Engineering,* vol. 53, no. 7, pp. 1-5, July 2014.

[57]   H. Samimi, "Performance of Subcarrier Intensity Modulated FSO Systems over Gamma–Gamma Turbulence Channels with Pointing Errors," *Wireless Personal Communications,* vol. 95, no. 2, pp. 1407-1416, July 2017.

[58]   H. G. Sandalidis, "Coded free-space optical links over strong turbulence and misalignment fading channels," *IEEE Transactions on Communications,* vol. 59, no. 3, pp. 669-674, March 2011.

[59]   X. Song, F. Yang, and J. Cheng, "Subcarrier intensity modulated optical wireless communications in atmospheric turbulence with pointing errors," *Journal of Optical Communications and Networking,* vol. 5, no. 4, pp. 349-358, April 2013.

[60] W. Gappmair, S. Hranilovic, and E. Leitgeb, "OOK performance for terrestrial FSO links in turbulent atmosphere with pointing errors modeled by Hoyt distributions," *IEEE Communications Letters,* vol. 15, no. 8, pp. 875-877, August 2011.

[61] F. Yang, J. Cheng, and T. A. Tsiftsis, "Free-space optical communication with nonzero boresight pointing errors," *IEEE Transactions on Communications,* vol. 62, no. 2, pp. 713-725, February 2014.

[62] G. Li, "Recent advances in coherent optical communication," *Advances in optics and photonics,* vol. 1, no. 2, pp. 279-307, April 2009.

[63] A. Belmonte and J. M. Kahn, "Performance of synchronous optical receivers using atmospheric compensation techniques," *Optics Express,* vol. 16, no. 18, pp. 14151-14162, September 2008.

[64] E. J. Lee and V. W. Chan, "Diversity coherent and incoherent receivers for free-space optical communication in the presence and absence of interference," *IEEE/OSA Journal of Optical Communications and Networking,* vol. 1, no. 5, pp. 463-483, October 2009.

[65] M. B. Niu, J. Cheng, and J. F. Holzman, "MIMO Architecture for Coherent Optical Wireless Communication: System Design and Performance," *Journal of Optical Communications and Networking,* vol. 5, no. 5, pp. 411-420, May 2013.

[66] Z. Ghassemlooy, W. O. Popoola, S. Rajbhandari, M. Amiri, and S. Hashemi, "A synopsis of modulation techniques for wireless infrared communication," In *Proceedings of ICTON Mediterranean Winter Conference*, Sousse,Tunisia, December 2007, pp. 1-6.

[67] S. S. Muhammad, T. Javornik, I. Jelovčan, Z. Ghassemlooy, and E. Leitgeb, "Comparison of hard-decision and soft-decision channel coded M-ary PPM performance over free space optical links," *Transactions on Emerging Telecommunications Technologies,* vol. 20, no. 8, pp. 746-757, December 2009.

[68] J. Li, J. Q. Liu, and D. P. Taylor, "Optical communication using subcarrier PSK intensity modulation through atmospheric turbulence channels," *IEEE Transactions on Communications,* vol. 55, no. 8, pp. 1598-1606, August 2007.

[69]   W. Huang, J. Takayanagi, T. Sakanaka, and M. Nakagawa, "Atmospheric optical communication system using subcarrier PSK modulation," *IEICE Transactions on Communications,* vol. 76, no. 9, pp. 1169-1177, September 1993.

[70]   W. O. Popoola and Z. Ghassemlooy, "BPSK subcarrier intensity modulated free-space optical communications in atmospheric turbulence," *Journal of Lightwave Technology,* vol. 27, no. 8, pp. 967-973, April 2009.

[71]   M. Aggarwal, P. Garg, and P. Puri, "Dual-hop optical wireless relaying over turbulence channels with pointing error impairments," *Journal of Lightwave Technology,* vol. 32, no. 9, pp. 1821-1828, May 2014.

[72]   N. D. Milosevic, M. I. Petkovic, and G. T. Djordjevic, "Average BER of SIM-DPSK FSO system with multiple receivers over M-distributed atmospheric channel with pointing errors," *IEEE Photonics Journal,* vol. 9, no. 4, pp. 1-10, 2017.

[73]   J. Park, C. B. Chae, and G. Yoon, "Amplify-and-forward two-way relaying system over free-space optics channels," *Journal of Communications and Networks,* vol. 19, no. 5, pp. 481-492, 2017.

[74]   P. V. Trinh, T. C. Thang, and A. T. Pham, "Mixed mmWave RF/FSO relaying systems over generalized fading channels with pointing errors," *IEEE Photonics Journal,* vol. 9, no. 1, pp. 1-14, 2017.

[75]   R. You and J. M. Kahn, "Average Power Reduction Techniques for Multiple-Subcarrier Intensity-Modulated Optical Signals," *IEEE Transactions on Communications,* vol. 49, no. 12, December 2001.

[76]   M. Di Renzo and H. Haas, "Performance comparison of different spatial modulation schemes in correlated fading channels," In *Proceedings of IEEE International Conference on Communications (ICC)*, Cape town, South Africa, May 2010, pp. 1-6.

[77]   R. Mesleh and S. S. Ikki, "Space shift keying with amplify-and-forward MIMO relaying," *Transactions on Emerging Telecommunications Technologies,* vol. 26, no. 4, pp. 520-531, April 2015.

[78] A. Mansour, R. Mesleh, and M. Abaza, "New challenges in wireless and free space optical communications," *Optics and Lasers in Engineering,* vol. 89, pp. 95-108, February 2017.

[79] N. Serafimovski, A. Younis, R. Mesleh, P. Chambers, M. Di Renzo, C.-X. Wang*, et al.*, "Practical implementation of spatial modulation," *IEEE Transactions on Vehicular Technology,* vol. 62, no. 9, pp. 4511-4523, November 2013.

[80] T. Fath, H. Haas, M. Di Renzo, and R. Mesleh, "Spatial modulation applied to optical wireless communications in indoor LOS environments," In *Proceedings of IEEE Global Telecommunications Conference (GLOBECOM)*, Texas, USA, December 2011, pp. 1-5.

[81] T. Fath, J. Klaue, and H. Haas, "Coded spatial modulation applied to optical wireless communications in indoor environments," In *Proceedings of IEEE Wireless Communications and Networking Conference (WCNC)*, Paris, France, April 2012, pp. 1000-1004.

[82] R. Mesleh, H. Elgala, R. Mehmood, and H. Haas, "Performance of optical spatial modulation with transmitters-receivers alignment," *IEEE Communications Letters,* vol. 15, no. 1, pp. 79-81, January 2011.

[83] L. Qiu and M. Jiang, "A generalized spatial modulation for indoor optical wireless communications," In *Proceedings of IEEE Opto-Electronics and Communications Conference (OECC)*, China, June 2015, pp. 1-3.

[84] R. Mesleh, H. Elgala, and H. Haas, "Optical spatial modulation," *Journal of Optical Communications and Networking,* vol. 3, no. 3, pp. 234-244, March 2011.

[85] Y. Cheng and S.-H. Hwang, "Subcarrier intensity modulation/spatial modulation for optical wireless communications," *IEICE Transactions on Communications,* vol. 97, no. 5, pp. 1044-1049, May 2013.

[86] W. O. Popoola, E. Poves, and H. Haas, "Spatial pulse position modulation for optical communications," *Journal of Lightwave Technology,* vol. 30, no. 18, pp. 2948-2954, September 2012.

[87]   E. Poves, W. Popoola, H. Haas, J. Thompson, and D. Cárdenas, "Experimental results on the performance of optical spatial modulation systems," In *Proceedings of IEEE Vehicular Technology Conference (VTC Fall)*, Quebec, Canada, September 2012, pp. 1-5.

[88]   H. T. Pham, D. B. Chu, and N. T. Dang, "Performance analysis of spatial PPM-based free-space optical communication systems with Gaussian beam," In *Proceedings of IEEE International Conference on Advanced Technologies for Communications (ATC)*, Hanoi, Vietanm, October 2014, pp. 144-148.

[89]   T. Özbilgin and M. Koca, "Optical spatial modulation over atmospheric turbulence channels," *Journal of Lightwave Technology,* vol. 33, no. 11, pp. 2313-2323, June 2015.

[90]   K. P. Peppas and P. T. Mathiopoulos, "Free-space optical communication with spatial modulation and coherent detection over HK atmospheric turbulence channels," *Journal of Lightwave Technology,* vol. 33, no. 20, pp. 4221-4232, October 2015.

[91]   X. Zhu and J. M. Kahn, "Markov chain model in maximum-likelihood sequence detection for free-space optical communication through atmospheric turbulence channels," *IEEE Transactions on Communications,* vol. 51, no. 3, pp. 509-516, March 2003.

[92]   L. C. Andrews and R. L. Phillips, *Laser beam propagation through random media* vol. 152: SPIE press Bellingham, WA, 2005.

[93]   L. C. Andrews, R. L. Phillips, and C. Y. Hopen, "Aperture averaging of optical scintillations: power fluctuations and the temporal spectrum," *Waves in Random Media,* vol. 10, no. 1, pp. 53-70, January 2000.

[94]   J. H. Churnside, "Aperture averaging of optical scintillations in the turbulent atmosphere," *Applied Optics,* vol. 30, no. 15, pp. 1982-1994, May 1991.

[95]   M. Khalighi, N. Aitamer, N. Schwartz, and S. Bourennane, "Turbulence mitigation by aperture averaging in wireless optical systems," In *Proceedings of International Conference onTelecommunications*, Zagreb, Croatia, June 2009, pp. 59-66.

[96] M.-A. Khalighi, N. Schwartz, N. Aitamer, and S. Bourennane, "Fading reduction by aperture averaging and spatial diversity in optical wireless systems," *Journal of optical communications and networking,* vol. 1, no. 6, pp. 580-593, November 2009.

[97] F. S. Vetelino, C. Young, and L. Andrews, "Fade statistics and aperture averaging for Gaussian beam waves in moderate-to-strong turbulence," *Applied optics,* vol. 46, no. 18, pp. 3780-3789, June 2007.

[98] H. Yuksel, S. Milner, and C. Davis, "Aperture averaging for optimizing receiver design and system performance on free-space optical communication links," *Journal of Optical Networking,* vol. 4, no. 8, pp. 462-475, June 2005.

[99] R. K. Tyson, "Bit-error rate for free-space adaptive optics laser communications," *Journal of the Optical Society of America* vol. 19, no. 4, pp. 753-758, April 2002.

[100] M. Uysal, S. M. Navidpour, and J. Li, "Error rate performance of coded free-space optical links over strong turbulence channels," *IEEE Communications Letters,* vol. 8, no. 10, pp. 635-637, October 2004.

[101] S. M. Navidpour, M. Uysal, and J. Li, "BER performance of MIMO free-space optical links," In *Proceedings of IEEE Vehicular Technology Conference*, California, USA, September 2004, pp. 3378-3382.

[102] N. Letzepis and A. G. I. Fabregas, "Outage probability of the Gaussian MIMO free-space optical channel with PPM," *IEEE Transactions on Communications,* vol. 57, no. 12, December 2009.

[103] M. Ibrahim and A. Ibrahim, "Performance analysis of optical receivers with space diversity reception," *IEE Proceedings-Communications,* vol. 143, no. 6, pp. 369-372, December 1996.

[104] W. O. Popoola, Z. Ghassemlooy, J. Allen, E. Leitgeb, and S. Gao, "Free-space optical communication employing subcarrier modulation and spatial diversity in atmospheric turbulence channel," *IET optoelectronics,* vol. 2, no. 1, pp. 16-23, February 2008.

[105] E. Bayaki, R. Schober, and R. K. Mallik, "Performance analysis of MIMO free-space optical systems in gamma-gamma fading," *IEEE Transactions on Communications,* vol. 57, no. 11, pp. 3415-3424, November 2009.

[106] X. Song and J. Cheng, "Subcarrier intensity modulated MIMO optical communications in atmospheric turbulence," *Journal of Optical Communications and Networking,* vol. 5, no. 9, pp. 1001-1009, September 2013.

[107] J.-H. Lee and S.-H. Hwang, "Selection diversity-aided subcarrier intensity modulation/spatial modulation for free-space optical communication," *IET Optoelectronics,* vol. 9, no. 2, pp. 116-124, February 2015.

[108] S. Kazemlou, S. Hranilovic, and S. Kumar, "All-optical multihop free-space optical communication systems," *Journal of Lightwave Technology,* vol. 29, no. 18, pp. 2663-2669, September 2011.

[109] M. Safari and M. Uysal, "Relay-assisted free-space optical communication," *IEEE Transactions on Wireless Communications,* vol. 7, no. 12, pp. 5441-5449, December 2008.

[110] A. S. Acampora and S. V. Krishnamurthy, "A broadband wireless access network based on mesh-connected free-space optical links," *IEEE Personal Communications,* vol. 6, no. 5, pp. 62-65, October 1999.

[111] J. Akella, M. Yuksel, and S. Kalyanaraman, "Error analysis of multi-hop free-space optical communication," In *Proceedings of IEEE International Conference on Communications*, Center Seoul, South Korea, May 2005, pp. 1777-1781.

[112] T. A. Tsiftsis, H. G. Sandalidis, G. K. Karagiannidis, and N. C. Sagias, "Multihop free-space optical communications over strong turbulence channels," In *Proceedings of IEEE International Conference on Communications*, Istanbul, Turkey, June 2006, pp. 2755-2759.

[113] H. H. Fu, P. Wang, R. R. Wang, X. X. Liu, L. X. Guo, and Y. T. Yang, "Performance analysis of relay-aided free-space optical communication system over gamma-gamma fading channels with pointing errors," *Optoelectronics Letters,* vol. 12, no. 4, pp. 294-298, July 2016.

[114] C. K. Datsikas, K. P. Peppas, N. C. Sagias, and G. S. Tombras, "Serial free-space optical relaying communications over gamma-gamma atmospheric turbulence channels," *Journal of Optical Communications and Networking,* vol. 2, no. 8, pp. 576-586, August 2010.

[115] M. Aggarwal, P. Garg, and P. Puri, "Analysis of subcarrier intensity modulation-based optical wireless DF relaying over turbulence channels with path loss and pointing error impairments," *IET Communications,* vol. 8, no. 17, pp. 3170-3178, September 2014.

[116] X. Tang, Z. Wang, Z. Xu, and Z. Ghassemlooy, "Multihop free-space optical communications over turbulence channels with pointing errors using heterodyne detection," *Journal of Lightwave Technology,* vol. 32, no. 15, pp. 2597-2604, August 2014.

[117] E. Zedini and M.-S. Alouini, "Multihop communications over CSI-assisted relay IM/DD FSO systems with pointing errors," In *Proceedings of IEEE International Conference on Communication Workshop (ICCW)*, London, UK, June 2015, pp. 937-942.

[118] C. Castillo-Vázquez, R. Boluda-Ruiz, B. Castillo-Vázquez, and A. García-Zambrana, "Outage performance of DF relay-assisted FSO communications using time diversity," In *Proceedings of IEEE Photonics Conference (IPC)*, Virginia, USA, October 2015, pp. 423-426.

[119] N. T. Dang, L. H. Nguyen, and H. T. Pham, "Performance of multi-hop M-ary PPM FSO systems with SIMO links over strong atmospheric turbulence channel and pointing errors," In *Proceedings of IEEE Third World Congress on Information and Communication Technologies (WICT)*, Hanoi, Vietnam, December 2013, pp. 121-126.

[120] E. Lee, J. Park, D. Han, and G. Yoon, "Performance analysis of the asymmetric dual-hop relay transmission with mixed RF/FSO links," *IEEE Photonics Technology Letters,* vol. 23, no. 21, pp. 1642-1644, November 2011.

[121] J. Park, G. Park, B. Roh, E. Lee, and G. Yoon, "Performance analysis of asymmetric RF/FSO dual-hop relaying systems for UAV applications," In *Proceedings of IEEE Military Communications Conference, MILCOM 2013*, San Diego, California, November, 2013, pp. 1651-1656.

[122] I. S. Ansari, F. Yilmaz, and M.-S. Alouini, "Impact of pointing errors on the performance of mixed RF/FSO dual-hop transmission systems," *IEEE Wireless Communications Letters,* vol. 2, no. 3, pp. 351-354, June 2013.

[123] J. Zhang, L. Dai, Y. Zhang, and Z. Wang, "Unified performance analysis of mixed radio frequency/free-space optical dual-hop transmission systems," *Journal of Lightwave Technology,* vol. 33, no. 11, pp. 2286-2293, June 2015.

[124] S. Anees and M. R. Bhatnagar, "Performance of an amplify-and-forward dual-hop asymmetric RF–FSO communication system," *Journal of Optical Communications and Networking,* vol. 7, no. 2, pp. 124-135, February 2015.

[125] E. Zedini, I. S. Ansari, and M.-S. Alouini, "Performance analysis of mixed Nakagami-m and Gamma–Gamma dual-hop FSO transmission systems," *IEEE Photonics Journal,* vol. 7, no. 1, pp. 1-20, February 2015.

[126] S. Anees and M. R. Bhatnagar, "Performance evaluation of decode-and-forward dual-hop asymmetric radio frequency-free space optical communication system," *IET Optoelectronics,* vol. 9, no. 5, pp. 232-240, October 2015.

[127] B. Maranda and C. Leung, "Block error performance of noncoherent FSK modulation on Rayleigh fading channels," *IEEE Transactions on Communications,* vol. 32, no. 2, pp. 206-209, February 1984.

[128] R. Eaves and A. Levesque, "Probability of block error for very slow Rayleigh fading in Gaussian noise," *IEEE Transactions on Communications,* vol. 25, no. 3, pp. 368-374, March 1977.

[129] C.-E. Sundberg, "Block error probability for noncoherent FSK with diversity for very slow Rayleigh fading in Gaussian noise," *IEEE Transactions on Communications,* vol. 29, no. 1, pp. 57-60, January 1981.

[130] Q. Zhang, J. Cheng, and G. K. Karagiannidis, "Block error rate of optical wireless communication systems over atmospheric turbulence channels," *IET Communications,* vol. 8, no. 5, pp. 616-625, February 2014.

[131] M. Cheng, J. Gao, W. Dan, and Y. Zhang, "Block error rate of FSO links over non-Kolmogorov turbulence with exponentiated Weibull distribution," *Optik-International Journal for Light and Electron Optics,* vol. 125, no. 22, pp. 6805-6809, November 2014.

[132] N. Serafimovski, S. Sinanovic, M. Di Renzo, and H. Haas, "Dual-hop spatial modulation (Dh-SM)," In *Proceedings of IEEE Vehicular Technology Conference (VTC Spring)*, Budapest, Hungary, May 2011, pp. 1-5.

[133] P. Som and A. Chockalingam, "Performance analysis of space-shift keying in decode-and-forward multihop MIMO networks," *IEEE Transactions on Vehicular Technology,* vol. 64, no. 1, pp. 132-146, January 2015.

[134] P. Som and A. Chockalingam, "End-to-end BER analysis of space shift keying in decode-and-forward cooperative relaying," In *Proceedings of IEEE Wireless Communications and Networking Conference (WCNC)*, Shanghai, China, April 2013, pp. 3465-3470.

[135] P. Som and A. Chockalingam, "BER analysis of space shift keying in cooperative multi-hop multi-branch DF relaying," In *Proceedings of IEEE Vehicular Technology Conference (VTC Fall)*, Las Vegas, USA, September 2013, pp. 1-5.

[136] P. Yang, B. Zhang, Y. Xiao, B. Dong, S. Li, M. El-Hajjar*, et al.*, "Detect-and-forward relaying aided cooperative spatial modulation for wireless networks," *IEEE Transactions on Communications,* vol. 61, no. 11, pp. 4500-4511, November 2013.

[137] S. B. Alexander, *Optical communication receiver design* vol. 37: SPIE Press, 1997.

[138] M. Niu, J. Cheng, and J. F. Holzman, "Terrestrial coherent free-space optical communication systems," in *Optical Communication*, ed: Intech, 2012.

[139] S. Bloom, E. Korevaar, J. Schuster, and H. Willebrand, "Understanding the performance of free-space optics," *Journal of optical Networking,* vol. 2, no. 6, pp. 178-200, June 2003.

[140] E. Bayaki and R. Schober, "Performance and design of coherent and differential space-time coded FSO systems," *Journal of Lightwave Technology,* vol. 30, no. 11, pp. 1569-1577, June 2012.

[141] G. P. Agrawal, *Fiber-optic communication systems* vol. 222: John Wiley & Sons, 2012.

[142] H. Nyquist, "Thermal agitation of electric charge in conductors," *Physical Review,* vol. 32, no. 1, p. 110, 1928.

[143] W. Schottky, "On spontaneous current fluctuations in different electricity conductors," *Annals of physics,* vol. 362, no. 23, pp. 541-567, January 1918.

[144] W. R. Bennett, *Electrical noise*: McGraw-Hill, 1960.

[145] F. N. H. Robinson, "Noise and fluctuations in electronic devices and circuits," *Oxford, Clarendon Press,* 1974.

[146] L. C. Andrews, R. L. Phillips, and C. Y. Hopen, *Laser beam scintillation with applications* vol. 99: SPIE press, 2001.

[147] H. Kaushal and G. Kaddoum, "Optical communication in space: Challenges and mitigation techniques," *IEEE Communications Surveys & Tutorials,* vol. 19, no. 1, pp. 57-96, 2017.

[148] A. Consortini, J. H. Churnside, R. J. Hill, and F. Cochetti, "Inner-scale effect on irradiance variance measured for weak-to-strong atmospheric scintillation," *Journal of Optical Society of America,* vol. 10, no. 11, pp. 2354-2362, November 1993.

[149] T. D. Katsilieris, G. P. Latsas, H. E. Nistazakis, and G. S. Tombras, "An Accurate Computational Tool for Performance Estimation of FSO Communication Links over Weak to Strong Atmospheric Turbulent Channels," *Computation,* vol. 5, no. 1, p. 18, March 2017.

[150] N. Perlot, *Characterization of signal fluctuations in optical communications with intensity modulation and direct detection through the turbulent atmospheric channel*: Shaker Verlag GmbH, 2006.

[151] N. Wang and J. Cheng, "Moment-based estimation for the shape parameters of the Gamma-Gamma atmospheric turbulence model," *Optics Express,* vol. 18, no. 12, pp. 12824-12831, June 2010.

[152] L. Yang, X. Song, J. Cheng, and J. F. Holzman, "Free-Space Optical Communications Over Lognormal Fading Channels Using OOK With Finite Extinction Ratios," *IEEE Access,* vol. 4, pp. 574-584, 2016.

[153] K. Kiasaleh, "Performance of coherent DPSK free-space optical communication systems in K-distributed turbulence," *IEEE Transactions on Communications,* vol. 54, no. 4, pp. 604-607, April 2006.

[154] V. I. Tatarski, *Wave propagation in a turbulent medium*: Courier Dover Publications, 2016.

[155] I. S. Ansari, M.-S. Alouini, and J. Cheng, "Ergodic capacity analysis of free-space optical links with nonzero boresight pointing errors," *IEEE Transactions on Wireless Communications,* vol. 14, no. 8, pp. 4248-4264, August 2015.

[156] Y. Ren, A. Dang, B. Luo, and H. Guo, "Capacities for long-distance free-space optical links under beam wander effects," *IEEE Photonics Technology Letters,* vol. 22, no. 14, pp. 1069-1071, July 2010.

[157] R. Boluda-Ruiz, A. García-Zambrana, B. Castillo-Vázquez, and C. Castillo-Vázquez, "Impact of nonzero boresight pointing error on ergodic capacity of MIMO FSO communication systems," *Optics Express,* vol. 24, no. 4, pp. 3513-3534, February 2016.

[158] N. Hayasaka and T. Ito, "Channel modeling of nondirected wireless infrared indoor diffuse link," *Electronics and Communications in Japan (Part I: Communications),* vol. 90, no. 6, pp. 9-19, June 2007.

[159] D. A. Rockwell and G. S. Mecherle, "Optical wireless: low-cost, broadband, optical access," *SONA Communications Corporation,* 2007.

[160] I. B. Djordjevic and B. Vasic, "100-Gb/s transmission using orthogonal frequency-division multiplexing," *IEEE Photonics Technology Letters,* vol. 18, no. 15, pp. 1576-1578, 2006.

[161] T. Ohtsuki, "Multiple-subcarrier modulation in optical wireless communications," *IEEE Communications magazine,* vol. 41, no. 3, pp. 74-79, March 2003.

[162] X. Song, F. Yang, J. Cheng, and M.-S. Alouini, "BER of subcarrier MPSK and MDPSK systems in atmospheric turbulence," *Journal of Lightwave Technology,* vol. 33, no. 1, pp. 161-170, January 2015.

[163] M. Di Renzo, H. Haas, A. Ghrayeb, S. Sugiura, and L. Hanzo, "Spatial modulation for generalized MIMO: Challenges, opportunities, and implementation," *Proceedings of the IEEE,* vol. 102, no. 1, pp. 56-103, January 2014.

[164] P. Yang, M. Di Renzo, Y. Xiao, S. Li, and L. Hanzo, "Design guidelines for spatial modulation," *IEEE Communications Surveys & Tutorials,* vol. 17, no. 1, pp. 6-26, March 2015.

[165] M. Di Renzo and H. Haas, "Bit error probability of space modulation over Nakagami-m fading: Asymptotic analysis," *IEEE Communications Letters,* vol. 15, no. 10, pp. 1026-1028, October 2011.

[166] M. Di Renzo and H. Haas, "Spatial modulation with partial-CSI at the receiver: optimal detector and performance evaluation," In *Proceedings of IEEE Sarnoff Symposium*, Princeton, USA, April 2010, pp. 1-6.

[167] T. Fath, M. Di Renzo, and H. Haas, "On the performance of space shift keying for optical wireless communications," In *Proceedings of IEEE GLOBECOM Workshops* Florida, USA, December 2010, pp. 990-994.

[168] O. S. Badarneh and R. Mesleh, "Spatial modulation performance analysis over generalized η-μ fading channels," In *Proceedings of IEEE International Symposium on Personal Indoor and Mobile Radio Communications (PIMRC)*, London, United Kingdom, September 2013, pp. 886-890.

[169] E. Soujeri and G. Kaddoum, "Performance comparison of spatial modulation detectors under channel impairments," In *Proceedings of IEEE International Conference on Ubiquitous Wireless Broadband (ICUWB)*, Quebec, Canada, October 2015, pp. 1-5.

[170] M. Di Renzo and H. Haas, "On the performance of space shift keying MIMO systems over correlated Rician fading channels," In *Proceedings of IEEE International ITG Workshop on Smart Antennas (WSA)*, Bremen, Germany, February 2010, pp. 72-79.

[171] J. Jeganathan, A. Ghrayeb, and L. Szczecinski, "Spatial modulation: Optimal detection and performance analysis," *IEEE Communications Letters,* vol. 12, no. 8, August 2008.

[172] S. M. Navidpour, M. Uysal, and M. Kavehrad, "BER performance of free-space optical transmission with spatial diversity," *IEEE transactions on Wireless Communications,* vol. 6, no. 8, August 2007.

[173] H. Manor and S. Arnon, "Performance of an optical wireless communication system as a function of wavelength," *Applied optics,* vol. 42, no. 21, pp. 4285-4294, July 2003.

[174] D. Shah, D. Kothari, and A. Ghosh, "Performance of free-space optical link with wavelength diversity over exponentiated Weibull channel," *Optical Engineering,* vol. 55, no. 11, pp. 116112-116112, November 2016.

[175] Z. Wang, W. D. Zhong, S. Fu, and C. Lin, "Performance comparison of different modulation formats over free-space optical (FSO) turbulence links with space diversity reception technique," *IEEE Photonics Journal,* vol. 1, no. 6, pp. 277-285, December 2009.

[176] W. O. Popoola, Z. Ghassemlooy, H. Haas, E. Leitgeb, and V. Ahmadi, "Error performance of terrestrial free space optical links with subcarrier time diversity," *IET communications,* vol. 6, no. 5, pp. 499-506, March 2012.

[177] K. Prabu, S. Cheepalli, and D. S. Kumar, "Analysis of PolSK based FSO system using wavelength and time diversity over strong atmospheric turbulence with pointing errors," *Optics Communications,* vol. 324, pp. 318-323, August 2014.

[178] F. Xu, A. Khalighi, P. Caussé, and S. Bourennane, "Channel coding and time-diversity for optical wireless links," *Optics express,* vol. 17, no. 2, pp. 872-887, Jaunary 2009.

[179] X. Tang, Z. Xu, and Z. Ghassemlooy, "Coherent polarization modulated transmission through MIMO atmospheric optical turbulence channel," *Journal of Lightwave Technology,* vol. 31, no. 20, pp. 3221-3228, October 2013.

[180] M. K. Simon and M. S. Alouini, *Digital communication over fading channels* vol. 95: John Wiley & Sons, 2005.

[181] M. K. Simon and M. S. Alouini, "A unified approach to the performance analysis of digital communication over generalized fading channels," *Proceedings of the IEEE,* vol. 86, no. 9, pp. 1860-1877, September 1998.

[182] Z. Wang and G. B. Giannakis, "A simple and general parameterization quantifying performance in fading channels," *IEEE Transactions on Communications,* vol. 51, no. 8, pp. 1389-1398, August 2003.

[183] K. P. Peppas, "A new formula for the average bit error probability of dual-hop amplify-and-forward relaying systems over generalized shadowed fading channels," *IEEE Wireless Communications Letters,* vol. 1, no. 2, pp. 85-88, April 2012.

[184] M. Lin, K. An, J. Ouyang, Y. Huang, and M. Li, "Effect of beamforming on multi-antenna two hop asymmetric fading channels with fixed gain relays," *Progress In Electromagnetics Research,* vol. 133, pp. 367-390, 2013.

[185] P. A. Anghel, M. Kaveh, and Z. Q. Luo, "An efficient algorithm for optimum power allocation in a decode-and-forward cooperative system with orthogonal transmissions," In *Proceedings of IEEE International Conference on Acoustics, Speech and Signal Processing*, Toulouse, France, May 2006, pp. 685-688.

[186] P. Wang, J. Xiao, and P. Li, "Comparison of orthogonal and non-orthogonal approaches to future wireless cellular systems," *IEEE Vehicular Technology Magazine,* vol. 1, no. 3, pp. 4-11, September 2006.

[187] K. V. Srinivas, K. Giridhar, and R. D. Koilpillai, "Orthogonal decode and forward relaying with improved spectral efficiency," *IEEE Communications Letters,* vol. 13, no. 2, pp. 109-111, February 2009.

[188] K. P. Peppas, A. Mansour, and G. S. Tombras, "Dual-hop transmissions with fixed-gain relays over generalized-gamma fading channels," *Journal of Telecommunications,* vol. 1, no. 1, pp. 87–93, February 2010.

[189] A. Cvetković, J. Anastasov, S. Panić, M. Stefanović, and D. Milić, "Performance of dual-hop relaying over shadowed ricean fading channels," *Journal of Electrical Engineering,* vol. 62, no. 4, pp. 244-248, July 2011.

[190] M. Aggarwal, P. Garg, and P. Puri, "Exact capacity of amplify-and-forward relayed optical wireless communication systems," *IEEE Photonics Technology Letters,* vol. 27, no. 8, pp. 903-906, April 2015.

[191] F. S. Al-Qahtani, T. Q. Duong, C. Zhong, K. A. Qaraqe, and H. Alnuweiri, "Performance analysis of dual-hop AF systems with interference in Nakagami-m fading channels," *IEEE Signal Processing Letters,* vol. 18, no. 8, pp. 454-457, August 2011.

[192] M. Dohler and Y. Li, *Cooperative communications: hardware, channel and PHY*: John Wiley & Sons, 2010.

[193] M. Karimi and M. Nasiri-Kenari, "BER analysis of cooperative systems in free-space optical networks," *Journal of Lightwave Technology,* vol. 27, no. 24, pp. 5639-5647, December 2009.

[194] J.-Y. Wang, J. B. Wang, M. Chen, Y. Tang, and Y. Zhang, "Outage analysis for relay-aided free-space optical communications over turbulence channels with nonzero boresight pointing errors," *IEEE Photonics Journal,* vol. 6, no. 4, pp. 1-15, 2014.

[195] M. A. Kashani, M. Safari, and M. Uysal, "Optimal relay placement and diversity analysis of relay-assisted free-space optical communication systems," *Journal of Optical Communications and Networking,* vol. 5, no. 1, pp. 37-47, January 2013.

[196] N. Sharma, A. Bansal, and P. Garg, "Relay selection in mixed RF/FSO system using DF relaying," *Photonic Network Communications,* vol. 33, no. 2, pp. 143-151, April 2017.

[197] S. S. Soliman, V. C. Leung, N. C. Beaulieu, and J. Cheng, "Analysis of general dual-hop AF systems over Rician fading links," In *Proceedings of IEEE Global Communications Conference (GLOBECOM)*, San Diego, CA, USA, December 2015, pp. 1-6.

[198] A. T. Pham and D. A. Luong, "Optical wireless communications over fading channels: Spatial diversity or multihop relaying?," In *Proceedings of International Conference on Advanced Technologies for Communications (ATC)*, Hanoi, Vietnam, October 2014, pp. 760-765.

[199] F. Yilmaz and O. Kucur, "Exact performance of wireless multihop transmission for M-ary coherent modulations over generalized gamma fading channels," In *Proceedings of IEEE International Symposium onPersonal, Indoor and Mobile Radio Communications*, Cannes, France, September 2008, pp. 1-5.

[200] M. Haenggi and D. Puccinelli, "Routing in ad hoc networks: a case for long hops," *IEEE Communications Magazine,* vol. 43, no. 10, pp. 93-101, October 2005.

[201] M. R. Bhatnagar and Z. Ghassemlooy, "Performance analysis of Gamma–gamma Fading FSO MIMO links with pointing errors," *Journal of Lightwave Technology,* vol. 34, no. 9, pp. 2158-2169, May 2016.

[202] M. Niu, J. Cheng, and J. F. Holzman, "Alamouti-type STBC for atmospheric optical communication using coherent detection," *IEEE Photonics Journal,* vol. 6, no. 1, pp. 1-17, February 2014.

[203] V. Adamchik and O. Marichev, "The algorithm for calculating integrals of hypergeometric type functions and its realization in REDUCE system," In *Proceedings of International Symposium on Symbolic and Algebraic computation*, July 1990, pp. 212-224.

[204] J. Park, E. Lee, and G. Yoon, "Average bit-error rate of the Alamouti scheme in Gamma-Gamma fading channels," *IEEE Photonics Technology Letters,* vol. 23, no. 4, pp. 269-271, February 2011.

[205] I. S. Gradshteyn and I. M. Ryzhik, *Table of integrals, series, and products*: Academic press, 2014.

[206] K. Prabu, D. S. Kumar, and T. Srinivas, "Performance analysis of FSO links under strong atmospheric turbulence conditions using various modulation schemes," *Optik-International Journal for Light and Electron Optics,* vol. 125, no. 19, pp. 5573-5581, October 2014.

[207] J. G. Proakis, "Digital communications fourth edition, 2001," ed: McGraw-Hill Companies, Inc., New York, NY, 1998.

[208] M. Di Renzo and H. Haas, "Space shift keying (SSK) MIMO over correlated Rician fading channels: Performance analysis and a new method for transmit-diversity," *IEEE Transactions on Communications,* vol. 59, no. 1, pp. 116-129, January 2011.

[209] S. A. Al-Semari and T. E. Fuja, "Performance analysis of coherent TCM systems with diversity reception in slow Rayleigh fading," *IEEE Transactions on Vehicular Technology,* vol. 48, no. 1, pp. 198-212, January 1999.

[210] A. Ramesh, A. Chockalingam, and L. B. Milstein, "Bounds on the performance of turbo codes on Nakagami fading channels with diversity combining," In *Proceedings of IEEE Global Telecommunications Conference*, San Antonio, USA, November 2001, pp. 1199-1204.

[211] M. Chiani, D. Dardari, and M. K. Simon, "New exponential bounds and approximations for the computation of error probability in fading channels," *IEEE Transactions on Wireless Communications,* vol. 2, no. 4, pp. 840-845, July 2003.

[212] M.-S. Alouini and A. J. Goldsmith, "A unified approach for calculating error rates of linearly modulated signals over generalized fading channels," *IEEE Transactions on Communications,* vol. 47, no. 9, pp. 1324-1334, September 1999.

[213] R. Annavajjala, A. Chockalingam, and L. B. Milstein, "Performance analysis of coded communication systems on Nakagami fading channels with selection combining diversity," *IEEE Transactions on Communications,* vol. 52, no. 7, pp. 1214-1220, July 2004.

[214] A. Viterbi, "Convolutional codes and their performance in communication systems," *IEEE Transactions on Communication Technology,* vol. 19, no. 5, pp. 751-772, October 1971.

[215] I. Djordjevic, W. Ryan, and B. Vasic, "Channel Coding for Optical Channels," in *Coding for Optical Channels*, ed: Springer, 2010, pp. 123-178.

[216] K. D. Rao, *Channel coding techniques for wireless communications*: Springer, 2016.

[217] Y. Jiang, *A practical guide to error-control coding using Matlab*: Artech House, 2010.

[218] S. H. Jamali and T. Le-Ngoc, *Coded-modulation techniques for fading channels* vol. 268: Springer Science & Business Media, 2012.

[219] S. Lin and D. J. Costello, *Error control coding* vol. 2: Prentice Hall Englewood Cliffs, 2004.

[220] P. Wang, J. Zhang, L. Guo, T. Shang, T. Cao, R. Wang, *et al.*, "Performance analysis for relay-aided multihop BPPM FSO communication system over exponentiated

Weibull fading channels with pointing error impairments," *IEEE Photonics Journal,* vol. 7, no. 4, pp. 1-20, August 2015.

[221] S. S. Soliman, "MRC and selection combining in dual-hop AF systems with Rician fading," In *Proceedings of International Conference on Computer Engineering & Systems (ICCES),* Cairo, Egypt, December 2015, pp. 314-320.

[222] G. K. Karagiannidis, T. A. Tsiftsis, and R. K. Mallik, "Bounds for multihop relayed communications in Nakagami-m fading," *IEEE Transactions on Communications,* vol. 54, no. 1, pp. 18-22, January 2006.

[223] A. P. Prudnikov, Y. A. Brychkov, O. I. Marichev, and R. H. Romer, "Integrals and series: Direct Laplace Transforms," vol. 4, ed: AAPT, 1988.

[224] D. Skraparlis, V. K. Sakarellos, A. D. Panagopoulos, and J. D. Kanellopoulos, "Performance of N-branch receive diversity combining in correlated lognormal channels," *IEEE Communications Letters,* vol. 13, no. 7, July 2009.

[225] N. D. Chatzidiamantis and G. K. Karagiannidis, "On the distribution of the sum of gamma-gamma variates and applications in RF and optical wireless communications," *IEEE Transactions on Communications,* vol. 59, no. 5, pp. 1298-1308, May 2011.

[226] F. A. Prisecaru and H. Hass, "Mutual information and capacity of spatial modulation systems," *School of Engineering and Science Jacobs University,* 2007.

[227] E. Soujeri and G. Kaddoum, "The impact of antenna switching time on spatial modulation," *IEEE Wireless Communications Letters,* vol. 5, no. 3, pp. 256-259, June 2016.

[228] M. K. Simon, S. M. Hinedi, and W. C. Lindsey, *Digital communication techniques: signal design and detection*: Prentice Hall PTR, 1995.

<div align="center">**Appendix**</div>

A. Special Function and Identities

A1. Meijer-G Function

The Meijer-G function is an extremely broad function, first presented as analytical continuation of the generalized hypergeometric function for divergent cases. It is characterized as a line integral in complex plane as:

$$G_{p,q}^{m,n}\left(x\left|\begin{matrix}(a_p)\\(b_q)\end{matrix}\right.\right) = \frac{1}{2\pi i}\int_L \frac{\prod_{j=1}^m \Gamma(b_j - s)\prod_{j=1}^n \Gamma(1 - a_j + s)}{\prod_{j=1}^q \Gamma(1 - b_j + s)\prod_{j=n+1}^p \Gamma(a_j - s)} x^s\, ds \qquad (A1.1)$$

where $a_p = a_1, \dots\dots, a_p$ and $b_q = b_1, \dots\dots, b_q$; and L is the integration path

A2. Identities to other Functions

$$K_v(x) = \frac{1}{2}G_{0,2}^{2,0}\left(\frac{x^2}{4}\left|\begin{matrix}-,-\\\frac{v}{2},\frac{-v}{2}\end{matrix}\right.\right) \qquad (A2.1)$$

$$\operatorname{erf} c(x) = \pi^{-1/2}G_{1,2}^{2,0}\left(x^2\left|\begin{matrix}-\\0,\frac{1}{2}\end{matrix}\right.\right) \qquad (A2.2)$$

$$e^{-x} = G_{0,1}^{1,0}\left(x\left|\begin{matrix}-\\0\end{matrix}\right.\right) \qquad (A2.4)$$

$$Z^k G_{p,q}^{m,n}\left(Z\left|\begin{matrix}a_p\\b_q\end{matrix}\right.\right) = G_{p,q}^{m,n}\left(Z\left|\begin{matrix}a_p + k\\b_q + k\end{matrix}\right.\right) \qquad (A2.5)$$

$$B(x,x) = 2^{1-2x}B\left(\frac{1}{2},\frac{x}{2}\right) \qquad (A2.6)$$

A3. Integral Identities

$$\int_0^\infty x^m exp(-tx^n)dx = \frac{\Gamma\left(\frac{m+1}{n}\right)}{nt^{\frac{m+1}{n}}} \tag{A3.1}$$

$$\int_0^{2\pi} (sin)^{x-1}\theta d\theta = 2^{x-2}B\left(\frac{x}{2},\frac{x}{2}\right) \tag{A3.2}$$

$$\int_0^\infty x^{-\rho}e^{-\beta x} G_{p,q}^{m,n}\left(\alpha x \left|\begin{matrix} a_1 \dots a_p \\ b_1 \dots b_q \end{matrix}\right.\right)dx = \beta^{\rho-1}G_{p+1,q}^{m,n+1}\left(\frac{\alpha}{\beta}\left|\begin{matrix}\rho, \ a_1, \dots\dots, a_p \\ b_1, \dots\dots, b_q\end{matrix}\right.\right) \tag{A3.3}$$

$$\int_0^y x^{\alpha-1}G_{p,q}^{m,n}\left(wx\left|\begin{matrix}(a_p)\\(b_q)\end{matrix}\right.\right)dx$$
$$= y^\alpha G_{p+1,q+1}^{m,n+1}\left(wy\left|\begin{matrix}a_1, \dots\dots, a_n, \ 1-\alpha, \ a_n, \dots\dots, a_p\\ b_1, \dots\dots, b_m, \ -\alpha, \ b_{m+1}, \dots\dots, b_q\end{matrix}\right.\right) \tag{A3.4}$$

$$\int_0^\infty x^{\alpha-1}G_{u,v}^{s,t}\left(\sigma x\left|\begin{matrix}(c_u)\\(d_v)\end{matrix}\right.\right)G_{p,q}^{m,n}\left(wx^{l/k}\left|\begin{matrix}(a_p)\\(b_q)\end{matrix}\right.\right)dx = \frac{k^\mu l^{\rho+\alpha(v-u)-1}\sigma^{-\alpha}}{(2\pi)^{b*(l-1)+c*(k-1)}}$$
$$\times G_{kp+lv,kq+lu}^{km+lt,kn+ls}\left(\frac{w^k k^{k(p-q)}}{\sigma^l l^{l(u-v)}}\left|\begin{matrix}\Delta(k,a_1), \dots\dots, \Delta(k,a_n), \ \Delta(l,1-\alpha-d_1),\\ \Delta(k,b_1), \dots\dots, \Delta(k,b_m), \ \Delta(l,1-\alpha-c_1),\end{matrix}\right.\right. \tag{A3.5}$$
$$\left.\begin{matrix}\dots\dots, \ \Delta(l,1-\alpha-d_v),\Delta(k,a_{n+1}), \dots\dots\Delta(k,a_p)\\ \dots\dots, \ \Delta(l,1-\alpha-c_u),\Delta(k,b_{m+1}), \dots\dots\Delta(k,b_q)\end{matrix}\right)$$

A4. Inverse Laplace Transform Identity

$$x^\lambda G_{p,q}^{m,n}\left(wx^{l/k}\left|\begin{matrix}(a_p)\\(b_q)\end{matrix}\right.\right) = \frac{k^\mu l^{\lambda+1/2}}{(2\pi)^{(l-1)/2+l(k-1)}p^{\lambda+1}}$$
$$\times G_{kp+l,kq}^{km,kn+l}\left(\frac{w^l l^l}{k^{k(p-q)}p^l}\left|\begin{matrix}\Delta(l,-\lambda),\Delta\left(k,(a_p)\right)\\ \Delta\left(k,(b_q)\right)\end{matrix}\right.\right) \tag{A4.1}$$

Generally,

where

- $m, n, p, q, s, t, u, v, l, and\ k$ are the integer numbers
- . Useful Expressions

$$b *= s = t - \frac{u + v}{2}$$

$$c *= m + n - \frac{p + q}{2}$$

$$\rho = \sum_{j=1}^{v} d_j - \sum_{j=1}^{u} c_j + \frac{u - v}{2} + 1$$

$$\mu = \sum_{j=1}^{q} b_j - \sum_{j=1}^{p} a_j + \frac{p - q}{2} + 1$$

$$\Delta(k, a) = \frac{a}{k}, \frac{a + 1}{k}, \dots \dots, \frac{a + k - 1}{k}$$

B. Derivation of Distribution Models

B1. Lognormal Distribution

The first order Rytov approximation of a random variable h of optical intensity through atmospheric turbulence can be expressed by as:

$$h = \langle h \rangle \exp(2\chi_1) \qquad\qquad \text{B1.1}$$

where χ_1 is the first order log-amplitude perturbation which obeys Gaussian distributions by normalized the intensity in the sense that $\langle h \rangle = 1$. Thus, the Lognormal PDF of h can be obtained as:

$$f_h(h) = f_{\chi_1}(\chi_1)\frac{d\chi_1}{dh}\bigg|_{\chi_1 = \frac{1}{2}\ln(h)}$$

$$\triangleq \frac{1}{2h\sqrt{2\pi\sigma_{\chi_1}^2}} exp\left(-\frac{\left(\frac{1}{2}\ln(h) + \langle\chi_1\rangle\right)^2}{2\sigma_{\chi_1}^2}\right) \qquad\qquad \text{B1.2}$$

When the variance of χ_1 is expressed as:

$$\sigma_{\ln h}^2 = 4\sigma_{\chi_1}^2 \qquad\qquad \text{B1.3}$$

and thus, by taking the expected value of (B1.1) result in:

$$\langle h \rangle = \langle h \rangle \exp\left(2\left(\chi_1 + \sigma_{\chi_1}^2\right)\right) \qquad\qquad \text{B1.4}$$

where this is valid only when the exponential is zero, then

$$\langle \chi_1 \rangle = -\sigma_{\chi_1}^2 = -\frac{1}{4}\sigma_h^2 \qquad\qquad \text{B1.5}$$

Substitute (B1.3) and (B1.4) into (B1.2), then the lognormal PDF of intensity can be expressed as:

$$f_h(h) = \frac{1}{h\sqrt{2\pi\sigma_h^2}} exp\left(-\frac{(\ln(h) + 1/2\sigma_h^2)^2}{2\sigma_h^2}\right) \qquad\qquad \text{B1.6}$$

B2. Gamma-Gamma Distribution

The Gamma-Gamma distributed random variable of h can be expressed as a product of large scale h_x and small scale h_y eddies proposed by Andrew et al [146] which can be defined as:

$$h = h_x h_y \qquad\qquad\qquad \text{B2.1}$$

Thus, the Gamma distribution PDF of h_x and h_y can be respectively expressed as:

$$f_{h_x}(h_x) = \frac{\alpha(\alpha h_x)^{\alpha-1}}{\Gamma(\alpha)} exp(-\alpha h_x), \qquad h_x > 0, \qquad \alpha = 0$$

$$\text{B2.2}$$

$$f_{h_y}(h_y) = \frac{\beta(\beta h_y)^{\beta-1}}{\Gamma(\beta)} exp(-\beta h_y), \qquad h_y > 0, \qquad \beta = 0$$

By first fixing h_x and using change of variable, $h_y = h/h_x$ then the conditional PDF is expressed as:

$$f_{h_y}(h/h_x) = \frac{\beta(\beta h/h_x)^{\beta-1}}{\Gamma(\beta)} exp(-\beta h/h_x), \qquad h = 0 \qquad \text{B2.3}$$

The unconditional PDF can therefore be obtained by averaging the Gamma distribution h_x to gives the Gamma-Gamma distribution as:

$$f_h(h) = \int_0^\infty f_{h_y}(h/h_x) f_{h_x}(h_x) dh_x$$

$$\text{B2.4}$$

$$\triangleq \frac{2(\alpha\beta)^{\frac{\alpha+\beta}{2}}}{\Gamma(\alpha)\Gamma(\beta)} h^{\frac{\alpha+\beta}{2}-1} K_{\alpha-\beta}(2\sqrt{\alpha\beta h}), \qquad h > 0$$